Université de Montréal

Caractérisation du rôle transcriptionnel et épigénétique de l'O-GlcNAcylation des histones et du facteur de transcription FOXK1

Par Jessica Gagnon

Département de Biochimie et médecine moléculaire, Faculté de médecine

Mémoire présenté à la faculté de Médecine en vue de
l'obtention du grade de Maîtrise en Biochimie et Médecine Moléculaire
option Génétique Moléculaire

Août 2015

I. RÉSUMÉ (Français)

L'O-GlcNAcylation est une modification post-traductionnelle qui consiste en l'ajout covalent du N-acetylglucosamine au groupement hydroxyle des sérines et thréonines des protéines nucléaires et cytoplasmiques. Ce type de glycosylation atypique est régulé de manière très dynamique par l'action de l'O-GlcNAc transférase (OGT) et de l'O-GlcNAcase (OGA) qui catalysent et hydrolysent cette modification respectivement. Aujourd'hui, OGT émerge comme un régulateur transcriptionnel et senseur critique du métabolisme où les protéines ciblées par l'O-GlcNAcylation couvrent la presque totalité des voies de signalisation cellulaire. Récemment, des études ont aussi proposé qu'OGT soit impliquée dans la régulation épigénétique par l'O-GlcNAcylation des histones. Dans le but de caractériser le rôle fonctionnel d'OGT dans la régulation épigénétique, nous avons revisité le concept d'O-GlcNAcylation des histones et, de manière surprenante, n'avons pu confirmer cette observation. En fait, nos données indiquent que les outils disponibles pour détecter l'O-GlcNAcylation des histones génèrent des artéfacts. De ce fait, nos travaux supportent plutôt un modèle où la régulation épigénétique médiée par OGT se fait par l'O-GlcNAcylation de régulateurs transcriptionnels recrutés à la chromatine. Parmi ceux-ci, OGT s'associe au complexe suppresseur de tumeurs BAP1. En étudiant le rôle d'OGT dans ce complexe, nous avons identifié le facteur de transcription FOXK1 comme un nouveau substrat d'OGT et démontrons qu'il est régulé par O-GlcNAcylation durant la prolifération cellulaire. Enfin, nous démontrons que FOXK1 est aussi requis pour l'adipogenèse. Ensemble, nos travaux suggèrent un rôle important d'OGT dans la régulation du complexe BAP1.

Mots clés : OGT, O-GlcNAcylation, Histones, H2BS112, BAP1, FOXK1, Transcription, Épigénétique, Chromatine, Adipogenèse

II. RÉSUMÉ (Anglais)

O-GlcNAcylation is a post-translational modification which consists in the covalent addition of an N-acetylglucosamine sugar to the hydroxyl group of serine and threonine residues of nuclear and cytoplasmic substrates. This atypical glycosylation is regulated in a very dynamic manner through the action of the O-GlcNAc transferase (OGT) and the O-GlcNAcase (OGA) that catalyze and hydrolyze this modification respectively. OGT has emerged as a critical transcriptional regulator and sensor of metabolism whereby proteins targeted by O-GlcNAcylation cover several cell signaling pathways. Recently, studies have also suggested that OGT may be involved in epigenetic regulation through the O-GlcNAcylation of histones. For the purpose of characterizing the functional role of OGT in epigenetic regulation, our group revisited the concept of histone O-GlcNAcylation and surprisingly, our work could not confirm this observation. In fact, our data indicate that the available tools for histone O-GlcNAcylation detection generate artifacts. Consequently, our work rather supports a model whereby OGT-mediated epigenetic regulation is indirectly achieved through O-GlcNAcylation of chromatin-associated transcriptional regulators. Among these, OGT strongly associates with the BAP1 tumor suppressor complex. Thus, by focusing on the role of OGT in this complex, we identified the transcription factor FOXK1 as a novel substrate of OGT and demonstrate that it is regulated throught O-GlcNAcylation during cell proliferation. Finally, we demonstrate that FOXK1 is also required for adipogenesis. Taken together, these data suggest an important role of OGT in regulating the BAP1 complex.

Key words: OGT, O-GlcNAcylation, Histones, H2BS112, BAP1, FOXK1, Transcription, Epigenetic, Chromatin, Adipogenesis.

TABLE DES MATIÈRES

I. RÉSUMÉ (FRANÇAIS) II
II. RÉSUMÉ (ANGLAIS) III
III. LISTE DES TABLEAUX VI
IV. LISTES DES FIGURES VII
V. LISTE DES ABBRÉVIATIONS IX
VI. REMERCIEMENTS XIV

CHAPITRE 1 1

1. REVUE DE LITTÉRATURE 1

1.1 O-GLCNAC TRANSFÉRASE (OGT) 2
1.1.1 Structure d'OGT 3
1.1.1.1 Répétitions tétratricopeptides d'OGT 4
1.1.1.2 Domaine catalytique d'OGT 5
1.1.1.3 Site actif d'OGT 6
1.1.2 Fonction enzymatique d'OGT 7
1.1.3 Régulation de l'O-GlcNAcylation 8
1.1.3.1 Voie Biosynthétique des Hexosamines 8
1.1.3.3 Régulation d'OGT 12
1.1.4 Rôle de l'O-GlcNAcylation 13
1.1.4.1 Régulation des interactions protéine-protéine 14
1.1.4.2 Régulation de la stabilité protéique 15
1.1.4.3 Régulation de la localisation cellulaire des protéines 16
1.1.4.4 Régulation de la phosphorylation 16
1.1.5 Implications biologiques majeures 17
1.1.5.1 Maturation de HCF-1 par O-GlcNacylation 17
1.1.5.2 Rôle polycomb d'OGT 17
1.1.5.3 Association d'OGT au complexe BAP1 19
1.1.5.4 Association d'OGT au régulateur épigénétique TET2 22
1.1.5.5 O-GlcNAcylation des Histones 23
1.2 FACTEUR DE TRANSCRIPTION FORKHEAD BOX K1 (FOXK1) 25
1.2.1 Famille *Forkhead Box* 25
1.2.1.1 Sous-familles K 27
1.2.2 Régulation de FOXK1 29
1.2.2 Maintien des cellules progénitrices myoblastiques (MPC) 30
1.2.2.1 Répression de l'activité transcriptionnelle de FOXO4 30
1.2.2.2 Répression des gènes cibles de Mef2 31
1.2.2.3 Répression des gènes dépendant de SRF 31
1.2.2.4 Association avec le complexe SIN3 et SDS3 33
1.2.3 Réponse à l'autophagie 34
1.2.4 Signalisation Wnt/β-caténine 34
1.3 HYPOTHÈSE ET OBJECTIFS DE RECHERCHE 35

CHAPITRE 2 35

2. ARTICLE 1 35

2.1 ABSTRACT 38
2.2 INTRODUCTION 39
2.3 RESULTS & DISCUSSION 40
2.4 ACKNOWLEDGEMENTS 58
2.5 MATERIAL & METHODS 59
2.6 SUPPLEMENTAL FIGURES AND TABLES 67

CHAPITRE 3 74

3. ARTICLE 2 74

3.1 ABSTRACT 77
3.2 INTRODUCTION 78
3.3 RESULTS 79
3.4 DISCUSSION 93
3.5 ACKNOWLEDGEMENTS 97
3.6 MATERIAL AND METHODS 97

CHAPITRE 4 102

4. DISCUSSION 102

4.1 LES HISTONES NE SONT PAS DES SUBSTRATS D'OGT 103
4.2 DÉTECTION ARTÉFACTUELLE DE L'O-GLCNAC SUR LES HISTONES 105
4.3 OGT RÉGULE FOXK1, MAIS PAS FOXK2 PAR O-GLCNACYLATION 106
4.4 FOXK1 EST REQUIS POUR L'ADIPOGENÈSE 108
4.5 CONCLUSION GÉNÉRALE 110

RÉFÉRENCES 113

CHAPITRE 5 XV

5. ANNEXE XV

5.1 ARTICLE 1 XVI
AUTODEUBIQUITINATION PROTECTS THE TUMOR SUPPRESSOR BAP1 FROM CYTOPLASMIC EXCLUSION MEDIATED BY THE ATYPICAL UBIQUITIN LIGASE UBE2O
5.2 ARTICLE 2 LXXIII
THE BAP1/ASXL2 HISTONE H2A DEUBIQUITINASE COMPLEX REGULATES CELL PROLIFERATION AND IS DISRUPTED IN CANCER

III. LISTE DES TABLEAUX

CHAPITRE 1

Tableau I.I. Liste et références des sites d'O-GlcNAcylation identifiés sur les histones corps du nucléosomes 24
Table 1. Identification of O-GlcNAcylation sites on HCF-1 73

IV. LISTES DES FIGURES

Figure 1. Schématisation des 3 isoformes humaines de l'O-GlcNAc transférase (OGT) codées par le chromosome X. 3
Figure 2. Structure tridimensionnelle de l'O-GlcNAc transférase (OGT) 5
Figure 3. Réaction d'O-GlcNAcylation 7
Figure 4. Schéma intégratif de la voie Biosynthétique des Hexosamines (HBP) simplifiée 10
Figure 5. Réversibilité de la réaction d'O-GlcNAcylation 11
Figure 6. Schématisation des 3 isoformes humaines de l'O-GlcNAcase (OGA) codées par le chromosome 10 11
Figure 7. Exemples de régulateurs transcriptionnels rapportés pour être ciblés par OGT 14
Figure 8. Régulation de la fonction des protéines polycombs et trithorax par l'O-GlcNAcylation 18
Figure 9. Composantes et implications du complexe suppresseur de tumeur BAP1 20
Figure 10. Représentation schématique des domaines de FOXK1 et FOXK2 humains 28
Figure 11. Exemples de régulation transcriptionnelle répressive par l'association de FOXK1 et FOXK2 avec certains complexes 29
Figure 12. Undetectable Histone O-GlcNAcylation following OGT and TET2 overexpression 42
Figure 13. Undetectable histone O-GlcNAcylation following various extraction procedures 45
Figure 14. Modulation of O-GlcNAcylation does not result in detectable histone O-GlcNAcylation. 49
Figure 15. Unspecific signal detected at the level of histones in various cell lines and during cell cycle progression 51
Figure 16 H2B Ser112 O-GlcNAc antibody is not specific and Ser112 O-GlcNAcylation is not linked to H2B K120 monoubiquitination 54
Figure 17. HCF-1 and several chromatin-associated proteins but not histones bind to WGA lectin. 56
Figure 18. Histones are not modified by Click-it biotin-alkyl chemistry or by *in vitro* OGT-mediated O-GlcNAcylation 57
Figure 2.S1 Undetectable O-GlcNAcylation of histone H2A. 67
Figure 2.S2 OGT O-GlcNAcylates both TET2 and HCF-1 and Modulates HCF-1 cleavage. 68
Figure 2.S3 Undetectable O-GlcNAcylation of endogenous histones. 69
Figure 2.S4 Detection of background immunoblotting of mammalian, yeast or recombinant histones 70
Figure 2.S5 The core histones are not enriched by WGA lectin resin in conditions that ensure complete HCF-1 depletion 71
Figure 2.S6 HCD MS/MS spectra for HCF-1 O-GlcNAcylated peptide containing T779 modification site 72
Figure 2.S7. HCD MS/MS spectra for H2B and H2A peptides containing Ser112 and Thr101 respectively 74
Figure 2.S8. HCD MS/MS spectra for H3 and H4 peptides containing Ser10 and Ser47 respectively 75
Figure 19 BAP1 structural conformation and Thr493 residue but not HCF-1 and OGT are important for FHA-dependant FOXKs binding to BAP1 83
Figure 20 FOXK1 but not FOXK2 is O-GlcNAcylated by OGT 85
Figure 21 FOXK1 O-GlcNAcylation by OGT is BAP1-independent 87
Figure 22 FOXK1 O-GlcNAcylation is modulated during cell cycle entry and in response to starvation 91

Figure 23 Foxk1 but not Foxk2 is required for adipogenesis.....94
Figure 24. Modèle proposé pour la régulation de l'adipogenèse par FOXK1.....110

V. LISTE DES ABBRÉVIATIONS

AceCS1	*Acetyl-CoA synthetase 1*
ADN	Acide désoxyribonucléique
AMPK	*AMP Activated Kinase*
ARN	Acide ribonucléique
ASXL1/2	*Additional Sex Comb-like 1 et 2*
BAP1	*BRCA1-associated protein 1*
BMAL1	*Aryl Hydrocarbon Receptor Nuclear Translocator-Like*
C-Cat	Domaine catalytique en C-terminal
ChIPseq	Immunoprécipitation de chromatine couplé au séquençage à haut débit
COX7C	*Cytochrome C Oxidase Subunit 7c*
DUB	Déubiquitinases
DVL	*Dishevelled*
EMC	Expansion mitotique clonale
EOGT	*EGF domain-specific OGT*
EZH2	*Enhancer of Zeste 2*
FH	*Forkhead box*
FHA	*Forkhead-associated domain*
FHL2	*Four and a Half LIM domain protein 2*
FHL3	*Four and a half LIM domain protein 3*
Fkh2p	*Forkhead Transcription Factor 2p*
FOXK1/2	*Forkhead box K1 and K2*
GFAT	*Glutamine fructose-6-phosphate amidotransferase*
GSK3β	*Glycogen synthase kinase 3 beta*
H2A	*Histone isoform 2A*
H2AK119Ub	Histone H2A lysine 119 mono-ubiquitination
H2B	*Histone isoform 2B*

H3	*Histone isoform 3*
H3K27me3	Histone H3 lysine 27 triméthylé
H4	*Histone isoform 4*
HAT	*Histone acetyltransferase*
HBP	Voie biosynthétique des hexosamines
HCF-1	*Host cell factor 1*
HDAC1/2	Histone deacetylases 1 and 2
HOX	Homeobox
Int-D	un domaine intervenant
Kb	Kilobase
KO	Knockout
LSD2/KDM1B	*Lysine-Specific demethylase 1B*
MADS	*Mothers against decapentaplegic*
MCM1p	*Minichromosome Maintenance Protein 1*
MDM2	*Mouse Double Minute 2 homolog*
MEF2	*myocyte enhancer factor-2*
miARN	micro ARN
MLL/SET1	*Mixed Lineage Leukemia Protein 1*
MNF	M*yocyte nuclear factor*
mOGT	OGT isoforme spécifique à la mitochondrie
MPC	Cellules progénitrices myoblastiques
MPT	Modification post-traductionnelle
mTOR	*mammalian target of rapamycin*
MTS	Signal de localisation mitochondrial
Myf5	*Myogenic Factor 5*
MyoD	*Myogenic Factor D*
N-Cat	Domaine catalytique en N-terminal
ncOGT	OGT isoforme nucléo-cytoplasmique longue

NeuroD1	*Neurogenic Differentiation 1*
Nup62/68	*Nucleoporin 62 and 68*
OGA	*O-GlcNAcase*
O-GlcNAc	*O-Linked β-N-Acetylglucosamine*
OGT	*O-Linked β-N-Acetylglucosamine Transferase*
PAH2	*Paired Amphipathic Helix*
PcG	protéine polycomb
PGC-1α	*Peroxisome proliferator-activated receptor gamma coactivator 1-alpha*
Ph	*Polyhomeotic*
PPARγ	*Peroxisome proliferator-activated receptors*
PPGB	*Protective protein de beta-galactosidase*
PRC1	Complexe polycomb répressif 1
PRC2	Complexe polycomb répressif 2
PR-DUB	Complexe polycomb répresseur déubiquitinase
PREs	*Polycomb Response Elements*
pT	phospho-thréonine
Rad53	*Checkpoint Kinase 2*
Rbbp4 et Rbbp7	Protéines de liaison au rétinoblastome 4 et 7
SAM	*Steril alpha motif*
SAP18/30	Protéines 18 et 30 associées à Sin3
Sds3	*Suppressor of defective silencing 3*
Ser	Sérine
SIN3	*SWI-independent-3*
Sin3a ou Sin3b	Protéine d'échafaudage Sin3
sOGT	OGT isoforme courte
SOX15	*SRY-related HMG-box protein* 15
Sp1	*Specificity Protein 1*
SRE	*Serum Response Element*

SREBP2	S*terol regulatory element binding protein 2*
SRF	Serum response factor
Sxc	*super sex combs*
TET	*Ten Eleven Translocation*
Thr	Thréonine
TPR	Répétition tetratricopeptide
UBE2O	Ubiquitine E2/E3 ligase
UCH	*Ubiquitin carboxyl hydrolase*
UDP-GlcNAc	Uridine di-phosphate N-Acétylglucosamine
UTP	Uridine triphosphate
WGA	*Wheat Germ Agglutinine*
β-TrCP1	*F-box/WD repeat-containing protein 1A*

Je dédie ce mémoire à mes parents

qui m'ont soutenue tout au long de mon cheminement,

qui m'ont encouragée, aimée et conseillée,

mais surtout qui m'ont appris que dans la vie,

on obtient ce que l'on veut en persévérant.

VI. REMERCIEMENTS

Tout d'abord j'aimerais remercier mon directeur de recherche Dr. El Bachir Affar pour m'avoir donné la chance de contribuer à d'excellents projets de recherche et de m'avoir donné tous les outils ainsi que les opportunités nécessaires à ma réussite dans le domaine de la science. Je voudrais aussi le remercier pour son engagement, son dévouement ainsi que son soutien durant mon cheminement académique, professionnel et personnel.

Ensuite, je voudrais aussi remercier tous mes collègues de travail qui m'ont supportée, aidée et guidée durant mes travaux de recherche et qui ont su partager leurs connaissances, leurs questionnements, leurs intérêts et leur passion pour la science.

Je remercie également les organismes subventionnaires tels que la Société de Leucémie et Lymphome du Canada, le groupe financier TD, la FRQS, le département de Biochimie ainsi que la Faculté de médecine de l'Université de Montréal pour leur soutien financier et l'intérêt qu'ils ont porté à l'égard de mes travaux de recherche.

Je voudrais aussi remercier ma famille, pour leur support moral, leur présence et leur encouragement qui m'ont permis de persévérer et de m'investir davantage dans cette longue route que représentent les études graduées.

Enfin, je voudrais spécialement remercier mon conjoint alias mon partenaire de vie et de laboratoire, pour son soutien, son implication et surtout pour son amour et sa patience inestimable qui contribuent, à tous les jours, à ma réussite et à mon enthousiame professionnel et personnel.

CHAPITRE 1

1. REVUE DE LITTÉRATURE

1.1 O-GlcNAc Transférase (OGT)

La régulation des mécanismes biochimiques par les modifications post-traductionnelles (MPT) est un processus de régulation complexe qui nécessite une collaboration et une coordination accrues des enzymes permettant de modifier des substrats spécifiques en réponse à un stimulus. Ces modifications permettent une régulation dynamique, rapide et variée de la fonction protéique par l'ajout de groupements fonctionnels permettant de changer les propriétés physicochimiques des protéines ciblées [1]. Cela peut résulter en l'ajout d'une charge, d'un sucre, d'un groupement lipidique, d'une protéine etc. Ces modifications sont majoritairement bénéfiques et constituent un élément fonctionnel important quant à l'activité, la localisation, l'affinité, la solubilité et la stabilité protéique. Par exemple, la phosphorylation qui consiste en l'ajout d'une molécule de phosphate chargée négativement est parmi les modifications les plus abondantes [2]. Par ailleurs, son importance est soulignée par le fait que plus d'une centaine de kinases et de phosphatases, qui catalysent l'ajout et l'enlèvement de cette modification respectivement, sont connues à ce jour et participent dans la presque totalité des voies de signalisation cellulaire. D'autre part, un autre exemple important de modifications post-traductionnelles est l'ubiquitination qui consiste en l'ajout d'une ou plusieurs protéines d'ubiquitines sur les résidus lysines. Cette dernière est principalement impliquée dans la régulation de la demi-vie en ciblant les protéines pour la dégradation dépendante du protéasome [3]. Ce mécanisme s'avère central quant au contrôle de la qualité des protéines et au recyclage des acides aminés.

Au cours des dernières décennies, l'identification de nouvelles molécules et enzymes modificatrices telles que l'ajout de l'O-Linked β-N-Acétylglucosamine (O-GlcNAc) catalysé par l'O-Linked β-N-Acétylglucosamine Transférase (OGT), a considérablement augmenté la complexité de ce réseau de modifications, mais a aussi contribué de manière importante à la compréhension des mécanismes à la base de diverses maladies dont le cancer. Depuis la découverte de l'O-GlcNAc par Dr. Gerald W. Hart en 1984, l'intérêt grandissant autour d'OGT émerge, entre autres, du fait qu'elle est la seule enzyme connue à ce jour responsable de cette MPT nommée O-GlcNAcylation, mais aussi à cause de son omniprésence au sein des voies de signalisation cellulaires ainsi que de son implication dans la régulation du

métabolisme [4]. L'identification grandissante de substrats ciblés par l'O-GlcNAcylation suggère une importance cruciale de cette modification dans les fonctions biologiques et révèle un mécanisme de régulation complexe où l'équilibre entre la disponibilité du substrat donneur et des substrats receveurs ainsi que la stabilité protéique d'OGT est finement régulé. Afin de mieux comprendre le rôle d'OGT dans l'O-GlcNAcylation de nombreuses cibles (nommé O-GlcNAcôme), il est important de comprendre les particularités de cette enzyme unique au niveau structural ainsi qu'au niveau de sa régulation.

1.1.1 Structure d'OGT

Le gène codant pour les formes prédominantes de la protéine humaine OGT se retrouve sur le chromosome X à proximité du locus *Xist* responsable du processus d'inactivation du chromosome X [5]. Le gène d'OGT est sujet à de nombreuses études et s'avère être essentiel à l'embryogenèse et à la survie cellulaire étant donné que sa suppression est létale a un stade embryonnaire précoce chez les souris KO [5, 6]. Ce gène est composé d'un total de 23 exons, qui suite au processus d'épissage alternatif, peuvent mener à la formation de 3 isoformes distinctes de la protéine OGT, soit la forme nucléo-cytoplasmique longue (ncOGT), mitochondriale (mOGT) ou nucléo-cytoplasmique courte (sOGT) (Figure 1) qui sont exprimées de manière ubiquitaire, mais différentielle dans les tissus [7, 8].

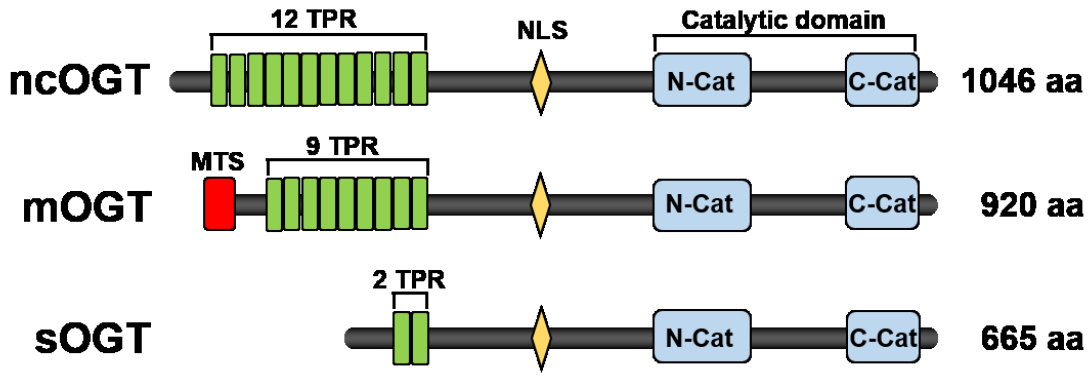

Figure 1. Schématisation des 3 isoformes humaines de l'O-GlcNAc transférase (OGT) codées par le chromosome X. Le nombre de répétitions tétratricopeptides (TPR), le signal de localisation mitochondriale (MTS), le signal de localisation nucléaire (NLS) et les lobes du domaine catalytique (N-Cat et C-Cat) sont représentés en vert, rouge, jaune et bleu respectivement. ncOGT; forme nucléocytoplasmique longue d'OGT, mOGT; forme mitocondriale d'OGT, sOGT; forme nucléocytoplasmique courte d'OGT.

Plus récemment, une étude sur la drosophile a mené à l'identification d'une forme atypique humaine d'OGT (EOGT) présente dans la lumière du réticulum endoplasmique qui serait responsable de l'O-GlcNAcylation de protéines de la matrice extracellulaire [9]. Le gène codant pour cette forme est présent sur le chromosome 3, mais n'a été que très peu caractérisé [9, 10]. De ce fait, la présente section portera uniquement sur une description détaillée de la structure et de la fonction des formes prédominantes d'OGT qui sont beaucoup plus caractérisées. Cependant, l'identification d'EOGT souligne l'importance de l'O-GlcNAcylation et indique qu'il reste encore beaucoup à découvrir sur son implication cellulaire.

1.1.1.1 Répétitions tétratricopeptides d'OGT

Comme indiqué précédemment, malgré le fait que les 3 isoformes prédominantes d'OGT possèdent une séquence presqu'identique, elles se sont révélées être différemment impliquées dans la fonction cellulaire et ce, principalement à cause de la différence entre leurs séquences N-terminales [11, 12]. La forme mOGT possède une séquence N-terminale contenant un signal de localisation mitochondrial (MTS), ce qui la situe dans la membrane interne de la mitochondrie où elle joue un rôle dans la réponse pro-apoptotique [11, 13, 14]. Les formes ncOGT et sOGT, quant à elles, se retrouvent dans le cytoplasme et dans le noyau et son impliquées dans de multiples voies de signalisation, en étant associées à différents partenaires [8, 15-17]. La distinction principale entre ces isoformes provient du nombre de répétitions du motif tetratricopeptide (TPR) situé en N-terminal. Ce motif est composé d'une répétition d'un groupe de 34 acides aminés qui s'arrange en une structure formée de 2 hélice-α antiparallèles [18]. La répétition de ce motif résulte en une accumulation de ces hélices-α antiparallèles permettant la formation d'une super hélice formant un canal amphipathique important dans la formation d'interactions protéine-protéine (Figure 2) [18].

Ce module d'interaction a été identifié dans la structure de nombreuses protéines impliquées dans des complexes multi-protéiques [19]. Par ailleurs, bien qu'aucune séquence consensus ciblée par OGT n'ait été identifiée, le site d'ancrage défini par le nombre de TPRs semble jouer un rôle déterminant dans la préférence de substrats entre les différentes isoformes d'OGT et suggère donc un rôle différentiel de ces derniers [20, 21]. En effet, la présence de

plusieurs résidus asparagine (Asp) sur la surface concave du tunnel formé par les TPRs serait importante dans la reconnaissance des substrats de différentes tailles [22]. Cette différence est

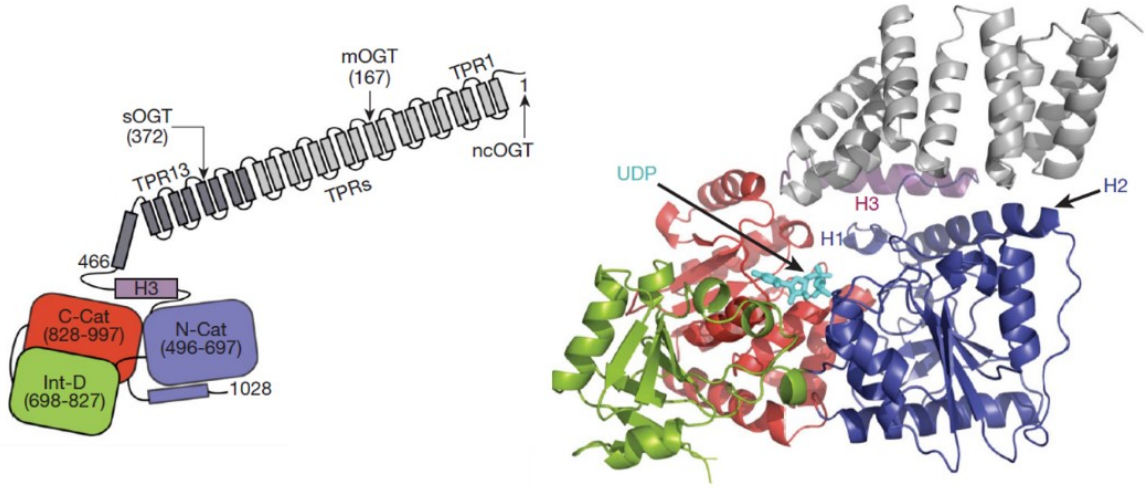

Figure 2. Structure tridimensionnelle de l'O-GlcNAc transférase (OGT) représentée de manière schématique simple (gauche) et détaillée (droite). Le nombre de répétitions tétratricopeptides (TPRs) propre aux différentes isoformes d'OGT est indiqué sur le schéma simple et représenté en gris sur les deux schémas. Le modèle tridimensionnel détaillé représente une forme tronquée contenant les 4 TPRs illustré en gris foncé sur le schéma simple. Les lobes N-terminal (C-Cat), *Intervening* (Int-D) et C-terminal (C-Cat) du domaine catalytique sont représentés en rouge, vert et violet respectivement. Les deux hélices additionnelles propres au domaine catalytique d'OGT sont représentées par H1 et H2. ncOGT; OGT nucléocytoplasmique, mOGT; OGT mitochondriale, sOGT; isoforme courte d'OGT nucléocytoplasmique. Tirée avec autorisation de Lazarus MB et al (2011) [21].

d'autant plus importante dans le cas de ncOGT et de sOGT qui se retrouvent dans les mêmes compartiments cellulaires et qui possèdent le même domaine catalytique fonctionnel [23].

1.1.1.2 Domaine catalytique d'OGT

Le domaine catalytique d'OGT comporte un lobe C-terminal (C-Cat) et un lobe N-terminal (N-Cat) qui sont séparés par un domaine *Intervening* (Int-D) qui forme chacun un repliement en sandwich de type α-β-α ressemblant à un pli de Rossmann (Figure 2) [24]. La structure de ce domaine catalytique ainsi que la présence de 2 hélices-α supplémentaires propre à la structure du lobe N-Cat d'OGT permettent la formation d'une poche de liaison à l'uridine di-phosphate N-Acétylglucosamine (UDP-GlcNAc) qui est le substrat donneur utilisé par OGT pour faire sa catalyse enzymatique [24, 25]. Cependant, bien que des études structurales aient démontré que le domaine Int-D se situe plus près du lobe C-Cat, son rôle

reste encore à déterminer. Les études cristallographiques et d'analyses mutagéniques d'OGT ont permis l'identification de résidus importants à la catalyse enzymatique. Les acides aminés Thr560, His920, Leu653 et Gly654 sont importants pour la stabilisation du sucre (GlcNAc) de l'UDP-N-Acétylglucosamine (UDP-GlcNAc) dans le site actif et les résidus Cys917, Met501 et Leu502 forment une poche hydrophobe pour interagir avec le groupe N-acétyl de ce dernier. Le groupement β-phosphate de l'UDP-GlcNAc se trouve dans une poche formée de His920, Thr921 et Thr922 ainsi que Lys842, ce qui favorise la conformation particulière de l'UDP-GlcNAc dans le site actif (Figure 2) [26]. La stabilité de la charge négative du phosphate résultant de l'attaque nucléophile du substrat est médiée par la charge positive du résidu Lys842 qui est absolument essentielle à la réaction enzymatique [26]. D'autres mutations abolissant la catalyse ont été identifiées telles que le mutant Asp925A (D925A) qui a été utilisé par notre groupe pour réaliser nos travaux [22].

1.1.1.3 Site actif d'OGT

Contrairement aux enzymes conventionnelles qui dépendent d'une diade ou triade catalytique pour déclencher la catalyse enzymatique entraînant la modification de leurs substrats, OGT semble plutôt favoriser un mécanisme de catalyse assistée par le substrat en imposant dans son site actif une conformation particulière à l'UDP-GlcNAc et au substrat, ce qui induit une attaque nucléophile entre la sérine (Ser) ou thréonine du substrat et l'UDP-GlcNAc [26]. Par ailleurs, les études de compétition indiquent qu'OGT effectue la catalyse par un mécanisme ordonné séquentiel bi-bi qui nécessite d'abord l'interaction de l'UDP-GlcNAc dans le site actif et ensuite l'interaction du peptide substrat [7, 27].

Enfin, ces études ont contribué de manière significative à la résolution de la structure d'OGT et de son complexe avec l'UDP-GlcNAc et certains peptides substrats, ce qui a permis d'éclaircir son mécanisme d'action ainsi que d'identifier les déterminants importants pour la reconnaissance de ses substrats. Les différents aspects de la structure d'OGT font d'elle une enzyme unique, capable de modifier une multitude de substrats impliqués dans des voies de signalisation variées et soulignent la complexité fonctionnelle de l'O-GlcNAcylation.

1.1.2 Fonction enzymatique d'OGT

OGT catalyse une modification post-traductionnelle cruciale et unique nommée O-GlcNAcylation. À ce jour, elle est la seule enzyme connue comme étant responsable de la catalyse de cette modification qui cible les résidus sérine et thréonine d'une multitude de protéines nucléo-cytoplasmiques pour l'ajout d'une molécule d'O-GlcNAc [28, 29]. Plus précisément, l'O-GlcNAcylation consiste en la modification réversible du groupement hydroxyle des sérines et thréonines par l'ajout covalent d'un sucre (O-GlcNAc) acétylé et non chargé provenant du substrat donneur d'OGT dérivé de la voie biosynthétique des hexosamines, l'UDP-GlcNAc (Figure 3) [30].

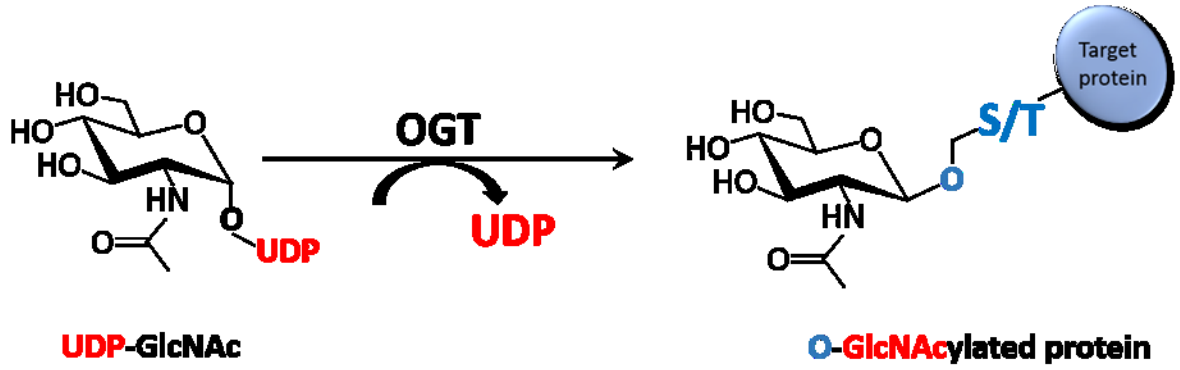

Figure 3. Réaction d'O-GlcNAcylation. Ajout de l'O-GlcNAc catalysé par l'O-GlcNAc transférase (OGT) utilisant l'UDP-GlcNAc. Le groupement hydroxyle de la sérine (S) ou de la thréonine (T) de la protéine cible est modifié par l'ajout du GlcNAc alors que l'UDP est relâché dans le milieu.

L'O-GlcNAcylation est une modification qui résulte d'interactions très transitoires qui compliquent l'analyse de son mécanisme. Les études cristallographiques qui ont mené à la compréhension du mécanisme moléculaire d'OGT ont nécessité l'utilisation d'inhibiteurs de son site actif, tels que l'UDP et l'UDP-5SGlcNAc, qui ont permis de stabiliser la présence du substrat donneur et du peptide en complexe avec OGT. Comme indiqué précédemment, le site actif d'OGT favoriserait une conformation et une proximité du substrat donneur et du substrat receveur où la sérine ou thréonine de la protéine cible (substrat receveur) attaque l'UDP-GlcNAc, ce qui résulte en l'addition du GlcNAc à cette dernière et en la libération de l'UDP [7]. D'ailleurs, bien qu'une protéine cible puisse être O-GlcNAcylée sur plusieurs résidus, OGT ne catalyse l'ajout que d'une seule molécule d'O-GlcNAc par résidu sérine ou thréonine,

ce qui ne mène pas à la formation de chaînes complexes d'O-GlcNAc [31]. Cette caractéristique ainsi que la localisation cellulaire des formes prédominantes d'OGT, favorisant majoritairement l'O-GlcNAcylation des protéines cytoplasmiques et nucléaires plutôt que celles dans la lumière du réticulum endoplasmique et du Golgi, font de l'O-GlcNAclation un type de glycosylation atypique et une modification unique. Cependant, malgré les avancées sur la compréhension du mécanisme d'action d'OGT, l'omniprésence de celle-ci ainsi que la liste exhaustive de protéines O-GlcNAcylées indiquent que les caractères structuraux identifiés jusqu'à maintenant ne sont pas les seuls déterminants qui régissent sa fonction. La manière dont OGT agit et cible spécifiquement certains substrats dans des contextes précis reste encore énigmatique. Des études ont cependant proposé que la présence d'OGT dans de nombreux complexes multi-protéiques suggère que sa spécificité pourrait provenir de son association contextuelle à ces complexes et à la disponibilité des protéines ciblées pour O-GlcNAcylation en fonction de leur expression, association ou régulation déterminées par le contexte cellulaire. Plus récemment, une étude a toutefois démontré que la structure du site actif d'OGT lui impose des contraintes quant à la séquence du substrat ciblé grâce aux positions -3 à +2 du résidu thréonine ou sérine modifié[32].

1.1.3 Régulation de l'O-GlcNAcylation

Contrairement à d'autres modifications comme la phosphorylation qui peut être modulée de manière spécifique par l'action de centaines de kinases et phosphatases qui interviennent dans différentes voies de signalisation, l'O-GlcNAcylation ne peut être généralement régulée que de manière globale par l'entremise de facteurs clés pouvant affecter 1) la formation du substrat donneur de la réaction, 2) la réversibilité de la réaction et/ou 3) la régulation d'OGT. Les modes possibles de régulation sont nombreux, mais la fluctuation du métabolisme et la disponibilité des nutriments sont sans aucun doute des déterminants importants qui contribuent au dynamisme de l'O-GlcNAc. Cette section met donc l'emphase sur les modes principaux de régulation de l'O-GlcNAcylation.

1.1.3.1 Voie Biosynthétique des Hexosamines

Comme mentionné précédemment, OGT nécessite l'intervention de l'UDP-GlcNAc dans son site actif qui agit à titre de substrat donneur du GlcNAc pour la catalyse enzymatique

[24]. L'UDP-GlcNAc joue un rôle fondamental dans la sensibilité de la réaction d'O-GlcNAcylation et procure à OGT une fonction métabolique majeure comparativement à d'autres glycosyltransférases [17, 33]. La particularité de l'utilisation de l'UDP-GlcNAc pour la réaction d'O-GlcNAcylation provient du fait que ce monosaccharide dérivé du glucose est le produit final de la voie Biosynthétique des Hexosamines (HBP), une voie impliquée dans la résistance à l'insuline et au développement du diabète [34, 35]. Normalement, l'activité limitante de la glutamine fructose-6-phosphate amidotransférase (GFAT) permet à environ 2-5% du glucose intracellulaire d'emprunter HBP plutôt que d'être dirigé vers la glycolyse (Figure 4) [35]. Ce glucose est soumis à de nombreux changements moléculaires nécessitant la collaboration d'une pléthore d'enzymes et voies métaboliques critiques pour la fonction cellulaire. Entre autres, le glucose, la glutamine, l'acétyl-CoA et l'Uridine tri-phosphate (UTP) sont des métabolites critiques pour la production de l'UDP-GlcNAc, ce qui implique une coordination accrue du métabolisme du glucose, des acides aminés, des acides gras et des nucléotides pour sa synthèse [7]. De nombreux inhibiteurs affectant le flux de HBP ont été synthétisés pour manipuler les niveaux d'O-GlcNAcylation et ont grandement contribués à la compréhension de la régulation des niveaux d'O-GlcNAc [7]. Tout changement métabolique pouvant affecter le flux de HBP peut résulter en un défaut dans la synthèse de novo de l'UDP-GlcNAc et par conséquent entraîner à long terme une diminution de l'O-GlcNAcylation globale qui aura des répercussions majeures sur la presque totalité des voies biologiques dans lesquelles cette modification est impliquée [30]. Par l'utilisation de l'UDP-GlcNAc, OGT se distingue donc par sa capacité à capter rapidement des changements métaboliques et en étant capable de convertir un stress en une réponse cellulaire globale vu l'étendu des substrats régulés par O-GlcNAcylation [36, 37]. De ce fait, OGT est décrite comme un senseur du métabolisme [38].

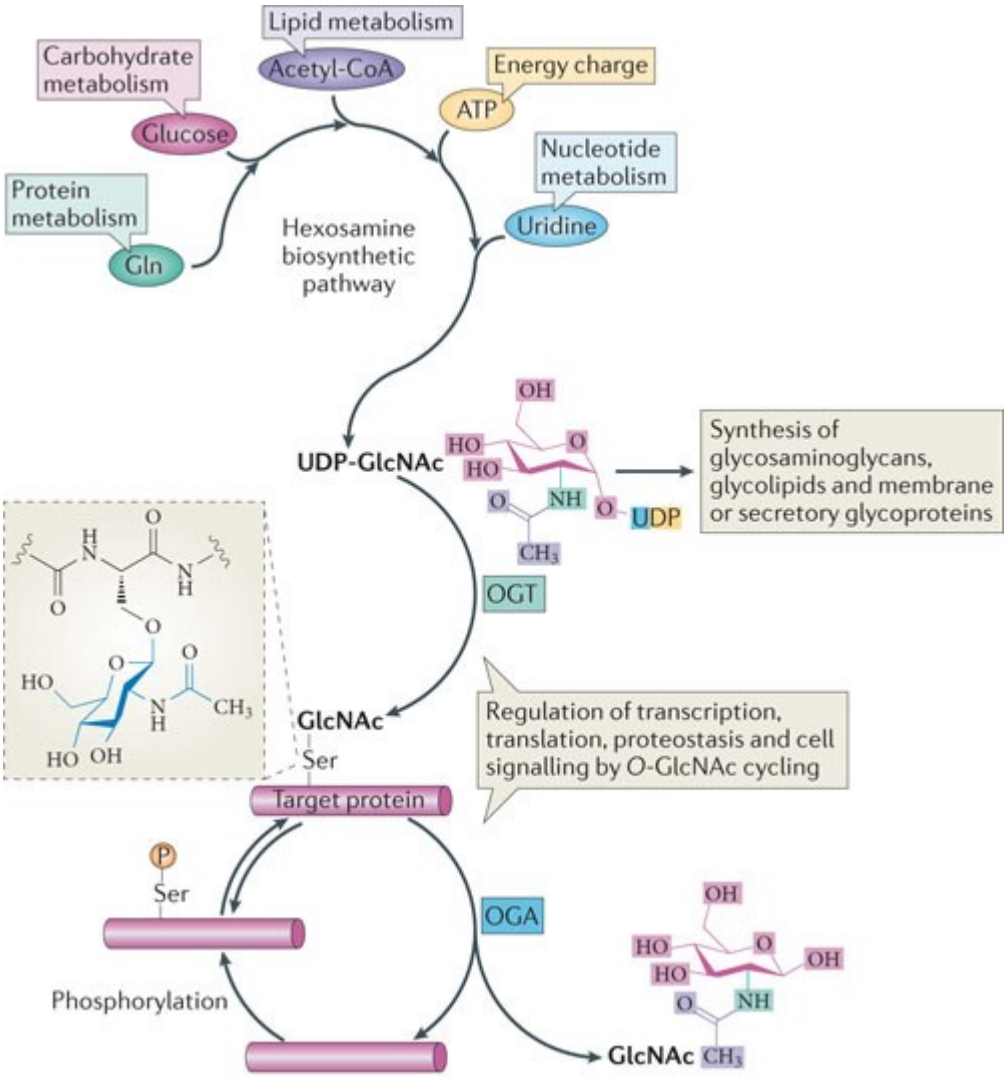

Figure 4. Schéma intégratif de la voie Biosynthétique des Hexosamines (HBP) simplifiée démontrant les voies métaboliques intermédiaires impliquées dans la synthèse de novo de l'UDP-GlcNAc et de la réaction d'O-GlcNAcylation où l'ajout de l'O-GlcNAc sur une protéine cible par OGT peut être contrecarré par l'action hydrolase d'OGA ou par compétition avec la phosphorylation. Tirée avec autorisation de Hanover JA et al (2012) [14].

1.1.3.2 O-GlcNAcase

L'O-GlcNAcylation est une modification dynamique qui est réversible par l'action unique de l'O-GlcNAcase (OGA). OGA est une glycoside hydrolase qui catalyse l'enlèvement du GlcNAc par une réaction d'hydrolyse qui libère ce dernier et qui est ensuite recyclé via la

voie de recyclage du GlcNAc (*GlcNAc salvage pathway)*. Durant leurs vies, les protéines ciblées par l'O-GlcNAcylation subissent donc des cycles variables d'ajout et d'enlèvement de la molécule d'O-GlcNAc en fonction du contexte cellulaire. Le dynamisme de cette modification est donc gouverné par l'action de deux enzymes uniques qui sont constamment soumises à une régulation fine permettant de maintenir et de contrôler les niveaux d'O-GlcNAcylation intracellulaires globaux (Figure 5).

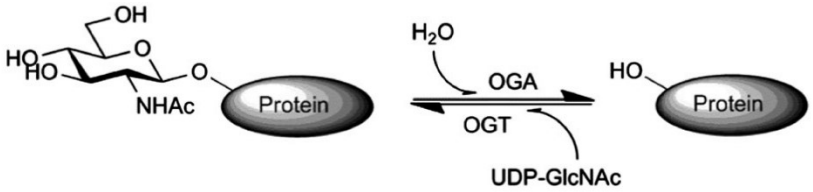

Figure 5. Réversibilité de la réaction d'O-GlcNAcylation catalysée par l'O-GlcNAc transférase (OGT) et l'O-GlcNAcase (OGA). OGT catalyse l'ajout de l'O-GlcNAc à l'aide de son substrat donneur, l'UDP-GlcNAc, alors qu'OGA hydrolyse le GlcNAc. Tirée avec autorisation de Zhu Y et al (2014) [204].

Contrairement à OGT, OGA n'a été que très peu caractérisée et sa structure cristalline n'a pas encore été résolue. Différentes études ont rapporté que la forme longue d'OGA est constituée d'un domaine GH84 en N-terminal contenant un motif catalytique à double aspartate (Asp174 et Asp175) caractéristique de son site actif et d'un amas d'hélices immédiatement suivi d'un domaine HAT en C-terminal (Figure 6) [39].

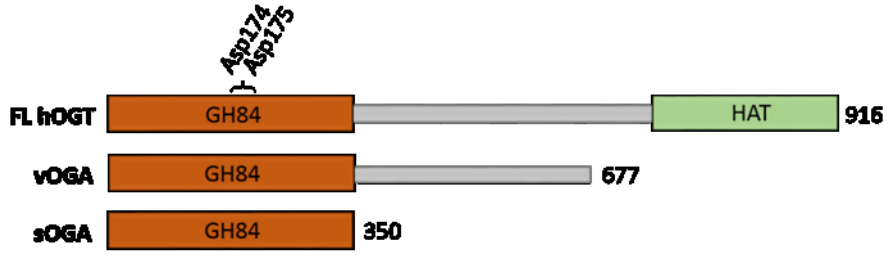

Figure 6. Schématisation des 3 isoformes humaines de l'O-GlcNAcase (OGA) codées par le chromosome 10. Les domaines O-GlcNAcase (GH84) et HAT sont représentés en orange et vert respectivement. Les deux résidus aspartate critiques du site catalytique Asp174 et Asp175 sont indiqués. La forme longue (FL), ainsi que les deux formes tronquées (vOGA et sOGA) correspondent à des protéines de 916, 677 et 350 acides aminés respectivement.

Néanmoins, bien que ce dernier domaine ait été identifié comme étant un domaine HAT, celui-ci n'a pas été associé à une activité acétyle transférase.

Trois isoformes prédominantes de la protéine OGA résultant de l'épissage alternatif du gène d'OGA sur le chromosome 10 ont été identifiées chez l'humain [40]. Chaque variant diffère en C-terminal où seule la forme longue possède le domaine HAT et où la forme la plus courte ne contient que le domaine GH84 ayant le site catalytique (Figure 5) [40, 41]. Ces isoformes ont pu être détectés dans les compartiments cytoplasmique et nucléaire et des évidences indiquent que leur expression est régulée par l'homéostasie de l'O-GlcNAc intracellulaire [41, 42]. Enfin, tout comme OGT, les déterminants qui régissent la spécificité d'OGA envers des centaines de substrats sont encore très peu compris et nécessitent des analyses beaucoup plus approfondies de son mécanisme d'action [43]. Évidemment, tous processus pouvant affecter la stabilité ou l'activité catalytique d'OGA auront des répercussions sur l'O-GlcNAcylation globale. De nombreuses molécules inhibitrices d'OGA, telles que l'O-(2-acetamido-2-deoxyglucopyranosylidene) amino N-phenylcarbamate (PUGNAc) utilisé dans nos travaux, ont été synthétisées et sont couramment utilisées pour étudier la fonction de cette modification [44].

1.1.3.3 Régulation d'OGT

Une autre façon de réguler l'ajout de l'O-GlcNAc provient d'évènements capables d'altérer ou d'accentuer de manière directe ou indirecte l'activité enzymatique ou les niveaux protéiques d'OGT. Il a été démontré qu'en réponse à une baisse de glucose intracellulaire et à une diminution du flux de HBP, l'expression d'OGT est augmentée paradoxalement suite à la diminution de la concentration en UDP-GlcNAc [45, 46]. Cependant, il n'est pas encore très clair si ce phénotype est dépendant ou non de l'AMPK qui est activée en réponse à une privation de glucose [46, 47]. De manière intrigante, la stabilité d'OGT a été montrée comme étant positivement régulée par les voies mTOR/ PI3K et c-MYC indépendamment de sa transcription [48, 49]. Lorsque la réponse autophagique est enclenchée, mTOR est inhibé et OGT est alors ciblée pour la dégradation par le protéasome résultant en une diminution de l'O-GlcNAcylation globale. Ceci démontre la complexité de la régulation d'OGT en réponse à un contexte particulier. D'autre part, les fluctuations en nutriments et autres influences

métaboliques ne sont cependant pas les seules responsables de la régulation d'OGT. En effet, OGT est la cible de multiples MPTs permettant à cette dernière de livrer une certaine sélectivité et/ou spécificité de réaction. Parmi ces MPTs, plusieurs sites de phosphorylation influençant l'activité ou la stabilité d'OGT ont été identifiés. En réponse à une stimulation par l'insuline, OGT est transloquée du noyau au cytoplasme et est phosphorylée sur une ou plusieurs tyrosines par le récepteur à l'insuline résultant en une augmentation de son activité catalytique [50, 51]. Une augmentation de l'activité d'OGT a aussi été observée par la phosphorylation de ses sérines 3 et 4 par GSK3β, un évènement important dans la régulation du rythme circadien [52]. Comme indiqué précédemment, la phosphorylation d'OGT par mTOR augmente sa stabilité [48, 49]. À l'inverse, OGT est aussi la cible des ubiquitines ligases LSD2 et β-TrCP1 qui provoquent sa dégradation médiée par le protéasome [53, 54]. Bien que la phosphorylation et l'ubiquitination semblent être les modifications prédominantes pour la régulation de la fonction d'OGT, OGT est aussi sujette à l'auto O-GlcNAcylation [55, 56]. Cependant, la conséquence fonctionnelle de cette auto régulation reste encore inconnue, mais semble être impliquée dans la régulation de son activité [52]. Enfin, autre que la voie de l'insuline, peu de régulateurs transcriptionnels d'OGT ont été identifiés [51].

1.1.4 Rôle de l'O-GlcNAcylation

Depuis sa découverte, l'O-GlcNAcylation a été étudiée dans plusieurs organismes modèles dans le but de déterminer sa fonction physiologique [6, 57-59]. Les travaux effectués chez le vers, la drosophile et la souris ont permis de déterminer que bien qu'OGT semble avoir des fonctions très différentes dans ces organismes, ses fonctions sont essentielles lorsqu'il s'agit de déterminer son rôle chez les eucaryotes complexes comme la souris et la drosophile [60]. De nombreuses études ont tenté de comprendre comment l'O-GlcNAcylation peut affecter la fonction protéique. Ces dernières ont révélé l'importance de l'O-GlcNAc dans la régulation fonctionnelle à plusieurs niveaux [61, 62]. De façon notable, OGT cible majoritairement des régulateurs et complexes transcriptionnels [63]. Malgré le fait que l'O-GlcNAcylation d'un résidu puisse avoir un rôle spécifique, il s'avère que la plupart des sites d'O-GlcNAcylation rapportés peuvent engendrer des répercussions diverses au niveau transcriptionnel et épigénétique (Figure 7). La section suivante présente donc quelques exemples spécifiques de régulation par O-GlcNAcylation rapportés dans la littérature qui

montrent l'implication répandue d'OGT dans la régulation du protéome. Cependant, à cause e son implication biologique majeure, cette liste d'exemples n'est pas du tout exhaustive et ne démontre que partiellement l'ampleur de la fonction d'OGT.

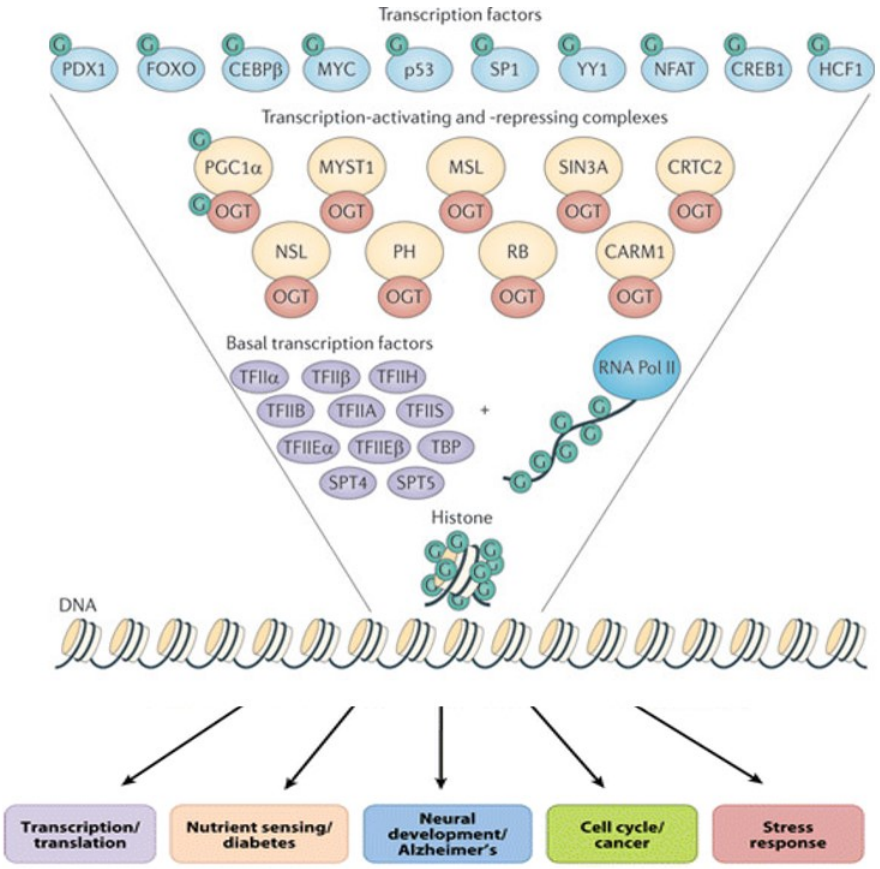

Figure 7. Exemples de régulateurs transcriptionnels rapportés pour être ciblés par OGT. L'O-GlcNAcylation de ces cibles a des répercussions sur la transcription, la traduction, le métabolisme, le développement neuronal, le cycle cellulaire et la réponse cellulaire au stress. Leur dérégulation contribue à de nombreuses maladies incluant le diabète, la maladie d'Alzheimer et le cancer. Adaptée avec autorisation de Slawson C et Hart GW (2011) [60].

1.1.4.1 Régulation des interactions protéine-protéine

De nombreux exemples sur le rôle de l'O-GlcNAction dans la régulation des interactions protéine-protéine ont été décrits dans la littérature. Un cas connu est la régulation

positive de l'assemblage du complexe de pré-initiation de la transcription par l'O-GlcNAcytion du domaine C-terminal de l'ARN polymérase II ayant un impact positif sur la transcription des gènes [64]. Un autre est la médiation de l'interaction entre les nucléoporines Nup62 et Nup68 où la co-immunoprécipitation de Nup62 avec Nup68 se trouve pratiquement abolie dans des conditions de déplétion d'OGT [65]. Ceci suggère que dans ce cas précis, l'O-GlcNAcylation augmente l'interaction entre ces deux protéines de manière favorable pour la fonction du complexe pore nucléaire qui est impliqué dans de nombreux processus en plus de sa fonction cruciale dans le transport nucléocytoplasmique [65, 66]. Un cas opposé a aussi été rapporté entre les facteurs de transcription Sp1 et SREBP2 où dans ce cas précis, l'O-GlcNAcylation de Sp1 interrompt son association avec SREBP2 et réduit l'expression de l'acétyl-CoA synthétase 1 (AceCS1) résultant en une diminution de la synthèse de lipides et d'autres processus dépendant de l'acétyl-CoA, tels que l'acétylation des histones [67-69]. Ces exemples et de nombreux autres, démontrent l'implication cruciale de l'O-GlcNAcylation dans la régulation positive et négative des interactions protéiques engagées dans des voies de signalisation variées.

1.1.4.2 Régulation de la stabilité protéique

L'O-GlcNAcylation a aussi été impliquée dans la régulation des niveaux protéiques et a récemment été décrite comme étant un régulateur du contrôle de qualité des protéines naissantes, impliquant que l'O-GlcNAcylation est aussi une modification co-traductionnelle [70]. Un exemple crucial de la régulation de la stabilité protéique ayant un impact important sur la régulation transcriptionnelle est l'O-GlcNAcylation de la Ser149 du suppresseur de tumeur et gardien du génome p53. Cette dernière empêche la dégradation de p53 par l'inhibition de son ancrage avec l'ubiquitine ligase MDM2 qui cible p53 pour la dégradation [71]. D'autre part, l'O-GlcNAcylation joue un rôle important dans l'homéostasie du glucose où la modification de PGC-1α favorise le recrutement du complexe de la déubiquitinase BAP1 qui permet la stabilisation des niveaux de PGC-1α en la protégeant contre la dégradation par le protéasome [72]. La stabilité de beaucoup d'autres protéines telles que la H3K27me3 méthyltransférase EZH2, le médiateur de la voie Wnt β-caténine, l'oncogène c-MYC [73] et les protéines du rythme circadien dont BMAL1/CLOCK sont aussi régulées par OGT et ont des répercussions majeures sur la fonction cellulaire [74-76].

1.1.4.3 Régulation de la localisation cellulaire des protéines

L'O-GlcNAcylation a aussi été impliquée dans le transport et le changement de localisation cellulaire de plusieurs protéines dans une variété de tissus. Au niveau neuronal, l'ajout de l'O-GlcNAc sur la Thr87 de synapsin I inhibe sa localisation aux synapses et diminue la densité des vésicules synaptiques et la taille des vésicules synaptiques de réserve dans les axones [77]. Ceci a été suggéré comme étant un mécanisme permettant de moduler la plasticité présynaptique. Dans les cellules β du pancréas, des niveaux élevés de glucose et donc une activité accrue d'OGT engendre la translocation nucléaire du facteur de transcription NeuroD1 afin d'induire l'expression des gènes en rapport avec la voie de l'insuline [78]. Par ailleurs, l'O-GlcNAcylation du proto-oncogène Ewing sarcoma induit sa translocation nucléaire où il participe à la maturation du miARN Let-7g qui contribue à l'adipogenèse [79-81]. Encore une fois, les cibles d'OGT sont diverses et celles-ci ne sont que quelques exemples permettant d'apprécier les multiples fonctions de l'O-GlcNAcylation.

1.1.4.4 Régulation de la phosphorylation

L'abondance de protéines modifiées par O-GlcNAcylation, le dynamisme de sa cyclisation dans les différents compartiments cellulaires ainsi que la spécificité ce cette modification pour les résidus sérine et thréonine rappelle la phosphorylation. En fait, des sites communs d'O-GlcNAcylation et de phosphorylation ont été identifiés sur un grand nombre de protéines telles que l'ARN polymérase II [82], la méthylcytosine déoxygénase TET2 [83] ainsi que la protéine tau [84] et ont rapidement mené à l'identification d'un mécanisme de régulation par compétition ayant des répercussions majeures sur la signalisation cellulaire [85-87]. De plus, OGT et OGA ont été trouvées en complexe avec de nombreuses kinases et phosphatases, ce qui implique que la compétition O-GlcNAc/phosphate nécessite l'intervention d'un mécanisme en 2 étapes où le phosphate doit d'abord être enlevé pour ensuite ajouter l'O-GlcNAc et vice versa [85, 87-89]. Cependant, la phosphorylation peut aussi être régulée par l'O-GlcNAcylation de manière indépendante de la compétition considérant que plusieurs kinases et phosphatases sont des substrats d'OGT [88, 90, 91]. Par ailleurs, plusieurs études ont aussi rapporté des impacts fonctionnels résultant d'un *crosstalk* entre des résidus phosphorylés et O-GlcNAcylés adjacents [92, 93]. Clairement, la

compréhension de la relation entre l'O-GlcNAcylation et la phosphorylation n'est encore qu'à ses débuts et des découvertes récentes suggèrent un mode de régulation encore plus complexe qu'attendu [94].

1.1.5 Implications biologiques majeures

1.1.5.1 Maturation de HCF-1 par O-GlcNacylation

OGT est une enzyme multifonctionnelle pour laquelle on ne cesse de découvrir de nouvelles fonctions. Un autre aspect unique de cette enzyme est le fait qu'elle retient une activité protéolytique envers le régulateur du cycle cellulaire HCF-1 (*Host cell factor 1).* OGT a d'abord été démontrée comme étant requise pour la maturation protéolytique de la forme précurseur de HCF-1 qui doit être clivée pour que ses formes HCF-1N et HCF-1C résultantes puissent permettre la transition G1/S et la cytokinèse respectivement [95, 96]. Les résidus aspartate et asparagine des TPRs d'OGT sont engagés dans une interaction avec une série de thréonines de la région répétitive HCF-1_{PRO} de la forme précurseur d'HCF-1 [97]. Durant cette interaction HCF-1 occupe une position spécifique dans le site actif d'OGT à proximité de l'UDP-GlcNAc. Des études mutationnelles et cristallographiques ont pu montrer qu'OGT O-GlcNAcyle et clive subséquemment HCF-1 dans sa région HCF-1_{PRO} qui contient plusieurs répétitions d'une séquence contenant un acide glutamique en position 10 qui semble important dans le mécanisme de clivage [97, 98]. Malgré que le mécanisme exact de protéolyse n'ait pas été identifié, les évidences structurales du site actif d'OGT en complexe avec l'inhibiteur analogue UDP-5SGlcNAc et un peptide tronqué d'HCF-1 contenant la région de clivage proposent que le clivage se fait via un mécanisme assisté impliquant la formation d'un intermédiaire glutamyl-sucre entre l'acide glutamique de la séquence HCF-1_{PRO} et le GlcNAc [97]. Bien que pour le moment cette activité protéolytique n'ait été identifiée qu'envers HCF-1, il ne serait pas étonnant que celle-ci s'applique aussi à d'autres protéines étant donné la quantité de substrats d'OGT qui s'élève maintenant à plusieurs centaines [87].

1.1.5.2 Rôle polycomb d'OGT

L'homologue d'OGT chez la drosophile est codé par le gène polycomb *sxc (super sex combs)* [99]. Sa fonction polycomb a été déterminée par l'identification de mutations causant un phénotype de transformation homéotique caractérisé par une dérégulation de l'expression

des gènes *Hox* [100]. OGT/sxc s'avère donc être cruciale pour la répression des gènes HOX, ce qui concorde avec le phénotype de létalité embryonnaire des souris $Ogt^{-/-}$ [6]. En fait, l'O-GlcNAcylation de protéines aux sites PREs *(Polycomb Response Elements)* a permis de déterminer qu'OGT régule ce processus de répression via l'O-GlcNAcylation d'autres protéines polycombs. Un exemple de cette régulation est l'O-GlcNAcylation de la protéine polycomb Ph *(Polyhomeotic)* qui est nécessaire à l'assemblage du Complexe Polycomb Répressif 1 (PRC1). Des défauts d'O-GlcNAcylation ont démontré que l'ajout d'O-GlcNAc sur une région spécifique de résidus Ser/Thr prévient l'agrégation du domaine SAM *(Steril alpha motif)* entre protéines Ph et permet une liaison ordonnée des protéines Ph nécessaire à la répression des gènes HOX [101]. Par ailleurs, OGT contrôle aussi la triméthylation de l'histone H3 sur la lysine 27 (H3K27me3) en régulant la stabilité de la protéine du Complexe Polycomb Répressif 2 (PRC2), EZH2, qui catalyse l'ajout de cette marque répressive [74]. En fait, de manière plus large, l'O-GlcNAcylation des protéines polycombs et thritorax joue un rôle primordial dans la régulation de leurs fonctions et indique qu'OGT est, en quelque sorte, un chef d'orchestre qui coordonne l'expression génique lors du développement embryonnaire (Figure 8).

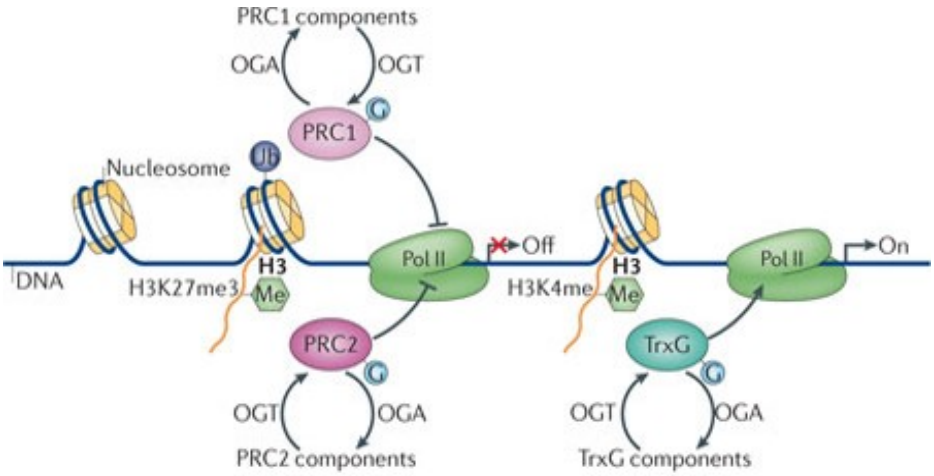

Figure 8. Régulation de la fonction des protéines polycombs et trithorax par l'O-GlcNAcylation. Les Complexes Polycombs Répressifs 1 et 2 (PRC1 et PRC2) catalysent l'ajout des marques répressives H2AK119Ub et H3K27me3 respectivement. Les groupes de protéines Trithorax (TrxG) catalysent l'ajout de la marque activatrice mono-, di- ou tri-méthyl sur H3K4. L'O-GlcNAcylation de certaines composantes de PRC1 et PRC2 ainsi que certaines composantes des TrxG permet la répression (Off) ou l'activation (On) de la transcription des gènes respectivement. Tirée avec autorisation de Hanover JA et al (2012) [17].

1.1.5.3 Association d'OGT au complexe BAP1

De manière importante, OGT est un partenaire majeur du complexe suppresseur de tumeur BAP1 qui est décrit comme un complexe polycomb répresseur déubiquitinase (PR-DUB). L'ubiquitination est une modification post-traductionnelle caractérisée par l'attachement covalent d'une molécule ubiquitine aux lysines de protéines cibles. L'ubiquitination joue un rôle crucial dans la régulation de nombreux processus biologiques. D'un point de vue clinique, les mutations des gènes impliqués dans le système ubiquitine sont associées à de nombreuses maladies humaines et sont souvent impliquées dans le développement et la progression de plusieurs types de cancers [102]. Entre autres, l'ubiquitination de l'histone H2A sur la lysine 119 (H2AK119Ub) par PRC1 a été décrite comme jouant un rôle majeur dans la cancérogenèse, où certaines composantes sont hautement surexprimées dans plusieurs cancers [103-105]. L'ubiquitination est une modification réversible grâce à l'action de protéases appelées déubiquitinases (DUBs) qui sont responsables de l'enlèvement de la molécule d'ubiquitine sur les protéines cibles. Bien que les DUBs émergent comme des régulateurs critiques des processus biologiques, les mécanismes fonctionnels et les déterminants de leurs spécificités sont encore des domaines très actifs de recherche [106].

BAP1 (*BRCA1-associated protein 1*) est une DUB particulière de la famille ubiquitine carboxyl hydrolase (UCH) qui a d'abord été identifiée par son interaction avec le suppresseur de tumeurs BRCA1 [107]. BAP1 est principalement caractérisée pour son action sur H2AK119Ub, agissant ainsi comme un antagoniste de PRC1. De façon importante, BAP1 est mutée dans un large éventail de cancers (mélanome, carcinome du rein, mésothéliome pleural, cancer du sein, du poumon, du pancréas etc.) et est à ce jour la déubiquitinase la plus mutée du génome humain [108, 109]. BAP1 forme un large complexe multi-protéines composé principalement de protéines Polycombs (PcG) et de régulateurs transcriptionnels (Figure 9) [110].

En plus de l'interaction majeure avec OGT, le corps du complexe BAP1 est composé d'HCF-1 (*Host cell factor 1*) qui est impliqué dans la prolifération cellulaire et dans la transition G1/S, d'ASXL1 et ASXL2 (*Additional Sex-Comb like protein 1 and 2*) qui sont des régulateurs

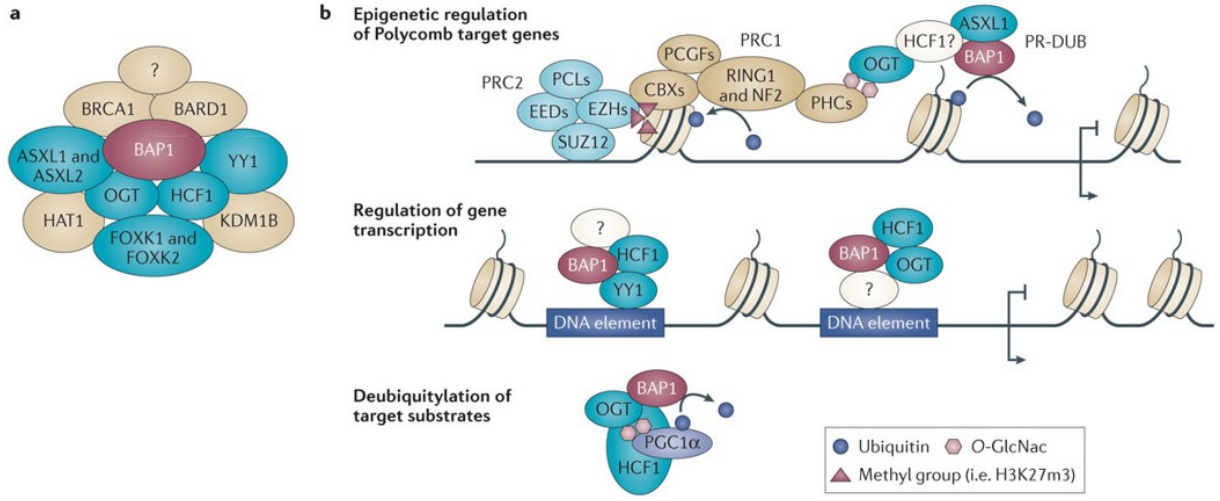

Figure 9. Composantes et implications du complexe suppresseur de tumeur BAP1. a) Composantes corps majeures du complexe BAP1 incluant OGT. b) (Haut) Implication épigénétique du complexe BAP1 opposant le Complexe Repressif 1 (PRC1) par la déubiquitination de l'histone H2A. (Milieu) Régulation de la transcription des gènes via le recrutement de BAP1 à la chromatine par les nombreux facteurs de transcription associés à BAP1. (Bas) Implication biologique par la déubiquitination de substrats cibles. Ces derniers incluent PGC1α, OGT et HCF-1. Tirée avec autorisation de Carbone M et al (2013) [104].

transcriptionnels et des PcG très impliqués dans l'intégrité du système hématologique, [111] de YY1 (*Ying Yang 1)* qui est un facteur de transcription et un facteur PcG impliqué dans la prolifération cellulaire et la différenciation [112] et de LSD2/KDM1B (*Lysine-Specific demethylase 1B*) qui est une histone déméthylase de H3K4me1/me2 antagoniste du complexe méthyltransférase MLL/SET1 et à la fois la E3 ubiquitine ligase responsable de la dégradation protéasomale d'OGT [54]. Ce complexe est aussi formé des deux facteurs de transcription FOXK1 et FOXK2 (*Forkhead box K1 and K2*) qui n'ont été que très peu caractérisés, mais qui sont impliqués de manière majeure dans la régulation du métabolisme et la différenciation cellulaire [113, 114]. Les évidences indiquent que l'intégrité du complexe ainsi que la coordination de ses différentes activités, incluant l'O-GlcNAcylation, sont cruciales pour sa fonction de suppression tumorale [108, 111, 115]. Le complexe BAP1 peut être décrit comme une plate-forme multifonctionnelle qui combine l'action de nombreuses MPTs nécessaires à la régulation transcriptionnelle très spécifique de régions régulatrices critiques impliquées dans la réponse anti-tumorale.

La fonction du complexe BAP1 dans la régulation de l'expression de nombreux gènes via la déubiquitination de H2AK119Ub a d'abord été mise en évidence par la présence du complexe ternaire BAP1/HCF-1/YY1 sur le promoteur du gène mitochondrial *COX7C* et par la régulation de ce gène de manière dépendante de l'activité déubiquitinase de BAP1 [116]. L'analyse par puce ARN de cellules déficientes du gène de BAP1 a cependant révélé la dérégulation d'un nombre élevé de gènes impliqués dans le cycle cellulaire, la réparation de l'ADN, l'apoptose et la prolifération [116]. En fait, des analyses d'immunoprécipitation de chromatine couplée au séquençage à haut débit (ChIPseq) de BAP1 ont révélé qu'environ 65% des sites de liaisons de BAP1 se trouvent sur des régions promotrices à environ (+/- 2kb) de l'origine de transcription, ce qui suggère un rôle déterminant quant à la régulation transcriptionnelle de nombreux processus biologiques [115]. Cependant, bien que des défauts transcriptionnels importants chez les patients atteints de cancers caractérisés par des mutations somatiques inactivatrices de BAP1 aient été observés, il n'a pas encore été déterminé si ce phénotype est uniquement causé par des niveaux trop élevés de H2AK119Ub ou s'il est aussi causé par l'impossibilité de recruter les autres protéines modificatrices du complexe BAP1 à des locus spécifiques [117].

La fonction d'OGT dans la complexe BAP1 est encore très peu connue. Bien que sa fonction dans la maturation protéolytique d'HCF-1 ait été très décrite et liée à un rôle dans le recrutement du complexe BAP1 à la chromatine, l'impact de l'O-GlcNAcylation d'autres composantes telles que YY1 sur la fonction du complexe BAP1 n'a pas encore été investigué [118]. Inversement, des études indiquent que BAP1 régule la stabilité des niveaux protéiques d'OGT [115, 119]. Néanmoins, indépendamment de leur interaction directe, OGT et BAP1 collaborent dans certains contextes cellulaires où, comme indiqué précédemment, l'O-GlcNAcylation de PGC-1α par exemple, favorise le recrutement du complexe BAP1 qui déubiquitine PGC-1α et stabilise ses niveaux protéiques en le protégeant contre la dégradation par le protéasome [72].

Toutefois, la présence stœchiométrique aussi importante d'OGT dans le complexe BAP1 suggère qu'il remplit une fonction critique et qu'il est possiblement essentiel à la spécificité et à la régulation de la fonction déubiquitinase et suppressive de tumeurs de ce complexe [110].

1.1.5.4 Association d'OGT au régulateur épigénétique TET2

La contribution importante d'OGT dans la régulation épigénétique a surtout été soulignée par la découverte de son interaction avec la déméthylase d'ADN TET2 [120]. La méthylation de l'ADN par les ADN méthyltransférases est la modification épigénétique la plus étudiée et probablement la plus importante du génome. La méthylation de l'ADN est cruciale non seulement dans la répression de la transcription, mais aussi dans le maintien de l'empreinte épigénétique et l'identité cellulaire [121]. Néanmoins, les joueurs clés responsables de la suppression de cette marque épigénétique n'avaient pas été identifiés jusqu'à tout récemment. En effet, la dernière décennie a mené à l'identification des premières déméthylases de l'ADN qui sont maintenant décrites comme faisant partie de la famille des protéines *Ten Eleven Translocation* (TET). Plus précisément, les trois membres de cette famille, TET1, TET2 et TET3, sont des méthylcytosine déoxygénases qui catalysent principalement l'hydroxylation du 5-méthylcytosine en 5-hydroxyméthylcytosine [122]. Il est maintenant établit que ces enzymes sont des régulateurs épigénétiques cruciaux et semblent prometteurs quant à leur utilisation comme marqueurs cliniques pour des fins diagnostiques ou pronostiques dans les cas de cancers où l'on observe des défauts dans les patrons de méthylation de l'ADN [123, 124]. Le rôle crucial du maintien de l'intégrité cellulaire des TETs a, entre autres, été démontré par la quantité impressionnante de mutations de TET2 identifiées dans les cellules hématopoïétiques de diverses leucémies myéloïdes [125, 126]. D'autre part, TET2 s'ajoute à la longue liste de substrats ciblés par l'O-GlcNAcylation et renforce l'idée que des défauts dans la fonction d'OGT puissent engendrer des dérégulations profondes de l'homéostasie cellulaire menant à des conséquences physiologiques considérables [127]. Cependant, les mécanismes découlant de cette interaction et l'implication au niveau de l'épigénome et de la transcription son encore incompris. Il a été proposé que l'O-GlcNAcylation de TET2 permette de réguler ses niveaux de phosphorylation [83]. D'autre part, TET2 serait nécessaire au recrutement d'OGT à la chromatine, ce qui permettrait de réguler la transcription via la régulation de certaines marques d'histones [127, 128]. Ce recrutement résulterait aussi en l'O-GlcNAcylation des histones corps du nucléosome, suggérant ainsi que l'O-GlcNAc serait une nouvelle marque épigénétique [125, 126].

1.1.5.5 O-GlcNAcylation des Histones

Les modifications post-traductionnelles des histones sont connues pour jouer un rôle critique dans les processus biologiques dépendants de l'ADN incluant la transcription, la réplication et la réparation de l'ADN. Entre autre, la queue N-terminale des histones émanant du corps du nucléosome, soit les histones H2A, H2B, H3 et H4, sont sujettes à un nombre important de combinaisons de marques activatrices ou répressives agissant de manière concertée et qui sont associées à la régulation de la structure ainsi qu'à la fonction de la chromatine. Certaines marques sont présentes de manière constitutive et sont tissus spécifiques, telles que la méthylation, et participent à l'élaboration de l'identité cellulaire et de l'empreinte épigénétique. D'autres marques sont hautement dynamiques et régulées par la coordination et l'association de complexes protéiques pouvant ou non exécuter la catalyse directe de ces modifications telles que l'acétylation, l'ubiquitination, la phosphorylation et encore une fois la méthylation. Ces MPTs contribuent au remodelage, au recrutement, à l'activation/répression de la transcription et à d'autres évènements impliquant le remaniement de la chromatine nécessaire pour orchestrer une réponse spécifique associée à un évènement cellulaire donné. Ce soit disant «code d'histones» est à la base de tous les processus cellulaires eucaryotes et tout un domaine de recherche est dévoué à l'étude fonctionnelle de ces marques [129]. Très récemment, des études ont proposé que plusieurs résidus des histones humaines soient O-GlcNAcylés *in vivo* ajoutant ainsi l'O-GlcNAcylation à la longue liste de marques épigénétiques (Tableau I.I) [130-132].

Toutefois, la majorité des sites rapportés par analyse de spectrométrie de masse ne sont pas concordants entre les différentes études. D'autre part, certains sites ont été étudiés de manière fonctionnelle et les études suggèrent différents rôles de régulation. Entre autres, l'O-GlcNAcylation de la Ser112 de H2B a été rapportée comme étant importante pour le dépôt subséquent de l'ubiquitine sur la lysine 120 de H2B pour induire l'activation de la transcription [133]. Les résidus Ser91 et Ser123 de H2B ont aussi été identifiés [134]. Les résidus Ser10 et Thr32 de H3 seraient aussi modifiés par O-GlcNAcylation et ont été suggérés dans la régulation de l'entrée en mitose en empêchant la phosphorylation des résidus Ser10, Ser28 et Thr32 [135]. L'O-GlcNAcylation de la Thr101 sur la queue C-terminale de H2A serait possiblement impliquée dans l'ancrage du tétramère H3H4 au nucléosome qui serait

aussi O-GlcNAcylé sur la Ser36 de H2B et la Ser47 de H4 [136]. Cependant cette même étude a aussi détecté de l'O-GlcNAcylation sur H3 à l'aide d'anticorps spécifiques contre l'O-GlcNAc, mais n'ont pas pu déterminer de sites spécifiques par analyse au spectromètre de masse.

Tableau I.I. Liste et références des sites d'O-GlcNAcylation identifiés sur les histones corps du nucléosomes. Tiré avec autorisation de Gambetta MC et al (2015) [57].

O-GlcNAc site		Ref
H2B	Ser 36	Sakabe et al., 2010
	Thr 52	Hahne et al., 2012
	Ser 55	Hahne et al., 2012
	Ser 56	Hahne et al., 2012
	Ser 64	Schouppe et al., 2011; Hahne et al., 2012
	Ser 91	Fujiki et al., 2011
	Ser 112	Fujiki et al., 2011
	Ser 123	Fujiki et al., 2011
H2A	Thr 101	Sakabe et al., 2010; Fujiki et al., 2011
H3	Ser 10	Zhang et al., 2011
	Thr 32	Fong et al., 2012
H3.3	Thr 80	Schouppe et al., 2011
H4	Ser 47	Sakabe et al., 2010

L'identification de l'O-GlcNAcylation sur les histones repose principalement sur des techniques de détection par spectrométrie de masse, par anticorps contre l'O-GlcNAc et par analyse mutationnelle. Dans le but de caractériser le rôle fonctionnel d'OGT dans la régulation épigénétique, notre groupe s'est intéressé à confirmer ce concept d'O-GlcNAcylation des histones. De manière surprenante, nos efforts pour valider ces observations ont mené à une conclusion différente, soit que les histones ne sont pas des substrats d'OGT. En fait, les travaux de recherche effectués par notre groupe soulèvent un doute raisonnable quant à l'occurrence de cette modification sur les histones et suggèrent plutôt une détection artéfactuelle provenant des anticorps contre l'O-GlcNAc ou contre des sites spécifiques d'histones menant à une interprétation biaisée de la fonction de l'O-GlcNAcylation dans ce contexte. Le chapitre 2 de ce mémoire présente donc l'ensemble des travaux qui ont mené à la remise en question de ce paradigme.

1.2 Facteur de transcription Forkhead box K1 (FOXK1)

FOXK1 aussi connu sous le nom de MNF (*myocyte nuclear factor*), est un facteur de transcription de la famille *Forkhead box* exprimé de manière ubiquitaire et codé par le chromosome 7. FOXK1 est majoritairement connu et étudié pour son rôle central dans la régulation de la régénération du muscle squelettique. Jusqu'à très récemment, la majorité des travaux sur FOXK1 portait principalement sur sa fonction dans la différenciation myoblastique et très peu d'études avaient démontré son implication dans d'autres processus biologiques. Depuis les 3 dernières années, FOXK1 émerge comme un régulateur transcriptionnel atypique qui ne se limite pas à une régulation transcriptionnelle dépendante de sa liaison à l'ADN. En effet, il est maintenant clair que FOXK1 est impliqué dans la régulation de l'autophagie, de la signalisation Wnt/β-caténine, de la transcription via le complexe BAP1 et de la réponse anti-virale [114, 137-139]. Notre groupe s'intéresse particulièrement à FOXK1 dans le contexte de son interaction avec le complexe BAP1, ce qui nous a menés à identifier FOXK1 comme un nouveau substrat d'OGT. De ce fait, notre étude sur le rôle de l'O-GlcNAcylation dans la régulation transcriptionnel s'est étendue à la détermination de la fonction de la régulation de FOXK1 par l'O-GlcNAcylation.

Cette section se consacre donc sur la revue des principales découvertes au sujet de FOXK1 en lien avec son rôle prépondérant dans la régulation de la myogenèse et dans la régulation d'autres voies de signalisation cellulaire métabolique.

1.2.1 Famille *Forkhead Box*

Les protéines *Forkhead box* (FOX) font partie d'une famille de facteurs de transcription comprenant 19 sous-familles dont les membres sont classés de FOXA à FOXR. Ces facteurs sont impliqués dans la régulation de l'expression génique et influencent une multitude de processus biologiques incluant l'embryogenèse, la progression du cycle cellulaire, la prolifération, la différenciation, la morphogenèse et la réparation de l'ADN [140]. Par exemple, certains membres des sous-familles FOXA, FOXD, FOXE et FOXO sont des facteurs pionniers essentiels au développement embryonnaire et à la régulation de l'identité cellulaire par leur capacité à lier la chromatine condensée et à permettre le recrutement de complexes régulateurs secondaires nécessaires à l'activation de la transcription de gènes

réprimés [141]. FOXM1 est un oncogène impliqué dans la régulation des phases G1/S et G2/M du cycle cellulaire et connu pour stimuler la transcription de la cycline B1 [142, 143]. FOXK1 est un facteur crucial dans le maintien de l'identité des cellules progénitrices myogéniques. Enfin, les membres de la sous-famille FOXP sont impliqués dans l'homéostasie du système immunitaire [113, 140, 141, 144]. Par ailleurs, les protéines FOX sont caractérisées par la présence du domaine de liaison à l'ADN *forkhead* (FH) (ou *winged-helix domain)* qui est composé de trois hélices-α flanquées par deux feuillets-β. Cette organisation structurale est hautement conservée entre les sous-familles FOX et permet de lier la séquence consensus de base (A/C)AA(C/T) [144]. Ainsi, puisque les protéines FOX reconnaissent la même séquence de base, la spécificité de chaque sous-famille est dictée par la reconnaissance spécifique des séquences d'ADN encadrant cette séquence minimale et par leur association à d'autres facteurs de transcription. En dépit de leur domaine FH très conservé, la différence dans leurs régulations et fonctions réside dans leurs régions non conservées [144].

Les protéines FOX sont soumises à de nombreux processus de régulation cellulaire principalement par l'entremise de MPTs. La phosphorylation, l'ubiquitination, l'acétylation et récemment l'O-GlcNAcylation ont été impliquées dans leur activation, répression, dégradation et même dans leur traffic intracellulaire [144]. Par exemple, la localisation cellulaire et la stabilité de certains FOX sont régulées par le système classique de dégradation par le protéasome via la polyubiquitination de type K48 conduisant à leur translocation et dégradation dans le cytoplasme [145]. De plus, la localisation cellulaire d'autres protéines FOX est régulée par des évènements dynamiques et très complexes de phosphorylation et d'acétylation [144]. Selon la nature de la protéine FOX ciblée, la phosphorylation et l'acétylation peuvent induire des changements servant à affecter leur association avec des protéines de transport ainsi qu'avec certaines chaperonnes et par conséquent permettent un contrôle strict de leur import et export nucléaire [144]. En raison de l'étendue des fonctions des membres de la famille de protéines FOX, plusieurs études ont montré que des défauts dans la régulation de ces MPTs peuvent entraîner de graves conséquences transcriptionnelles pouvant contribuer au développement et à la progression de cancers [146, 147].

1.2.1.1 Sous-familles K

Chez l'humain, FOXK1 et FOXK2 sont les deux seules protéines de la sous-famille K. La particularité de ces facteurs de transcription provient du fait qu'ils sont les deux seules protéines FOX qui contiennent à la fois, le domaine FH et un domaine FHA (*Forkhead-associated domain)*. Le domaine FHA est un module de liaison au phosphate strictement spécifique pour les résidus phospho-thréonine (pT) et est donc engagé dans des interactions de type protéine-protéine [148]. Ce domaine protéique est largement répandu chez les eucaryotes et est retrouvé dans la séquence de groupes de protéines ayant des fonctions régulatrices incluant des kinases, des phosphatases, des facteurs de transcription, des protéines *ring-finger* etc [149]. La spécificité de liaison des protéines contenant un FHA est assurée par la règle pT+3 où la propriété de l'acide aminé à la position +3 de la thréonine phosphorylée est importante pour la liaison et la spécificité du FHA [148]. Par exemple, la protéine de réparation de l'ADN Rad53 contient deux domaines FHA chacun ayant une préférence pour un résidu pT+3 différent soit un résidu acide aspartique et un résidu isoleucine [150]. Toutefois, les éléments biochimiques et physicochimiques qui déterminent la préférence des FHA pours des résidus pT+3 différents sont encore incompris. Ainsi, l'acquisition du domaine FHA chez la sous-famille FOXK leur confère un avantage mécanistique considérable ne limitant pas leur spécificité à seulement une séquence consensus d'ADN, mais en permettant un mode de régulation plus complexe en collaboration avec la phosphorylation.

Une autre particularité de la sous-famille K est leur association commune au complexe suppresseur de tumeur BAP1. Bien que FOXK1 et FOXK2 aient des domaines semblables et qu'ils soient souvent impliqués dans des voies de régulation communes, leur homologie de séquence n'est que d'environ 50% suggérant qu'ils puissent avoir des fonctions non redondantes (Figure 10). Ceci est concordant avec le fait que FOXK1 peut interagir avec Sin3. En général, FOXK1 est décrit comme un répresseur transcriptionnel alors que FOXK2 est plutôt décrit comme un activateur. Cependant, l'association de FOXK2 au complexe BAP1 a récemment été montrée comme un processus répressif de la transcription [138]. Leur rôle répresseur ou activateur semble donc être dicté par les complexes protéiques auxquels ils s'associent (Figure 11). De plus, l'identification de leur liaison à BAP1 via la même phospho-sérine de BAP1 indique qu'ils forment des complexes mutuellement exclusifs. Ceci est aussi

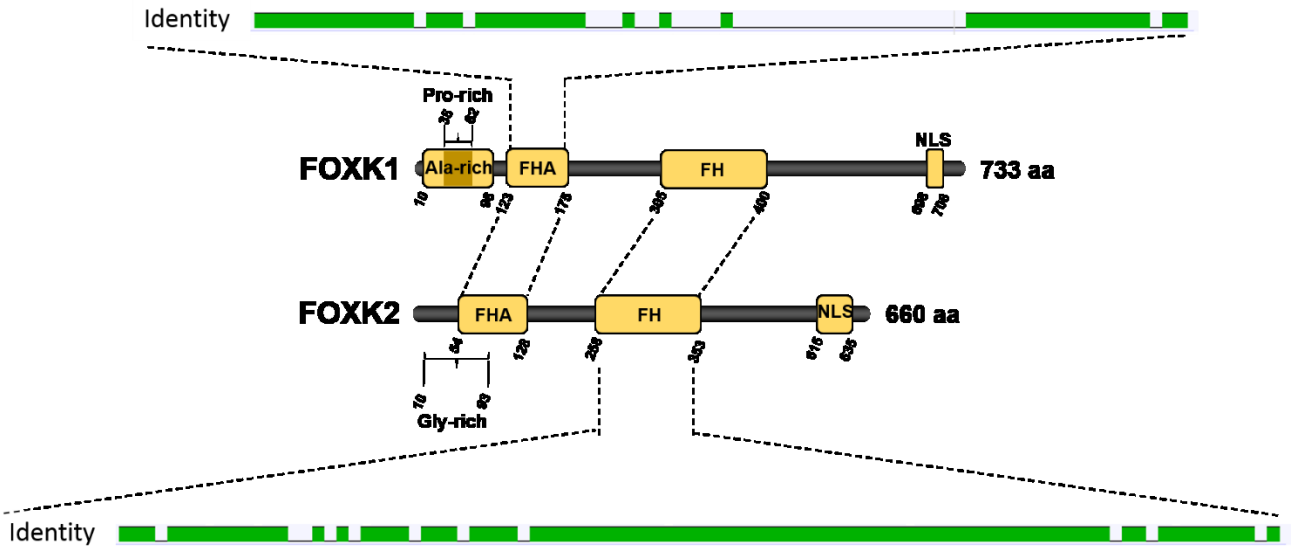

Figure 10. Représentation schématique des domaines de FOXK1 et FOXK2 humains. La séquence de 733 acides aminés (aa) de FOXK1 est composée d'une région riche en résidus alanine (Ala-rich) et proline (Pro-rich) en N-Terminale, des domaines Forkhead (FH), Forkhead-associated (FHA) et d'un signal de localisation nucléaire (NLS). La séquence de 660 aa de FOXK2 est composée d'une région riche en résidus glycine (Gly-rich) en N-Terminale, des domaines Forkhead (FH), Forkhead-associated (FHA) et d'un signal de localisation nucléaire (NLS). Les résidus définissant les domaines sont indiqués. L'homologie de séquence des domaines FH et FHA a été réalisé à l'aide du logiciel Geneius (Global alignment with free end gaps, matrix Blosum45).

vrai pour leur interaction avec la protéine d'échaffaudage DVL impliquée dans la voie Wnt/β-caténine. Ceci laisse croire que ces facteurs peuvent intégrer la phosphorylation et la fonction modificatrice de la chromatine du complexe BAP1 en réponse à une transduction du signal afin de réguler l'expression génique en réponse à des stimuli spécifiques.

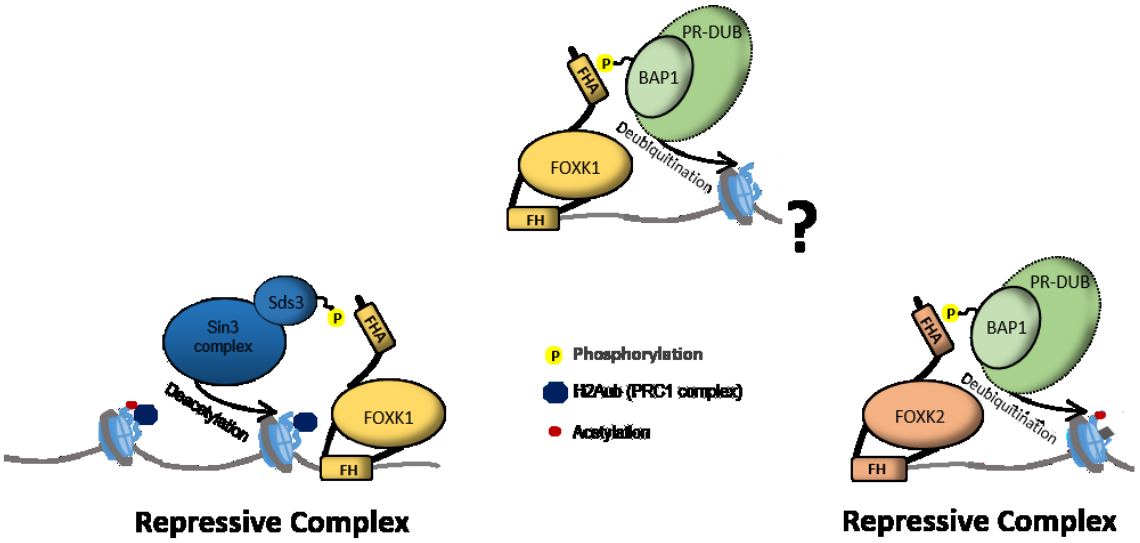

Figure 11. Exemples de régulation transcriptionnelle répressive par l'association de FOXK1 et FOXK2 avec certains complexes. Bien que l'action répressive de FOXK2 par son association avec le complexe BAP1 soit connue, l'action de FOXK1 quant à elle n'a pas été déterminée.

1.2.2 Régulation de FOXK1

Des travaux récents ont identifié un élément de liaison Sox (SBE) en amont du promoteur de FOXK1. Une analyse plus approfondie a permis d'identifier le régulateur transcriptionnel SOX15 (*SRY-related HMG-box protein*) comme un activateur majeur du gène FOXK1 via la liaison à ce motif SBE [151]. Le rôle de SOX15 quant à la régulation de FOXK1 est concordant avec le fait que SOX15 est aussi exprimé dans les cellules satellites du muscle squelettique et que sa déplétion provoque aussi des défauts de régénération musculaire en plus d'un arrêt des cellules progénitrices en phase G0/G1 [152]. De plus, des études ont confirmé l'implication de Fhl3 (*Four and a half LIM domain protein 3*) en tant que co-régulateur de la transcription de FOXK1 via son interaction avec SOX15 et ont démontré que ce mécanisme d'activation est critique pour la régulation positive de FOXK1 [151]. Toutefois, la déplétion de Fhl3 n'est pas associée à des défauts phénotypiques similaires à ceux observés suite à la déplétion de SOX15 ou de FOXK1. Puisque les protéines LIM sont exprimées dans une large gamme de tissus, il a été suggéré et plus tard confirmé que Fhl2 (*Four and a half LIM domain protein* 2) est un co-activateur synergique de FOXK1 bien qu'il n'interagisse pas

avec SOX15 [151]. Ceci concorde avec une autre étude qui a conduit à l'identification de Fhl2 comme partenaire d'interaction de FOXK1 [153]. Étonnamment, l'expression de FOXK1 est aussi contrôlée par son paralogue FOXK2 qui induit sa répression transcriptionnelle [114]. Enfin, ces études mettent en évidence une régulation complexe du gène de FOXK1 impliquant de multiples protéines engagées dans diverses voies de signalisation. Cependant, il reste encore beaucoup de facteurs à identifier et les mécanismes de régulation autour de l'activité et de l'expression de FOXK1 sont encore incompris.

1.2.2 Maintien des cellules progénitrices myoblastiques (MPC)

Les souris Foxk1$^{-/-}$ montrent des défauts graves et un retard de la régénération musculaire où l'on note une importante diminution de la population de cellules progénitrices myoblastiques (MPC) en plus d'une dérégulation importante du cycle cellulaire [154]. En réponse à une blessure du muscle, les cellules satellites quiescentes entourant les myofibres endommagées reprennent le cycle cellulaire, prolifèrent et entreprennent le programme de différenciation pour fusionner et former de nouveaux myotubes multi-nucléaires [155]. Dans le tissu musculaire, FOXK1 est limité à la population de MPC et son expression est réduite dans les myotubes différenciés, soulignant son importance dans le maintien de la population MPC [153, 154].

1.2.2.1 Répression de l'activité transcriptionnelle de FOXO4

Les études sur les souris Fhl2$^{-/-}$ ont démontré un phénotype similaire à celui observé pour les souris Foxk1$^{-/-}$ et Sox15$^{-/-}$, soit des défauts de régénération musculaire et l'arrêt du cycle cellulaire en phase G0/G1 [153]. Ceci peut être expliqué par le fait que l'interaction entre FOXK1 et Fhl2 médie la répression de l'activité transcriptionnelle de FOXO4 [153]. FOXO4 est une protéine de la famille *Forkhead* impliquée entre autres dans l'activation de la transcription de l'inhibiteur du cycle cellulaire p21 [113]. En plus d'interagir avec Fhl2, FOXK1 interagit avec le domaine FH de FOXO4 par sa région contenant les domaines FH et FHA [113]. La séquence minimale d'interaction n'a cependant pas été déterminée. Étonnamment, en contraste avec plusieurs autres partenaires d'interaction de FOXK1 identifiés jusqu'à maintenant, FOXK1 interagit avec Fhl2 via sa région C-terminale distale aux domaines FH et FHA. Ce réseau d'interactions démontre que la régulation médiée par

FOXK1 peut impliquer des mécanismes indépendants de son activité transcriptionnelle. En resumé, la capacité de répression de FOXO4 renforce l'idée que FOXK1 est impliqué dans le maintien de l'état prolifératif des MPC par la régulation de facteurs qui contrôlent le cycle cellulaire.

1.2.2.2 Répression des gènes cibles de Mef2

Basée sur l'observation que la surexpression de FOXK1 provoque aussi des défauts de différenciation du muscle squelettique, des analyses du transcriptôme ont identifié MEF2 comme une cible potentielle de FOXK1. En effet, tout comme FOXK1 a un effet sur la prolifération cellulaire par l'inhibition de FOXO4, des travaux récents ont montré que FOXK1 peut retarder l'activation du programme de différenciation grâce à l'inhibition du facteur de transcription MEF2. En effet, MEF2 est un régulateur important de la myogenèse par son action combinatoire avec le facteur de transcription spécifique de la lignée myogénique MYOD [113, 156, 157]. De manière importante, la déplétion du facteur de transcription MyoD et la surexpression du facteur de régulation myogénique précoce Myf5 observées dans les cellules myogéniques $Sox15^{-/-}$ pourraient être une conséquence indirecte de la régulation négative de FOXK1. En effet, ce mécanisme de répression est médié par une interaction directe entre MEF2 et FOXK1 via le domaine MADS (*Mothers against decapentaplegic)* de MEF2 et une région comprenant les domaines FH et FHA de FOXK1. Étant donné que le domaine MADS est un domaine de liaison à l'ADN en plus d'un domaine impliqué dans des interactions protéiques, la liaison de FOXK1 résulte en une inhibition de la capacité transcriptionnelle de MEF2. Ces données concordent avec le modèle selon lequel FOXK1 régule la population MPC en agissant simultanément sur différentes cascades de signalisation qui convergent afin de retenir l'état prolifération des MPC [113].

1.2.2.3 Répression des gènes dépendant de SRF

Des études antérieures chez *Saccharomyces cerevisiae* ont identifié le facteur de transcription forkhead Fkh2p et le facteur de transcription MADS-box MCM1p comme partenaires d'interaction dans divers processus cellulaires montrant ainsi l'importance de la formation de complexes multi-protéines ainsi que l'association des facteurs de transcription dans la régulation de l'expression génique [158]. Ces études ont conduit à l'extrapolation d'un mécanisme d'interaction similaire chez les mammifères, puisque la plupart des

mécanismes de base qui se produisent dans la levure sont conservés. De ce fait, FOXK1 a été identifié comme un partenaire d'interaction du facteur de transcription à domaine MAD-box SRF (Serum response factor). SRF est une protéine nucléaire qui régule la prolifération et la différenciation par sa liaison à un motif SRE (*Serum Response Element*) trouvé dans le promoteur de plusieurs gènes tel que FOS [159]. La protéine FOS de structure leucine-zipper a la capacité d'hétérodimériser avec JUN formant ainsi le facteur de transcription AP1 largement impliqué dans la régulation génique. AP1 affecte la prolifération et la différenciation. Il est donc possible de spéculer que FOXK1 agit en amont ou en collaboration avec ce régulateur. De plus, l'interaction FOXK1-SRF réprime la transcription de gènes dépendants de SRF [160]. Cette répression est la conséquence de l'interaction entre le domaine FHA de FOXK1 et le domaine de liaison à l'ADN de SRF. Par conséquent, SRF ne peut plus lier les motifs SRE de ses gènes cibles ce qui réprime son activité transcriptionnelle. Il est à noter que des expériences de co-immunoprécipitation ont déterminé que FOXK1 n'a que très peu d'affinité pour SRF. Ainsi, l'interaction est rare lors d'une atténuation de la prolifération cellulaire, tandis qu'elle se produit plus fréquemment suite à une augmentation de la prolifération afin de réguler ce dernier. FOXK1 régule donc l'activité de SRF via une boucle de rétroaction négative. De plus, SRF est fortement phosphorylé [161, 162]. Il serait donc intéressant de déterminer quel(s) site(s) sont responsables de l'interaction entre FOXK1 et SRF. Il serait ensuite possible d'identifier les kinases responsables de cette phosphorylation et ainsi identifier la cascade de signalisation menant à la régulation de SRF via FOXK1. Toutefois, il est possible que cette interaction soit médiée par un mécanisme indépendant d'une dynamique de kinase/phospho-résidu de SRF comme c'est le cas pour l'interaction entre FOXK1 et Fhl2.

Par ailleurs, les gènes α-actine de muscles lisses et PPGB (*protective protein de beta-galactosidase*) sont indirectement régulés par FOXK1 via son interaction avec SRF. En effet, l'inhibition de l'expression de FOXK1 et/ou la surexpression de SRF engendre une augmentation de l'expression de ces deux gènes. Aussi, des analyses d'interaction ont pu élucider deux mécanismes par lesquels FOXK1 agit en tant que répresseur transcriptionnel. Le premier est un mécanisme indépendant de sa liaison à l'ADN où FOXK1 peut lier SRF directement et inhiber sa fonction. Le deuxième en est un dépendant de sa liaison à l'ADN où

FOXK1 peut être recruté à la chromatine via SRF et inhiber la transcription. Ces résultats suggèrent que FOXK1 peut réguler des processus cellulaires à différents niveaux d'une cascade de signalisation et que les modifications post-traductionnelles sont critiques pour la régulation de sa fonction.

1.2.2.4 Association avec le complexe SIN3 et SDS3

L'importance de la contribution de complexes modificateurs d'histones pour la fonction de FOXK1 est démontrée par son association avec le complexe SIN3 (*SWI-independent-3*) [163]. SIN3 est un complexe contenant les histones déacétylases 1 et 2 (HDAC1 et HDAC2) capable de réprimer la transcription en provoquant le remodelage de la chromatine. Ce complexe est composé d'un des trois isoformes de la protéine d'échafaudage Sin3, soit Sin3a, Sin3b ou Sin3b(293), des déacétylases HDAC1 et HDAC2, des protéines de liaison au rétinoblastome Rbbp4 et Rbbp7 et des protéines associées à Sin3, SAP18 et SAP30 et Sds3 *(suppressor of defective silencing 3)*. L'interaction entre FOXK1 et Sin3 est médiée par la région N-terminale de FOXK1 (1-40) et le domaine PAH2 présent dans les trois isoformes de Sin3. Par ailleurs, bien que les trois isoformes puissent lier FOXK1, elles n'ont pas toutes le même effet sur la transcription. En effet, Sin3a et Sin3b inhibent p21 et p27 tandis que Sin3b peut aussi inhiber p57, ce qui suggère que leur spécificité pourrait être déterminée via des domaines autres que ceux qui interagissent avec FOXK1. Il existe aussi une deuxième interaction entre FOXK1 et le complexe SIN3. En effet, le domaine FHA de FOXK1 lie le résidu phosphorylé Thr49 de Sds3. De ce fait, une même molécule de FOXK1 peut lier à la fois la protéine d'échafaudage Sin3 ainsi que Sds3 à l'aide de son domaine N-terminal et de son FHA et encore avoir la capacité de lier l'ADN via son domaine FH. De plus, il a été montré que Sin3 inhibe l'expression de FOXK1. Il existe donc une boucle de rétroaction négative entre Sin3 et FOXK1 qui peut servir à maintenir un certain niveau de FOXK1 en réponse à un contexte cellulaire particulier. Aussi, des études ont démontré l'implication de Sin3 dans plusieurs complexes répressifs et indiquent qu'il existe peut-être une cascade de signalisation ayant comme but d'inhiber l'expression de FOXK1 pendant la différenciation [164]. Plus de données expérimentales sont nécessaires afin de comprendre la complexité de la régulation de FOXK1 et son rôle dans des boucles de régulation négative.

1.2.3 Réponse à l'autophagie

Le tissu musculaire est très dépendant du glucose et une restriction peut engendrer des défauts de différenciation myoblastique [165]. L'implication de FOXK1 dans la maintenance de l'état prolifératif des myoblastes suggère que ce dernier soit lié à la régulation du métabolisme [113]. Une analyse de ChIPseq couplée à une analyse d'ontologie de gènes a démontré que FOXK1 régule de manière transcriptionnelle de nombreux gènes liés au métabolisme. Ceci n'est pas surprenant compte tenu de son interaction avec le complexe BAP1 qui est lui-même impliqué dans la gluconéogenèse par l'entremise d'OGT [72]. Cependant, il se trouve que Foxk1 murin est aussi ciblé par la phosphorylation dépendante de la voie mTOR et que ses sites de phosphorylation (Ser225, Ser229, Thr231, Ser427 et Ser431) sont critiques à sa localisation nucléaire [114]. Cette translocation au noyau mène au recrutement du complexe Sin3-HDAC aux gènes d'autophagies via FOXK1 résultant en la répression de ces derniers par déacétylation [114]. De ce fait, lors d'une privation de glucose qui cause l'inhibition du complexe mTOR, FOXK1 ne peut être phosphorylé et demeure cytoplasmique, ce qui permet une activation des gènes de la réponse à l'autophagie. Cette privation de glucose engendre aussi la phosphorylation de FOXK1 nucléaire par d'autres kinases qui n'ont pas été identifiées, ce qui cause sa translocation au cytoplasme. En d'autres termes, le transport nucléo-cytoplasmique de FOXK1 est essentiel à la réponse au stress métabolique et indique que la phosphorylation joue un rôle prédominant dans cette régulation.

1.2.4 Signalisation Wnt/β-caténine

La signalisation canonique de Wnt est une voie de régulation complexe principalement impliquée dans des processus à potentiel oncogénique qui contribuent aux mécanismes de développement et de progression de nombreuses tumeurs ainsi qu'à la résistance de plusieurs cancers aux traitements chimio-thérapeutiques [166]. Récemment, FOXK1 et FOXK2 ont été identifiés comme facteurs clés requis dans la régulation de la voie canonique Wnt dépendante de β-caténine en régulant la translocation nucléaire de la protéine d'échaffaudage DVL (*Dishevelled*) [137]. En fait, FOXK1 et FOXK2 provoquent l'évènement initial qui contribue à l'activation de la voie Wnt/β-caténine qui nécessite la translocation nucléaire dépendante de la phosphorylation des protéines DVL [137]. Encore une fois, cette interaction entre FOXKs et

DVL sollicite la contribution du domaine FHA et intègre un mécanisme de régulation indépendant de l'activité transcriptionnelle de FOXK1 et FOXK2. Par ailleurs, cette étude a permis l'identification de deux nouvelles caractéristiques de FOXK1 et FOXK2 qui était jusqu'à maintenant inconnues, soit 1) leurs potentiels de régulation via le cytoplasme par interaction directe avec des protéines cytoplasmiques et 2) la présence d'un motif hydrophobe (Leu137-phe145-phe154) dans une région en aval de la séquence FHA qui est conservée entre FOXK1 et FOXK2 et qui peut contribuer aux interactions protéine-protéine.

En résumé, toutes ces études ont mené à la découverte de nouveaux mécanismes de régulation de l'expression et de la fonction de FOXK1 indépendants de son rôle en tant que régulateur myogénique et indiquent que ce dernier est en fait un régulateur essentiel à beaucoup d'autres voies de signalisation cellulaire. De plus, FOXK1 démontre un autre niveau de complexité de régulation transcriptionnelle, car il agit de façon indépendante de sa liaison à l'ADN. Son association avec de nombreux complexes de fonctions diverses indique aussi que FOXK1 peut agir à titre d'oncogène et de suppresseur de tumeur spécifique en réponse à un stress cellulaire précis. D'autres études sont nécessaires à l'identification de nouvelles fonctions et implications de FOXK1 afin d'établir sa contribution dans l'oncogenèse et son potentiel comme cible thérapeutique.

1.3 Hypothèse et Objectifs de recherche

OGT est une enzyme multifonctionnelle qui a la capacité de médier une réponse précise et spécifique malgré le fait qu'aucune séquence consensus cible n'ait été identifiée. La complexité de son réseau de régulation propose un défi de taille quant à l'élaboration d'inhibiteurs spécifiques à une fonction ciblée d'OGT et demande une compréhension sans équivoque de son implication cellulaire. Cependant, il est notable qu'OGT régule principalement des complexes impliqués dans le contrôle de l'expression génique. De ce fait, l'O-GlcNAcylation doit avoir un impact essentiel sur la régulation transcriptionnelle et épigénétique en régulant le remodelage de la chromatine. La présence d'OGT dans le complexe suppresseur de tumeur BAP1 suggère qu'elle contribue a un mécanisme de régulation transcriptionelle et épigénétique important à investiguer incluant 1)

la possibilité qu'il existe un *crosstalk* entre l'O-GlcNAcylation et la déubiquitination de l'histone H2A en lien avec la O-GlcNAcylation des histones qui a récemment été rapportée et 2) l'implication d'OGT dans la régulation de la fonction suppressive de tumeur du complexe BAP1 par O-GlcNAcylation des composantes corps du complexe et/ou par O-GlcNAcylation de joueurs clés intermédiaires qui sont recutés aux gènes cibles de BAP1 et qui collaborent avec ce dernier. De ce fait, en fonction des connaissances actuelles sur OGT et sur le complexe BAP1 et en fonction de notre intérêt quant à la compréhension des mécanismes de régulation transcriptionnelle et épigénétique modulés par le complexe BAP1, nous avons postulé l'hypothèse que l'O-GlcNAcylation des histones par OGT coordonne la déubiquitination de l'histone H2A médiée par le complexe BAP1. De plus, sachant que certaines composantes centrales du complexe BAP1 sont sujettes à l'O-GlcNAcylation et que l'absence d'OGT n'affecte pas l'activité déubiquitinase de BAP1, nous croyons qu'OGT est importante quant à la régulation fonctionnelle de ce complexe dans un contexte cellulaire donné. Nos objectifs généraux de recherche étaient donc principalement axés sur :

1) La validation du rôle d'OGT dans la régulation épigénétique en lien avec le concept d'O-GlcNAcylation des histones (Chapitre 2),
2) La caractérisation biochimique et fonctionnelle des facteurs de transcription FOXK1 et FOXK2 dans le rôle suppresseur de tumeur du complexe BAP1. (Chapitre 3)

Afin de répondre au premier objectif, nous nous sommes intéressé à :

1.1 Reproduire et revisiter les techniques employées pour identifier l'O-GlcNAcylation des histones dans le but de déterminer le lien entre l'O-GlcNAcylation et la déubiquitination des histones.

1.2 Investiguer la spécificité des anticorps actuels générés pour détecter l'O-GlcNAcylation globale ou spécifique à la sérine 112 de l'histone H2B.

1.3 Indentifier des contextes cellulaires pouvant mener à l'O-GlcNAcylation des histones.

Afin de répondre au second objectif, nous nous sommes, entre autre, intéressé à :

2.1 Comprendre la dynamique des interactions au sein du complexe BAP1 en présence ou en absence des FOXKs.

2.2 Identifier des modifications post-traductionelles pouvant réguler la fonction de FOXK1 et FOXK2.

2.3 Investiguer le rôle fonctionnel de l'O-GlcNAcylation de FOXK1 dans la fonction du complexe BAP1.

CHAPITRE 2

2. Article 1

Statut de l'article: Publié

Référence: Gagnon J, Daou S, Zamorano N, Iannantuono NV, Hammond-Martel I, Mashtalir N, Bonneil E, Wurtele H, Thibault P, Affar el B. Undetectable histone O-GlcNAcylation in mammalian cells. Epigenetics. 2015;10(8):677-91. doi: 10.1080/15592294.2015.1060387. PubMed PMID: 26075789; PubMed Central PMCID: PMC4622518.

Contribution des co-auteurs:

Pour cet article intitulé *«Undetectable Histone O-GlcNAcylation in Mammalian Cells»*, en tant que co-première auteure et donc au même titre que Salima Daou, j'ai participé à la conception des expériences, j'ai exécuté et analysé la majorité des expériences, supervisé les co-auteurs et discuté des expériences complémentaires ainsi que des questions devant être abordées. J'ai contribué de manière significative à la préparation des figures, à l'écriture et à la correction du manuscrit durant les étapes de soumission, de révision et de re-soumission et j'ai participé à la lettre de réponses aux évaluateurs. Entre autre, j'ai réalisé les travaux présentés aux figures 14 a) b), 16 a) c), 17, 18 a), 2S5 et participé pour les travaux présentés aux figures 14 c), 2S4 et 2S6, 2S7 et 2S8. Salima Daou a réalisé les travaux présentés aux figures 12, 13, 15, 16 b), 2S1, 2S2, 2S3, 2S4, 2S6, 2S7 et 2S8 et a participé pour les travaux présentés aux figures 18 b) c) et d). Natalia Zamorano a réalisé les travaux présentés aux figures 14 c), 15 b) 18 b) c) d) et 2S4. Nicholas VG Iannantuono a participé aux travaux des figures 15 a) et 16 b). Ian Hammond-Martel réalisé les travaux présentés aux figures 12, 13, 2S1, 2S3 et a purifié les histones de levure utilisé pour la figure 2S4. Nazar Masthalir a contribué aux travaux en lien avec les figures présentés aux figures 12, 13, 2S1 et 2S3. Éric Bonneil a réalisé les travaux et l'analyse des figures de spectrométrie de masse présentés aux figures 2S6, 2S7 et 2S8. Tous les auteurs ont participé à l'interprétation des résultats et a éditer et révisé le manuscrit.

Undetectable Histone O-GlcNAcylation in Mammalian Cells

Jessica Gagnon[1,†], Salima Daou[1,†], Natalia Zamorano[1], Nicholas VG Iannantuono[1], Ian Hammond-Martel[1], Nazar Mashtalir[1], Eric Bonneil[2], Hugo Wurtele[1], Pierre Thibault[2] and El Bachir Affar[1,#]

[1]Maisonneuve-Rosemont Hospital Research Center and Department of Medicine, University of Montréal, Montréal H3C 3J7, Québec, Canada

[2]Institute for Research in Immunology and Cancer, University of Montréal, Montréal H3C 3J7, Québec, Canada

[†]Equal contribution

[#]Correspondence

Conflict of interest

The authors declare no conflict of interest

Running title: Undetectable Histones O-GlcNAcylation

Key words: Histone, OGT, O-GlcNAc, O-GlcNAcylation, Chromatin, Epigenetics, Polycomb, post-translational modification, HCF-1, TET2.

Abbreviation: O-Linked N-acetylglucosamine (O-GlcNAc), O-Linked N-acetylglucosamine transferase (OGT), O-GlcNAcase (OGA), Host Cell Factor-1 (HCF-1), Ten-Eleven Translocation protein 2 (TET2), serine (Ser), threonine (Thr), Uridine Diphosphate *N*-Acetylglucosamine (UDP-GlcNAc), Wheat Germ Agglutinin (WGA), Histone H2B serine 112 O-GlcNAc (H2B Ser112 O-GlcNAc), Histone H2B lysine 120 monoubiquitination (H2Bub Lys120), O-(2-acetamido-2-deoxyglucopyranosylidene) amino N-phenylcarbamate (PUGNAc)

2.1 Abstract

O-GlcNAcylation is a post-translational modification catalyzed by the O-Linked *N*-acetylglucosamine (O-GlcNAc) transferase (OGT) and reversed by O-GlcNAcase (OGA). Numerous transcriptional regulators including chromatin modifying enzymes, transcription factors and co-factors are targeted by O-GlcNAcylation indicating that this modification is central for chromatin-associated processes. Recently, OGT-mediated O-GlcNAcylation was reported to be a novel histone modification, suggesting a potential role in directly coordinating chromatin structure and function. In contrast, using multiple biochemical approaches, we report here that histone O-GlcNAcylation is undetectable in mammalian cells. Conversely, O-GlcNAcylation of the transcription regulators Host Cell Factor-1 (HCF-1) and the Ten-Eleven Translocation protein 2 (TET2) could be readily observed. Our study raises questions on the occurrence and abundance of O-GlcNAcylation as a histone modification in mammalian cells and reveals technical complications regarding the detection of genuine protein O-GlcNAcylation. Therefore, the identification of the specific contexts in which histone O-GlcNAcylation might occur is still to be established.

2.2 Introduction

O-GlcNAcylation is a widespread post-translational modification corresponding to the addition of a single O-Linked *N*-acetylglucosamine (O-GlcNAc) moiety to nuclear and cytosolic proteins [27-29]. Similar to other post-translational modifications, O-GlcNAcylation regulates protein function by influencing protein-protein interactions, enzymatic activity and sub-cellular localization [167, 168]. In mammals, this modification is coordinated by two enzymes, the O-Linked β-*N*-acetylglucosamine transferase (OGT) which catalyzes the attachment of the O-GlcNAc moiety on serine and threonine residues of target proteins, while the O-GlcNAcase (OGA) ensures its removal through hydrolysis [43, 169]. O-GlcNAcylation signaling is dependent on the availability of the donor substrate, Uridine Diphosphate *N*-Acetylglucosamine (UDP-GlcNAc), which is produced via the Hexosamine Biosynthetic Pathway [34]. O-GlcNAcylation is a highly dynamic modification, being regulated by a plethora of intracellular and extracellular cues, including growth factor signaling, fluctuation of nutrient levels, as well as stress responses [17, 33, 170]. Indeed, O-GlcNAcylation signaling acts as a metabolic sensor that links changes in the cellular metabolism to downstream regulation of numerous cellular pathways [168, 171, 172]. Moreover, recent studies have shown that direct competition between phosphorylation and O-GlcNAcylation can occur for the same amino acid residue, thus adding another layer of complexity to the outcome and regulation of this post-translational modification [135, 173]. The physiological importance of O-GlcNAcylation is further emphasized by the fact that defects in its regulation have been associated with human pathologies such as diabetes, neurodegenerative diseases and cancer [15, 31, 38, 174, 175].

O-GlcNAcylation signaling was proposed to play important roles in regulating the epigenome [28, 176]. Indeed, several transcriptional regulators and chromatin-modifying enzymes are modified by O-GlcNAcylation, thus impacting their recruitment to chromatin, assembly into functional transcription regulatory complexes, stability and activity [61, 177-179]. For instance, we and others have identified a non-canonical mechanism of OGT-mediated transcriptional regulation which involves the O-GlcNAcylation of the Host Cell Factor 1 (HCF-1) transcriptional regulator inducing its proteolytic maturation [95, 97, 98].

Recent studies have also reported that histones are modified by O-GlcNAcylation, suggesting an interesting possibility of crosstalk with other well-established histone marks [136, 180, 181]. Moreover, it was suggested that the methylcytosine dioxygenase Ten Eleven Translocation 2 (TET2) enzyme directly interacts with OGT to stimulate histone H2B S112 O-GlcNAcylation (H2B S112 O-GlcNAc) and gene expression [182]. Several methods were used to detect histone O-GlcNAcylation, including mass spectrometry, immunodetection with O-GlcNAc-specific antibodies and affinity binding to Wheat Germ Agglutinin lectin (WGA) [133, 136, 173]. However, discrepancies regarding the occurrence and the identity of the histones being modified were also reported. For instance, some studies suggested that histones H2A and H2B might be the principal targets for O-GlcNAcylation while others have shown that histone H3 would be the main substrate [133, 135, 173, 181]. Upon further characterization, it was reported that histone H2B S112 O-GlcNAcylation promotes H2B monoubiquitination on lysine 120 (H2B K120ub), an event associated with transcriptional activation [133, 183]. On the other hand, histone H3 serine 10 was also reported to be O-GlcNAcylated, and this appears to compete with the phosphorylation of this site as well as modulate the transcriptional state of chromatin [135, 173]. Other O-GlcNAcylation sites were reported within the globular domains of histones suggesting that they may function in maintaining higher-order chromatin structure [181]. Strikingly, during our investigation on the role of OGT in chromatin function; we were unable to reproduce the previous findings regarding histone O-GlcNAcylation in mammalian cells, whereas modification of other known OGT substrates was readily detected. Our results raise questions about the occurrence of histone O-GlcNAcylation and its proposed function in chromatin regulation.

2.3 Results & discussion

2.3.1 Undetectable Histone O-GlcNAcylation using various extraction techniques

OGT interacts with the TET family of methylcytosine dioxygenase enzymes, notably TET2, which appear to be required for the chromatin association of OGT and this was suggested to promote histone O-GlcNAcylation [182, 184]. To further investigate the potential biological significance of histone O-GlcNAcylation, we initially sought to reproduce

previously published results on the modification of histones H2B and H2A [133, 136, 173, 182, 183]. We co-expressed Flag-H2B or Flag-H2A with either Myc-OGT or the D925A catalytic inactive mutant (Myc-OGT CD) [22]. Coexpression of Myc-TET2 with Myc-OGT was also included since their association was expected to significantly increase OGT-mediated histone O-GlcNAcylation [182, 185]. We conducted an immunoprecipitation of Flag-H2B or Flag-H2A under denaturing conditions to determine their potential O-GlcNAcylation levelsby

using the widely employed anti-O-GlcNAc antibodies RL2 and CTD110.6 (Figure 12 and Figure 2.S1). We did not detect a specific signal at the molecular weight region corresponding to histones Flag-H2B or Flag-H2A using the two anti-O-GlcNAc antibodies. However, using similar conditions, we were able to detect HCF-1 and TET2 O-GlcNAcylation, two known substrates of OGT (Figure 2.S1) [95, 178]. Of note, as expected, OGT-mediated HCF-1 proteolytic cleavage also confirmed the activity of OGT in our co-transfection conditions

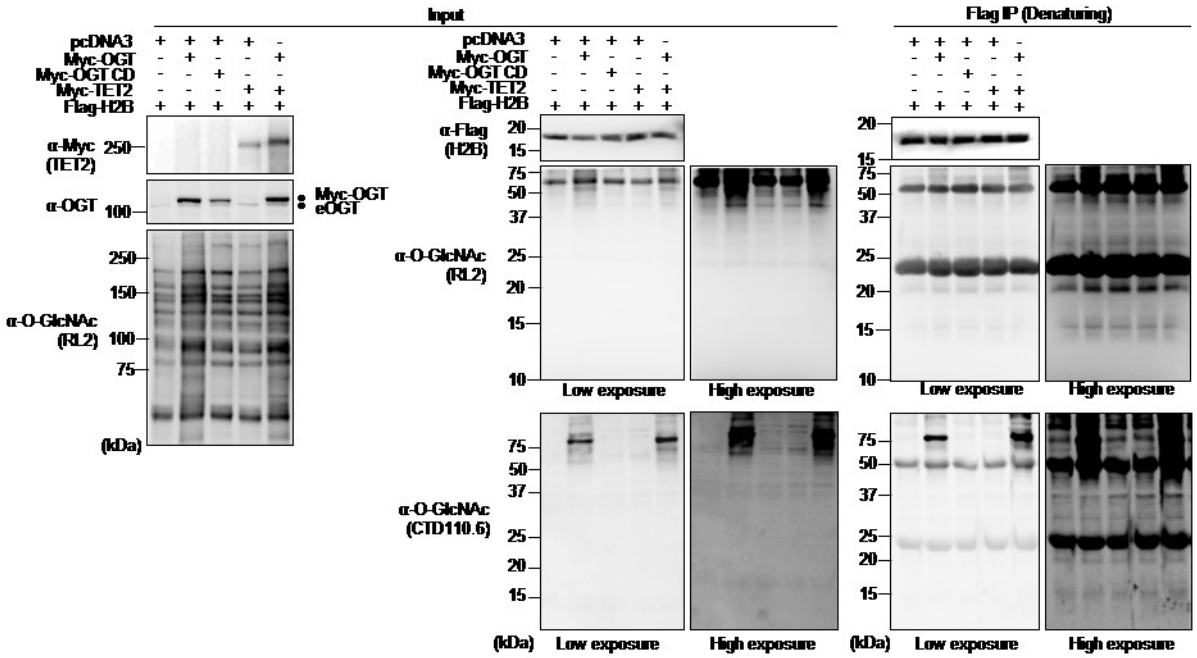

Figure 12. Undetectable Histone O-GlcNAcylation following OGT and TET2 overexpression. (A) HEK293T cells were transfected with Flag-H2B along with either pcDNA3 empty vector, Myc-OGT or Myc-OGT catalytic dead (CD), as well as Myc-TET2 alone or in combination with Myc-OGT. Three days post-transfection, cells pellets were harvested and immunoprecipitation (Flag-IP) following protein denaturation was conducted to obtain purified Flag-H2B. The immuno-purified histones were subjected to western blotting analysis using the indicated antibodies. Dots indicate Myc-OGT and endogenous OGT (eOGT). (B) HEK293T cells were transfected with either GFP-OGT or GFP-OGT catalytic dead (CD) in the presence of HA-HCF-1 full length (FL) or Myc-TET2 expression vectors. Three days post-transfection, cells were harvested and total cell lysates were subjected to immunoprecipitation (IP), following sample denaturation, using anti-Myc or anti-HA antibodies to purify TET2 and HCF-1 respectively. Total cell lysates (Input fractions) as well as immunopurifications were subjected to western blotting analysis using the indicated antibodies. Arrow indicates the full length (precursor) form of HCF-1 and brace indicates the cleaved forms of HCF-1. Dots indicate GFP-OGT and endogenous OGT (eOGT). kDa; Molecular weight marker in Kilodalton.

(Figure 2.S1) [95, 97, 98]. Next, using the same transfection conditions indicated above, we performed several established extraction methods in order to enrich endogenous histones for O-GlcNAcylation detection. Chromatin and Histones were isolated using both high salt/detergent (300 mM NaCl, 1% NP-40) extraction (Figure 13A and Figure 2.S3A) and acid extraction (0.2 N HCl) (Figure 13B and Figure 2.S3B) methods, respectively. First, immunoblotting with RL2 or CTD110.6 antibodies was conducted on the soluble fractions to detect global O-GlcNAcylation levels (Figure 13 and Figure 2.S3, Left panels). As expected, we observed an increase of cellular O-GlcNAcylation levels following OGT overexpression. However, chromatin fractions revealed faint signals between 10 and 20 kDa when the blots probed with RL2 antibody were overexposed. The CTD110.6 antibody occasionally produced more pronounced signals at the levels of histones (Figure 13 and Figure 2.S3, Right panels). Overall, we did not observe increasing signals following overexpression of OGT or TET2, regardless of the O-GlcNAc antibody used, the quantity of proteins loaded or the method of extraction performed (Figure 13 and Figure 2.S3). On the other hand, upon OGT overexpression, we detected increased O-GlcNAcylation of certain chromatin-associated proteins corresponding to bands ≥ 37 kDa. Based on these results, we concluded that the faint and inconsistent signals produced between 10 and 20 kDa by the RL2 or CTD110.6 antibodies are not indicative of histone O-GlcNAcylation.

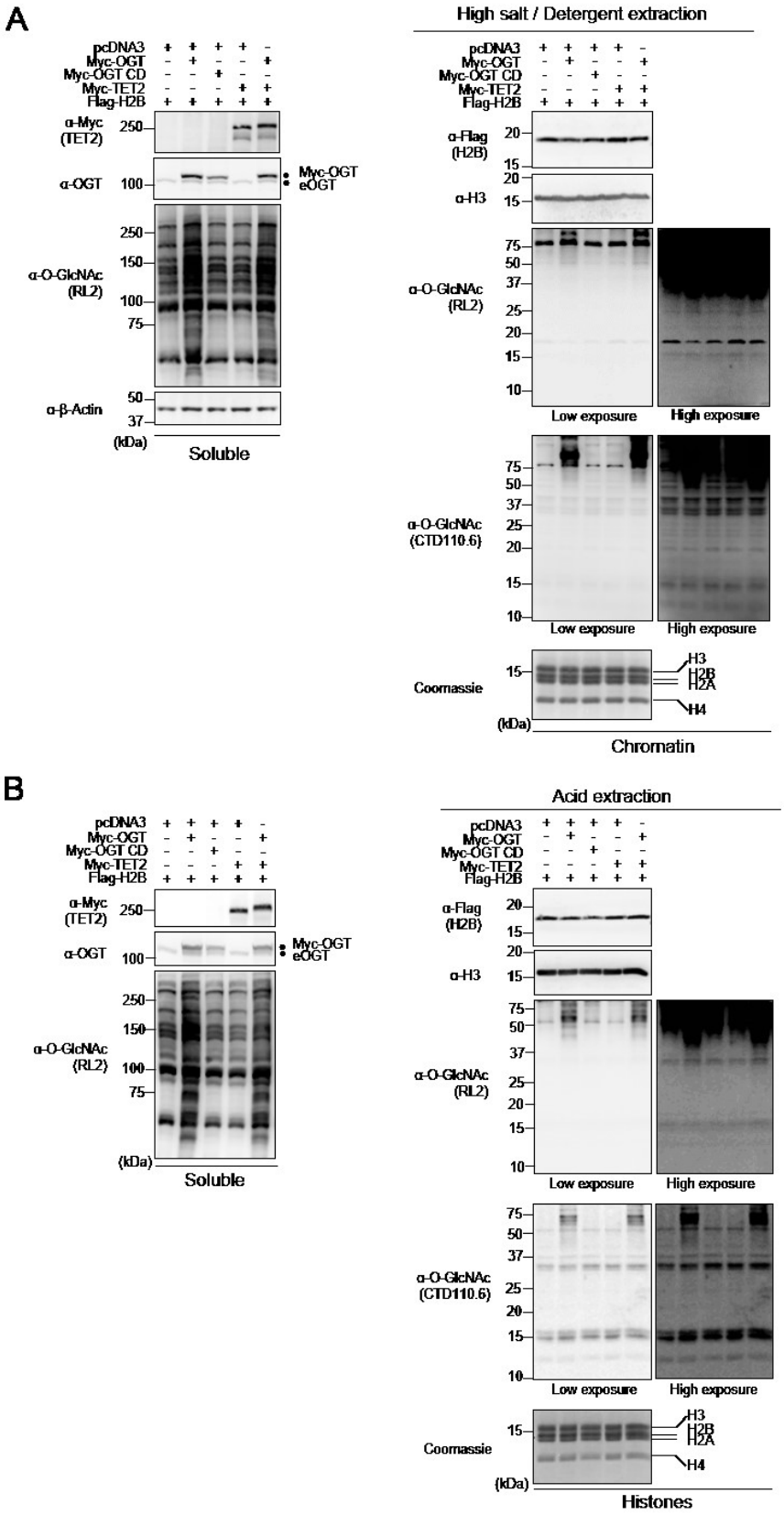
A
High salt / Detergent extraction
pcDNA3
Myc-OGT
Myc-OGT CD
Myc-TET2
Flag-H2B
α-Myc (TET2)
α-OGT
Myc-OGT
eOGT
α-O-GlcNAc (RL2)
α-β-Actin
(kDa)
Soluble
α-Flag (H2B)
α-H3
Low exposure
High exposure
α-O-GlcNAc (CTD110.6)
Coomassie
H3
H2B
H2A
H4
Chromatin
B
Acid extraction
Histones

Figure 13. Undetectable histone O-GlcNAcylation following various extraction procedures. (**A**) HEK293T cells were transfected with Flag-H2B along with either pcDNA3 empty vector, Myc-OGT, Myc-OGT catalytic dead (CD) or Myc-TET2, as well as the combination of Myc-OGT with Myc-TET2. Three days post-transfection, cells pellets were collected for subsequent high salt/detergent extraction and cellular extracts were then analysed by western blotting with the indicated antibodies. (Left panel) Soluble fraction showing global increase of O-GlcNAcylation following OGT overexpression. (Right panel) Immunodetection of histone O-GlcNAcylation by RL2 and CTD110.6 antibodies on chromatin fraction. β-Actin and histone H3 were used as loading controls. (**B**) HEK293T cells were transfected as in (**A**). Three days post-transfection, cells were harvested and histones were extracted. The samples were analysed by western blotting with the indicated antibodies. (Left panel) Soluble fraction showing global O-GlcNAcylation levels. (Right panel) Histones fraction detected with both RL2 and CTD110.6 anti-O-GlcNAc antibodies. Coomassie Brilliant Blue staining indicates abundance of histones loaded. Histone H3 was use as a loading control. Dots indicate Myc-OGT and endogenous OGT (eOGT). kDa; Molecular weight marker in Kilodalton.

2.3.2 Modulation of O-GlcNAc levels does not result in the detection of specific histone O-GlcNAcylation

We reasoned that if the signals detected by RL2 or CTD110.6 around 10-20 kDa correspond to histone O-GlcNAcylation, then it might be possible to modulate these signals by depleting endogenous OGT. Thus, we conducted siRNA knockdown of OGT in U2OS cells and performed cellular fractionation to separate the soluble and histone-containing chromatin fractions. As shown in figure 14A (Right panel), the signals detected with RL2 or CTD110.6 antibodies around 10-20 kDa, did not decrease following OGT depletion suggesting that these signals are unspecific. In contrast, using both antibodies, we detected a significant decrease in global O-GlcNAcylation in the soluble fraction upon siRNA treatment (Figure 14A, Left panel). Again, we noted that while the signal obtained with RL2 antibody in the 10-20 KDa region can be seen only upon overexposure of the membrane, the CTD110.6 antibody produced a much more readily detectable signal in this region. As RL2 and CTD110.6 are respectively IgG and IgM isotypes, we sought to determine if the signal detected at the level of histones with CTD110.6 could be due to the peroxidase-coupled secondary anti-IgM antibody. This is particularly relevant as high quantities of histones were probed with anti-O-GlcNAc antibodies. Thus, we incubated the blots with a non-relevant anti-rhodamine IgM antibody prior to incubation with the same anti-IgM HRP-conjugated antibody or with this secondary antibody alone (Figure 14A, Right panel). Interestingly, both combinations displayed a similar signal pattern as that obtained using the CTD110.6, suggesting that the non-specific signal originates from the combination of secondary anti-IgM antibody and high protein density of histone bands. In addition, probing the membranes with a non-relevant anti-BAP1 antibody also resulted in background signals at molecular weights corresponding to histone bands

(Figure 14A, Right panel). These data indicate that the high abundance of histones present on membranes renders the detection of O-GlcNAcylation amenable to false-positive immunoblotting signals. Of note, previous studies questioned the specificity of CTD110.6 towards O-GlcNAc and revealed cross-reactivity with N-GlcNAc$_2$-modified glycoprotein and GlcNAcylated O-mannose modified proteins [186, 187]. Consequently, we used the RL2 antibody to continue our investigation since it was not shown to cross react with other GlcNAc modifications. Nonetheless, our data suggested that the faint signal obtained with RL2 corresponds to a non-specific background caused by high amounts of histones. To further support our data, we extracted endogenous histones from HeLa cells for comparison with purified yeast H2B (yH2B) and recombinant human H2B (hH2B) produced in bacteria. We reasoned that if the faint signal produced by RL2 corresponds to histone O-GlcNAcylation, then this signal should not be detected for histones purified from yeast or bacteria which are not O-GlcNAcylated. We observed that the RL2 antibody produced low signals following overexposure of the blot, and these signals increased proportionally with the amount of histones loaded, irrespective of the species from which the histones were isolated (Figure 2.S4, panels A, B). Next, we conducted competition assays and found that, as expected, *N*-Acetylglucosamine (GlcNAc) inhibited RL2 binding to high molecular weight O-GlcNAcylated proteins present in the soluble fraction or associated with the chromatin fraction (Figure 2.S4C). However, GlcNAc also strongly reduced the signal produced by RL2, in the region of histone bands, for both mammalian chromatin and recombinant human H2B (Figure S4C). These results are not surprising as a non-specific and low affinity binding of the RL2 antibody to histone fraction could also be potentially blocked by GlcNAc. Thus, these results further suggest that the RL2 antibody recognizes non-specifically antigenic determinants on histones through its paratope.

To further investigate potential histone O-GlcNAcylation, we sought to determine if inhibiting O-GlcNAcase (OGA), the enzyme responsible for O-GlcNAc removal, with O-(2-acetamido-2-deoxyglucopyranosylidene) amino N-phenylcarbamate (PUGNAc) would increase the signal of histone O-GlcNAcylation above background levels. Treatment of HeLa and HEK293T cells with PUGNAc promoted the accumulation of O-GlcNAcylated proteins but not of the background signal at the level of histones (Figure 14B, Left and Right panel).

We also conducted a nutrient starvation in C2C12 myoblasts, and analysed global protein and potential histone O-GlcNAcylation. As expected, AMPK phosphorylation progressively increased and decreased with starvation and medium replenishment (R) respectively (Figure 14C, Left panel) [188]. We observed that while chromatin-associated high molecular weight protein O-GlcNAcylation was reduced upon starvation, only weak and inconsistent background signals were detected for histones (Figure 14C, Right panel).

Taken altogether, our results indicate that the immunoblot signal detected by RL2 in the region corresponding to histones, is a non-specific O-GlcNAcylation-independent background signal.

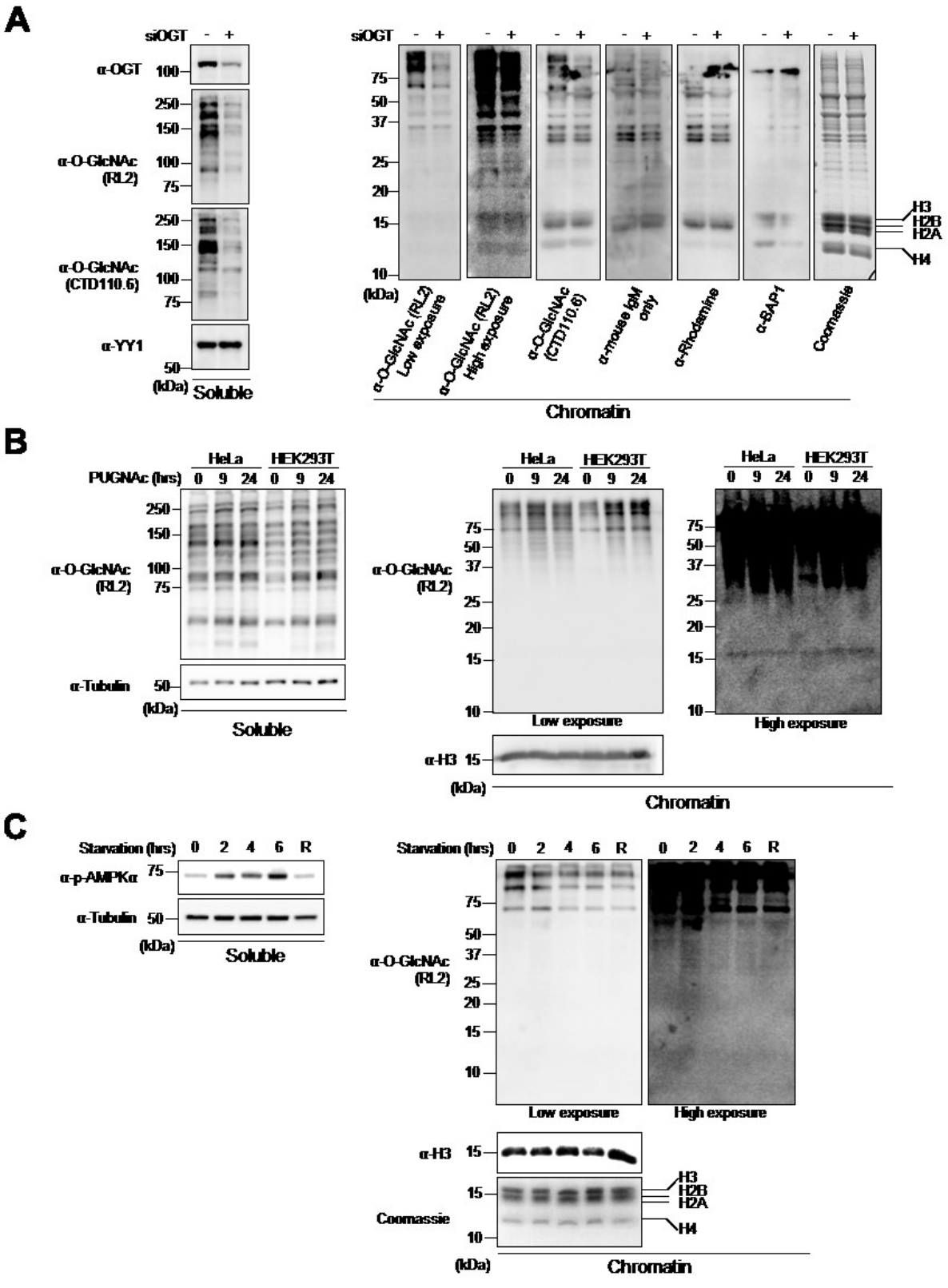
A
siOGT - +
α-OGT
100
250
150
α-O-GlcNAc (RL2)
100
75
250
150
α-O-GlcNAc (CTD110.6)
100
75
α-YY1
50
(kDa)
Soluble
siOGT - + - + - + - + - + - +
75
50
37
25
20
15
10
(kDa)
α-O-GlcNAc (RL2) Low exposure
α-O-GlcNAc (RL2) High exposure
α-O-GlcNAc (CTD110.6)
α-mouse IgM only
α-Rhodamine
α-BAP1
Coomassie
H3
H2B
H2A
H4
Chromatin
B
HeLa HEK293T
PUGNAc (hrs) 0 9 24 0 9 24
250
150
α-O-GlcNAc (RL2)
100
75
α-Tubulin
50
(kDa)
Soluble
HeLa HEK293T
0 9 24 0 9 24
75
50
37
α-O-GlcNAc (RL2)
25
20
15
10
Low exposure
α-H3
15
(kDa)
Chromatin
HeLa HEK293T
0 9 24 0 9 24
75
50
37
25
20
15
10
High exposure
C
Starvation (hrs) 0 2 4 6 R
α-p-AMPKα
75
α-Tubulin
50
(kDa)
Soluble
Starvation (hrs) 0 2 4 6 R 0 2 4 6 R
75
50
37
α-O-GlcNAc (RL2)
25
20
15
10
Low exposure
High exposure
α-H3
15
Coomassie
15
10
H3
H2B
H2A
H4
(kDa)
Chromatin

Figure 14. Modulation of O-GlcNAcylation does not result in detectable histone O-GlcNAcylation. (**A**) U2OS cells were transfected twice with OGT siRNA and three days post-transfection, cells were harvested. Chromatin fraction was isolated and protein levels were analysed by western blotting with the indicated antibodies. (Left) U2OS soluble fraction showing OGT depletion and decrease of global O-GlcNAcylation levels. YY1 was used as a loading control. (Right) Chromatin fraction showing O-GlcNAcylation background detection of histones using various antibodies. (**B**) HeLa and HEK293T cells that were treated with 100 μM PUGNAc for 0, 9 and 24 hours. The soluble and chromatin fractions were blotted with RL2 antibody. Histone H3 and Tubulin were used as loading controls. (**C**) C2C12 mouse myoblast cell line were starved by incubation in HBSS buffer, and harvested at the indicated times for cellular fractionation. R; 4 hours of starvation followed by 2 hours of replenishment with complete culture medium. (Left) Western blot analysis of the soluble fraction showing increasing levels of phosphorylated AMPKα (α-p-AMPKα) as a control of the starvation treatment. Tubulin was used as a loading control. (Right) The chromatin fraction was analysed by western blotting using the indicated antibodies. Histone H3 was used as a loading control and Coomassie Brilliant Blue staining indicates the abundance of histones loaded. kDa; Molecular weight marker in Kilodalton.

2.3.3 Undetectable histone O-GlcNAcylation in different cell lines and during cell cycle progression

Although our data did not reveal constitutive histone O-GlcNAcylation, we could not exclude that this post-translational modification might occur on histones in specific cell types. Thus, we investigated potential histone O-GlcNAcylation in a variety of previously used cell lines including mouse Embryonic Fibroblast (MEF) as well as mouse Embryonic Stem Cells (mESCs) [182, 183, 185]. We also included the mouse pre-adipocyte 3T3-L1 cell line often used in differentiation studies as well as several multiple myeloma cell lines, RPMI-8226, JJN-3, NCI-H292 cells, that we had in culture at the time of our investigation. We find that this cell line panel is representative of multiple tissue-origins as well as primary and cancer cells. When immunoblotting the insoluble chromatin fraction for O-GlcNAcylation, we detected a very faint signal at the level of histones (Figure 15A, Top panel). This signal, obtained only following extended exposure of the blot, does not correlate with the cell-specific levels of endogenous O-GlcNAcylation detected for high molecular weight proteins. Instead, by probing total H2A levels, it can be noticed that the RL2 signal follows the trend of histones abundance (Figure 4A, Bottom blot).

To further determine whether histone O-GlcNAcylation might be enriched in a specific phase of the cell cycle, U2OS cells were synchronized at the G1/S boundary with a double thymidine block and released to progress through the cell cycle [189]. These cells were also treated with the CDK1 inhibitor (RO-3306) to enrich for late G2 cells (Figure 15B, Top panel) [190]. The chromatin fraction was isolated from cells at different phases of the cell cycle and histone O-GlcNAcylation was monitored by western blotting using the RL2 antibody. We

noticed the expected faint signal at the level of histones and that this signal did not change during cell cycle progression. However, high molecular weight chromatin-associated proteins show significantly increased O-GlcNAcylation at G1/S transition. Therefore, we concluded that fluctuating histone O-GlcNAcylation could not be observed during cell cycle. Moreover, along with our previous data, these results strengthen the notion that the signal detected by RL2 at the level of histones following blot overexposure corresponds to background.

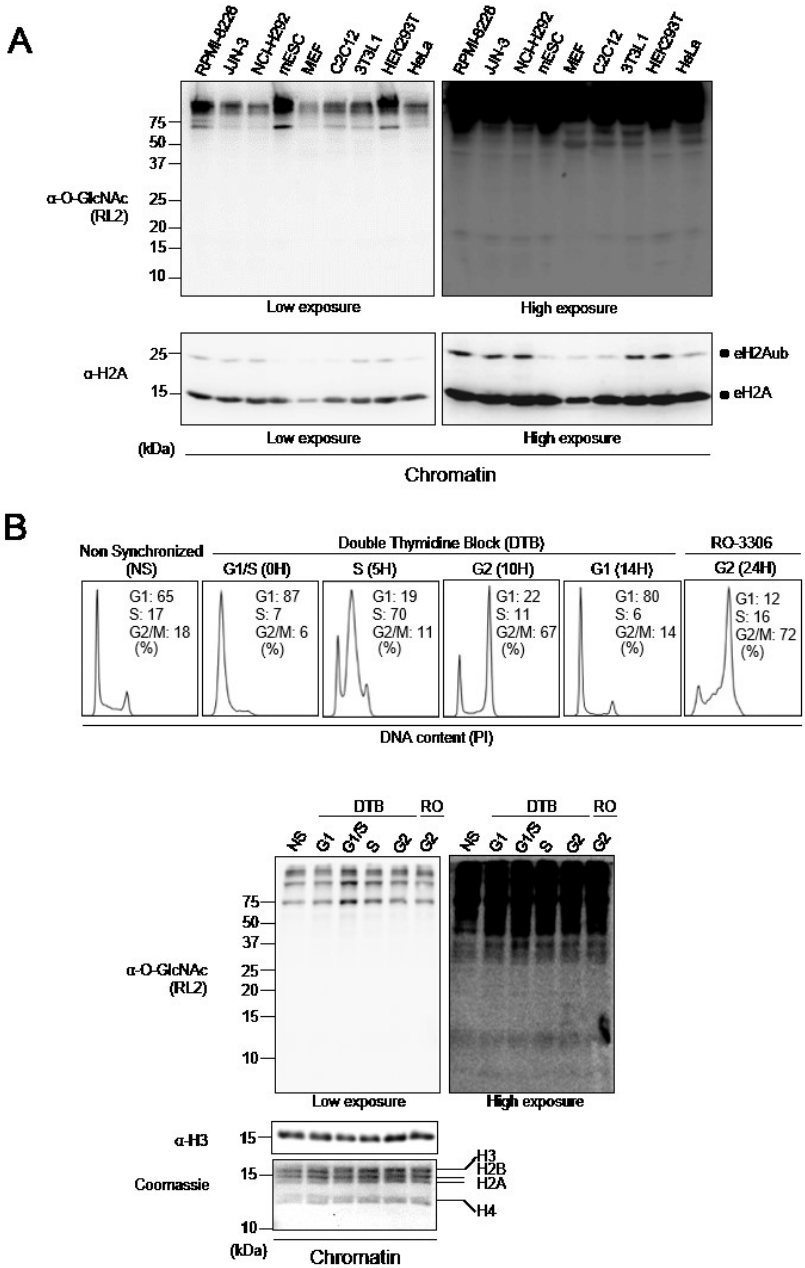

Figure 15. Unspecific signal detected at the level of histones in various cell lines and during cell cycle progression. (A) Various cell lines were cultured and harvested to perform chromatin extraction. The chromatin fraction was analysed by western blotting with the indicated antibodies. Total histone H2A was used as a loading control. Dots indicate endogenous H2A ubiquitination (eH2Aub) and total H2A (eH2A). (B) Histones O-GlcNAcylation analysis of synchronized U2OS cells. Cells were blocked in G1/S boundary by double thymidine block (DTB) and then released to progress through the cell cycle. U2OS cells were also treated with the CDK1 inhibitor, RO-3306, for 24 hours to block cells in late G2. Cells were harvested at the indicated times for FACS analysis (Upper panel) and for chromatin extraction (Bottom panel). The chromatin fraction was analysed by western blotting with the indicated antibodies and by Coomassie Brilliant Blue staining. Histone H3 was used as a loading control. NS; Non-Synchronized, DTB; Double Thymidine Block. kDa; Molecular weight marker in Kilodalton.

2.3.4 Lack of evidence supporting H2B Ser112 O-GlcNAcylation and its link with H2B Lys120 monoubiquitination

It was reported that H2B S112 is O-GlcNAcylated (H2B S112 O-GlcNAc), an event that appears to promote the monoubiquitination of H2B Lys120 (H2B K120ub) thus coordinating gene expression [133]. It was also described that AMPK-mediated OGT Thr444 phosphorylation hindered its ability to associate with chromatin, and this was shown to reduce the reported H2B S112 O-GlcNAc signal [170]. In turn, this effect was proposed to inhibit monoubiquitination of H2B K120, thus repressing gene expression in MEF cells [183]. As an anti-O-GlcNAcylated H2B S112 is commercially available [183], we first inquired about the specificity of this antibody. Since H2B S112 O-GlcNAc was shown to decrease dramatically following knockdown of OGT by RNAi, we used a similar approach to deplete OGT by siRNA in HeLa cells (Figure 16A) [133, 183]. As expected, OGT knockdown resulted in the accumulation of the precursor form of HCF-1, as its proteolytic maturation is O-GlcNAcylation-dependent (Figure 16A, Left panel) [95, 97, 98]. However, neither the signal generated by the anti-H2B S112 O-GlcNAc nor that for anti-H2B K120ub changed following OGT depletion (Figure 16A, Right panel). In addition, we expressed Flag-H2B WT and Flag-H2B S112A mutant in HEK293T cells and conducted anti-Flag immunoprecipitation under denaturing conditions (Figure 16B). Unexpectedly, the anti-H2B S112 O-GlcNAc signal decreases by only ~3-fold in the H2B S112A mutant, instead of completely disappearing. In addition, we observed no change in H2B K120ub levels. Our results could not validate the reported link between H2B S112 O-GlcNAc and H2B K120ub and moreover further suggest that the anti-H2B S112O-GlcNAc antibody might not confer specific detection for H2B O-GlcNAcylation. Next, we sought to further investigate the anti-H2B S112 O-GlcNAc antibody specificity by producing recombinant human histones H2B (His-hH2B) and H2B S112A (his-

hH2B S112A) purified from bacteria (Figure 16C). We also used a GST-H2A construct as a negative control. Following relative quantification of recombinant histones shown by Coomassie Brilliant Blue staining (Figure 16C, Top panel), we subsequently probed increasing quantities of these proteins by immunoblotting using the anti-H2B S112O-GlcNAc antibody. We found that purified recombinant proteins are detectable using this antibody and that this signal decreased by about two to three folds when the serine was mutated to alanine (His-hH2B S112A) (Figure 16C, Middle panel). Moreover, the H2B S112O-GlcNAc signal detected for the recombinant His-hH2B protein is comparable to that detected for a similar amount of mammalian endogenous H2B in the chromatin fraction (Figure 16C, Bottom panel). Thus, these results indicate that this antibody recognizes the H2B backbone itself rather than O-GlcNAc moiety and that unmodified S112 is a major determinant in epitope recognition by this antibody.

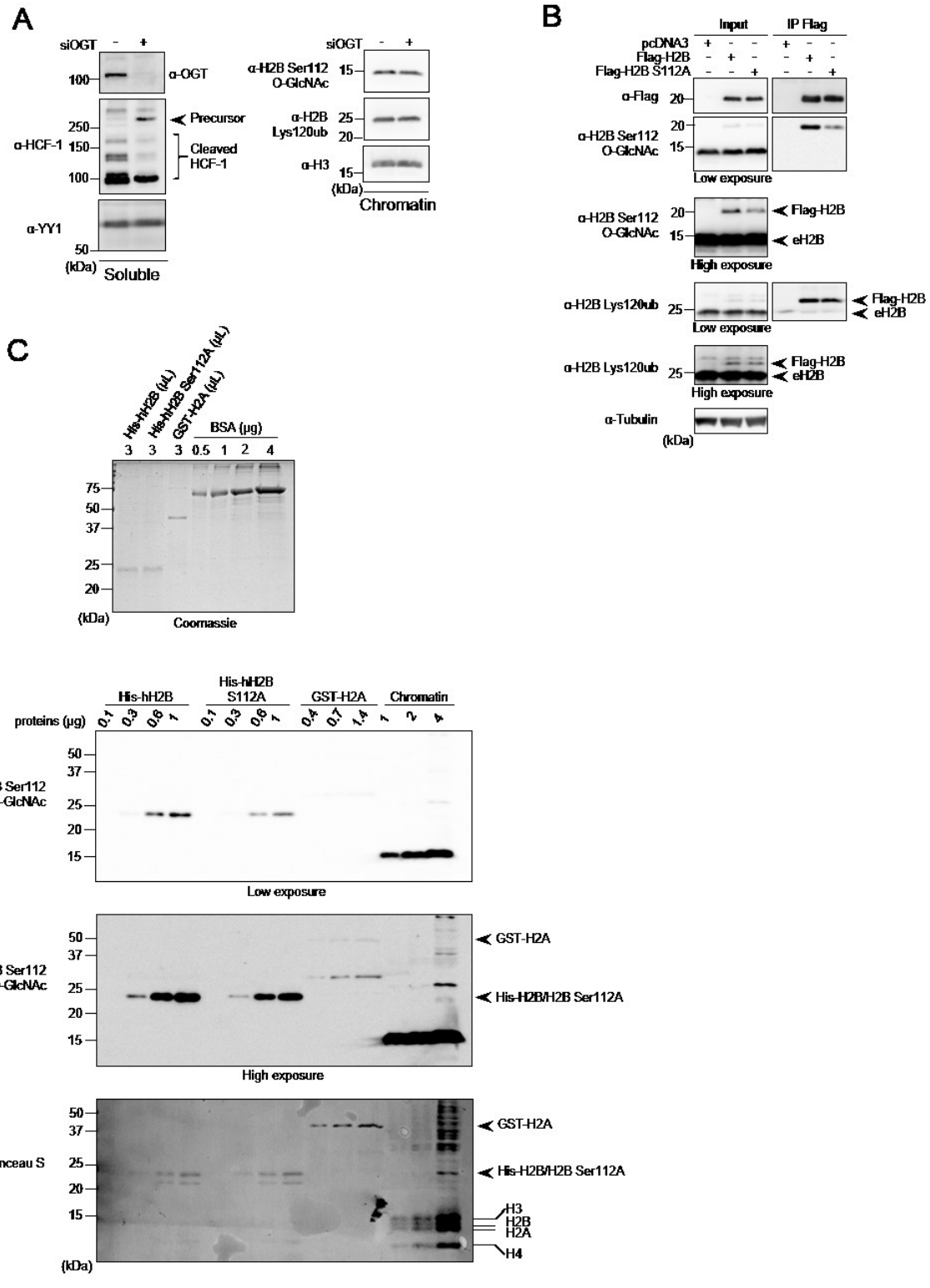
A
siOGT
α-OGT
Precursor
α-HCF-1
Cleaved HCF-1
α-YY1
Soluble
α-H2B Ser112 O-GlcNAc
α-H2B Lys120ub
α-H3
Chromatin
(kDa)
B
Input
IP Flag
pcDNA3
Flag-H2B
Flag-H2B S112A
α-Flag
α-H2B Ser112 O-GlcNAc
Low exposure
High exposure
Flag-H2B
eH2B
α-H2B Lys120ub
α-Tubulin
C
His-hH2B (μL)
His-hH2B Ser112A (μL)
GST-H2A (μL)
BSA (μg)
Coomassie
His-hH2B
His-hH2B S112A
GST-H2A
Chromatin
proteins (μg)
GST-H2A
His-H2B/H2B Ser112A
Ponceau S
H3
H2B
H2A
H4

Figure 16 H2B Ser112 O-GlcNAc antibody is not specific and Ser112 O-GlcNAcylation is not linked to H2B K120 monoubiquitination. (A) HeLa cells were transfected twice with OGT siRNA and three days post-transfection, cells were harvested to perform cellular fractionation. Protein levels were analysed by western blotting with the indicated antibodies. HeLa soluble fraction was analysed for HCF-1 proteolytic cleavage. YY1 was used as a loading control (left panel). Chromatin fraction was analysed for H2B Ser112 O-GlcNAc and H2B Lys120ub levels (Right panel). (B) HEK293T cells were transfected with Flag-H2B or Flag-H2B Ser112A. Three days post-transfection, cells were harvested and total cell lysates were subjected to protein denaturation and immunoprecipitation (IP) using α-Flag antibody. Input as well as IP fractions were subjected to immunoblotting analysis using the indicated antibodies. Arrows indicate Flag-H2B and endogenous H2B (eH2B). Tubulin was used as a loading control for the input fraction. (C) Relative quantification of eluted purified recombinant histones detected by Coomassie Brilliant Blue staining. Known amounts of BSA protein were used as standards for relative quantification (top panel). Increasing amounts of recombinant His-hH2B, His-hH2B Ser112A mutant, GST-H2A as well as chromatin extract from HEK293T cells were analysed by western blot using the indicated antibodies. Red Ponceau S staining of the membrane used for subsequent western blotting showing the loading of purified proteins (bottom panel). Arrows and lines indicate the position of recombinant and endogenous histones respectively. kDa; Molecular weight marker in Kilodalton.

2.3.5 Undetectable binding of mammalian histones to the Wheat Germ Agglutinin (WGA) lectin

It was previously reported that HeLa cell nucleosomes obtained by micrococcal digestion can be enriched with a WGA lectin resin which is known to strongly bind O-GlcNAcylated proteins [133]. However, the extraction procedure does not preclude histone binding to the WGA column as a consequence of interaction of histones with O-GlcNAcylated proteins associated with nucleosomes. Thus, we sought to use an acid extraction procedure to separate the soluble histones from all other proteins that remain in the insoluble fraction. Moreover, acid treatment ensures denaturation of proteins, thereby preventing potential interactions of histones with O-GlcNAcylated proteins associated with chromatin. We cultured HEK293T cells with PUGNAc for 24 hours and also included this inhibitor during the extraction steps to exclude the possibility of losing protein O-GlcNAc modification [173]. Moreover, to ensure that acid treatment does not influence detection of O-GlcNAc modification, we also analyzed the ability of chromatin-associated-proteins in the acid extraction mixture to bind the WGA column (Figure 17). Importantly, HCF-1 and several chromatin-associated proteins were enriched approximately 5 to 10 times compared to the input signal, thus confirming that the WGA resin strongly and efficiently binds O-GlcNAcylated proteins (Figure 17, Left panel). This result also indicates that acid treatment did not covalently modify or disrupt the O-GlcNAc moiety. In contrast, immunoblotting with RL2, anti-H2B S112 O-GlcNAc or anti-H2A revealed that histones were found only in the input and the flow through fractions (Figure 17, Right panel). Consistently, staining of

histones with Coomassie Brilliant Blue did not reveal histones binding to WGA-agarose. Note that the background signal produced by the RL2 antibody at the level of histones was observed in the input and the flow through fractions. To further exclude the possibility that only a small fraction of histones are modified in proliferating human cells, and that such limited amounts of modified histones are below immunoblotting detection thresholds, we carried out a WGA pull-down experiment in conditions that would allow for the total depletion of HCF-1 from the cell lysate (Figure 2.S5, Left panel). Even in these conditions, histones were again only detected in the inputs and the flow through fractions by immunodetection and silver staining (Figure 2.S5, Right panels). Altogether, these data support our findings that histone O-GlcNAcylation is undetectable in mammalian cells.

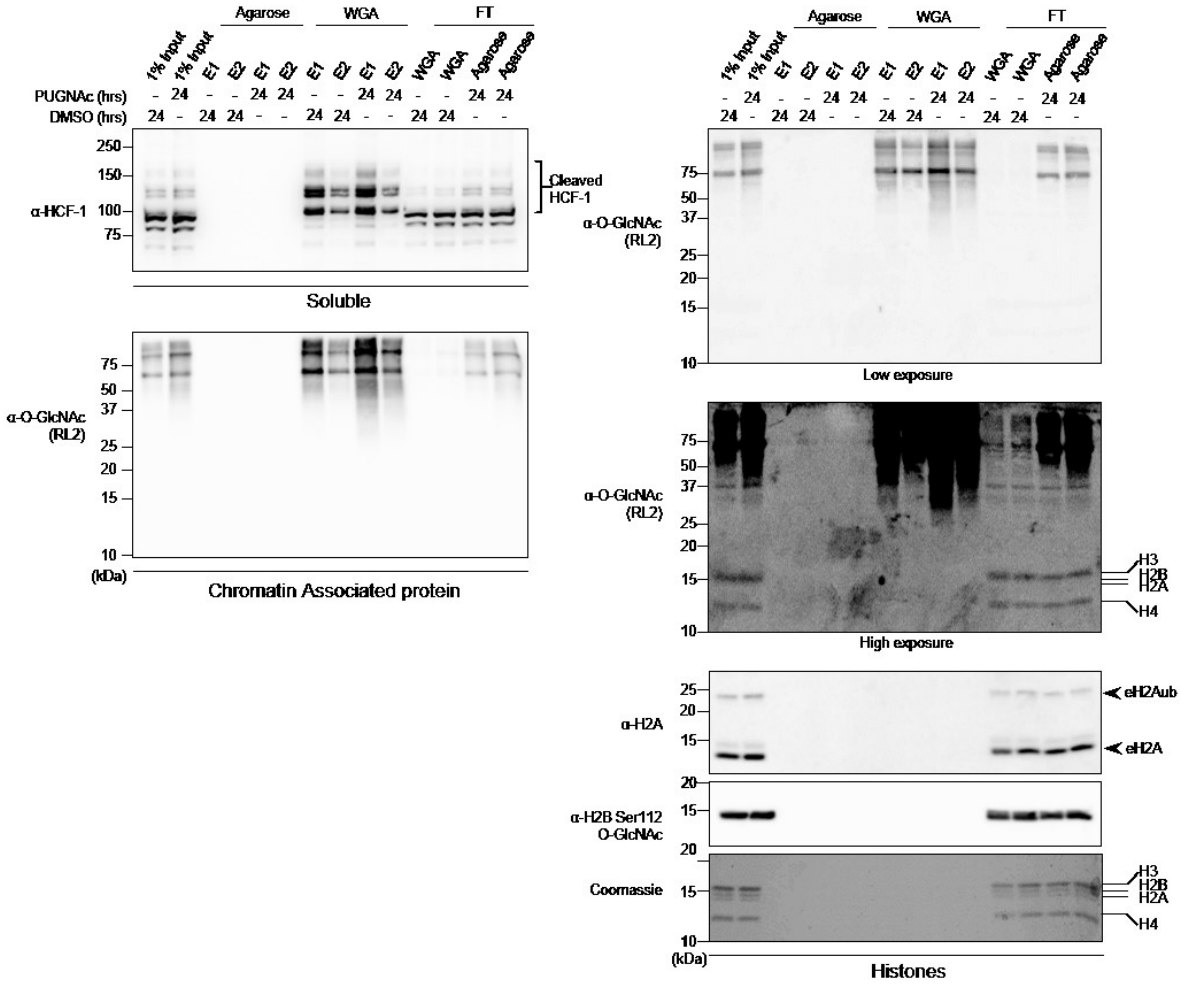

Figure 17. HCF-1 and several chromatin-associated proteins but not histones bind to WGA lectin. HEK293T cells were treated with 100 μM PUGNAc or equal volume of DMSO for 24 hours as indicated and harvested to perform acid extraction of histones. The indicated soluble and chromatin-associated-proteins fractions (Left panels), and histone fraction (Right panels) were incubated for 2 hours with agarose bound WGA lectin or with agarose resin to control for non-specific binding. Two elutions (E1 and E2) of agarose and WGA bound proteins as well as the flow through (FT) fractions were analysed by western blot using the indicated antibodies. The Coomassie Brilliant Blue staining and the anti-H2A antibody indicate that histones are found in the input and the FT fractions. Arrows indicate endogenous H2A ubiquitination (eH2Aub) and total H2A (eH2A). kDa; Molecular weight marker in Kilodalton.

2.3.6 Histone O-GlcNAcylation is not detected by *Click-it* biotin-alkyl chemistry, mass spectrometry or following *in vitro* O-GlcNAcylation reactions

To further corroborate our observations, we sought to use other methods for O-GlcNAcylation detection. We first used the commercially available *in vitro Click-it* chemistry system. This procedure consists in modifying O-GlcNAcylated proteins with an azido sugar (GalNAz), which can then react with biotin-alkyne thus becoming detectable via streptavidin-conjugated HRP [191]. This approach is highly sensitive since it allows for the detection of the O-GlcNAcylation of α-crystallin, a lens protein that was reported to be O-GlcNAcylated at a very low stoichiometric ratio [191, 192]. Thus, we performed the *Click-it* chemistry reaction on histones extracted from HeLa cells, as well as on α-crystallin, used as the positive control. As shown in Figure 7A, although similar amount of both purified histones and α-crystallin were used (Figure 18A, Right panel), we could only detect O-GlcNAcylation of α-crystallin in these conditions (Figure 18A, Left panel). Moreover, O-GlcNAcylation of co-purified high molecular weight proteins could be readily observed, thus demonstrating the efficiency of GalNAz labeling in the same reaction conditions as histones.

Next, we sought to determine, by performing ETD-MS/MS analysis, if we could recapitulate the reported histone O-GlcNAcylation sites using acid extracted histones from HeLa cells. We also purified HCF-1 from HEK293T cells and included it as a positive control. Mass spectrometry analysis by HCD and ETD for proper glycan localization was conducted [193]. As shown in Figure 2.S6 and Supplemental Table 1, in addition to several novel sites, we were able to identify 6 of the reported HCF-1 O-GlcNAcylation sites [95, 98, 194-198]. However, we were unable to detect O-GlcNAcylation of the core histones. Indeed, even though the MS analysis revealed the presence of histone peptides that were reported to be modified (e.g., H2B S112, H2A T101, H3 S10 and H4 S47), we did not detect their corresponding O-GlcNAcylated forms (Figures 2.S7 and 2.S8).

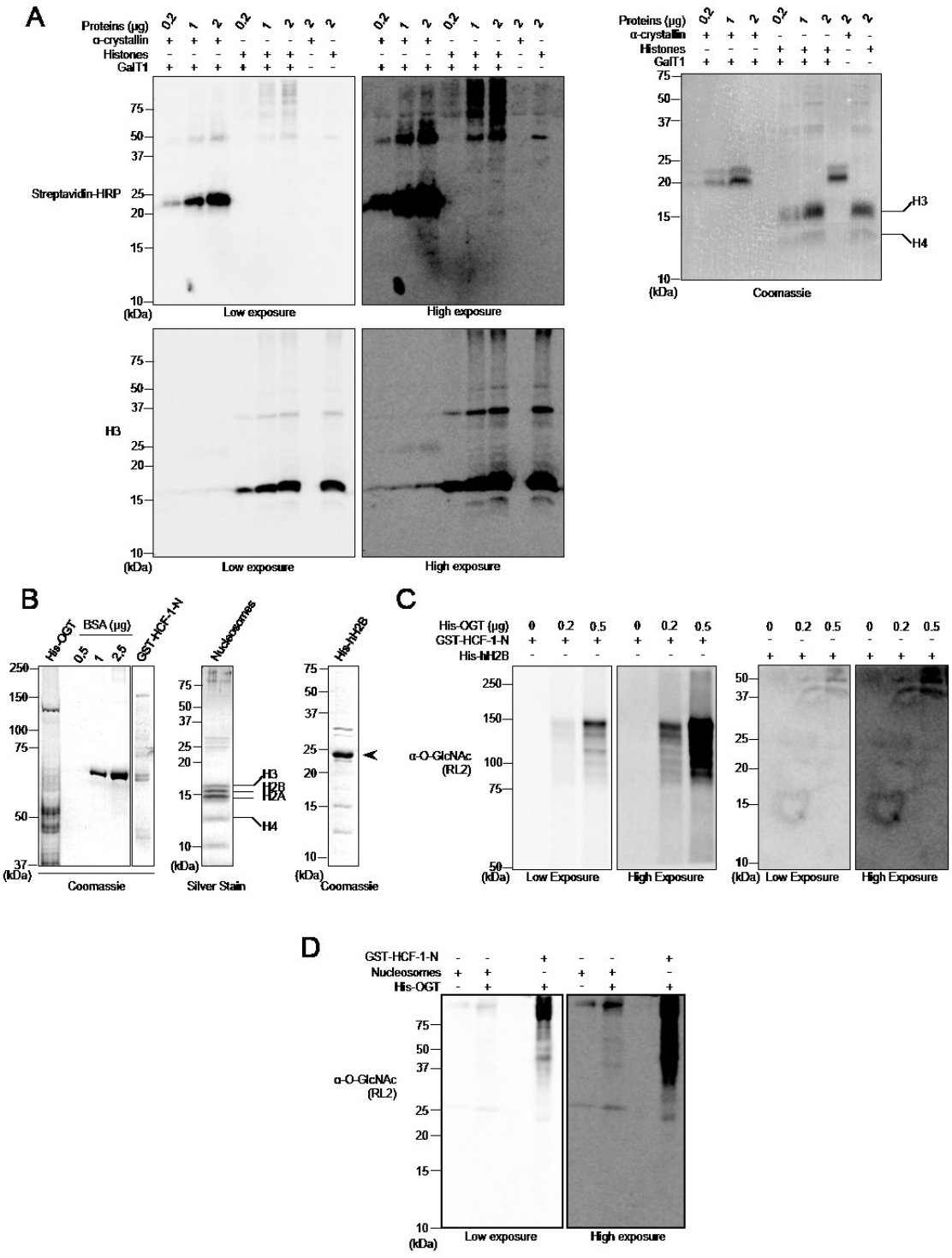

Figure 18. Histones are not modified by Click-it biotin-alkyl chemistry or by *in vitro* OGT-mediated O-GlcNAcylation. (A) The poorly O-GlcNAcylated α-crystallin is detected with the click-it biotin-alkyl chemistry but not histones. HeLa cells were harvested and acid extraction followed by acetone precipitation was performed to purify histones. The GalNAz labeling reaction was carried out for a minimum of 16 hours and the biotin-alkyl

reaction was performed in the presence or absence of the GalT1 enzyme. (Left panel) O-GlcNAcylation was analysed by blotting with streptavidin-HRP. (Right panel) Coomassie Brilliant Blue staining shows the indicated amounts of used purified proteins. (B-D) Histones are not O-GlcNAcylated *in vitro* by OGT. (B) Purified proteins analysed by Coomassie Brilliant Blue or silver staining as indicated. (Left panel) Relative quantification of purified recombinant His-OGT and GST-HCF-1-N to known amounts of BSA. (Middle and Right panels) Integrity of Flag-H2A-purified mammalian nucleosomes and recombinant His-hH2B. (C) *In vitro* O-GlcNAcylation reaction of the purified recombinant His-hH2B. GST-HCF-1-N and recombinant His-hH2B were incubated with increasing amounts of recombinant His-OGT for 4 hours. O-GlcNAcylation was detected by western blotting using the anti-O-GlcNAc antibody (RL2). (D) *In vitro* O-GlcNAcylation reaction of the purified mammalian nucleosomes by OGT. GST-HCF-1-N and nucleosomes were incubated in the absence or presence of His-OGT for 11 hours. The O-GlcNAcylation was detected as in (C). kDa; Molecular weight marker in Kilodalton.

Previous studies reported that histones can be modified by OGT *in vitro* [133]. Thus, we performed *in vitro* O-GlcNAcylation reactions using purified recombinant human His-hH2B and purified mammalian nucleosomes. As a positive control, we also used purified recombinant GST-HCF-1N (for N-Terminal HCF-1) [199] as this domain is a well-established substrate of OGT [95, 98, 199]. The relative quantity and integrity of the purified proteins were assessed by Coomassie Brilliant Blue staining or silver staining as indicated (Figure 18B). As shown in Figures 18C and 18D, we detected a strong O-GlcNAcylation of HCF-1-N, but not of the recombinant His-hH2B (Figure 18C) or nucleosomal histones (Figure 18D).

In summary, using various approaches, we were unable to detect histone O-GlcNAcylation. Thus, our study provides strong evidence that histone O-GlcNAcylation, if occurring, must be present at levels below detection limits of commonly available tools, while O-GlcNAcylation of other known proteins including HCF-1 and TET2 can be observed. We emphasize that histones are hundreds- to thousands-folds more abundant than the majority of cellular proteins and their modifications, even in relatively low abundance, are in general easily monitored. On the other hand, detection of histone modifications can be prone to false-positive signals, especially when analyzing a large amount of proteins by immunoblotting.

2.4 Acknowledgements

We thank Haider Dar and Diana Adjaoud for technical assistance. This work was supported by grants from the Canadian Institutes of Health Research (CIHR) (MOP-115132) and the Natural Sciences and Engineering Research Council of Canada (NSERC) (355814-2010) to E.B.A and (435636-2013) to H.W.. E.B.A. is a scholar of the Fonds de la Recherche du Québec - Santé (FRQ-S) and the CIHR. H.W is a scholar of the FRQ-S, J.G. has a M.Sc.

scholarship from the FRQ-S. The Proteomics facility at The Institute for Research in Immunology and Cancer (IRIC) receives infrastructure support from IRICoR, the Canadian Foundation for Innovation, and the Fonds de Recherche du Québec- Santé (FRQS).

2.5 Material & Methods

Plasmids and mutagenesis

The cDNA of human of OGT and TET2 were cloned from HeLa total RNA by reverse transcription and inserted into pENTR D-Topo plasmid (Life Technologies). Expression construct of Myc-TET2 was generated by recombination using LR clonase kit (Life Technologies) into pDEST-Myc construct. pCGN-HCF-1 FL was previously described [200, 201]. Myc-OGT, Myc- OGT D925A catalytic inactive mutant (Myc-OGT CD) were also previously described [95] GFP-OGT and GFP-OGT CD were generated by recombination into pDEST-GFP expression construct. pcDNA3-Flag-H2A and pcDNA3-Flag-H2B were obtained from Dr. Moshe Oren [202]. H2B and H2A were generated using gene synthesis (BioBasic) and then subcloned into modified pENTR D-Topo plasmid. H2B S112A construct was generated by site direct mutagenesis using Q5 High-Fidelity DNA Polymerase. The Primers used are: Forward primer: CACGCCGTG**G**CGGAGGGCACCAAGGCCGTCA; Reverse primer: TGCCCTCCG**C**CACGGCGTGCTTGGCCAGCTC. HCF-1N was amplified from pCGN-HCF-1 FL and inserted into pENTR D-Topo plasmid. The T antigen NLS coding sequence was added in the primers. His-OGT was generated by subcloning the OGT cDNA into pET30a+ vector. Expression constructs of H2B and H2B S112A were generated by recombination using LR clonase kit into pDEST-Flag or pDEST-6xHis constructs. Expression constructs of H2B and HCF-1N were generated by recombination into pDEST-Flag or pDEST-GST constructs. All DNA constructs were sequenced.

Immunoblotting and antibodies.

Total cell lysates were prepared by harvesting cells with buffer containing 25 mM Tris-HCl pH 7.3 and 1% sodium dodecyl sulfate (SDS). Cell extracts were boiled at 95°C for 10 min and sonicated. Quantification of total proteins was conducted using the bicinchoninic acid (BCA) assay [203]. Total cell extracts as well as chromatin fractions and

immunoprecipitation samples were diluted in 2X or 4X Laemmli buffer**.** SDS-PAGE and immunoblotting were conducted according to standard procedures. The band signals were acquired with a LAS-3000 LCD camera coupled to MultiGauge software (Fuji, Stamford, CT, USA).

Mouse monoclonal anti-BAP1 (C4, sc-28383), rabbit polyclonal anti-YY1 (H414, sc-1703), rabbit polyclonal anti-OGT (H300, sc-32921), mouse monoclonal anti-Tubulin (B-5-1-2, sc-SC-23948), were from Santa Cruz. Rabbit polyclonal anti-HCF-1 (A301-400A) was from Bethyl Laboratories. Mouse monoclonal anti-Flag (M2) was from Sigma-Aldrich. Mouse monoclonal anti-MYC (9E10) was from Covance. Rabbit polyclonal anti-H2B K120ub (D11 XP) was from Cell Signaling. Rabbit polyclonal anti-H2B S112 O-GlcNAc (ab130951), rabbit polyclonal anti-H2A (ab18255) Rabbit polyclonal anti-H3 (ab1791) and mouse monoclonal anti-O-Linked *N*-acetylglucosamine (RL2, ab2739) were from Abcam. The mouse monoclonal anti-O-Linked *N*-acetylglucosamine (CTD110.6) was kindly provided by Dr. Gerald Hart [204]. Mouse monoclonal anti-β-Actin (MAB1501, clone C4) was from Millipore. Anti-rhodamine (IgM) was a generous gift from Dr. Li-Huei Tsai. Peroxidase Affini-Pure Goat anti-mouse IgM μ chain specific secondary antibody was from Jackson Laboratories.

Cell culture and cell transfection

U2OS osteosarcoma, HeLa, human embryonic kidney HEK293T, 3T3-L1 mouse preadipocytes, C2C12 mouse myoblasts, mouse embryonic fibroblasts (MEF) cell lines were grown in Dulbecco's modified Eagle's medium (DMEM) supplemented with 10 % of foetal bovine serum (FBS), L-glutamine and penicillin/streptomycin. Multiple myeloma cell lines (JJN-3, RPMI-8226, NCI-H292) were cultured in RPMI-1640 medium supplemented with 10 % of foetal bovine serum (FBS), L-glutamine and penicillin/streptomycin. Mouse embryonic stem cells (mESCs) were maintained in DMEM medium supplemented with 15% of embryonic stem cells qualified FBS (Gibco), L-glutamine, penicillin/streptomycin, 0.1 mM β-mercaptoethanol, 0.1 mM MEM (Non-essential amino acids), 1 mM sodium pyruvate and 1,000 U/ml of leukemia inhibitory factor (LIF) (Life technologies).

HeLa or HEK293T cells were treated with 100 μM of PUGNAc or equal volume of DMSO for 0, 9 and 24 hours and were subjected to sub-cellular fractionation (soluble and

chromatin) or histone extraction. HEK293T cells were transfected with mammalian expressing vectors using polyethylenimine (PEI) (Sigma-Aldrich). Three days post-transfection, cells were harvested for immunoblotting using total cell extracts or following cellular fractionation and histones extraction. Prior to immunoblotting, histones were also immunoprecipitated using anti-Flag antibody following denaturation of cell extracts. HeLa or U2OS cells were transfected using Lipofectamine 2000 (Life technologies) with 200 pmol of either ON-TARGET plus Non-targeting pool (D-001810-10-50) or ON-TARGET plus SMARTpool OGT (L-019111-00-0050) (Thermo Scientific, Dharmacon). Cells were transfected in a serum-free DMEM medium for 16 hours, then changed with DMEM complemented with 5 % FBS, 1 % Glutamine and 1 % Penicillin-Streptomycin and 8 hours later, cells were transfected again as described above. Three days following the first transfection, cells were harvested in PBS and soluble and chromatin extractions were conducted and used for immunoblotting.

Histone and chromatin extraction

For histone extraction, HEK293T cells were transfected with Flag-H2A or Flag-H2B with or without Myc-OGT, Myc-OGT CD, Myc-TET2 or with the combination of Myc-OGT and Myc-TET2 and harvested three days post-transfection. For high salt/detergent chromatin extraction, cells were lysed in 300 mM NaCl, 1% NP-40, 2 µM PUGNAc, 1 mM PMSF and 1 X protease inhibitors (Sigma). Samples were kept on ice for 15 min and then centrifuged at 6,000 rpm for 10 min. The supernatant was kept as the soluble fraction for western blotting analysis. The pellet was washed 2 times with the previous buffer and resuspended in 1% SDS for protein quantification. For the histones acid extraction, cells were lysed in 50 mM Tris-HCl pH 7.4, 300 mM NaCl, 2 mM EDTA and 2 µM PUGNAc. The lysate was centrifuged at 6,000 rpm for 10 min and the supernatant was kept as the soluble fraction. The pellet was washed 2 times with the same buffer and treated with 0.2 N HCl (1 volume of buffer for 1 volume 0.4 HCl) for 1 hour on ice. After centrifugation at 14,000 rpm for 5 min, the supernatant containing histones was neutralized by adding equal volume of 100 mM Tris-HCl pH 8.8. The pellet was also resuspended in 1% SDS. To quantify proteins, part of the histones fraction was precipitated using 100% acetone at -20°C for 2 hours, centrifuged at 14,000 rpm for 10 min and resuspended in 1% SDS. Proteins were then quantified using the BCA assay. For chromatin extraction, the cell pellet was resuspended in 50 mM Tris-HCl pH 7.3, 300 mM

NaCl, 5 mM EDTA, 1% Triton, 2 μM PUGNAc, 1X protease inhibitors (Sigma) and 1 mM PMSF and kept on ice for 30 min. The chromatin was pelleted by centrifugation at 10,000 rpm for 10 min at 4^0C, the supernatant was kept (soluble fraction) and the chromatin pellet was resuspended in 25 mM Tris-HCl pH 7.3 and 1 % SDS. Both fractions were quantified using the BCA protein quantification method.

Wheat Germ Agglutinin lectin Pull-Down

HEK293T cells were either treated with 100 μM PUGNAc or DMSO for 24 hours. Cells were then harvested in 1X PBS and the cell pellet was lysed with 0.25 M sucrose, 3 mM $CaCl_2$, 1 mM Tris-HCl pH 8.0, 0.5 % triton, 2 μM PUGNAc and 1X protease inhibitors (Sigma). The chromatin was pelleted by centrifugation at 3,900 rpm for 5 minutes at 4°C and the supernatant was kept (soluble fraction). Next, the pellet was washed with 300 mM NaCl, 5 mM $MgCl_2$, 1% Triton, 50 mM Tris-HCl pH 8.0, 5 mM DTT and 2 μM PUGNAc and centrifuged at 3,900 rpm for 5 min at 4°C. Supernatant was discarded and the pellet was very quickly resuspended in 3 volumes of acid extraction buffer containing 0.5 M HCl, 10% glycerol and 0.1 M β-mercaptoethanol and left on ice for 30 min. The sample was centrifuged at 14,000 rpm for 5 min at 4°C, the supernatant containing the histones was transferred in a new tube and 10 volumes of acetone were added to both the pellet (chromatin-associated proteins) and the supernatant (histones) fractions and were left at -20 °C overnight. The next day, protein precipitates were pelleted at 14,000 rpm for 1 hour at 4°C, resuspended in 25 mM Tris-HCl pH7.3 and 1 % SDS, sonicated and diluted in 10 volumes of EB300 Buffer containing 50 mM Tris-HCl pH7.5, 300 mM NaCl, 5 mM EDTA, 1% Triton X-100, 1X protease inhibitors (Sigma), 1 mM PMSF, 1 mM DTT and 2 μM PUGNAc. The samples were incubated for 2 hours with WGA lectin resin (Vector Laboratories, #AL-1023) or agarose beads, washed with EB300 buffer and eluted with 500 mM *N*-acetylglucosamine. Sample were then analysed by western blotting.

Immunoprecipitation

For histone immunoprecipitation following denaturation, HEK293T cells were transfected with Flag-H2A or Flag-H2B with pcDNA3 empty vector, Myc-OGT or Myc-OGt CD, Myc-TET2 or the combination of Myc-OGT with Myc-TET2 using Polyethylenimine

(PEI). Three days post-transfection, cells were harvested and the cell pellets were lysed in 20 mM Tris-HCl pH 8.0, 600 mM NaCl, 0.5% NP-40, 0.5% SDS, 0.5% sodium deoxycholate, 1 mM EDTA and 2 μM PUGNAc. Samples were sonicated and centrifuged at 14,000 rpm for 10 min. The lysate was then diluted in 5 volumes of 50 mM Tris-HCl pH 7.4, 2 mM EDTA and 100 mM NaCl. For TET2 and HCF-1 immunoprecipitation, HEK293T cells were transfected with Myc-TET2 or HA-HCF-1 FL with and without GFP-OGT or GFP-OGT CD. Three days post-transfection, cells were harvested to perform denaturing immunoprecipitation. Briefly cells pellets were lysed using 300 mM NaCl containing buffer (50 mM Tris-HCl pH 7.5, 300 mM NaCl, 1% Triton, 1% SDS, 10 mM NaF, 5 mM EDTA 1 mM PMSF, 2 μM PUGNAc and 1X protease inhibitors (Sigma)). After boiling for 3 min in the lysis buffer, cell lysate was sonicated and samples were diluted 10 folds with the same buffer but without SDS prior to immunoprecititation using anti-Myc or anti-HA antibodies. For mutant histones, HEK293T cells were transfected with PEI with either FLAG-H2B or FLAG-H2B S112A. Three days post-transfection, cells were harvested for denaturing immunoprecipitation in 25 mM Tris pH 7.3 and 1.5 % SDS. Next, suspensions were diluted 10 times with dilution buffer containing 50 mM Tris-HCl pH7.5, 100 mM NaCl, 1% Triton, 1 mM EDTA, 1 mM DTT, 1 mM PMSF, 1X protease inhibitors (Sigma), 2 μM PUGNAc and 20 mM N-Ethylmaleimide (NEM, Sigma). Suspensions were mixed with anti-FLAG M2 resin (Sigma Aldrich #A2220) overnight at 4 ^{0}C. Next day, beads were washed 5 times with the dilution buffer. Proteins were then eluted from the beads by adding Laemmli Buffer 2X and analysed by western blotting.

Recombinant proteins

pDEST-6xHis-H2B, pDEST-6xHis-H2BS112A, pDEST-GST-HCF-1-N and pET30a+ OGT were transformed into RIL bacteria. Following induction with 400 μM IPTG, recombinant proteins were purified either under native or denaturing conditions. For the denaturing immunopurification, the bacterial pellets were lysed in 50 mM Tris-HCl pH 8, 8 M Urea and 3 mM DTT and left on ice for 30 min. After incubation, suspensions were sonicated and centrifuged at 16,000 rpm for 20 min. Supernatants were incubated with Ni-NTA Agarose resin (Invitrogen #R901-15) overnight at 4 ^{0}C and the resin was then washed with 50 mM Tris-HCl pH 8.0, 500 mM NaCl, 3 mM DTT and 20 mM imidazole and transferred into a Bio-Spin Disposable Chromatography columns (Bio Rad #732-6008). Proteins were eluted with

200 mM Imidazole. For the native purification of His-H2B, His-H2B S112A and His-OGT, cell pellets were lysed in 50 mM Tris pH 8, 500 mM NaCl and 3 mM DTT, 1 mM PMSF, 1X protease inhibitors (Sigma) and left on ice for 30 min. After incubation and sonication, the purified proteins were obtained as described above except for His-OGT which was kept on the Ni-NTA Agarose resin in order to use it for the *in-vitro* O-GlcNAcylation reaction. The OGT Ni-NTA Agarose resin beads were washed 6 times and kept in 50 mM Tris-HCl pH 7.5, 12.5 mM $MgCl_2$, 3 mM DTT, 10% glycerol, 1 mM PMSF, 1X protease inhibitors (Sigma). The induction of GST-H2A expression in bacteria was done in the same manner as indicated above. Pellets of cells were lysed on ice in 50 mM Tris-HCl pH 8, 150 mM NaCl, 1 mM EDTA, 1 % Triton, and 1 mM PMSF, 1 mM DTT, 1X protease inhibitors (Sigma). The lysates were sonicated, centrifuged at 16,000 rpm for 20 min and supernatants were incubated with GSH-Agarose (Sigma Aldrich #A8580) overnight at 4 ^{0}C. Then, the resin was washed with 50 mM Tris-HCl pH 7.5, 150 mM NaCl, 1 mM EDTA, 0.1% Tween20, 1 mM PMSF, 200 µM DTT and 1X protease inhibitors (Sigma)). Proteins were eluted with the same buffer containing 250 mM reduced gluthatione. GST-HCF-1-N was purified in the same manner as GST-H2A. Elutions of His-H2B, His-H2B S112A, GST-H2A and GST-HCF-1N were loaded on SDS-PAGE for Coomassie Brilliant Blue staining using BSA for relative quantification.

Purification of the nucleosomes

For mammalian nucleosomes purification, HEK293T cells were transfected with 7 µg of pCDNA-Flag-H2A using PEI in serum free media. Three days post-transfection, cells were harvested and chromatin fraction extraction and nucleosomes were purified using anti-Flag beads as previously described [205]. For yeast Flag-H2B nucleosomes purification, 2 liters of cells expressing Flag-H2B were grown under standard conditions and 4 grams of cell pellet were used for the purification. Briefly, cells were resuspended in the SP Buffer (20 mM HEPES 7.4, 1.2 M sorbitol, 10 mM DTT) supplemented with 5 mg/ml of Zymolyase 20T. When the spheroplasting is completed, the cell pellet is washed again with the SP buffer and then resuspended in the Buffer L (20 mM HEPES 7.4, 18% Ficoll 400, 20 mM KCl, 5 mM $MgCl_2$, 1 mM EDTA, protease inhibitors (1 µg/ml leupeptin, pepstatin, aprotinin), 3 mM

DTT, 1 mM PMSF) prior to the dounce homogenization. The extract was then diluted with the Buffer S (buffer L supplemented with 2.4 M sorbitol instead of Ficoll) and chromatin fraction was recovered by centrifugation at 11,000 rpm for 20 min. The chromatin pellet was washed with the IP buffer (20 mM HEPES 7.6, 150 mM KCl, 5% glycerol, 5 mM $MgCl_2$, 1 mM $CaCl_2$, 0.1% NP-40, protease inhibitors, 1 mM PMSF prior to the MNase treatment. After MNase treatment (15KU/ml for 30 min at room temperature), the reaction was stopped with 1 mM EDTA and 5 mM EGTA. Following centrifugation at 20,000g for 5 min at 4°C, the soluble chromatin fraction was incubated 1 hour at 4°C with anti-Flag M2 beads. The beads were washed four times with the IP2 buffer (same as IP buffer but with 1 mM EDTA, 1 mM EGTA and without $CaCl_2$). Bound nucleosomes were then eluted with 200 µg/ml of Flag peptides (Biobasic Inc.)

Click-it chemistry

HeLa cells were harvested and acid extraction was performed to purify histones as described for the WGA pull-down. Following acetone precipitation the histones were resuspended in 1% SDS, 20mM HEPES pH 7.9 and quantified using the BCA assay. The GalNAz labeling reaction was performed following the manufacturer's instructions using the Click-iT® GalNAz metabolic glycoprotein labeling reagent kit (Life Technologies). α-crystalline was included as a positive control. Following labeling of histones and α-crystalline, the detection was carried out with the Click-iT® Biotin Glycoprotein Detection Kit (Life Technologies) and the reaction was loaded on SDS-PAGE for blotting analysis using streptavidin-HRP (Cell Signaling #3999S) affinity detection.

In Purified GST-HCF-1-N (0.2 µg) and recombinant His-H2B (0.4 µg) were incubated with purified His-OGT (0.2 to 0.5 µg) in the presence of UDP-GlcNAc (1 mM) at 37°C overnight for 4 or 11 hours. The reaction was carried out in 50 mM Tris-HCl pH 7.5 containing 12.5 mM $MgCl_2$ and 3 mM DTT. Purified nucleosomes were also included in the O-GlcNAcylation reaction as described above. The reaction was stopped by adding Laemmli buffer and analysed by immunoblotting.

Synchronization and cell cycle analysis

U2OS cells were synchronized at the G1/S border using the method of thymidine (2 mM) double block as previously described [189]. Cells were then released into new media to follow the progression through S and G2/M phases. U2OS cells were also arrested in late G2 by treating them with 10 μM of the CDK1 inhibitor RO-3306 for 24 hours [190]. Cell cycle analysis was carried out as described [189].

Cell starvation.

C2C12 cells were incubated for 6 hours in the Hanks Balanced Salt Solution (HBSS) medium completed with 10 mM HEPES pH 7.5 and penicillin/streptomycin. After 4 hours of treatment, a separate plate dish of cells was replenished with fresh media and released for another 2 hours. Cells pellets were harvested at the indicated times for chromatin extraction.

Mass spectrometry analysis

Reduction of histone and HCF-1 samples was performed by adding 5 mM DTT in 50 mM ammonium bicarbonate. Alkylation was performed with chloroacetamide 50 mM with ammonium bicarbonate 50 mM. The digestion with trypsin was performed for 8 h at 37°C. Samples were loaded and separated on a homemade reversed-phase column (150 μm i.d. x 150 mm) with a 106-min gradient from 0–40% acetonitrile (0.2% FA) and a 600 nl/min flow rate on an Easy nLC-1000 (Thermo Fisher Scientific) connected to an LTQ-Orbitrap Fusion (Thermo Fisher Scientific). Each full MS spectrum acquired with a 70,000 resolution was followed by 10 MS/MS spectra, where the 10 most abundant multiply charged ions were selected for MS/MS sequencing. Tandem MS experiments were performed using high-energy C-trap dissociation (HCD) and electron transfer dissociation (ETD) acquired in the Orbitrap. Peaks were identified using a Peaks 7.0 (Bioinformatics Solution Inc.) and peptide sequences were blasted against the human Uniprot database (74,530 sequences). Tolerance was set at 10 ppm for precursor and 0.01 Da for fragment ions during data processing and with carbamidomethylation (C), oxidation (M), deamidation (NQ), and Hex-N-acylation (ST) as variable modifications.

2.6 Supplemental Figures and Tables

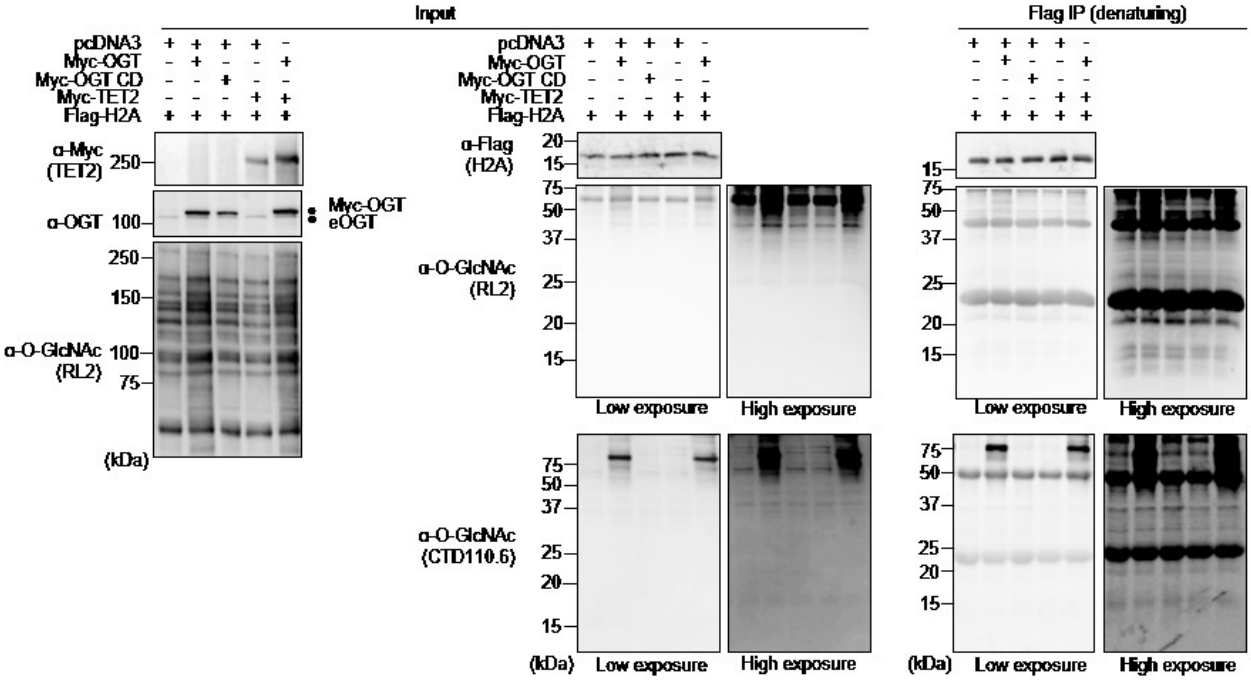

Figure 2.S1 Undetectable O-GlcNAcylation of histone H2A. HEK293T cells were transfected with Flag-H2A along with either pcDNA3 empty vector, Myc-OGT, Myc-OGT catalytic dead (MYC-OGT CD) or Myc-TET2, as well as the combination of Myc-OGT with Myc-TET2. Three days post-transfection, cells were harvested and analysed for Flag-H2A O-GlcNAcylation as conducted for Flag-H2B (see Fig.1). Flag immunoprecipitation (Flag-IP) of exogenous H2A was conducted following sample denaturation. Dots indicate Myc-OGT and endogenous OGT (eOGT). kDa; Molecular weight marker in Kilodalton.

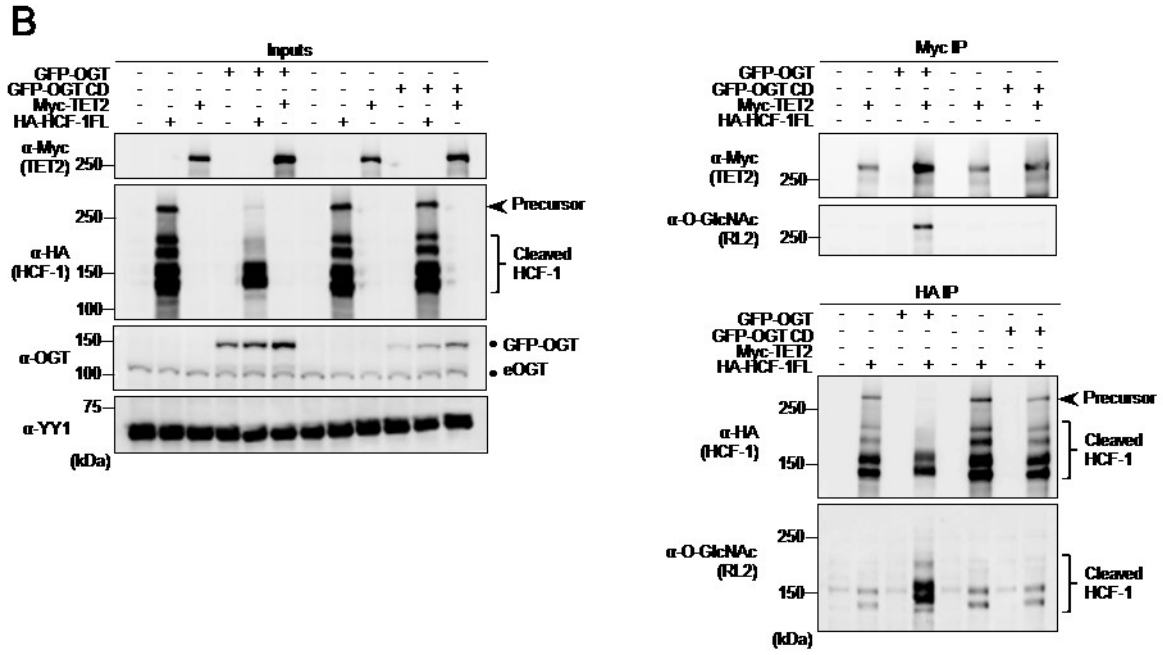

Figure 2.S2 OGT O-GlcNAcylates both TET2 and HCF-1 and Modulates HCF-1 cleavage. HEK293T **c**ells were transfected with either GFP-OGT or GFP-OGT catalytic dead (CD) in the presence of HA-HCF-1 full length (FL) or Myc-TET2 expression vectors. Three days post-transfection, cells were harvested and total cell lysates were subjected to immunoprecipitation (IP), following sample denaturation, using anti-Myc or anti-HA antibodies to purify TET2 and HCF-1 respectively. Total cell lysates (Input fractions) as well as immunoprecipitations were subjected to western blotting analysis using the indicated antibodies. Arrow indicates the full length (precursor) form of HCF-1 and brace indicates the cleaved forms of HCF-1. Dots indicate GFP-OGT and endogenous OGT (eOGT). kDa; Molecular weight marker in Kilodalton.

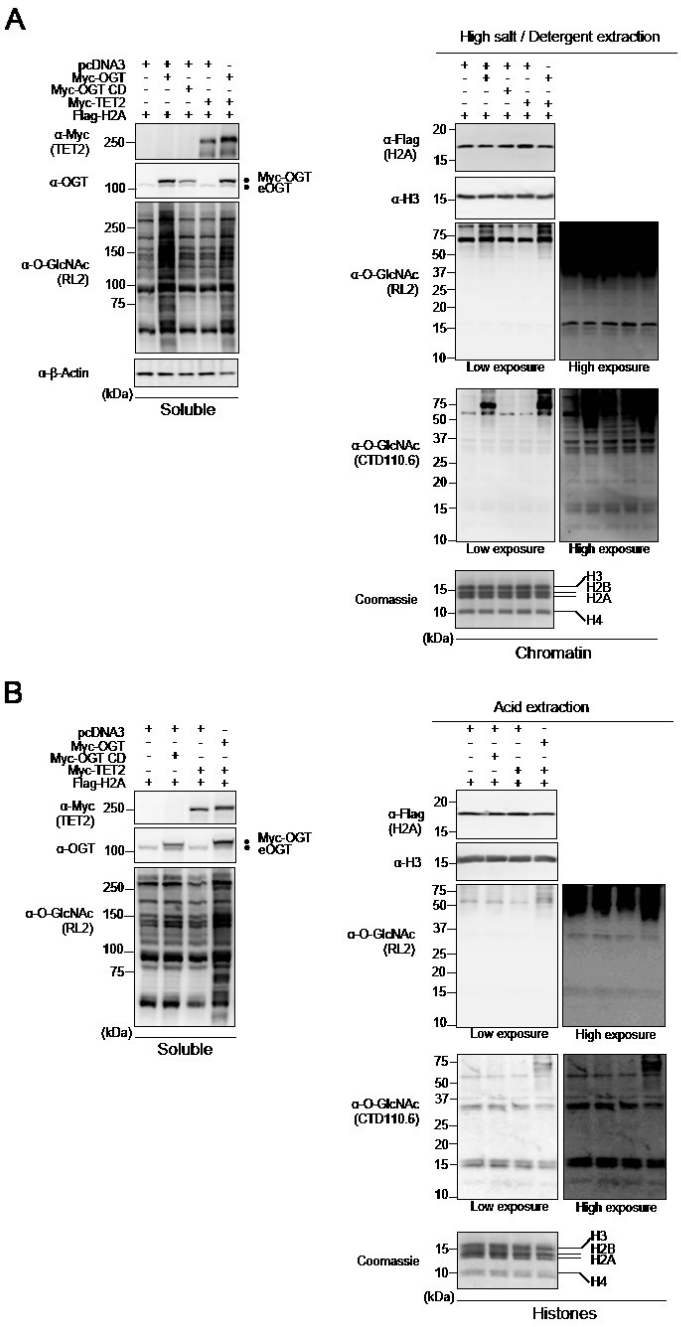

Figure 2.S3 Undetectable O-GlcNAcylation of endogenous histones. HEK293T cells were transfected as in Supplemental Fig.1. Three days post-transfection, cells pellets were collected for subsequent high salt / high detergent extraction as well as histones acid extraction and cellular extracts were analysed by western blotting with the indicated antibodies. (**A**) Chromatin high salt extraction. (Left) Soluble fraction showing global increase of O-GlcNAcylation following OGT overexpression. (Right) Detection of O-GlcNAcylation using RL2 and CTD110.6 antibodies on chromatin fraction. (**B**) Histone acid extraction showing (Left) the soluble fraction and global O-GlcNAcylation levels and (Right) the histone fraction detected with both O-GlcNAc antibodies. β-Actin and histone H3 were used as loading controls. Coomassie Brilliant Blue staining indicates abundance of histones loaded. Dots indicate Myc-OGT and endogenous OGT (eOGT). kDa; Molecular weight marker in Kilodalton.

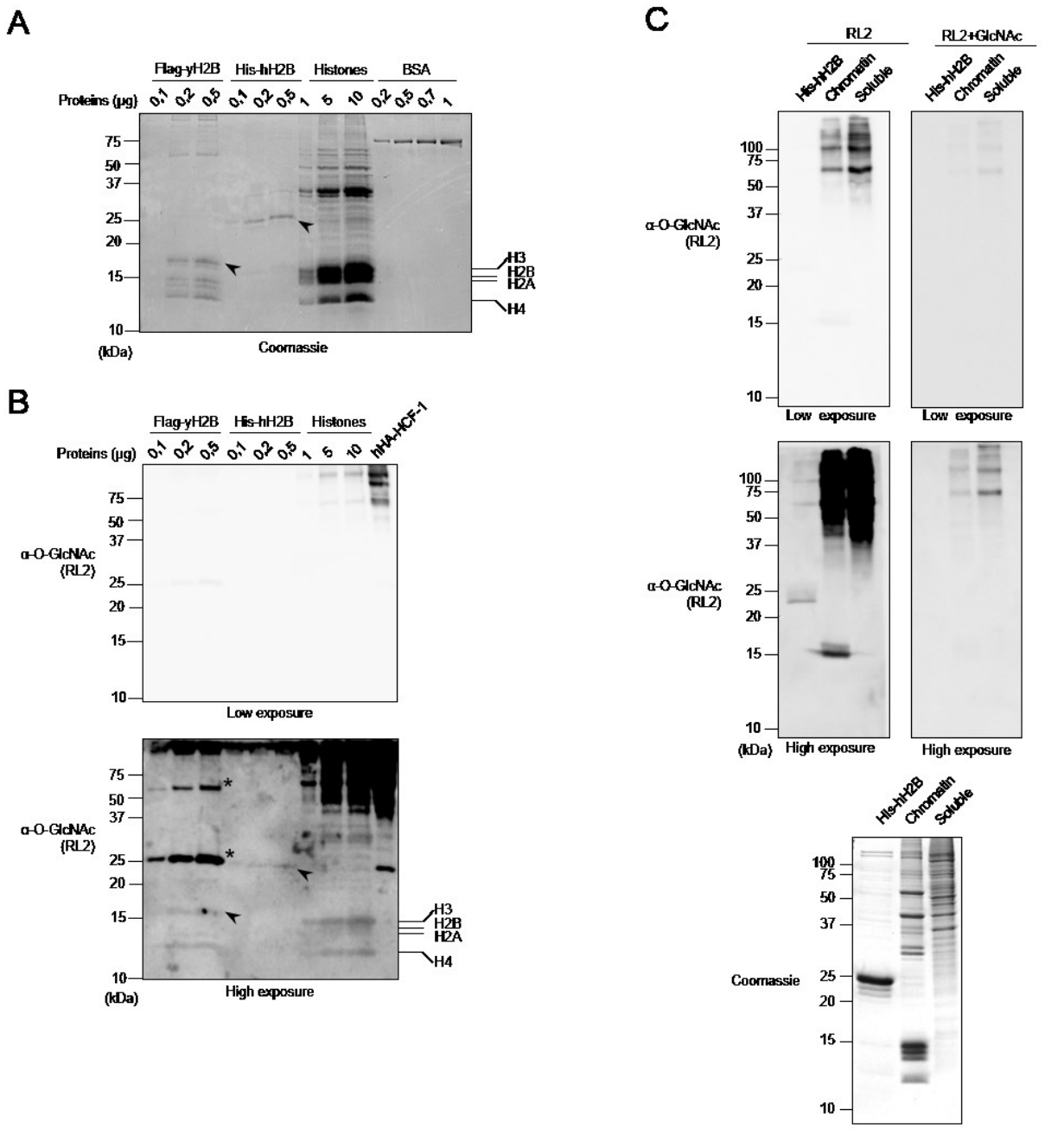

Figure 2.S4 Detection of background immunoblotting of mammalian, yeast or recombinant histones (A) Coomassie Brilliant Blue staining showing molecular weight and relative quantification of purified recombinant yeast Flag-H2B (Flag-yH2B), human His-H2B (His-hH2B) and acid extracted histones purified from HeLa cells relative to bovine serum albumin (BSA). (B) Increasing amounts of recombinant Flag-yH2B, His-hH2B and acid extracted histones from HeLa cells quantified in (A) were analysed by western blot using α-O-GlcNAc (RL2) antibody. Purified human HCF-1(hHA-HCF-1) from HEK293T cells was used as a control for RL2 detection. Lines indicate purified endogenous histones from HeLa cells and Flag-yH2B. Arrows indicate Flag-yH2B and His-hH2B position. Asterisks indicate non-specific signal from the heavy and light chains of Flag antibody respectively. (C) N-Acetyl-D-Glucosamine competition with RL2 antibody. RL2 antibody was incubated with 1M of N-acetylglucosamine (GlcNAc) for 1 hour. Antibody mixture was then used to immunoblot recombinant human His-hH2B, chromatin and soluble fractions from U2OS cells. Coomassie Brilliant Blue staining was used as a loading control. kDa; Molecular weight marker in Kilodalton.

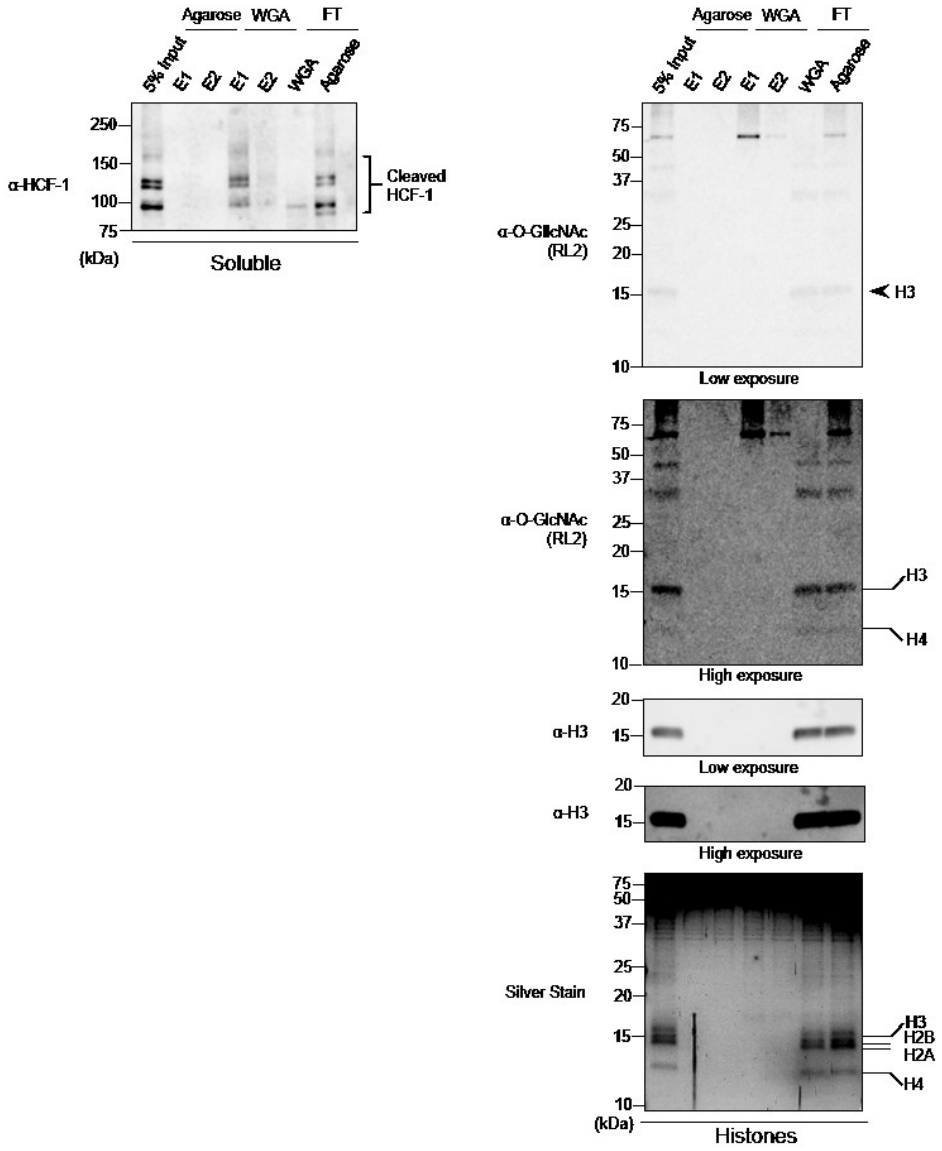

Figure 2.S5 The core histones are not enriched by WGA lectin resin in conditions that ensure complete HCF-1 depletion from extracts. HeLa cells were harvested and acid extraction of histones was performed. The indicated soluble (Left panel) and histone fractions (Right panel) were incubated overnight with the agarose bound WGA lectin resin or with the agarose resin to control for non-specific binding. The flow through (FT) was kept and the proteins were eluted from the resins (E1 and E2) with N-acetylglucosamine (GlcNAc). Soluble fraction showing depletion of HCF-1 on the WGA lectin resin (Left panel) . Western blot and silver stain analysis of the collected elutions revealed no interaction between the core histones and the WGA lectin resin (Right panel). Arrows and lines indicate histones molecular weight. kDa; Molecular marker in Kilodalton.

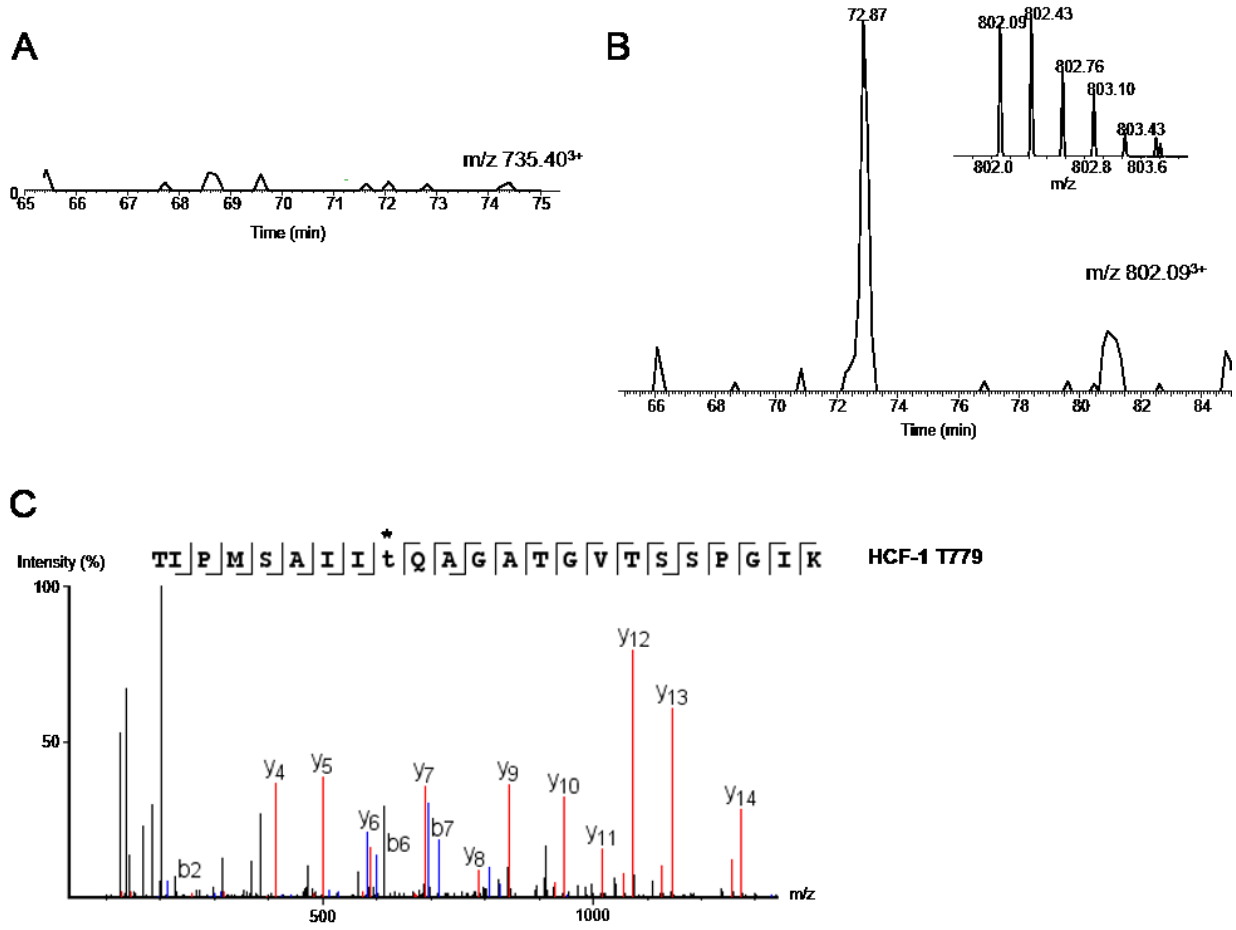

Figure 2.S6 HCD MS/MS spectra for HCF-1 O-GlcNAcylated peptide containing T779 modification site. (A) extracted ion chromatogram for the HCF-1 peptide TIPMSAIITQAGATGVTSSPGIK at m/z 735.40^{2+} showing that the peptide was not detected. (B) Extracted ion chromatogram for the HCF-1 peptide TIPMSAIIT(GlcNAc)QAGATGVTSSPGIK at m/z 802.09^{2+} with the corresponding MS spectrum at 72.87 min. (C) MS/MS spectrum showing that the Thr9 indicated with the star is modified with the GlcNAc moiety.

Table 1. Identification of O-GlcNAcylation sites on HCF-1

m/z	PTM sites of HCF-1	Peptide Sequence	References	ppm
927.77	T575	IPPSSAPTVLSVPAGTtVKTMAVTPGTTTLPATVK	Novel	1.07
896.47	T588	TMAVTPGTTtLPATVK	Novel	-2.9
751.89	S620?/S622	TAAAQVGTsVsSATNTSTRPIITVHK	Ref. 47, 48, 50	-0.88
1,002.19	T625?/S628?	TAAAQVGTSVSSAtNTsTRPIITVHK	Ref. 51	0.12
846.12	T640?/T642	SGtVtVAQQAQVVTTVVGGVTK	Novel	0.3
778.42	T654	SGTVTVAQQAQVVtTVVGGVTK	Novel	0.67
1,084.85	T694	VMSVVQTKPVQtSAVTGQASTGPVTQIIQTKGPLPAG TILK	Novel	-1.9
847.70	T698	VMSVVQTKPVQTSAVtGQASTGPVTQIIQTKGPLPAG TILK	Novel	-2.9
1,001.94	T738?/S742	LVTSADGKPTTIITtTQAsGAGTKPTILGISSVSPSTTK PGTTTIIK	Novel	0.04
802.09	T771	tIPMSAIITQAGATGVTSSPGIK	Ref. 26, 27	1.0
1,187.97	S775?	TIPMsAIItQAGATGVTSSPGIKSPITIITTK	Novel	-3.7
802.09	T779	TIPMSAIItQAGATGVTSSPGIK	Ref. 26, 27, 47, 48, 50	0.32
1,141.36	T784	TIPMSAIItQAGAtGVTSSPGIKSPITIITTKVMTSGTGA PAK	Novel	1.2
726.40	T800	SPITIItTKVMTSGTGAPAK	Ref. 26, 27	-0.2
1,089.09	T801	SPITIITtKVMTSGTGAPAK	Ref. 47, 48, 49, 50	-0.2
742.45	T858	LVtPVTVSAVKPAVTTLVVK	Novel	0.11

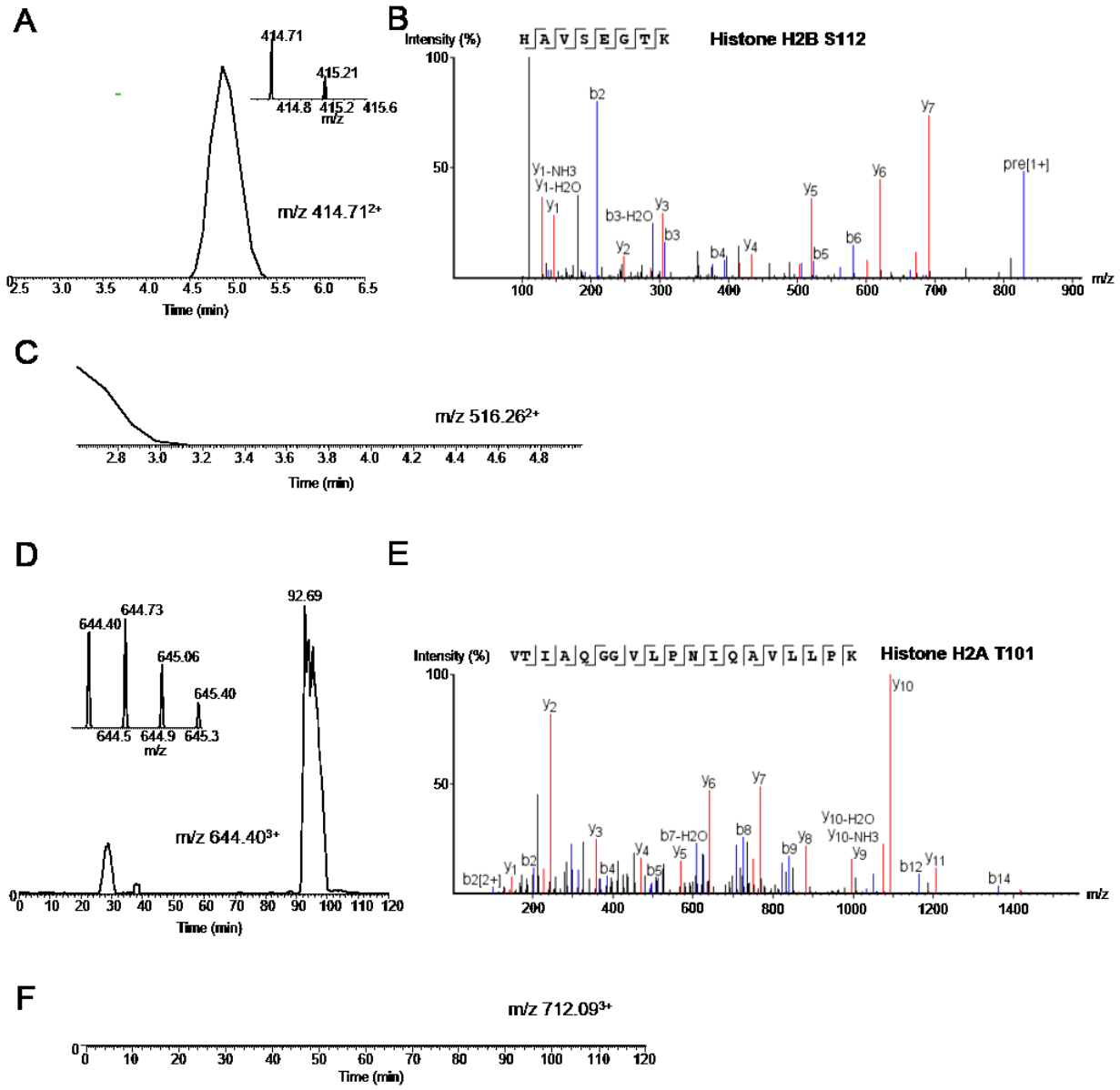

Figure 2.S7. HCD MS/MS spectra for H2B and H2A peptides containing Ser112 and Thr101 respectively.(A-C) HCD MS/MS spectra for H2B. Extracted ion chromatogram for the H2B peptide HAVSEGTK at m/z 414.712+ showing that the peptide was detected (A) along with the corresponding MS spectrum at 4.9 min and its MS/MS spectrum (B). (C) Extracted ion Chromatogram for m/z 516,262+ corresponding to the expected peptide HAVSEGTK with a GlcNAC moiety. The absence of signal at m/z 516,262+ indicates that the corresponding glycopeptide was not detected. (D-F) HCD MS/MS spectra for H2A. Extracted ion chromatogram for the H2A peptide VTIAQGGVLPNIQAVLLPK at m/z 644.403+ showing that the peptide was detected (D) along with the corresponding MS spectrum at 92.69 min and its MS/MS spectrum (E). (F) Extracted ion Chromatogram at m/z 712.093+ corresponding to the expected peptide VTIAQGGVLPNIQAVLLPK bearing a GlcNAC moiety. The absence of a signal at m/z 712.093+ indicates that the corresponding glycopeptide was not detected.

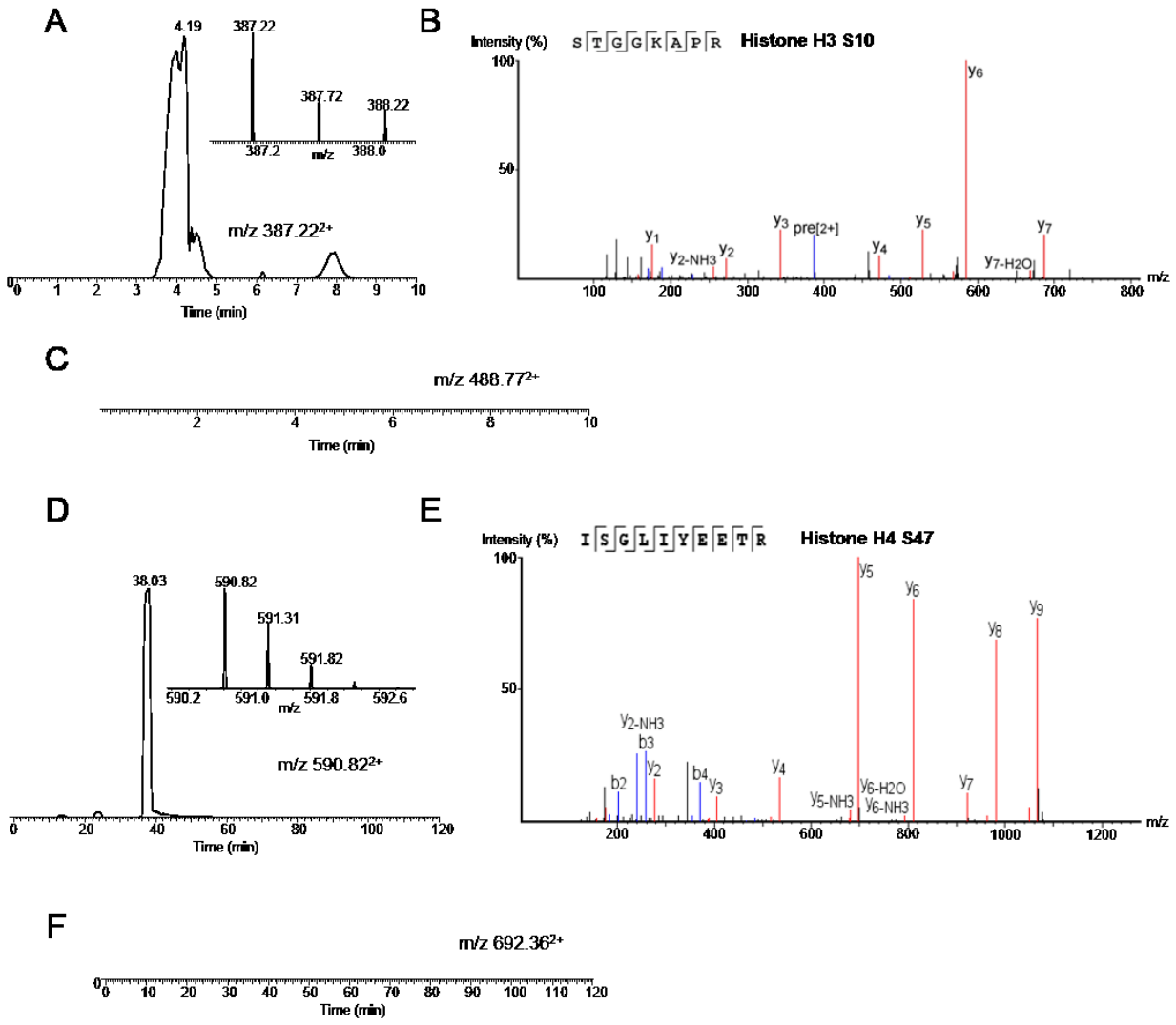

Figure 2.S8. HCD MS/MS spectra for H3 and H4 peptides containing Ser10 and Ser47 respectively.(A-C) HCD MS/MS spectra for H3. Extracted ion chromatogram for the H3 peptide STGGKAPR at m/z 387.222+ showing that the peptide was detected as evidenced from its (A) corresponding MS spectrum at 4.01 min and its MS/MS spectrum (B). (C) Extracted ion Chromatogram for the expected peptide STGGKAPR bearing a GlcNAC moiety at m/z 488.773+, the absence of a signal indicates that the corresponding glycopeptide was not detected. (D-F) HCD MS/MS spectra for H4. Extracted ion chromatogram for the H4 peptide ISGLIYEETR at m/z 590.822+ showing that the peptide was detected as evidenced from the corresponding (D) MS spectrum at 39.03 min and its MS/MS spectrum (E). (F) Extracted ion Chromatogram for the expected peptide ISGLIYEETR bearing a GlcNAC moiety at m/z 692.362+, the absence of signal indicates that the corresponding glycopeptide was not detected.

CHAPITRE 3

3. Article 2

Statut de l'article: en préparation pour publication

Contribution des co-auteurs:

Pour cet article intitulé «*FOXK1 Transcription Factor is Regulated by O-GlcNAcylation and is Required for Adipogenesis*», en tant que co-première auteure et donc au même titre que Nicholas V.G. Iannantuono, j'ai contribué de manière significative à la planification, à la conception, à l'exécution et à l'analyse de la majeure partie des expériences. J'ai aussi considérablement contribué aux discussions, à la préparation des figures ainsi qu'à l'écriture du manuscrit. Entre autre, j'ai réalisé les travaux présentés aux figures 21 A, 22 C et D, 23 A, B, C et D et j'ai participé aux travaux de la figure 22 B. J'ai aussi purifié FOXK1 pour analyse par spectrométrie de masse. Nicholas Iannantuono a réalisé les travaux présentés aux figures 19, 20, 21 B, 22 A et B et 23 E. Haithem Barbour a participé aux travaux de la figure 23C et a contribué à mettre en place le système CRISPR/Cas9 pour la déplétion de FOXK1 et FOXK2 qui sera utilisé pour des travaux futurs. Éric Bonneil a réalisé l'analyse des sites d'O-GlcNAcylation de FOXK1 par spectrométrie de masse *(data not shown)*.

FOXK1 Transcription Factor is Regulated by O-GlcNAcylation and is Required for Adipogenesis

Nicholas VG Iannantuono[1,†], Jessica Gagnon[1,†], Haithem Barbour[1], Eric Bonneil[2], Pierre Thibault[2] and El Bachir Affar[1,#]

[1]Maisonneuve-Rosemont Hospital Research Center and Department of Medicine, University of Montréal, Montréal H3C 3J7, Québec, Canada

[2]Institute for Research in Immunology and Cancer, University of Montréal, Montréal H3C 3J7, Québec, Canada

[†]Equal contribution

[#]Correspondence

Conflict of interest

The authors declare no conflict of interest

Running title: FOXK1 is O-GlcNAcylated and Required for Adipogenesis

Key words: FOXK1, FOXK2, OGT, O-GlcNAcylation, BAP1, Adipogenesis, post-translational modification, starvation, differentiation, FHA

Abbreviation: Forkhead box Associated protein 1 and 2 (FOXK1 and FOXK2), Forkhead box Associated domain (FHA), O-Linked N-acetylglucosamine transferase (OGT), Host Cell Factor-1 (HCF-1), serine (Ser), threonine (Thr), post-translational modifications (PTMs), Hexosamine Biosynthetic Pathway (HBP), HCF-1 Binding Motif (HBM), Ubiquitin Carboxyl Hydrolase (UCH), C-terminal domain (CTD), Coiled-Coil1 and 2 (CC1 and CC2)

3.1 Abstract

O-GlcNAcylation, catalyzed by OGT, is an extensively studied modification which consists in the addition of an O-GlcNAc moiety to serine and threonine residues of targeted proteins. OGT is known to be a core partner of BRCA1 Associated Protein 1 (BAP1) which is an important tumor suppressor complex mainly composed of transcriptional regulators and transcription factors whose main function is the deubiquitination of histone H2A. Furthermore, the BAP1 complex is subjected to a plethora of post-translational modifications that were shown to be crucial for the regulation of its function including O-GlcNAcylation. Among the different partners of BAP1, the transcription factor of the K subfamily of Forkhead Box protein (FOXK1 and FOXK2) have recently emerged as important regulators of BAP1-mediated deubiquitination of specific gene promoters. These factors are uniquely characterized by the presence of both, a Forkhead box Associated domain (FHA) which binds phosphothreonine residues and a DNA-binding Forkhead box domain (FH). Recent studies have demonstrated the importance of the phosphorylation of BAP1 for the binding of the FOXKs. However, why both FOXK1 and FOXK2 interact with the BAP1 complex and how they are differentially regulated is still unclear. In this study, we report that FOXK1, but not FOXK2 is a novel target for O-GlcNAcylation and that FOXK1's interaction with BAP1 is greatly compromised in response to cellular starvation. Our data also demonstrates that FOXK1 O-GlcNAcylation is modulated during the entry of cell cycle as well as during differentiation. Using the 3T3L1 adipocyte differentiation model, we also provide new evidence that FOXK1 is critical for adipogenesis

3.2 Introduction

Networks of post-translational modifications (MPTs) in eukaryotic cells participate in the regulation of a wide variety of signaling cascades whose main output is modulation of gene transcription [2, 29, 167, 168, 206-215]. Such collaboration between modifying enzymes results in a highly complex crosstalk of marks crucial for cell fate determination [216-219]. Such networks can be observed within chromatin modifying complexes that interpret multiple signaling cascades to trigger different cellular outcomes. For instance, the BRCA1 Associated Protein 1 (BAP1) forms a large protein complex containing several transcription regulators and factors [220-222]. O-GlcNAcylation and ubiquitination are MPTs that have been shown to be critical for the function of several of the BAP1 complex subunits [54, 95, 97, 118, 205, 223]. Indeed, recent studies have shown that Lysine-Specific Demethylase 1B (LSD2/KDM1B) ubiquitinates the O-linked-β-N-acetylglucosamine transferase (OGT) in order to trigger its degradation [54]. This is counteracted by deubiquitination via BAP1 so as to protect OGT for it to O-GlcNAcylate other components of the BAP1 complex to regulate their function [95]. O-GlcNAcylation is of great interest as its addition onto serine and threonine residues has been shown to compete with phosphorylation. In this way, O-GlcNAcylation may protect specific sites from kinase activity thus interfering with phosphorylation-dependent events whereby O-GlcNAcylation may have broad cellular repercussions [224, 225]. Furthermore, O-GlcNAcylation is emerging as a direct and critical mediator of metabolic signaling as the synthesis of its donor substrate is derived from the hexosamine biosynthetic pathway (HBP), resulting in dynamic O-GlcNAcylation in response to fluctuations in the major metabolic pathways including the metabolism of nucleotides, free fatty acids, amino acids and glucose [31, 37, 226, 227]. Hence, the dynamic competition with phosphorylation would also be sensitive to metabolic fluctuations. The ternary complex of OGT/HCF1/BAP1 has also been shown to regulate gluconeogenesis via O-GlcNAcylation and deubiquitination of PGC-1α, thereby solidifying the BAP1 complex's implication in metabolic regulation [72]. Other components of the BAP1 complex have also been shown to be O-GlcNAcylated such as Yin Yang 1 (YY1) and HCF-1, attesting to the importance of O-GlcNAcylation in the regulation of this complex [95, 97, 98].

Two other factors in the BAP1 complex are the Forkhead Box Proteins 1 and 2 (FOXK1 and FOXK2) whose functions remain poorly understood. FOXK1 and FOXK2 are two ubiquitously expressed FOX transcription factors. The FOX factors are known to bind DNA with a highly conserved FH domain but the FOXK subfamily is unique in that FOXK1 and FOXK2 contain an FHA phospho-threonine binding domain. Both FOXK1 and FOXK2 are present in the BAP1 complex, are highly similar in structure but have been reported to have very different functions. FOXK2 has been shown to recruit the BAP1 complex to chromatin in order to modulate PRC1-mediated gene expression [138, 228]. It has also been shown to act in concert with AP-1 signaling and to bind G/T mismatches [229, 230]. Further, it has been shown to mediate cell survival and most recently was shown to suppress tumour growth of ERα-positive breast cancers [231]. FOXK1, on the other hand, has been shown to be a critical regulator of myogenesis through both cell cycle control and direct protein inhibition of the differentiation program [151, 153, 163, 232-234]. Recently it has been shown that mTOR phosphorylates FOXK1, promoting its nuclear accumulation, in order to inhibit autophagy gene expression through the recruitment of the Sin3 repressive complex in normal growth conditions [114]. Importantly, both FOXK1 and FOXK2 have been shown to be regulated by phosphorylation and have been implicated in Wnt Signaling through the nuclear transport of DVL proteins[137], and the antiviral response via Nup98[139], however the link between metabolic regulation, OGT and the FOXK proteins has not been thoroughly explored. Here we show that FOXK1 is specifically O-GlcNAcylated compared to FOXK2 and that this modification is modulated during various cellular processes including adipogenesis where we show that FOXK1 is critical for this process.

3.3 Results

2.5.1 BAP1 structural conformation and Thr493 residue but not HCF-1 and OGT are important for FHA-dependant FOXKs binding to BAP1.

Several studies have mapped the potential binding domain between the FOXKs transcription factors and BAP1 identifying the FHA domain of FOXKs as the main domain responsible for the interaction with BAP1. However, it is still unclear if this interaction is mediated via BAP1 phosphorylation of its threonine 493, and/or also through its structural

conformation [138, 228]. Thus, we sought to investigate the phosphorylation dependency of the interaction between BAP1 and FOXK proteins. To do so, we used GST-tagged constructs of FOXK1 and FOXK2 to perform GST-pulldowns using recombinant proteins. GST-YY1 was used as a positive control, as previous studies have demonstrated its direct interaction with BAP1 [220]. As shown in Figure 19A, both GST-FOXK1 and GST-FOXK2 strongly enrich recombinant BAP1 suggesting that its phosphorylation is not necessary for the interaction. Therefore, we sought to better characterise the interacting region of BAP1 with the FOXKs. Since the FHA and FH domains of FOXK1 and FOXK2 are highly conserved and that Okino et al [138] showed that FOXK1 and FOXK2 interact with the same region of BAP1, we sought to validate that the FOXKs interact with BAP1 in a mutually exclusive manner. As such, HeLa nuclear extracts were prepared and native immunoprecipitations of endogenous FOXK1 and FOXK2 were performed. Our data clearly show that FOXK2 does not co-immunoprecipitate with FOXK1 and vice versa suggesting that they are indeed mutually exclusive (Figure 19B). Therefore, further mapping experiments with BAP1 were performed using GST-FOXK1 only. As shown in figure 19C (Right), we generated several BAP1 deletion constructs in order to validate previous identified binding region of BAP1 [223]. Our results demonstrate that FOXK1 interacts with the full length form of BAP1 as well as with the ΔUCH fragment, indicating that the NORS and the CTD of BAP1 are either completely or partially important for proper binding of BAP1 with FOXK1. However, the BAP1-Thr493A mutant reported by Okino et al [138] completely abolished FOXKs binding as shown by the FLAG co-immunoprecipitation (Figure 19D and 19E). Reciprocally, we produced the FOXK1-Arg127A mutant, known to be critical for FHA function as it recognizes the phosphate moiety and as reported, co-immunoprecipitation of BAP1 is significantly reduced with FOXK1-Arg127A mutant (Figure 19E). Altogether, these contradictory data suggest that the Thr493 residue as well as the structural conformation of BAP1 are both important for the binding of BAP1 by the FHA domain of FOXK1. Also, due to the proximity of Thr493 to the HCF-1 binding motif (HBM) of BAP1 and since HCF-1 is a core component of the BAP1 complex, we examined if the presence of HCF-1 could regulate the presence of the FOXKs in the BAP1 complex. We reasoned that the proximity of HCF-1 to the Thr493 residue in the flexible loop of BAP1 might create steric hindrance regulating FOXKs interaction with BAP1 as schematised in Figure 19F, therefore, ablation of the HBM might

increase FOXKs binding to BAP1. To verify this hypothesis, we generated HeLa S3 cells stably expressing either FLAG-HA-BAP1 or FLAG-HA-BAP1 ΔHBM and purified these complexes by FLAG immunoprecipitation. As shown in figure 19G, FOXKs levels in the BAP1 complex are not affected by HCF-1 or OGT presence. Collectively, these data suggest that FOXK proteins bind a precise structural conformation of BAP1 as well as its Thr493 residue independently of HCF-1 and OGT presence in the complex.

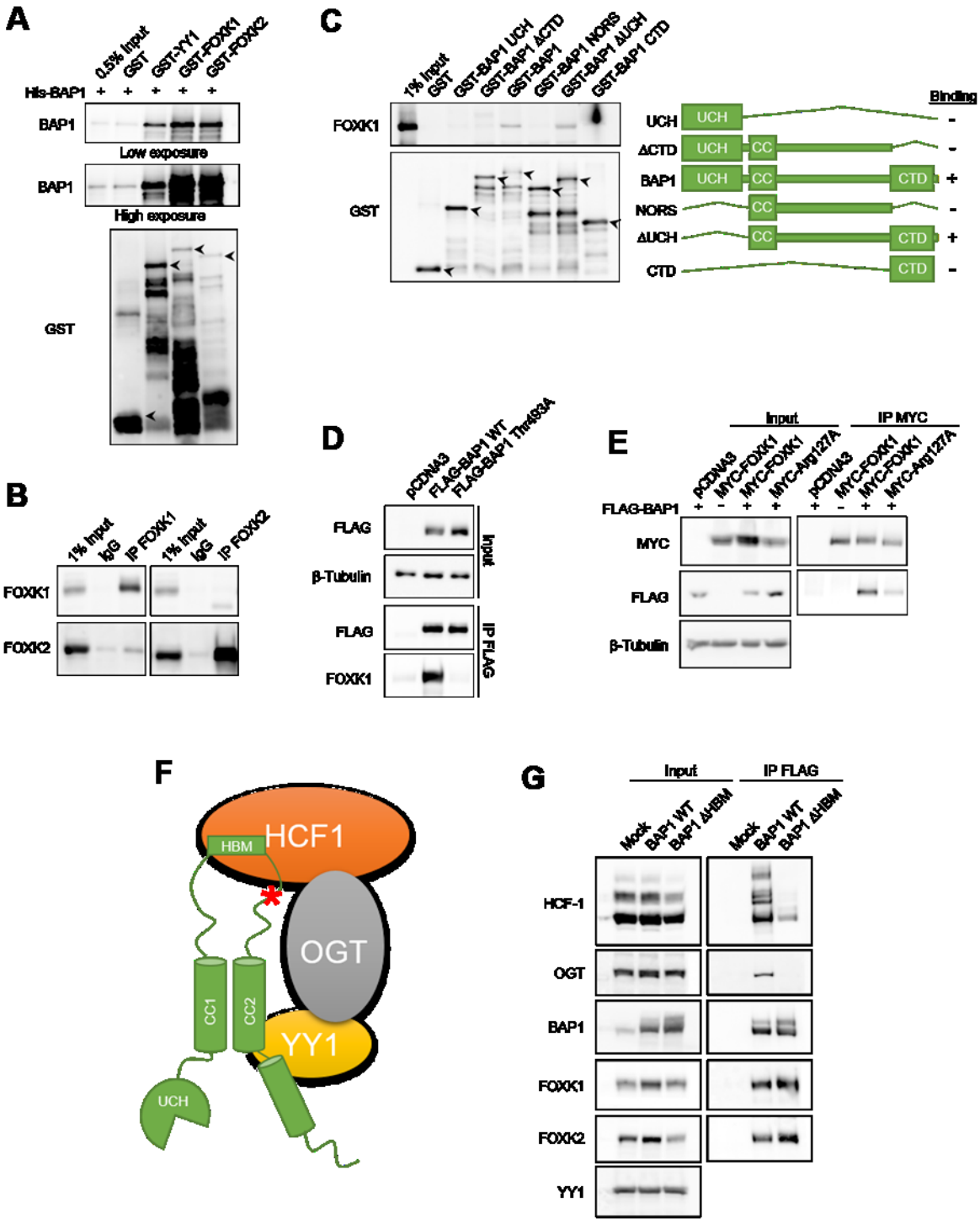
A
0.5% Input
GST
GST-YY1
GST-FOXK1
GST-FOXK2
His-BAP1 + + + + +
BAP1
Low exposure
BAP1
High exposure
GST
B
1% Input
IgG
IP FOXK1
1% Input
IgG
IP FOXK2
FOXK1
FOXK2
C
1% Input
GST
GST-BAP1 UCH
GST-BAP1 ΔCTD
GST-BAP1
GST-BAP1 NORS
GST-BAP1 ΔUCH
GST-BAP1 CTD
FOXK1
GST
Binding
UCH
ΔCTD
BAP1
NORS
ΔUCH
CTD
D
pCDNA3
FLAG-BAP1 WT
FLAG-BAP1 Thr493A
FLAG
β-Tubulin
Input
FLAG
FOXK1
IP FLAG
E
Input
IP MYC
pCDNA3
MYC-FOXK1
MYC-FOXK1
MYC-Arg127A
pCDNA3
MYC-FOXK1
MYC-FOXK1
MYC-Arg127A
FLAG-BAP1 + - + + + - + +
MYC
FLAG
β-Tubulin
F
HBM
HCF1
OGT
CC1
CC2
YY1
UCH
G
Input
IP FLAG
Mock
BAP1 WT
BAP1 ΔHBM
Mock
BAP1 WT
BAP1 ΔHBM
HCF-1
OGT
BAP1
FOXK1
FOXK2
YY1

Figure 19 BAP1 structural conformation and Thr493 residue but not HCF-1 and OGT are important for FHA-dependant FOXKs binding to BAP1 (A) GST-pulldown of recombinant purified His-BAP1, GST, GST-FOXK1, GST-FOXK2 and GST-YY1. His-BAP1 was used as the pray. Proteins levels were analysed by western blotting using the indicated antibodies. Arrows indicate GST-tagged proteins (B) HeLa nuclear extracts were lysed and native immunoprecipitations of FOXK1 and FOXK2 were performed overnight. Control IgG immunoprecipitations was performed as a negative control and proteins levels were analyzed by immunoblotting with the indicated antibodies. (C) (Left) GST-pulldown of recombinant BAP1 fragments with purified recombinant His-FOXK1. Arrows indicate GST-tagged BAP1 fragments. (Right) Schematics of BAP1 fragments used for the GST-pulldown. (D) HEK293T cells were transfected with either FLAG-BAP1 wild-type (WT) or FLAG-BAP1 Thr493A mutant. Three days post-transfection, cells were lysed and native anti-FLAG immunoprecipitation was performed. Endogenous FOXK1 co-immunoprecipitation was analyzed by western blotting. (E) HEK293T cells were transfected with MYC-FOXK1 WT or MYC-FOXK1 Arg127A with or without FLAG-BAP1. Three days post-transfection, cells were harvested and native anti-MYC immunoprecipitation was performed. BAP1 binding was analysed by western blotting. (F) BAP1 schematic illustrating the location of Thr493A with regards to the reported binding locations of HCF1/OGT/YY1 axis. Asterisk indicates the position of threonine 493 residue. (G) HeLa S3 cells stably expressing either pOZN, pOZN-FLAG-HA-BAP1 or pOZN-Flag-HA-BAP1 ΔHBM were grown and harvested for complex purification by overnight anti-flag immunoprecipitation. Core components of the complex were analysed by western blotting with the indicated antibodies. IP; Immunoprecipitation

2.5.2 FOXK1 but not FOXK2 is O-GlcNAcylated by OGT

MPTs of the core proteins in the BAP1 complex have been extensively studied and characterized [54, 118, 221-223, 235]. The presence of protein modifying proteins such as LSD2, OGT, UBE2O, HAT1 and BAP1 itself strongly advocate for the importance of MPTs in the function of this tumor suppressor complex. However, the identification and function of the various MPTs in the BAP1 complex are still largely unknown. For example, although several phosphorylation sites of FOXKs were identified, the study of the MPTs of the FOXKs transcription factors remains in its infancy [114, 236]. Therefore, we sought to identify novel MPTs of FOXKs and how they might regulate the dynamic of the BAP1 complex. Since the binding of FOXK proteins to BAP1 Thr493 would bring them in close proximity to the O-linked N-acetylglucosamine transferase (OGT), already known to modulate the function of components of the BAP1 complex through O-GlcNAcylation, we verified if FOXK proteins may be O-GlcNAcylated in vivo [95, 97, 98, 118, 221]. We co-overexpressed MYC-FOXK1 or MYC-FOXK2 with either FLAG-OGT WT or FLAG-OGT CD to perform MYC immunoprecipitations under denaturing conditions. As shown in figure 20A, a mobility shift can be observed for FOXK1 in the presence of OGT WT but not in the presence of OGT CD, indicative of a higher molecular weight for all of the ectopic FOXK1 in this condition. This modification was further confirmed to be O-GlcNAcylation as it was detected by the highly used RL2 antibody, which is specific for the O-GlcNAc moiety[237]. Moreover, these data

suggest that this O-GlcNAcylation is specific to FOXK1. To further confirm previous results on endogenous FOXK1, we harvested HEK293T to performed FOXKs immunoprecipitation under denaturing conditions. As shown in figure 20B, immunoprecipitated FOXK1 but not FOXK2 yields an O-GlcNAcylation signal. The same result was obtain using the non-cancerous murin cell line 3T3L1 albeit FOXKs are expressed at lower levels. To verify the specificity of the detected O-GlcNAcylation signal, we depleted OGT by siRNA in U2OS cells and performed a FOXK1 immunoprecipitation under denaturing condition (Figure 20D). As expected, levels of OGT were almost completely ablated under siRNA treatment which resulted in a complete loss of the O-GlcNAcylation signal previously observed for FOXK1. Moreover, a slight decrease in BAP1 binding can be observed following depletion of OGT (Figure 20D). As O-GlcNAcylation is known to mediate certain protein functions such as localization and protein-protein interactions, we sought to determine if O-GlcNAcylation of FOXK1 could modulate its interaction with BAP1. Thus, we co-expressed OGT WT or CD in the presence of BAP1 WT or the BAP1-Thr493A mutant but observed no change in FOXK1 binding in all conditions (Figure 20E). Also, the O-GlcNAcylation of FOXK1 had no effect on the FOXK2-BAP1 interaction suggesting that FOXK1 O-GlcNAcylation does not regulate FOXKs binding to the BAP1 complex. Taken together, these results suggest that FOXK1 but not FOXK2 is specifically O-GlcNAcylated by OGT and that this modification does not regulate FOXKs presence in the complex.

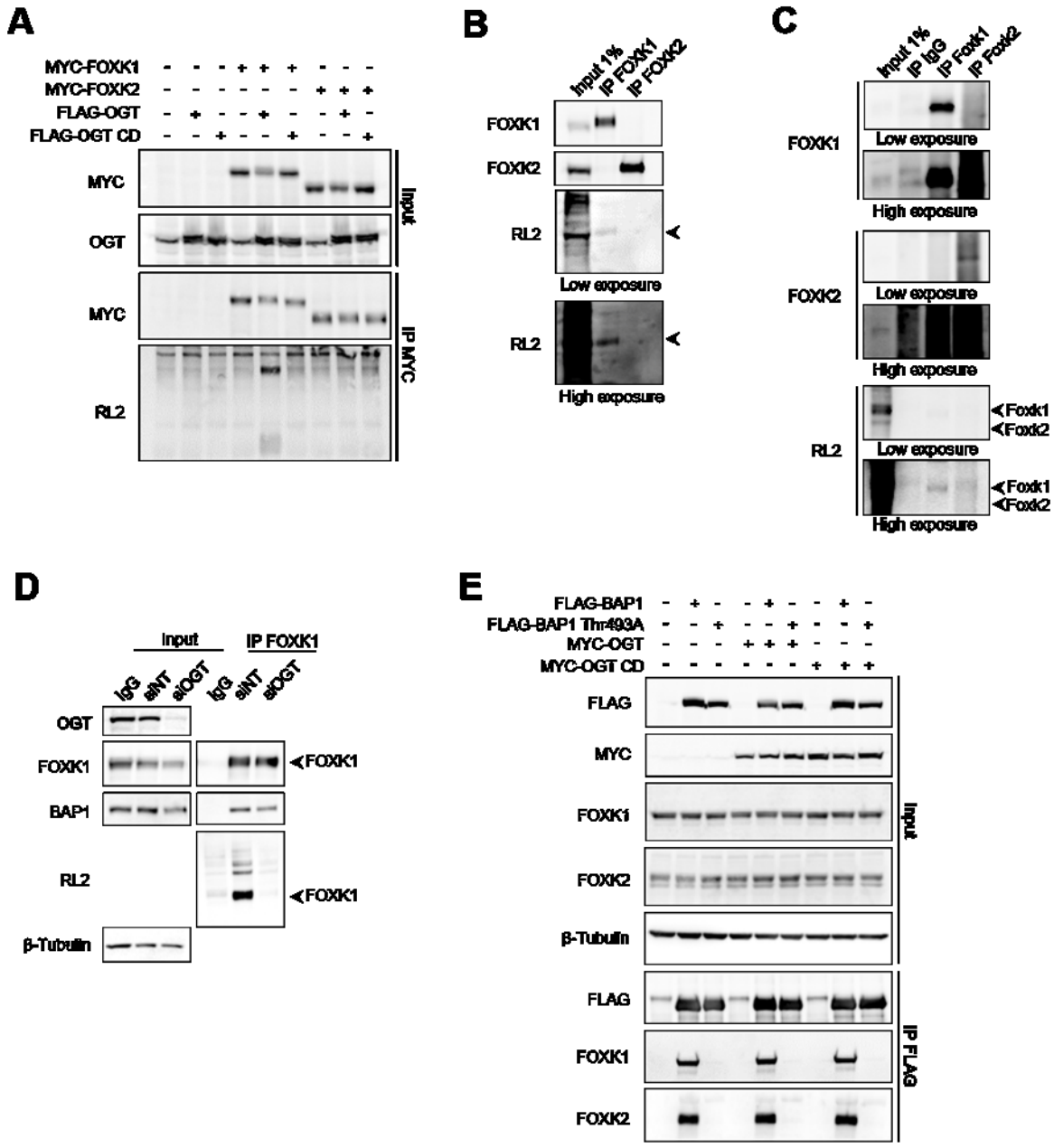

]

transfection, cells were harvested for denaturing anti-MYC immunoprecipitation and proteins levels were immunoblotted with indicated antibodies. (**B**) HEK293T cells were harvested and denaturing immunoprecipitation of endogenous FOXKs was performed. O-GlcNAcylation of FOXKs was analyzed by western blotting using RL2 antibody. (**C**) O-GlcNAcylation of endogenous Foxk1 and Foxk2 in murine 3T3L1 cell line was analysed as in (B). (**D**) U2OS cells were double treated with siRNA against OGT. Three days post-transfection, cells were harvested for native immunoprecipitation of FOXK1. Protein levels were analysed by western blotting with indicated antibodies. Control correspond to untreated U2OS cells used for the IgG immunoprecipitation. (**E**) HEK293T cells were transfected with either FLAG-BAP1 WT or FLAG-BAP1 Thr493A with either MYC-OGT WT or MYC-OGT CD. Three days post-transfection, cells were harvested for anti-FLAG immunoprecipitation and results were revealed by western blotting using indicated antibodies. IP; Immunoprecipitation

2.5.3 FOXK1 O-GlcNAcylation by OGT is BAP1-independent.

OGT is a ubiquitous protein that is involved in a plethora of cellular processes and is known to interact with hundreds of substrates outside of its interaction with BAP1. Since our previous data indicates that O-GlcNAcylation does not affect FOXK1 binding with BAP1, we then wanted to verify if BAP1 is required for FOXK1 O-GlcNAcylation. We reasoned that BAP1 might serve as a bridge allowing OGT to modify FOXK1. To explore this possibility, we performed immunoprecipitation of endogenous OGT and FOXKs in H226 mesothelioma cells, known to be knockout for BAP1, as well as in an H226-BAP1 cell line in which we rescued BAP1 expression in order to compare the O-GlcNAcylation level of FOXK1. As shown in figure 21A, FOXK1 O-GlcNAcylation level is similar in the presence or absence of BAP1. These data suggest that BAP1 is not required for FOXK1 O-GlcNAcylation. To further confirm that the O-GlcNAcylation of FOXK1 is independent of BAP1 and that FOXK1 may be modified by OGT outside of the BAP1 complex, we conducted a denaturing immunoprecipitation of FOXK1 from the elutions of the FLAG-BAP1 WT and FLAG-BAP1 ΔHBM purified complexes shown in figure 19G. As expected, the O-GlcNAcylation levels of FOXK1 are similar regardless of the presence of HCF-1 and OGT in the BAP1 complex. Altogether, these data strongly suggest that FOXK1 O-GlcNAcylation is independent of BAP1.

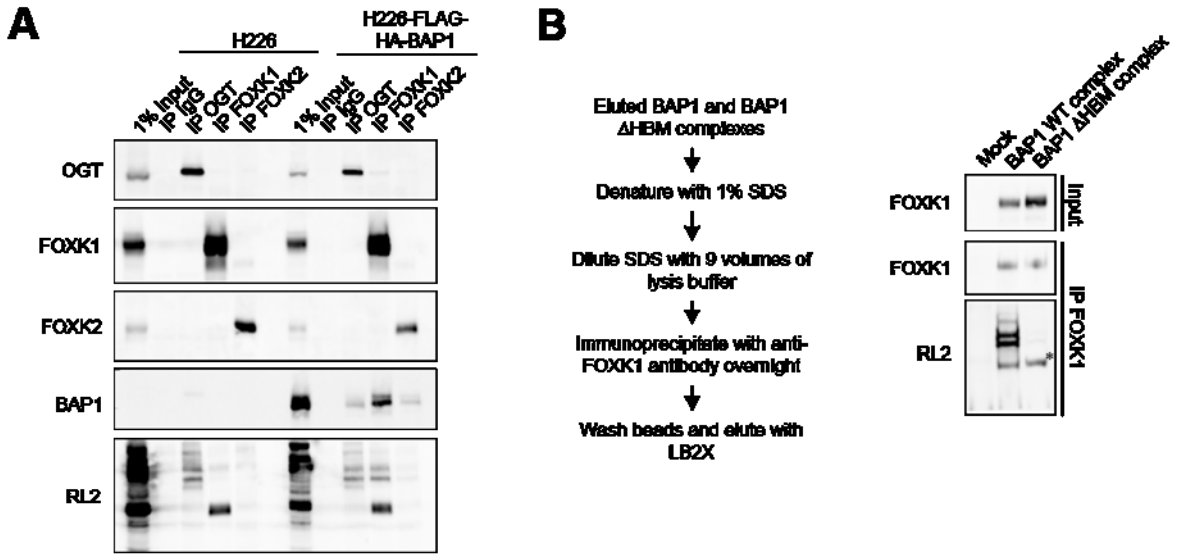

expressing FLAG-HA-BAP1 were harvested for native immunoprecipitation of endogenouos OGT, FOXK1 and FOXK2. Protein levels and O-GlcNAcylation were analyzed by western blotting with indicated antibodies. (**B**) (Left) Schematic of the different steps performed to immunoprecipitate FOXK1 out of the BAP1 complexes purified in Figure 1G. (Right) O-GlcNAcylation level of FOXK1 in either BAP1 or BAP1 ΔHBM complex following denaturing immunoprecipitation of FOXK1 as indicated on the left. Immunodetection was conducted with the indicated antibodies.Asterisk indicates FOXK1 corresponding band. IP; Immunoprecipitation

2.5.4 FOXK1 O-GlcNAcylation is modulated during cell cycle entry and in response to starvation.

We next explored if this O-GlcNAc modification of FOXK1 may be modulated during a specific cellular event. It is known that cells go through a restriction point before the decision to enter into the cell cycle is made [238, 239]. Indeed, the availability of nutrients, physical space, cell-cell communications and extracellular signaling are critical inputs to this decision. As for the availability of sufficient nutrients, OGT has been previously described as a sensor for the metabolic state of the cell [72, 168, 170]. Thus, we verified if the O-GlcNAcylation of FOXK1 may be modulated during the entry into cell cycle. We therefore, grew U2OS osteosarcoma cells to confluence and starved them of serum for 24 hours in order to arrest them in G0. We then released these cells by feeding them with 20% serum in order to provoke a flux of cells enter into the cell cycle. As shown in figure 22A, protein levels of FOXK1 and BAP1 remain relatively stable over the course of the 12 hours of release. As expected, a spike in CDC6 levels correlates with a slight entry of cells into G1/S, as seen in the corresponding FACS analysis for the point of 12h release (Figure 22A, right panel).

Interestingly, over the full course of the cell cycle entry, FOXK1 O-GlcNAcylation levels increase steadily and reach a maximum at 6h prior to the restriction point where cells begin moving towards the G1/S boundary (Figure 22A, left panel). Then, the levels decrease slightly once cells have begun cycling. Furthermore, the interaction between BAP1 and FOXK1 increases as cells begin to cycle (Figure 22A, left panel). These data strongly suggest that FOXK1 O-GlcNAcylation is modulated during the entry of the cell cycle and that FOXK1 and BAP1 interaction may be important for the proliferative state of cells. However, it cannot be excluded that this observation may be caused by a cancer-derived process. To eliminate this possibility, the same experiment was redone using primary human fibroblasts. After maintaining cells at confluence for two days in order to trigger cell-cell contact inhibition, we further serum starved them for 24h to completely arrest cell growth. The cells were then fed 20% serum media. As expected, FOXK1 and BAP1 levels remain stable and a spike in CDC6 level corresponding to the entry of cells into G1/S, albeit later than in U2OS, was observed. Again, as previously described, O-GlcNAcylation of FOXK1 is most evident at the onset of the cell cycle entry and decreases as cells are actively cycling. These results clearly demonstrate that FOXK1 O-GlcNAcylation is modulated during the decision to enter cell cycle.

Previous studies have demonstrated that FOXK1 phosphorylation and cellular localization are modulated in response to fluctuations in cellular metabolism through mTOR signaling [114]. Moreover, mTOR was shown to regulate OGT stability [49, 240]. Since it was reported that OGT levels decrease during starvation, we sought to determine if FOXK1 O-GlcNAcylation is also modulated during this process. Hence, we deprived LL human fibroblasts of all nutrients and examined the differential O-GlcNAcylation of endogenous FOXK1 following denaturing immunoprecipitation. As shown in figure 22C, at the onset of cellular starvation, the reported mobility shift of FOXK1 can be observed concording with its reported phosphorylation [114]. Also as expected, the O-GlcNAcylation levels of FOXK1 steadily decrease over the course of the starvation kinetic and this signal restabilizes itself once cells are fed complete media (Figure 22C). Since both the O-GlcNacylation of FOXK1 and its binding to BAP1 increase during the entry into cell cycle (Figure 22A and 22B) and that the O-GlcNAcylation of FOXK1 decreases during starvation (Figure 22C), we verified if

the BAP1 complex may be subjected to changes during starvation. We therefore, starved cells and co-immunoprecipitated the BAP1 complex via ASXL2 as we had K562-FLAG ASXL2 stable cell lines in culture at the time of our investigation. As shown in figure 22D, total levels of the core components of the BAP1 complex, namely, ASXL2, BAP1 and OGT decrease overtime. However the levels of both FOXKs seem unaffected. Notably however, FOXK1 and to a lesser extent FOXK2 become excluded from the BAP1 complex as cells undergo starvation, returning to the complex once cells are re-fed complete media. These data are consistent with previous studies showing that both FOXK1 and FOXK2 are shuttled out of the nucleus in response to starvation, however since FOXK1 becomes excluded much more rapidly, it is possible that the tie between FOXK1 and cellular metabolism, strictly speaking its O-GlcNAcylation may confer a sensitivity to this process.

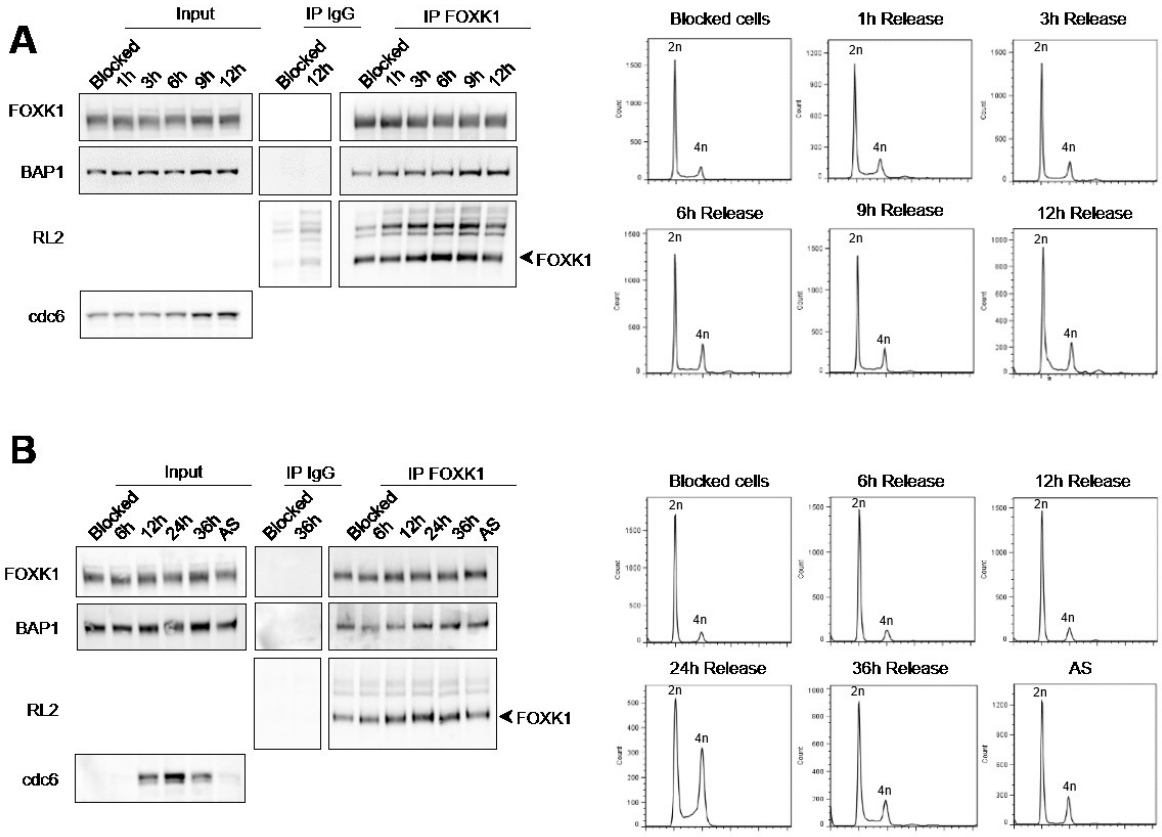
A
Input
IP IgG
IP FOXK1
Blocked
1h
3h
6h
9h
12h
FOXK1
BAP1
RL2
cdc6
FOXK1
Blocked cells
1h Release
3h Release
6h Release
9h Release
12h Release
2n
4n
B
Input
IP IgG
IP FOXK1
Blocked
6h
12h
24h
36h
AS
FOXK1
BAP1
RL2
cdc6
FOXK1
Blocked cells
6h Release
12h Release
24h Release
36h Release
AS
2n
4n
C
Input
IP FOXK1
Starvation (hrs)
0
4
8
10
R
IgG
FOXK1
RL2
β-Tubulin
D
Input
IP FLAG
Starvation (hrs)
0
6
2
4
R
FLAG
OGT
BAP1
FOXK1
FOXK2
β-Tubulin
K562
K562-FLAG-HA-ASXL2

Figure 22 FOXK1 O-GlcNAcylation is modulated during cell cycle entry and in response to starvation. (**A**) (Left) U2OS cells were grown to confluence and then cells were serum starved for 24h. The next day, blocked cells were harvested and remaining cells were fed with media containing 20% serum. At the indicated time points, cells were harvested for both FACS analysis and immunoprecipitation. IgG control or anti-FOXK1 native immunoprecipitation was performed overnight and western blotting was performed with indicated antibodies. (Right) FACS analysis showing very slight entry into G1/S between 9h and 12h. (**B**) (Left) Primary LL human fibroblasts were grown to confluence and left at confluence for 48h. Then, cells were serum starved for an additional 24h, replated in 20% serum containing media and finally harvested at indicated time-points for FACS analysis and immunoprecipitation as indicated in (A). (Right) FACS analysis of each time-point showing that cells began to enter the cell cycle between 12 and 24h. IP; Immunoprecipitation, AS; Asynchronous population, hrs; hours. (C) LL human primary fibroblasts were starved according to Bowman et al. (206) with (HBSS) supplemented with 10 mM HEPES pH 7.5 and 1% Penicillin-Streptomycin for the indicated time. When indicated, cells were replenished for 2h by feeding back the cells with growing medium. Cells were then harvested for subsequent denaturing immunoprecipitation. IgG immunoprecipitations was done as a negative control and proteins were revealed using indicated antibodies. (D) K562 cells stably expressing a FLAG-HA-ASXL2 construct were starved in the same manner as (C) and harvested at indicated time points for native FLAG immunoprecipitations. Control K562 cells were used as negative controls for the FLAG immunoprecipitations and proteins were revealed using indicated antibodies. Experiments A, B and C were performed twice. Experiment D was performed once.

2.5.5 Foxk1, but not Foxk2, is required for adipogenesis

Since our results have shown that not only FOXK1 O-GlcNAcylation but also its presence in the BAP1 complex are modulated in response to cellular starvation, we reasoned that FOXK1 itself may play a role in cellular metabolism. Furthermore, previous studies have shown that FOXK1 is a critical regulator of the differentiation of the highly metabolic C2C12 myogenic progenitor cells whereby its loss impairs muscle regeneration in KO mice [154, 241]. Therefore, we sought to determine if in fact FOXK1 regulation of differentiation could be a consequence of its regulation of metabolism rather than being specific for myogenic differentiation. 3T3L1 adipogenesis is also a highly metabolic-dependent process, thus, we investigated if FOXK1 regulation of differentiation could be extended to adipogenic tissues. Hence, using standard 3T3L1 differentiation procedures (see material and methods) in parallel with double siRNA treatments of Foxk1, we knocked-down Foxk1 levels to study its effect on adipogenic differentiation. As shown in the upper blot of figure 23A, knockdown of Foxk1 with several different individual siRNA as well as the mix reduced Foxk1 levels by roughly 50%. Interestingly, siRNAs 2 and 4 and to a lesser extent siRNAs 1 and 3 caused a media color change (become purple) compared to scrambled siRNA (siNT) indicative of media alkalinity (Figure 23A, lower panel). As the differentiation of 3T3L1 triggers cell cycle arrest and a flux in triglycerides and free fatty acids synthesis, normal differentiation of these cells will tend to acidify the media. Further Oil Red O staining analysis of neutral triglyceride and

lipid accumulation revealed that knockdown of Foxk1 also impairs adipogenesis although to varying degrees (Figure 23B). Furthermore, the siRNA treatments that blocked differentiation the most correspond to stronger alkalinity of the media. As we identified Foxk1 as a major regulator of adipogenesis we next determine if it was also the case for Foxk2. Surprisingly, siFoxk2 showed no significant effect on differentiation compared to control siRNA albeit causing a slightly more acidic media (Figure 23C). In order to explore the molecular bases of this differentiation block and to validate that the observable effect of siFoxk1 is not an off-target effect, we differentiated 3T3L1 cells under the treatment of an additional set of Foxk1 siRNA and verified commonly used adipogenesis markers. As shown in figure 23D all siRNA treatments, except for 1 and 3, almost completely blocked differentiation as shown by Fabp4 and Perilipin levels. These results strongly suggest that Foxk1 but not Foxk2 is critical for 3T3L1 differentiation.

As our group already demonstrated the importance of the BAP1 complex in adipogenesis via the Ube2o-Bap1 axis, we explored its kinetics as well as the O-GlcNAcylation state of Foxk1 during this process [223]. Interestingly, components of the BAP1 complex change quite drastically over the course of the differentiation process (Figure 23E). Moreover, many of the protein levels of the components of the BAP1 complex differentially decrease during differentiation but most strikingly at the onset of the production of adipogenic markers at day 4, except for Ogt, whose levels remain stable (Figure 23E). Finally, normalized native immunoprecipitations of Foxk1 suggest that its interaction with Bap1 does not change in a significant way over the course of the differentiation. However, FOXK1 O-GlcNAcylation is almost completely ablated near terminal differentiation, and this, despite identical levels of OGT in cells. Taken together, our results suggest that not only is FOXK1 critical for 3T3L1 differentiation, but its O-GlcNAcylation is modulated during this process.

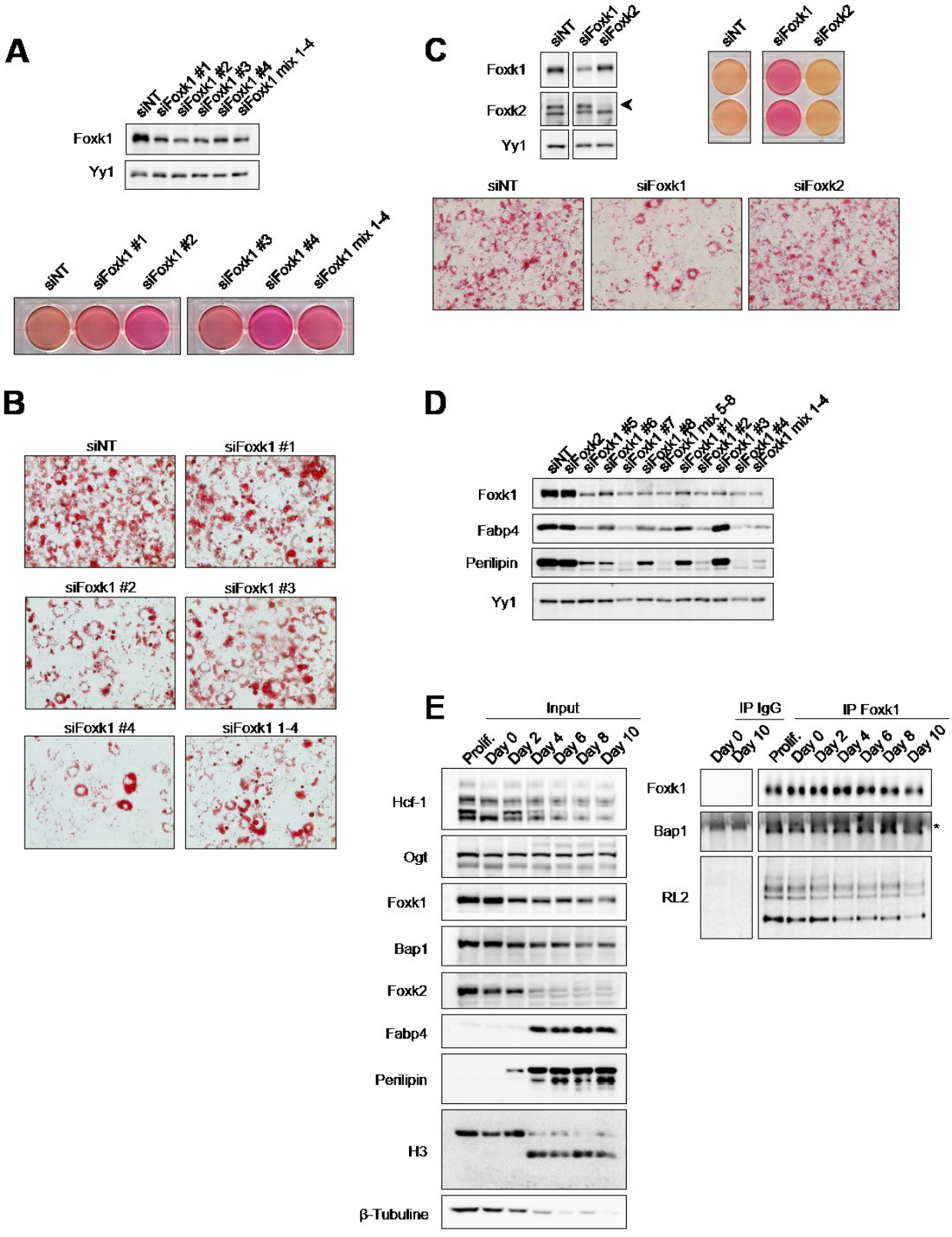
A
siNT
siFoxk1 #1
siFoxk1 #2
siFoxk1 #3
siFoxk1 #4
siFoxk1 mix 1-4
Foxk1
Yy1
B
siNT
siFoxk1 #1
siFoxk1 #2
siFoxk1 #3
siFoxk1 #4
siFoxk1 1-4
C
siNT
siFoxk1
siFoxk2
Foxk1
Foxk2
Yy1
D
siNT
siFoxk2
siFoxk1 #5
siFoxk1 #6
siFoxk1 #7
siFoxk1 #8
siFoxk1 mix 5-8
siFoxk1 #1
siFoxk1 #2
siFoxk1 #3
siFoxk1 #4
siFoxk1 mix 1-4
Foxk1
Fabp4
Perilipin
Yy1
E
Input
IP IgG
IP Foxk1
Prolif.
Day 0
Day 2
Day 4
Day 6
Day 8
Day 10
Hcf-1
Ogt
Foxk1
Bap1
Foxk2
Fabp4
Perilipin
H3
β-Tubuline
RL2

Figure 23 Foxk1 but not Foxk2 is required for adipogenesis (**A**) (Top) 3T3L1 cells were differentiated under siRNA treatment against Foxk1 as described in material and methods. Scrambled siRNA was used as a negative control. Indicated protein levels were analyzed by western blotting. YY1 was used as a loading control. (Bottom) Differential media colour following siRNA treatments from top panel. (**B**) Oil Red O staining of differentiated 3T3L1 from (A). (**C**) (Top left) 3T3L1 cells were differentiated under siRNA treatment against Foxk1 and Foxk2 as in (A). (Top right) Differential media colour following siRNA treatments. (Bottom) Oil Red O staining corresponding to siFoxk1 and siFoxk2 treatment previously described. (**D**) 3T3L1 cells were differentiated under a more extensive panel of siRNA against Foxk1 as described in (A). Scrambled and Foxk2 siRNA were used as negative controls. Indicated protein levels were analyzed by western blotting. YY1 was used as a loading control. (**E**) 3T3L1 cells were either harvested while proliferating or differentiated according to standard procedures (see material and methods). Cells were harvested for native immunoprecipitation at indicated time-points. IgG control or anti-FOXK1 native immunoprecipitation was performed overnight and western blotting was conducted with indicated antibodies. IP; Immunoprecipitation, Prolif; Proliferating.

3.4 Discussion

In this study, we show that the transcription factors FOXK1 and FOXK2 form mutually exclusive complexes with BAP1, whereby their FHA-dependant binding to BAP1 is mediated by a specific structural folding of BAP1 as well as its Thr493 residue in the NORS domain. Most interestingly, here we show that FOXK1 is specifically O-GlcNAcylated compared to FOXK2 but also that this modification is modulated during various metabolic events such as cell cycle entry, starvation and adipogenesis. Moreover, we show that FOXK1 but not FOXK2 is critical for adipogenic differentiation.

Our study suggests that FOXK1 and FOXK2 may bind BAP1 through conformational changes that expose the residue Thr493 of BAP1, however further mutational studies are needed to pinpoint the biochemistry behind this assertion. A previous study by Ji NAR, using similar techniques, showed that deletion of either the N or C-terminal domains of BAP1 greatly hindered binding to FOXK1 [228]. However, another study by Okino et al [138] showed that deletion of the N and C-terminal of BAP1 had no effect on binding of FOXK1 in vivo. Although our study does confirm that the deletion of the C-terminal domain eliminated binding between FOXK1 and BAP1, we were unable to confirm loss of binding upon the deletion of the UCH domain of BAP1 [228]. Interestingly, not all of our constructs containing the reported critical Thr493 residue could bind FOXK1 in our pulldowns [228]. We have previously shown that BAP1 engages in intramolecular binding between the CC1 (amino acids 236-265) of the NORS region and the CC2 (amino acids 631-660) of the CTD [223]. Only our constructs able to perform these interactions could bind FOXK1. However, our in vivo data also confirm that the Thr493 residue reported to be important for binding between the FHA

domain of FOXK1 or FOXK2 and BAP1 is indeed critical for binding [138, 228]. Nonetheless, the use of recombinant proteins to perform the pulldowns indicates that phosphorylation of Thr493 might not be necessary to allow the binding although it might greatly amplify it. In fact, FHA domains are known to bind not only the phosphate group on the threonine itself but also to have stabilizing interactions with the methyl group of the threonine as well as interactions with the pT+3 residue. Furthermore non canonical phospho-independent interactions between FHA domains and substrates have been described [242, 243]. It is possible that our GST-pulldowns were successful due to these secondary interactions. We reason that in fact, in the context of the full length of BAP1, a concert of intramolecular binding events are necessary to properly expose BAP1 Thr493 to be bound by the FHA of FOXK proteins.

The BAP1 tumour suppressor complex contains a plethora of different transcription regulators and factors that attest to its importance in gene expression regulation [138, 220-222]. MPTs have been shown to be of great importance in the regulation of the function of several of BAP1's partners as well as BAP1 itself [95, 97, 118, 205, 221, 223, 235]. Among identified MPTs, our group and others have already demonstrated the importance of OGT in regulating the function of the main partner of BAP1, namely HCF-1, as well as the Yin Yang 1 (YY1) transcription factor. This study identified the BAP1 partner FOXK1 but not FOXK2 as a novel substrate for O-GlcNAcylation. It is still unclear if FOXK1 and FOXK2 share similar or antagonist function since they were both reported to be regulated in similar context but also shown to act as a repressor and activator respectively. [114, 137] The presence of both factors in the BAP1 complex however hint at them having different functions. In fact, the identification of FOXK1 but not FOXK2 as a major substrate of OGT sheds light on the potential differential modulation of these factors through MPTs. We observed that FOXK1 interaction with the BAP1 complex is much more affected by starvation compared to FOXK2 which hints at its transcriptional function being important in metabolic sensing response. This could be explained by the fact that the reported mTOR-mediated phosphorylation sites of FOXK1 have been shown to be implicated in the nuclear translocation of FOXK1 whereby starvation-induced mTOR deactivation would trigger cytoplasmic relocation of FOXK1. This relocation was also shown to be triggered by other phosphorylation sites. Further, OGT

stability has been shown to be regulated by mTOR signaling. Consequently, during cellular starvation, mTOR is deactivated and the nuclear-transport phosphorylation sites of FOXK1 would remain unmodified, thus hindering its nuclear transport and retention. Moreover, destabilized OGT levels would reduce O-GlcNAcylation levels of FOXK1. As it is known that phosphorylation and O-GlcNAcylation can modify the same residues, it is possible that under normal cell growth O-GlcNAcylation might protect certain serine and threonine residues from phosphorylation but starvation induced accessibility to these sites via OGT destabilization would trigger their phosphorylation and the cytoplasmic retention, examples of which have been described [244-246]. In other words, two groups of phosphorylation sites would exist on FOXK1, a group critical for nuclear import and a second group critical for export. Under normal conditions however, the nuclear export sites would be protected from phosphorylation via OGT-mediated O-GlcNAcylation but these sites would be replaced by phosphorylation as cells undergo starvation. Therefore, crosstalk between phosphorylation and O-GlcNAcylation would allow a very fine tuning of FOXK1 function in response to starvation.

Finally, previous studies on the function of FOXK1 have revealed its critical importance in the differentiation of C2C12 myoblasts. On the other hand, our data clearly demonstrate an important role of FOXK1 in adipogenesis. As both adipogenic and myogenic tissues are derived from the mesoderm, it is possible that FOXK1 may in fact play a role in the regulation of earlier progenitor cells in these lineages. Indeed, the reported function of FOXK1 in myogenesis is in fact to impede differentiation of satellite cells by promoting sufficient clonal expansion prior to differentiation. This is accomplished through inhibition of p21 signaling whereby insufficient FOXK1 activity leads to inefficient muscle repair. Adipogenesis also triggers a clonal expansion event. In fact, a previous study showed that while this expansion was not necessary for the differentiation program to occur, its inhibition generated less Oil Red O staining reminiscent of our siFOXK1 data [247-249]. In line with this, although significantly less cells differentiate under siFOXK1 treatments, the few do differentiation often appear normal. It is possible that in adipogenesis, FOXK1 acts during the clonal expansion event, as it does in myogenesis, in order to increase the number of cells that will later differentiate. Importantly however, as both FOXK1 and FOXK2 have been shown to mediate Wnt signaling through DVL nuclear translocation, and that Wnt signaling is known to

inhibit adipogenesis, our data show that indeed FOXKs expression decreases at the onset of the differentiation program. Taken together, FOXK1 is O-GlcNAcylated by OGT, presumably as an output for the metabolic regulation of its function, and its activity is required for efficient differentiation of mesoderm-derived tissues, however the link between this mark and its activity remains to be elucidated.

In summary, our study provides new evidence for the regulation of adipogenesis through the transcription factor FOXK1 and demonstrates a differential regulation from its paralog FOXK2 via O-GlcNAcylation. These findings will help decipher complex post-translation modification networks in the BAP1 complex and deepen our understanding of the molecular basis of this tumour suppressor complex

3.5 Acknowledgements

We thank all the members of Dr. El Bachir Affar's laboratory for technical assistance. This work was supported by grants from the Canadian Institutes of Health Research (CIHR) (MOP-115132) and the Natural Sciences and Engineering Research Council of Canada (NSERC) (355814-2010) to E.B.A. E.B.A. is a scholar of the Fonds de la Recherche du Québec - Santé (FRQ-S) and the CIHR. J.G. has a M.Sc. scholarship from the FRQ-S. The Proteomics facility at The Institute for Research in Immunology and Cancer (IRIC) receives infrastructure support from IRICoR, the Canadian Foundation for Innovation, and the Fonds de Recherche du Québec- Santé (FRQS).

3.6 Material and methods

Bacterial induction, purification and GST-Pulldown

GST-Pulldown was performed as previously described [220]. Briefly, purified GST-tagged recombinant protein were purified from *E. Coli* bacteria with Glutathione-agarose resin (Sigma). As for His-tagged proteins, they were induced in the same manner as the GST-tagged proteins except they were purified with Ni-NTA Agarose resin (Life Technologies). Protein were induced over day with 400 µM of IPTG. For GST-Pulldown, 2 µg of beads were incubated overnight at 4ºC with the indicated recombinant His-tagged protein in a GST-pulldown binding buffer (50 mM Tris-HCl, pH 7.5, 50 mM NaCl, 0.02% Tween 20, 1 mM

PMSF and 500 μM DTT). Next day, beads were washed 8 times with GST-pulldown wash buffer (50mM Tris pH 7.5, 150mM NaCl, 1mM EDTA, 0.1% Tween 20, 1mM PMSF, 200 μM DTT). Proteins were then eluted with 2X Laemmli buffer and protein interaction were analyzed by western blotting.

Cell culture and G0 synchronization

Human embryonic kindney (HEK293T), human osteosarcoma (U2OS), HeLa S3, and human lung carcinoma (H226) were cultured according to standard procedures in DMEM supplemented with 5% Foetal Bovine Serum (FBS), 1% Glutamine and 1% Penicillin/Streptomycin except for murin adipocyte progenitors (3T3L1) and human fibroblast (LL) which were cultured with 10% FBS. Human chronic myelogenous leukemia K562 and K562-ASXL2 suspension cells were maintained in RPMI medium supplemented with 5% FBS, 1% Glutamine and 1% Penicillin/Streptomycin. Cell cycle synchronizations in G0 were done as previously described [189] and cell cycle analysis was performed using FACScan flow cytometer fitted with CellQuestPro software (BD Biosciences) as previously described [250] and figures were made using FlowJo software.

Plasmids, transfections and siRNA treatments

GST-, FLAG- and MYC-tagged constructs were generated using the recombination technology of the Gateway system from Life Technologies. siRNA-resistant cDNA coding for FOXK1 and FOXK2 were synthesized from Biobasic Int directly into Bluescript plasmid. His-YY1 was previously described [251]. pOZN, pOZN-FLAG-HA-BAP1 WT and pOZN-FLAG-HA-BAP1ΔHBM were previously generated [220]. Both MYC-OGT, FLAG-OGT WT and catalytic dead mutants were produced as described [22] and GST-tagged deletion mutants of BAP1 were previously generated [223]. Plasmids transfections were done in HEK293T with mammalian expressing vectors using polyethylenimine (PEI) (Sigma-Aldrich). Three days post-transfection cells were harvested in PBS or in lysis buffer (25 mM Tris-HCl pH 7.5) for subsequent analysis.

U2OS double siRNA transfections were done in serum-free DMEM medium for 16h with Lipofectamine 2000 (Life Technologies) as previously described [237] 3T3L1 double siRNA transfection were done in serum-free DMEM medium for 16h with RNAi Max Lipofectamine (Life Technologies) using 200 pmol of either ON-TARGET plus Non-targeting

pool (D-001810-10-50) (Thermo Scientific, Dharmacon) or siFoxk1 (SASI_Mm01_00032593) (SASI_Mm01_00032594) (SASI_Mm01_00032595) (SASI_Mm01_00032596) (SASI_Mm02_00351347) (SASI_Mm02_00351348) (SASI_Mm01_00160371) (SASI_Mm01_00160372) or siFoxk2 (SASI_Mm02_00294023) (SASI_Mm02_00294024) (SASI_Mm02_00294025) (SASI_Mm02_00294026). Then, medium was changed for complete DMEM supplemented with 10% FBS, 1% Glutamine and 1% Streptomycin and a second siRNA transfection was done 72h following the first siRNA transfection so as to start 3T3L1 differentiation.

Immunoprecipitation and complex purification

For native immunoprecipitations, cells were harvested in PBS and pellets were lysed for 30 minutes on ice in EB150 buffer (50mM Tris pH 7.5, 150mM NaCl, 5mM EDTA, 1% Triton, 1mM DTT, 1mM PMSF, 2µM PUGNAc, 10mM BGP, 1mM Na_3VO_4, 50 mM NaF,1X anti-protease cocktail (Sigma)). Lysates were then spun for 20 minutes at 14 000 rpm at 4ºC to pellet insoluble material and supernatants were incubated overnight with rotation at 4ºC with either anti-FLAG resin (Sigma) or anti-Protein G Sepharose and 4µg of the appropriate antibody. The following day, beads were washed with EB150. Bound proteins were eluted with 2X Laemmli buffer and subjected to Western Blotting. As for the stable cell line complex purifications, 1 liter of HeLa S3 pOZN, pOZN-FLAG-HA-BAP1 or pOZN-FLAG-HA-BAP1ΔHBM were grown to ~$1x10^6$ cells/ml and then cells were harvested and pelleted. Pellets were lysed on ice for 30 minutes in EB150 (50mM Tris pH 7.5, 150mM NaCl, 1mM EDTA, 0.5% Triton, 1mM DTT, 1mM PMSF, 2µM PUGNAc, 10mM BGP, 1mM Na_3VO_4, 50mM NaF, 1X anti-protease cocktail (Sigma)). Lysates were then spun at 20 000 rpm for 20 minutes at 4ºC. Supernatant was then filtered through a 0.45 µm filter onto anti-FLAG resin (Sigma) for overnight rotation at 4ºC. The following day, beads were washed and bound proteins were eluted with 150 µg/ml of FLAG peptide and subjected to Western Blotting. For denaturing immunoprecipitations, cells were first harvested in a lysis buffer (25 mM Tris-HCl pH 7.5 and 1% SDS). Samples were boiled for 10 minutes, sonicated and samples were diluted with 9 volumes of EB150. Immunoprecipitations was performed as previously described for native immunoprecipitations.

Site-directed mutagenesis

Site-Directed Mutagenesis was performed using standard laboratory techniques and all mutants were sequenced. Primers used for site-directed mutagenesis are as follows: FOXK1 R127A primer_F: ACGATAGGGGCGAATAGCAGCCAAGGGAGCGT, FOXK1 R127A primer_R: TGCTATTCGCCCCTATCGTCACCGACGGTTGC, BAP1 T493A primer_F: ACCCCCAGCAATGAGAGTGCAGACAC, BAP1 T493A primer_R: GATCTCAGAGGCCGTGTCTGCACT

Differentiation and starvation

3T3L1 differentiation assays were performed as previously described [223] in parallel with siRNA treatment. Briefly, 3T3L1 cells were plated at the same density and transfected with siRNA using Lipofectamine RNAi Max as described above. Cells were then grown to confluence and left at confluency for 48h. The cells were then transfected with siRNA a second time but in differentiation media (DMEM supplemented with 10% foetal bovine serum, 1% Glutamine, 1% penicillin/streptomycin, 1 µM dexamethasone, 1 µg/ml insulin and 500 µM isobutylmethylxanthine (IBMX) (Sigma)). Two days post-induction, media was changed for DMEM medium supplemented with 10 % FBS, 1% Glutamine, 1% penicillin/streptomycin and 1 µg/ml insulin. Media was changed every 48 hours and cells were harvested at indicated time points. For LL and K562 stably expressing FLAG-HA-tagged ASXL2 starvation, cells were starved according to Bowman et al [114] with Hank's Balanced Salt Solution (HBSS) supplemented with 10 mM HEPES pH 7.5 and 1% Penicillin-Streptomycin for the indicated time. When indicated, cells were replenished for 2h by feeding back the cells with growing medium. Cells were then harvested for subsequent immunoprecipitation.

Oil Red O staining

Prior to Oil Red O staining, scans of media colour were rapidly taken using a HP Scanjet 8300. 3T3L1 cells were fixed in 10% formalin for 10 minutes at room temperature (RT). Cells were then washed with PBS, ddH2O and incubated with 60% isopropanol for 5 minutes at RT. Cells were completely dried at RT and then incubated in Oil Red O working solution composed of a filtered 60% solution of Oil Red O stain (Sigma #O0625-25G) for 10 minutes. Cells were then rapidly washed 4 times with ddH2O and images were taken using an inverted microscope Olympus BX53F.

Immunoblotting and antibodies

Cells were harvested either in PBS for subsequent immunoprecipitation or in a lysis buffer composed of 25 mM Tris-HCl pH 7.3 and 1% SDS. Total cell lysates harvested in lysis buffer were boiled at 95°C for 10 min and sonicated. Protein quantification was done by bicinchoninic acid (BCA) assay. For western blotting, samples were diluted in 2X or 4X Laemmli buffer and SDS-PAGE and immunoblotting were performed following standard procedure. The band signals were acquired with a LAS-3000 LCD camera coupled to MultiGauge software (Fuji, Stamford, CT, USA).

Mouse monoclonal anti-BAP1 (C4, sc-28383), rabbit polyclonal anti-FOXK1 (H140, sc-134550), rabbit polyclonal anti-YY1 (H414, sc-1703), rabbit polyclonal anti-OGT (H300, sc-32921), mouse monoclonal anti-tubulin (B-5-1-2, sc-23948) and mouse monoclonal anti-CDC6 (180.2 sc-9964) were from Santa Cruz. We generated the rabbit polyclonal anti-FOXK2. Rabbit polyclonal anti-HCF-1 (A301-400A) was from Bethyl Laboratories. Mouse monoclonal anti-Flag (M2) was from Sigma-Aldrich. Mouse monoclonal anti-MYC (9E10) was from Covance. Monoclonal anti-O-Linked N-acetylglucosamine (RL2, ab2739), rabbit polyclonal anti-H3 (ab1791) were from Abcam. Mouse monoclonal anti-β-Actin (MAB1501, clone C4) was from Millipore. Rabbit monoclonal anti-perillipin (D1D8, #9341) was from Cell Signaling. Rabbit polyclonal anti-FABP4 (#10004944) was from Cayman Chemical.

CHAPITRE 4

4. Discussion

Durant la dernière décennie, de nombreuses études ont démontré le rôle fondamental qu'occupe l'O-GlcNAcylation au sein de la fonction cellulaire. À ce jour, l'identification de protéines ciblées par OGT couvrent la presque totalité des voies de signalisation et jouent un rôle central dans la régulation de la plupart des processus biologiques chez les eukaryotes. Par ailleurs, il est maintenant clair qu'OGT agit de manière prépondérante au niveau de la régulation transcriptionnelle et épigénétique étant donné le nombre croissant de régulateurs transcriptionnels modifés et modulés par O-GlcNAcylation. Toutefois, la fonction de sa présence dans plusieurs complexes transcriptionnels est encore inconnue et de ce fait, son rôle dans les mécanismes de répression et d'activation oncogéniques est encore très peu clair. De plus, bien que de nombreuses études cherchent à construire le réseau de régulation de l'O-GlcNAcome, la plupart des substrats d'OGT identifiés par analyse de criblage à haut débit couplé à la spectrométrie de masse doivent être validés à l'aide d'outil plus spécifique à l'O-GlcNAcylation. À ce sujet, le rôle épigénétique d'OGT par l'O-GlcNAcylation des histones récemment rapporté nécessite une attention particulière quant à la validation et la détermination de sa fonction et de son intégration au «code d'histone». D'autre part, la caractérisation de la fonction d'OGT dans la régulation de la transcription via son association à certains complexes transcriptionnels essentiels à l'hométostasie cellulaire, tels que le complexe suppresseur de tumeurs BAP1 n'a pas encore été faite. De ce fait, les travaux de recherche présentés dans ce mémoire permettront non seulement de rediriger le mécanisme d'action épigénétique d'OGT, mais aussi d'approfondir l'implication de l'O-GlcNAcome au niveau transcriptionnel.

4.1 Les histones ne sont pas des substrats d'OGT

Étant donné la diversité et le nombre important de substrats ciblés par OGT, il est tout à fait plausible que les histones puissent être O-GlcNAcylées. De plus, la structure d'OGT laisse croire que les queues flexibles et non-structurées des histones peuvent aisément se positionner dans son site actif. Afin d'investiguer le rôle d'OGT dans la régulation épigénétique impliquant la modification des histones, nous avons tenté de valider leur O-GlcNAcylation à l'aide de différentes méthodes d'extraction utilisées lors des études ayant rapporté que les histones sont O-GlcNAcylées. En plus des différentes méthodes d'extraction, nous avons mis au point plusieurs conditions d'expression d'histones FLAG-H2A ou FLAG-H2B en parallèle avec la co-expression d'OGT pouvant permettre de déterminer clairement que le signal détecté correspond à

de l'O-GlcNAcylation. La diversité des méthodes d'extraction par sel/détergent, par immunoprécipitation dénaturante et par acide aurait dû permettre de valider au moins de trois manières différentes les travaux rapportés. Cependant, nous n'avons pu détecter qu'un très faible signal au poids moléculaire correspondant aux histones qui n'a pas augmenté avec la surexpression d'OGT contrairement à d'autres protéines de plus haut poids moléculaire. Cette observation a également été supportée par le fait que la déplétion d'OGT par ARN interférant n'a pas résulté en une diminution du signal détecté, ni en la diminution de H2BK120Ub. Cette impossibilité de corréler le signal détecté avec la tendance normale de l'O-GlcNAc à être modulé en réponse à la fluctuation des niveaux d'OGT nous a menés à nous questionner sur les conclusions des travaux rapportés et sur l'occurrence et la fonction de l'O-GlcNAcylation des histones.

Depuis la découverte de l'O-GlcNAc, un grand nombre de techniques ont été développées pour faciliter l'analyse de l'O-GlcNAcome. Étant donné, que l'O-GlcNAcylation est une modification extrêmement dynamique et que le nombre de sites modifiés est très variable d'une protéine à une autre, il est possible que dans certains types cellulaires ou dans certaines conditions spécifiques les niveaux d'O-GlcNAcylation soient imperceptibles et que la purification d'une quantité abondante de protéines soit nécessaire à sa détection. Face à cette réalité et bien qu'une grande quantité d'histones aient été purifiées pour réaliser la totalité de nos travaux, nous avons utilisé un plus large éventail de techniques de détection in vivo et in vitro de l'O-GlcNAc de manière à optimiser et à faciliter sa détection. Ainsi, les résultats obtenus par WGA Pull-Down, chimie *Click-it*, essais d'O-GlcNAcylation in vitro et spectrométrie de masse indiquent que les histones, endogènes ou recombinantes, ne sont pas modifiées par OGT ou, du moins, pas à un niveau au-dessus de la limite de détection des techniques employées. Par ailleurs, la plupart des MPTs sont catalysées en réponse à un évènement cellulaire précis et leur occurrence peut changer d'un type cellulaire à un autre [252]. L'analyse de différents types cellulaires ainsi que de conditions de privation en glucose et de synchronisation cellulaire nous a permis de renforcer nos conclusions quant à la non O-GlcNAcylation des histones. De manière surprenante, ceci ne concorde pas avec les études rapportées qui ont utilisé des méthodes semblables.

Comment est-ce possible que des effets biologiques aient été attribués à l'O-GlcNAcylation de certains sites d'histones si ces dernières ne sont pas O-GlcNAcylées? Comme mentionné précédemment, OGT joue un rôle central dans la régulation de la plupart des processus biologiques. De ce fait, il est possible d'imaginer plusieurs scénarios où OGT peut spécifiquement moduler un évènement en régulant la chromatine sans modifier les histones. D'abord, OGT pourrait agir en régulant les kinases spécifiques à certains sites d'histones. De ce fait, la surexpression d'OGT résultant en une diminution de certains sites de phosphorylation ne serait pas due à une compétition pour ces sites ou par l'encombrement stérique d'un site adjacent, mais plutôt par une augmentation des niveaux d'O-GlcNAcylation de ces kinases résultant en une diminution de leur stabilité ou activité [135]. Aussi, l'association d'OGT à plusieurs complexes modificateurs d'histones suggère qu'OGT peut réguler l'activité de ces derniers et provoquer un remodelage de la chromatine générant ainsi une réponse spécifique en modulant par exemple le *crosstalk* entre les marques d'histones. Pour résumer, les méthodes de régulation de la chromatine par OGT via le recrutement, la stabilité et/ou l'activité de protéines impliquées dans le remodelage et la régulation de la chromatine peuvent être nombreuses et peuvent tout de même permettre une régulation transcriptionnelle et épigénétique précises sans impliquer directement les histones. De ce fait, nos travaux supportent plutôt un modèle de régulation épigénétique qui exclue l'O-GlcNAcylation des histones.

4.2 Détection artéfactuelle de l'O-GlcNAc sur les histones

Les analyses par immunodétection peuvent souvent être difficiles à interpréter lorsque le signal généré est faible et que la membrane doit être longuement exposée. La détection d'un très faible signal au niveau du poids moléculaire des histones en utilisant des anticorps spécifiques contre l'O-GlcNAc à considérablement compliqué l'analyse des résultats expérimentaux. L'importance de discerner un évènement réelle d'un évènement artéfactuel est considérable puisque cela peut changer l'interprétation d'un mécanisme moléculaire et rediriger les travaux de recherche. Le fait que la plupart des *immunoblots* montrent un faible signal au niveau des histones qui n'est pas modulé en réponse aux fluctuations d'OGT suggère que ce signal pourrait en être de l'O-GlcNAcylation constitutive, mais peu abondante. Par contre, en plus de ne pas avoir pu confirmer la régulation entre les niveaux d'H2BS112 et H2BK120Ub, l'ensemble de nos résultats in vivo et in vitro suggèrent plutôt que ce signal est non spécifique et qu'il ne correspond donc pas à de l'O-GlcNAcylation. Il aurait aussi été intéressant de surexprimer la

forme nucléaire d'OGA afin de déterminer si le signal détecté diminue en présence d'OGA. Ceci aurait aussi pu aider à déterminer si le signal détecté est spécifique ou non à de l'O-GlcNAcylation [253]. Afin de faire une interprétation appropriée d'un phénomène biologique, il est primordial de valider de manière rigoureuse la spécificité, la sélectivité et la reproductibilité des anticorps utilisés, surtout lorsque les résultats sont ambigus [254]. En effet, notre analyse de la spécificité des anticorps disponibles générés contre l'O-GlcNAc a révélé qu'ils causent une détection artéfactuelle qui peut être due 1) à l'abondance des histones analysées et/ou 2) à la reconnaissance non spécifique générée par l'anticorps primaire ou 3) secondaire. Entre autres, l'analyse de la spécificité de l'anticorps CTD110.6 a déjà démontré qu'il a une affinité pour d'autres épitopes que l'O-GlcNAc [186]. Ceci concorde avec la tendance de l'anticorps CTD110.6 à générer un signal plus fort que celui de RL2. De plus, les analyses mutationnelles de H2BS112A n'ont pas permis d'éliminer complètement le signal exogène, ce qui supporte encore le fait que la grande quantité d'histones utilisées contribuent fortement à la non-spécificité du signal. Dans ces cas précis, il est impératif d'intégrer des contrôles négatifs à l'analyse qui permettent de distinguer un signal spécifique d'un signal non-spécifique. De ce fait, la détection des histones de levures et de bactéries avec RL2 et H2BS112 a grandement contribué à renforcer nos conclusions sur le fait que les histones ne sont pas O-GlcNAcylées et que les anticorps contre l'O-GlcNAcylation globale ou contre des sites spécifiques O-GlcNAcylés peuvent générer des artéfacts de détection.

4.3 OGT régule FOXK1, mais pas FOXK2 par O-GlcNAcylation

Bien que nous n'ayons pu confirmer le rôle d'OGT dans l'O-GlcNAcylation des histones, nous avons identifié un autre rôle possible d'OGT dans la régulation transcriptionnel et épigénétique par l'entremise du complexe PcG suppresseur de tumeur BAP1. L'utilisation de techniques de détection de l'O-GlcNAc en parallèle avec des expériences d'immunoprécipitation ont permis d'identifier FOXK1 comme nouveau substrat d'OGT. De manière encore plus intéressante, cette observation est spécifique à FOXK1, mais pas à son paralogue FOXK2 qui se trouve aussi dans le complexe. Donc, en plus d'identifier un nouveau rôle d'OGT dans la régulation du complexe BAP1, nos travaux démontrent un nouveau mécanisme de régulation différentiel entre FOXK1 et FOXK2 qui sont normalement impliqués similairement dans de nombreux processus biologiques [114, 137]. Entre autres, FOXK1 et FOXK2 interagissent de

manière mutuellement exclusive avec la même Thr493 de BAP1 et comme la mutation de ce résidu abolit complètement l'interaction entre FOXK1 et BAP1 in vivo, la phosphorylation de ce résidu semble importante pour leur interaction. L'O-GlcNAcylation de FOXK1 dans le complexe BAP1 suggère fortement que FOXK1 lie ce complexe à la régulation du métabolisme. De plus, l'intensité du signal d'O-GlcNAc ainsi que le retard de migration de FOXK1 observable sur plusieurs *immunoblots* est indicatif de plusieurs sites modifiés. En effet, il est connu que TET2 est modifiée par O-GlcNAcylation sur plusieurs sites, ce qui résulte aussi en un retard de migration et génère un fort signal d'O-GlcNAcylation lorsque l'on analyse TET2 par Western blot. Bien que la modulation de l'O-GlcNAcylation de FOXK1 ne semble pas affecter son interaction avec BAP1, il est possible d'imaginer qu'en réponse à un changement métabolique, OGT O-GlcNAcyle FOXK1 sur des sites précis et par conséquent permet le recrutement différentiel du complexe BAP1 à des gènes spécifiques en fonction de la réponse attendue. Cette hypothèse est pertinente sachant que l'O-GlcNAcylation de différents sites résulte souvent en des conséquences fonctionnelles distinctes [255]. L'identification des sites d'O-GlcNAcylation de FOXK1 par spectrométrie de masse nous permettrait d'effectuer une analyse mutationnelle de FOXK1 afin d'investiguer le rôle précis de l'ensemble et/ou de chaque site d'O-GlcNAcylation. Parallèlement, une analyse ChIPseq permettrait de déterminer si l'O-GlcNAcylation différentielle influence le recrutement du complexe à certains gènes cibles. Jusqu'à présent, nos travaux ne permettent donc pas de déterminer si les sites d'O-GlcNAcylation de FOXK1 peuvent changer en fonction du contexte cellulaire. Cependant, l'augmentation des niveaux de BAP1 associés à FOXK1 observée en parallèle avec l'augmentation de l'O-GlcNAcylation de FOXK1 en réponse à l'entrée du cycle cellulaire ne concorde pas avec les résultats démontrant que la diminution de l'O-GlcNAcylation de FOXK1 par déplétion d'OGT n'affecte pas son interaction avec BAP1. Cette contradiction expérimentale supporte un modèle où OGT régulerait l'interaction FOXK1-BAP1 dans un contexte spécifique. Cela est aussi appuyé par le fait que la présence de FOXK1 dans le complexe BAP1 est considérablement affectée par la privation en glucose.

Il a été démontré que FOXK1 est fortement phosphorylé en réponse à l'autophagie cellulaire et que cette phosphorylation provoque sa translocation cytoplasmique. [114] De plus, la stabilité d'OGT est grandement affectée par l'inactivation de mTOR lors de ce processus [49]. Par conséquent, il est possible qu'un rôle potentiel de l'O-GlcNAcylation de FOXK1 implique

une régulation de sa localisation cellulaire par une compétition phosphorylation/O-GlcNAcylation. En réponse à une concentration limitante de nutriments, mTOR est inhibé, ce qui engendre la dégradation protéasomale d'OGT. Il est alors possible de spéculer que cela affecte l'O-GlcNAcylation de certains sites de FOXK1, ce qui promeut la phosphorylation nécessaire à son exclusion nucléaire. Ainsi localisé dans deux compartiments différents, BAP1 ne pourrait plus être recrutée aux gènes cibles de FOXK1 résultant en l'activation ou la répression de ces gènes. Toutefois, cela ne concorde pas avec la régulation de FOXK2 qui est aussi transloqué dans le cytoplasme lors de l'autophagie [114]. D'autres modes de régulation sont donc probablement impliqués. Il est tout de même possible que l'O-GlcNAcylation contribue à la régulation plus fine et plus rapide de FOXK1 qui est beaucoup plus affecté par la privation de glucose que FOXK2 en termes d'association avec le complexe BAP1. En conclusion, nos travaux suggèrent une implication importante de l'O-GlcNAcylation de FOXK1 dans la régulation de processus métaboliques et propose que cette dernière contribue, entre autres, à la régulation de la fonction du complexe BAP1. Cependant, plus d'analyses des niveaux d'H2AK119Ub aux gènes ciblés par le complexe FOXK1-BAP1 dans ces conditions sont nécessaires pour identifier le mécanisme fonctionnel.

4.4 FOXK1 est requis pour l'adipogenèse

Une analyse fonctionnelle par déplétion de Foxk1 utilisant des ARN interférants dans le modèle murin 3T3-L1 nous a permis d'identifier Foxk1 comme régulateur crucial de l'adipogenèse. En effet, la déplétion de Foxk1 à l'aide de petits ARN interférants réduit significativement la formation de gouttelettes lipidiques détectées à l'aide de la coloration *Oil Red O.* Ce phénotype est spécifique puisque l'utilisation individuelle de plusieurs ARNi ciblant une région différente de la séquence de Foxk1 génère le même défaut de différenciation. Cette nouvelle implication de FOXK1 ainsi que son rôle connu dans le maintien de la population de cellules myoblastiques, indique que FOXK1 est largement engagé dans le programme de différenciation cellulaire et suggère que son action est étendue au-delà de ces deux tissus. En fait, la surexpression de FOXK1 a récemment été associée à l'hyperprolifération des cellules intestinales contribuant au développement d'adénocarcinomes du colon et suggère donc un rôle dans la régulation de la différenciation des cellules des cryptes intestinales qui sont constamment

renouvelées [137]. Ces observations suggèrent que FOXK1 régule la différenciation par l'entremise de la régulation de la prolifération cellulaire. D'ailleurs, notre groupe a déjà démontré que le complexe BAP1 est impliqué de manière fonctionnelle dans l'adipogenèse via son ubiquitination par l'ubiquitine hybride E2/E3 ligase UBE2O et qu'il contrôle la prolifération cellulaire via ASXL1 et ASXL2 (voir annexes) [223].

Dans le tissu musculaire, FOXK1 inhibe FOXO4 et MEF2, ce qui résulte en le soutien d'un état prolifératif nécessaire à repeupler la population de cellules différenciées [113]. Plus précisément, ce mécanisme d'inhibition de Foxo4 par Foxk1 empêche l'activation de l'inhibiteur du cycle cellulaire p21. En ce qui concerne le tissu adipeux, l'adipogenèse peut être divisée en deux grands stades, soit en un stade précoce défini par une expansion mitotique clonale (EMC) et en un stade tardif durant lequel le programme de différenciation est engagé. Lorsque la différenciation est induite, les préadipocytes qui sont dans un état d'inhibition de contact ré-entrent de manière synchrone dans le cycle cellulaire pour faire l'EMC qui consiste à environ 2-3 cycles de réplication pour ensuite enclencher le programme de différentiation [256]. Bien que nos travaux n'expliquent pas le mécanisme par lequel FOXK1 régule cette fonction, il est possible que FOXK1 soit impliqué dans la régulation de l'EMC qui selon plusieurs études, est requise pour la différenciation terminale des adipocytes [257]. En fait, alors qu'il a déjà été démontré que Foxk1 inhibe l'activité transcriptionnelle de Foxo4 en interagissant avec son domaine FH, il pourrait aussi réguler l'activité transcriptionnelle d'autres Fox de la même façon puisque le domaine FH est très conservé. De manière intéressante, Foxo1 est un régulateur clé de la différenciation adipocytaire et régule la transcription de p21 dans ce tissu [258]. Il ne serait donc pas surprenant que Foxk1 puisse inhiber l'activité transcriptionnelle de Foxo1 afin de permettre l'EMC. Dans ce cas, la déplétion de Foxk1 dans les 3T3-L1 empêcherait l'inhibition de p21, ce qui entraînerait un défaut de l'EMC et par conséquent un défaut de différenciation. Ceci peut aussi être supporté par l'implication de FOXK1 récemment découverte dans la régulation de la voie Wnt/β-caténine [137]. En fait, la voie canonique Wnt/β-caténine inhibe PPARγ qui est le régulateur maître du programme de différenciation adipocytaire [257]. De ce fait, il est possible de spéculer qu'en réponse à la déplétion de Foxk1 dans les cellules 3T3-L1, l'EMC serait empêchée par l'activation de p21 et le programme de différenciation serait lancé trop tôt. Cette combinaison de défauts mécanistiques entraînerait ainsi une différenciation aberrante. Quant à la diminution de l'O-GlcNAcylation de Foxk1 durant l'adipogenèse, elle est

possiblement une conséquence de la différenciation terminale sachant que durant ce processus, OGT est relocalisée dans le cytoplasme des cellules différenciées [170]. Il est alors possible que Foxk1 non-glycosylé joue un autre rôle particulier dans la régulation des cellules post-mitotiques. Cependant, il est fort probable qu'OGT modifie FOXK1 dans le but de réguler sa fonction adipocytaire et que sa O-GlcNAcylation soit nécessaire au lancement du programme de différenciation cellulaire.

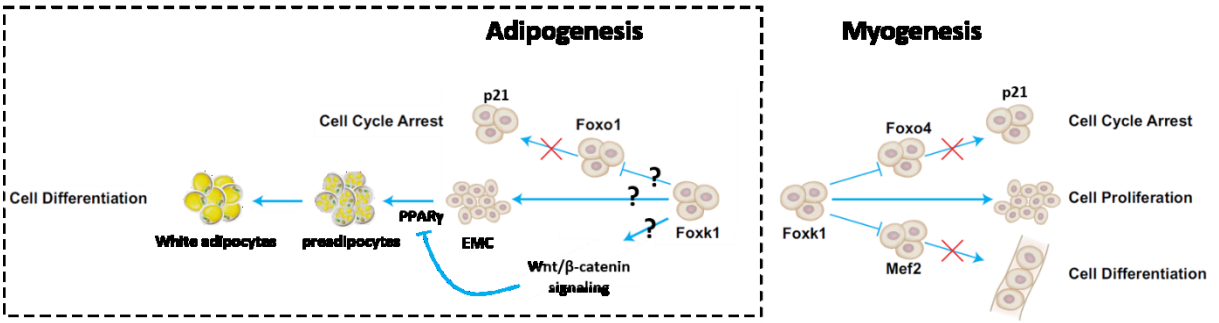

Figure 24. Modèle proposé pour la régulation de l'adipogenèse par FOXK1. Durant la myogenèse Foxk1 inhibe Foxo4 et Mef2, ce qui empêche l'arrêt du cycle cellulaire et la différenciation respectivement. De ce fait, Foxk1 soutient la prolifération nécessaire à la formation de la population de cellules progénitrices myoblastiques nécessaire à la réparation du tissu musculaire. Il est alors possible d'extrapoler la fonction de Foxk1 dans le tissu adipeux par des mécanismes de régulations similaires. Foxk1 empêcherait donc l'arrêt du cycle cellulaire par son interaction avec le paralogue de Foxo4, Foxo1. De plus, la fonction récente de Foxk1 dans l'activation de la voie Wnt/β-caténine suggère que Foxk1 peut inhiber PPARγ et empêcher une différenciation cellulaire précoce. Par conséquent, Foxk1 régulerait l'expansion mitotique clonale (EMC) nécessaire à la différenciation adipocytaire adéquate. Modifié de Shi X et al. (2012).

4.5 Conclusion générale

En conclusion, dans l'effort de déterminer la fonction épigénétique d'OGT, nous avons revisité le concept d'O-GlcNAcylation des histones récemment rapporté. De manière surprenante, nous n'avons pu reproduire les résultats obtenus lors de ces études. De ce fait, nos travaux supportent plutôt un modèle où la régulation épigénétique médiée par OGT se fait indirectement par l'O-GlcNAcylation de régulateurs transcriptionnels recrutés à la chromatine. Parmi ces complexes régulateurs, notre groupe s'intéresse au complexe suppresseur de tumeurs BAP1. Ainsi, en se concentrant sur le rôle d'OGT dans le complexe BAP1, nous avons identifié FOXK1 comme un nouveau substrat ciblé par l'O-GlcNAcylation et par le fait même identifié un

nouveau mécanisme de régulation différentiel entre FOXK1 et FOXK2 par modifications post-traductionnelles. De plus, nos travaux ont identifié une nouvelle fonction de FOXK1 dans la régulation de l'adipogenèse.

L'importance de comprendre les mécanismes de régulation du complexe BAP1 est soulignée par le fait que la dérégulation de ce dernier cause une susceptibilité élevée au développement de cancers. Son association récente à un syndrome de prédisposition tumorale démontre à quel point il est urgent de développer des outils thérapeutiques spécifiques pouvant améliorer le pronostic clinique [259]. Pour ce faire, il est primordial de décortiquer les mécanismes moléculaires du complexe BAP1. De ce fait, la plupart des membres centraux du complexe BAP1, tels que les PcG ASXL1 et ASXL2, sont sujets à de nombreuses études qui ont démontré que l'intégrité du complexe est aussi essentielle à sa fonction qui sont nécessaire à l'activité de déubiquitination de H2AK119Ub [119]. Malgré tout, la façon dont BAP1 régule la transcription des gènes est encore très peu comprise. Parmi les protéines associées, les facteurs de transcription FOXK1 et FOXK2 sont probablement les moins étudiés et ont pourtant été montrés comme pouvant réguler la transcription de manière atypique [137, 260]. La caractérisation de leur fonction permettra d'améliorer la compréhension générale du complexe BAP1, mais aussi de définir un lien plus clair entre le métabolisme et la dérégulation de la fonction de BAP1 pouvant mener au développement et à la progression de cancers.

En perspective, bien que nos travaux n'aient pu confirmer l'O-GlcNAcylation des histones, ils soulignent sans aucun doute l'importance de valider les outils utilisés et d'inclure des contrôles pertinents lors de validations expérimentales. Ces travaux soulèvent un doute raisonnable quant à l'intégration de cette modification au «code d'histones», ce qui permettra à ce domaine de recherche d'apporter une réflexion plus approfondie et prudente à ce sujet. De plus, en n'ayant pu identifier les histones comme substrats directs d'OGT, cette étude suggère plutôt un rôle beaucoup plus complexe qu'attendu de l'O-GlcNAcylation dans la régulation épigénétique via un mécanisme indirect. Une investigation plus approfondie de l'impact de l'O-GlcNAcylation sur les complexes régulateurs de la chromatine sera nécessaire afin de répondre à cette question.

Par ailleurs, les mécanismes moléculaires qui définissent le maintien des cellules souches sont peu connus et l'implication de l'axe BAP1/FOXK1/OGT dans la régulation de l'adipogenèse

ouvre tout un champ d'investigation sur le rôle de la déubiquitination et de l'O-GlcNAcylation dans ce contexte. La compréhension des mécanismes entourant la prolifération, la différenciation et surtout le maintien de l'identité des cellules permettra de démystifier d'avantages l'importance de la régulation de la transcription durant la différenciation cellulaire et de comprendre comment une dérégulation de ce système engendre la formation de cancer ou un retard de développent. Alors que les études sur FOXK1 indiquent que ce facteur de transcription est déterminant pour le maintien de la population de cellules progénitrices musculaires, notre groupe a identifié une nouvelle implication de FOXK1, mais cette fois-ci dans un contexte de différenciation cellulaire. L'homéostasie des organes est dépendante de la faculté des cellules souches à se renouveller et à se différencier, il est donc important de faire avancer les connaissances à ce sujet afin de pouvoir contribuer au développement de thérapies contre le cancer et les maladies dégénératives.

RÉFÉRENCES

1. Karve, T.M. and A.K. Cheema, *Small changes huge impact: the role of protein posttranslational modifications in cellular homeostasis and disease.* J Amino Acids, 2011. **2011**: p. 207691.
2. Tarrant, M.K. and P.A. Cole, *The Chemical Biology of Protein Phosphorylation.* Annual Review of Biochemistry, 2009. **78**(1): p. 797-825.
3. Komander, D. and M. Rape, *The ubiquitin code.* Annu Rev Biochem, 2012. **81**: p. 203-29.
4. Torres, C.R. and G.W. Hart, *Topography and polypeptide distribution of terminal N-acetylglucosamine residues on the surfaces of intact lymphocytes. Evidence for O-linked GlcNAc.* J Biol Chem, 1984. **259**(5): p. 3308-17.
5. Shafi, R., et al., *The O-GlcNAc transferase gene resides on the X chromosome and is essential for embryonic stem cell viability and mouse ontogeny.* Proc Natl Acad Sci U S A, 2000. **97**(11): p. 5735-9.
6. Watson, L.J., et al., *Cardiomyocyte Ogt is essential for postnatal viability.* Am J Physiol Heart Circ Physiol, 2014. **306**(1): p. H142-53.
7. Kim, E.J., et al., *Chemical tools to explore nutrient-driven O-GlcNAc cycling.* Crit Rev Biochem Mol Biol, 2014. **49**(4): p. 327-42.
8. Hanover, J.A., et al., *Mitochondrial and nucleocytoplasmic isoforms of O-linked GlcNAc transferase encoded by a single mammalian gene.* Arch Biochem Biophys, 2003. **409**(2): p. 287-97.
9. Sakaidani, Y., et al., *O-linked-N-acetylglucosamine on extracellular protein domains mediates epithelial cell-matrix interactions.* Nat Commun, 2011. **2**: p. 583.
10. Sakaidani, Y., et al., *O-linked-N-acetylglucosamine modification of mammalian Notch receptors by an atypical O-GlcNAc transferase Eogt1.* Biochem Biophys Res Commun, 2012. **419**(1): p. 14-9.
11. Love, D.C., et al., *Mitochondrial and nucleocytoplasmic targeting of O-linked GlcNAc transferase.* J Cell Sci, 2003. **116**(Pt 4): p. 647-54.
12. Lazarus, B.D., D.C. Love, and J.A. Hanover, *Recombinant O-GlcNAc transferase isoforms: identification of O-GlcNAcase, yes tyrosine kinase, and tau as isoform-specific substrates.* Glycobiology, 2006. **16**(5): p. 415-21.
13. Lozano, L., et al., *The mitochondrial O-linked N-acetylglucosamine transferase (mOGT) in the diabetic patient could be the initial trigger to develop Alzheimer disease.* Exp Gerontol, 2014. **58**: p. 198-202.
14. Shin, S.H., D.C. Love, and J.A. Hanover, *Elevated O-GlcNAc-dependent signaling through inducible mOGT expression selectively triggers apoptosis.* Amino Acids, 2011. **40**(3): p. 885-93.
15. Lazarus, B.D., D.C. Love, and J.A. Hanover, *O-GlcNAc cycling: implications for neurodegenerative disorders.* Int J Biochem Cell Biol, 2009. **41**(11): p. 2134-46.
16. Fletcher, B.S., et al., *Functional cloning of SPIN-2, a nuclear anti-apoptotic protein with roles in cell cycle progression.* Leukemia, 2002. **16**(8): p. 1507-18.
17. Hanover, J.A., M.W. Krause, and D.C. Love, *Bittersweet memories: linking metabolism to epigenetics through O-GlcNAcylation.* Nat Rev Mol Cell Biol, 2012. **13**(5): p. 312-21.
18. Blatch, G.L. and M. Lassle, *The tetratricopeptide repeat: a structural motif mediating protein-protein interactions.* Bioessays, 1999. **21**(11): p. 932-9.
19. Zeytuni, N. and R. Zarivach, *Structural and functional discussion of the tetra-trico-peptide repeat, a protein interaction module.* Structure, 2012. **20**(3): p. 397-405.
20. Iyer, S.P. and G.W. Hart, *Roles of the tetratricopeptide repeat domain in O-GlcNAc transferase targeting and protein substrate specificity.* J Biol Chem, 2003. **278**(27): p. 24608-16.

21. Cheung, W.D., et al., *O-linked beta-N-acetylglucosaminyltransferase substrate specificity is regulated by myosin phosphatase targeting and other interacting proteins.* J Biol Chem, 2008. **283**(49): p. 33935-41.
22. Clarke, A.J., et al., *Structural insights into mechanism and specificity of O-GlcNAc transferase.* Embo j, 2008. **27**(20): p. 2780-8.
23. Liu, Y., et al., *Developmental regulation of protein O-GlcNAcylation, O-GlcNAc transferase, and O-GlcNAcase in mammalian brain.* PLoS One, 2012. **7**(8): p. e43724.
24. Lazarus, M.B., et al., *Structure of human O-GlcNAc transferase and its complex with a peptide substrate.* Nature, 2011. **469**(7331): p. 564-7.
25. Kreppel, L.K., M.A. Blomberg, and G.W. Hart, *Dynamic glycosylation of nuclear and cytosolic proteins. Cloning and characterization of a unique O-GlcNAc transferase with multiple tetratricopeptide repeats.* J Biol Chem, 1997. **272**(14): p. 9308-15.
26. Schimpl, M., et al., *O-GlcNAc transferase invokes nucleotide sugar pyrophosphate participation in catalysis.* Nat Chem Biol, 2012. **8**(12): p. 969-74.
27. Janetzko, J. and S. Walker, *The Making of a Sweet Modification: Structure and Function of O-GlcNAc Transferase.* J Biol Chem, 2014.
28. Lewis, B.A. and J.A. Hanover, *O-GlcNAc and the Epigenetic Regulation of Gene Expression.* J Biol Chem, 2014.
29. Hart, G.W., M.P. Housley, and C. Slawson, *Cycling of O-linked beta-N-acetylglucosamine on nucleocytoplasmic proteins.* Nature, 2007. **446**(7139): p. 1017-22.
30. Bond, M.R. and J.A. Hanover, *A little sugar goes a long way: the cell biology of O-GlcNAc.* J Cell Biol, 2015. **208**(7): p. 869-80.
31. Slawson, C., R.J. Copeland, and G.W. Hart, *O-GlcNAc signaling: a metabolic link between diabetes and cancer?* Trends Biochem Sci, 2010. **35**(10): p. 547-55.
32. Pathak, S., et al., *The active site of O-GlcNAc transferase imposes constraints on substrate sequence.* Nat Struct Mol Biol, 2015.
33. Harwood, K.R. and J.A. Hanover, *Nutrient-driven O-GlcNAc cycling - think globally but act locally.* J Cell Sci, 2014. **127**(Pt 9): p. 1857-67.
34. Hanover, J.A., M.W. Krause, and D.C. Love, *The hexosamine signaling pathway: O-GlcNAc cycling in feast or famine.* Biochim Biophys Acta, 2010. **1800**(2): p. 80-95.
35. Schleicher, E.D. and C. Weigert, *Role of the hexosamine biosynthetic pathway in diabetic nephropathy.* Kidney Int Suppl, 2000. **77**: p. S13-8.
36. Bond, M.R., et al., *Conserved nutrient sensor O-GlcNAc transferase is integral to C. elegans pathogen-specific immunity.* PLoS One, 2014. **9**(12): p. e113231.
37. Wells, L., K. Vosseller, and G.W. Hart, *A role for N-acetylglucosamine as a nutrient sensor and mediator of insulin resistance.* Cell Mol Life Sci, 2003. **60**(2): p. 222-8.
38. Jozwiak, P., et al., *O-GlcNAcylation and Metabolic Reprograming in Cancer.* Front Endocrinol (Lausanne), 2014. **5**: p. 145.
39. Alonso, J., M. Schimpl, and D.M. van Aalten, *O-GlcNAcase: promiscuous hexosaminidase or key regulator of O-GlcNAc signaling?* J Biol Chem, 2014. **289**(50): p. 34433-9.
40. Li, J., et al., *Isoforms of human O-GlcNAcase show distinct catalytic efficiencies.* Biochemistry (Mosc), 2010. **75**(7): p. 938-43.
41. Comtesse, N., E. Maldener, and E. Meese, *Identification of a nuclear variant of MGEA5, a cytoplasmic hyaluronidase and a beta-N-acetylglucosaminidase.* Biochem Biophys Res Commun, 2001. **283**(3): p. 634-40.
42. Zhang, Z., et al., *O-GlcNAcase Expression is Sensitive to Changes in O-GlcNAc Homeostasis.* Front Endocrinol (Lausanne), 2014. **5**: p. 206.

43. Vocadlo, D.J., *O-GlcNAc processing enzymes: catalytic mechanisms, substrate specificity, and enzyme regulation.* Curr Opin Chem Biol, 2012. **16**(5-6): p. 488-97.
44. Macauley, M.S. and D.J. Vocadlo, *Increasing O-GlcNAc levels: An overview of small-molecule inhibitors of O-GlcNAcase.* Biochim Biophys Acta, 2010. **1800**(2): p. 107-21.
45. Taylor, R.P., et al., *Glucose deprivation stimulates O-GlcNAc modification of proteins through up-regulation of O-linked N-acetylglucosaminyltransferase.* J Biol Chem, 2008. **283**(10): p. 6050-7.
46. Taylor, R.P., et al., *Up-regulation of O-GlcNAc transferase with glucose deprivation in HepG2 cells is mediated by decreased hexosamine pathway flux.* J Biol Chem, 2009. **284**(6): p. 3425-32.
47. Cheung, W.D. and G.W. Hart, *AMP-activated protein kinase and p38 MAPK activate O-GlcNAcylation of neuronal proteins during glucose deprivation.* J Biol Chem, 2008. **283**(19): p. 13009-20.
48. Sodi, V.L., et al., *mTOR/MYC Axis Regulates O-GlcNAc Transferase Expression and O-GlcNAcylation in Breast Cancer.* Mol Cancer Res, 2015. **13**(5): p. 923-33.
49. Park, S., et al., *Inhibition of mTOR affects protein stability of OGT.* Biochem Biophys Res Commun, 2014. **453**(2): p. 208-12.
50. Whelan, S.A., M.D. Lane, and G.W. Hart, *Regulation of the O-linked beta-N-acetylglucosamine transferase by insulin signaling.* J Biol Chem, 2008. **283**(31): p. 21411-7.
51. Perez-Cervera, Y., et al., *Insulin signaling controls the expression of O-GlcNAc transferase and its interaction with lipid microdomains.* Faseb j, 2013. **27**(9): p. 3478-86.
52. Kaasik, K., et al., *Glucose sensor O-GlcNAcylation coordinates with phosphorylation to regulate circadian clock.* Cell Metab, 2013. **17**(2): p. 291-302.
53. Liu, H., et al., *Proteasomal degradation of O-GlcNAc transferase elevates hypoxia-induced vascular endothelial inflammatory responsedagger.* Cardiovasc Res, 2014. **103**(1): p. 131-9.
54. Yang, Y., et al., *Histone Demethylase LSD2 Acts as an E3 Ubiquitin Ligase and Inhibits Cancer Cell Growth through Promoting Proteasomal Degradation of OGT.* Mol Cell, 2015. **58**(1): p. 47-59.
55. Kreppel, L.K. and G.W. Hart, *Regulation of a cytosolic and nuclear O-GlcNAc transferase. Role of the tetratricopeptide repeats.* J Biol Chem, 1999. **274**(45): p. 32015-22.
56. Lubas, W.A. and J.A. Hanover, *Functional expression of O-linked GlcNAc transferase. Domain structure and substrate specificity.* J Biol Chem, 2000. **275**(15): p. 10983-8.
57. Park, S., et al., *O-GlcNAc modification is essential for the regulation of autophagy in Drosophila melanogaster.* Cell Mol Life Sci, 2015.
58. Selvan, N., et al., *The Early Metazoan Trichoplax adhaerens Possesses a Functional O-GlcNAc System.* J Biol Chem, 2015. **290**(19): p. 11969-82.
59. Gambetta, M.C., K. Oktaba, and J. Muller, *Essential role of the glycosyltransferase sxc/Ogt in polycomb repression.* Science, 2009. **325**(5936): p. 93-6.
60. Gambetta, M.C. and J. Muller, *A critical perspective of the diverse roles of O-GlcNAc transferase in chromatin.* Chromosoma, 2015.
61. Deng, R.P., et al., *Global identification of O-GlcNAc transferase (OGT) interactors by a human proteome microarray and the construction of an OGT interactome.* Proteomics, 2014. **14**(9): p. 1020-30.
62. Vosseller, K., L. Wells, and G.W. Hart, *Nucleocytoplasmic O-glycosylation: O-GlcNAc and functional proteomics.* Biochimie, 2001. **83**(7): p. 575-81.
63. Slawson, C. and G.W. Hart, *O-GlcNAc signalling: implications for cancer cell biology.* Nat Rev Cancer, 2011. **11**(9): p. 678-84.
64. Ranuncolo, S.M., et al., *Evidence of the involvement of O-GlcNAc-modified human RNA polymerase II CTD in transcription in vitro and in vivo.* J Biol Chem, 2012. **287**(28): p. 23549-61.
65. Mizuguchi-Hata, C., et al., *Quantitative regulation of nuclear pore complex proteins by O-GlcNAcylation.* Biochim Biophys Acta, 2013. **1833**(12): p. 2682-9.

66. Simon, D.N. and M.P. Rout, *Cancer and the nuclear pore complex.* Adv Exp Med Biol, 2014. **773**: p. 285-307.
67. Lim, K. and H.I. Chang, *O-GlcNAc inhibits interaction between Sp1 and sterol regulatory element binding protein 2.* Biochem Biophys Res Commun, 2010. **393**(2): p. 314-8.
68. Choudhary, C., et al., *The growing landscape of lysine acetylation links metabolism and cell signalling.* Nat Rev Mol Cell Biol, 2014. **15**(8): p. 536-50.
69. Takahashi, H., et al., *Nucleocytosolic acetyl-coenzyme a synthetase is required for histone acetylation and global transcription.* Mol Cell, 2006. **23**(2): p. 207-17.
70. Zhu, Y., et al., *O-GlcNAc occurs cotranslationally to stabilize nascent polypeptide chains.* Nat Chem Biol, 2015. **11**(5): p. 319-25.
71. Yang, W.H., et al., *Modification of p53 with O-linked N-acetylglucosamine regulates p53 activity and stability.* Nat Cell Biol, 2006. **8**(10): p. 1074-83.
72. Ruan, H.B., et al., *O-GlcNAc transferase/host cell factor C1 complex regulates gluconeogenesis by modulating PGC-1alpha stability.* Cell Metab, 2012. **16**(2): p. 226-37.
73. Li, M.D., et al., *O-GlcNAc signaling entrains the circadian clock by inhibiting BMAL1/CLOCK ubiquitination.* Cell Metab, 2013. **17**(2): p. 303-10.
74. Chu, C.S., et al., *O-GlcNAcylation regulates EZH2 protein stability and function.* Proc Natl Acad Sci U S A, 2014. **111**(4): p. 1355-60.
75. Olivier-Van Stichelen, S., et al., *O-GlcNAcylation stabilizes beta-catenin through direct competition with phosphorylation at threonine 41.* Faseb j, 2014. **28**(8): p. 3325-38.
76. Itkonen, H.M., et al., *O-GlcNAc transferase integrates metabolic pathways to regulate the stability of c-MYC in human prostate cancer cells.* Cancer Res, 2013. **73**(16): p. 5277-87.
77. Skorobogatko, Y., et al., *O-linked beta-N-acetylglucosamine (O-GlcNAc) site thr-87 regulates synapsin I localization to synapses and size of the reserve pool of synaptic vesicles.* J Biol Chem, 2014. **289**(6): p. 3602-12.
78. Andrali, S.S., Q. Qian, and S. Ozcan, *Glucose mediates the translocation of NeuroD1 by O-linked glycosylation.* J Biol Chem, 2007. **282**(21): p. 15589-96.
79. Li, Q. and K. Kamemura, *Adipogenesis stimulates the nuclear localization of EWS with an increase in its O-GlcNAc glycosylation in 3T3-L1 cells.* Biochem Biophys Res Commun, 2014. **450**(1): p. 588-92.
80. Sohn, E.J., et al., *Accumulation of pre-let-7g and downregulation of mature let-7g with the depletion of EWS.* Biochem Biophys Res Commun, 2012. **426**(1): p. 89-93.
81. Sun, T., et al., *MicroRNA let-7 regulates 3T3-L1 adipogenesis.* Mol Endocrinol, 2009. **23**(6): p. 925-31.
82. Comer, F.I. and G.W. Hart, *Reciprocity between O-GlcNAc and O-phosphate on the carboxyl terminal domain of RNA polymerase II.* Biochemistry, 2001. **40**(26): p. 7845-52.
83. Bauer, C., et al., *Phosphorylation of TET proteins is regulated via O-GlcNAcylation by the O-linked N-acetylglucosamine transferase (OGT).* J Biol Chem, 2015. **290**(8): p. 4801-12.
84. Brister, M.A., et al., *OGlcNAcylation and phosphorylation have opposing structural effects in tau: phosphothreonine induces particular conformational order.* J Am Chem Soc, 2014. **136**(10): p. 3803-16.
85. Zeidan, Q. and G.W. Hart, *The intersections between O-GlcNAcylation and phosphorylation: implications for multiple signaling pathways.* J Cell Sci, 2010. **123**(Pt 1): p. 13-22.
86. Hu, P., S. Shimoji, and G.W. Hart, *Site-specific interplay between O-GlcNAcylation and phosphorylation in cellular regulation.* FEBS Lett, 2010. **584**(12): p. 2526-38.
87. Hart, G.W., et al., *Cross Talk Between O-GlcNAcylation and Phosphorylation: Roles in Signaling, Transcription, and Chronic Disease.* Annual Review of Biochemistry, 2011. **80**(1): p. 825-858.

88. Wells, L., et al., *O-GlcNAc transferase is in a functional complex with protein phosphatase 1 catalytic subunits.* J Biol Chem, 2004. **279**(37): p. 38466-70.
89. Slawson, C., et al., *A mitotic GlcNAcylation/phosphorylation signaling complex alters the posttranslational state of the cytoskeletal protein vimentin.* Mol Biol Cell, 2008. **19**(10): p. 4130-40.
90. Dias, W.B., W.D. Cheung, and G.W. Hart, *O-GlcNAcylation of kinases.* Biochem Biophys Res Commun, 2012. **422**(2): p. 224-8.
91. Koo, J. and Y.Y. Bahk, *In vivo putative O-GlcNAcylation of human SCP1 and evidence for possible role of its N-terminal disordered structure.* BMB Rep, 2014. **47**(10): p. 593-8.
92. Smet-Nocca, C., et al., *Identification of O-GlcNAc sites within peptides of the Tau protein and their impact on phosphorylation.* Mol Biosyst, 2011. **7**(5): p. 1420-9.
93. Wang, Z., et al., *Extensive crosstalk between O-GlcNAcylation and phosphorylation regulates cytokinesis.* Sci Signal, 2010. **3**(104): p. ra2.
94. Mishra, S., S.R. Ande, and N.W. Salter, *O-GlcNAc modification: why so intimately associated with phosphorylation?* Cell Commun Signal, 2011. **9**(1): p. 1.
95. Daou, S., et al., *Crosstalk between O-GlcNAcylation and proteolytic cleavage regulates the host cell factor-1 maturation pathway.* Proc Natl Acad Sci U S A, 2011. **108**(7): p. 2747-52.
96. Zargar, Z. and S. Tyagi, *Role of host cell factor-1 in cell cycle regulation.* Transcription, 2012. **3**(4): p. 187-92.
97. Lazarus, M.B., et al., *HCF-1 is cleaved in the active site of O-GlcNAc transferase.* Science, 2013. **342**(6163): p. 1235-9.
98. Capotosti, F., et al., *O-GlcNAc transferase catalyzes site-specific proteolysis of HCF-1.* Cell, 2011. **144**(3): p. 376-88.
99. Sinclair, D.A., et al., *Drosophila O-GlcNAc transferase (OGT) is encoded by the Polycomb group (PcG) gene, super sex combs (sxc).* Proc Natl Acad Sci U S A, 2009. **106**(32): p. 13427-32.
100. Ingham, P.W., *A gene that regulates the bithorax complex differentially in larval and adult cells of Drosophila.* Cell, 1984. **37**(3): p. 815-23.
101. Gambetta, M.C. and J. Muller, *O-GlcNAcylation prevents aggregation of the Polycomb group repressor polyhomeotic.* Dev Cell, 2014. **31**(5): p. 629-39.
102. Endoh, M., et al., *Histone H2A Mono-Ubiquitination Is a Crucial Step to Mediate PRC1-Dependent Repression of Developmental Genes to Maintain ES Cell Identity.* PLoS Genet, 2012. **8**(7): p. e1002774.
103. Endoh, M., et al., *Histone H2A mono-ubiquitination is a crucial step to mediate PRC1-dependent repression of developmental genes to maintain ES cell identity.* PLoS Genet, 2012. **8**(7): p. e1002774.
104. Hoeller, D. and I. Dikic, *Review Article Targeting the ubiquitin system in cancer therapy.* Nature, 2009. **458**: p. 438-444.
105. Gil, J., D. Bernard, and G. Peters, *Role of polycomb group proteins in stem cell self-renewal and cancer.* DNA Cell Biol, 2005. **24**(2): p. 117-25.
106. Reyes Turcu, F., K. Ventii, and K. Wilkinson, *Regulation and Cellular Roles of Ubiquitin-specific Deubiquitinating Enzymes.* Annu Rev Biochem, 2009. **78**: p. 363-397.
107. Jensen, D.E., et al., *BAP1: a novel ubiquitin hydrolase which binds to the BRCA1 RING finger and enhances BRCA1-mediated cell growth suppression.* Oncogene, 1998. **16**(9): p. 1097-112.
108. Carbone, M., et al., *BAP1 and cancer.* Nat Rev Cancer, 2013. **13**(3): p. 153-9.
109. Murali, R., T. Wiesner, and R.A. Scolyer, *Tumours associated with BAP1 mutations.* Pathology, 2013. **45**(2): p. 116-26.
110. Yu, H., et al., *The Ubiquitin Carboxyl Hydrolase BAP1 Forms a Ternary Complex with YY1 and HCF-1 and Is a Critical Regulator of Gene Expression* Mol. Cell. Biol., 2010. **30**(21): p. 5071-5085.

111. Katoh, M., *Functional and cancer genomics of ASXL family members.* Br J Cancer, 2013. **109**(2): p. 299-306.
112. Gordon, S., et al., *Transcription factor YY1: structure, function, and therapeutic implications in cancer biology.* Oncogene, 2006. **25**(8): p. 1125-42.
113. Shi, X., et al., *Foxk1 promotes cell proliferation and represses myogenic differentiation by regulating Foxo4 and Mef2.* J. Cell Sci., 2012. **125**(Pt 22): p. 5329-5337.
114. Bowman, C.J., D.E. Ayer, and B.D. Dynlacht, *Foxk proteins repress the initiation of starvation-induced atrophy and autophagy programs.* Nat Cell Biol, 2014. **16**(12): p. 1202-14.
115. Dey, A., et al., *Loss of the tumor suppressor BAP1 causes myeloid transformation.* Science, 2012. **337**(6101): p. 1541-6.
116. Yu, H., et al., *The ubiquitin carboxyl hydrolase BAP1 forms a ternary complex with YY1 and HCF-1 and is a critical regulator of gene expression.* Mol Cell Biol, 2010. **30**(21): p. 5071-85.
117. Bott, M., et al., *The nuclear deubiquitinase BAP1 is commonly inactivated by somatic mutations and 3p21.1 losses in malignant pleural mesothelioma.* Nat Genet, 2011. **43**(7): p. 668-72.
118. Hiromura, M., et al., *YY1 is regulated by O-linked N-acetylglucosaminylation (O-glcNAcylation).* J Biol Chem, 2003. **278**(16): p. 14046-52.
119. Abdel-Wahab, O. and A. Dey, *The ASXL-BAP1 axis: new factors in myelopoiesis, cancer and epigenetics.* Leukemia, 2013. **27**(1): p. 10-5.
120. Chen, Q., et al., *TET2 promotes histone O-GlcNAcylation during gene transcription.* Nature, 2013. **493**(7433): p. 561-564.
121. Bilian, J. and D.R. Keith, *DNA Methyltransferases (DNMTs), DNA Damage Repair, and Cancer.* Adv Exp Med Biol, 2013. **754**: p. 3-29.
122. Ito, S., et al., *Tet Proteins Can Convert 5-Methylcytosine to 5-Formylcytosine and 5-Carboxylcytosine.* Science, 2011. **333**(6047): p. 1300-1303.
123. Zhang, L.Y., et al., *Prognostic values of 5-hmC, 5-mC and TET2 in epithelial ovarian cancer.* Arch Gynecol Obstet, 2015.
124. Liu, W.J., et al., *Prognostic significance of Tet methylcytosine dioxygenase 2 (TET2) gene mutations in adult patients with acute myeloid leukemia: a meta-analysis.* Leuk Lymphoma, 2014. **55**(12): p. 2691-8.
125. Moran-Crusio, K. and al., *Tet2 loss leads to increased hematopoietic stem cell self-renewal and myeloid transformation.* Cancer Cell, 2011. **20**(1): p. 11-24.
126. Ko, M., et al., *Ten-eleven-Translocation 2 (TET2) negatively regulated homeostasis and differentiation of hematopoietic stem cells in mice.* . Proc. Natl. Acad. Sci. U. S. A. , 2011. **108**(35): p. 14566-14571.
127. Deplus, R., et al., *TET2 and TET3 regulate GlcNAcylation and H3K4 methylation through OGT and SET1/COMPASS.* EMBO J., 2013. **32**(5): p. 645-655.
128. Delatte, B., *[TET-OGT interaction potentiates transcription by regulating histone H3 methylation].* Med Sci (Paris), 2014. **30**(6-7): p. 619-21.
129. Rothbart, S.B. and B.D. Strahl, *Interpreting the language of histone and DNA modifications.* Biochim Biophys Acta, 2014. **1839**(8): p. 627-43.
130. Sakabe, K., Z. Wang, and G. Hart, *Beta-N-acetylglucosamine (O-GlcNAc) is part of the histone code.* Proc Natl Acad Sci U S A, 2010. **107,**: p. 19915-19920.
131. Hanover, J., *Epigenetics gets sweeter: O-GlcNAc joins the "histone code".* Chem Biol, 2010. **17**: p. 1271-1274.
132. Fujiki, R. and al., *GlcNAcylation of histone H2B facilitates its monoubiquitination.* Nature, 2011. **480**: p. 557-560.
133. Fujiki, R., et al., *GlcNAcylation of histone H2B facilitates its monoubiquitination.* Nature, 2011. **480**(7378): p. 557-60.

134. Bonizec, M., et al., *The ubiquitin-selective chaperone Cdc48/p97 associates with Ubx3 to modulate monoubiquitylation of histone H2B.* Nucleic Acids Res, 2014. **42**(17): p. 10975-86.
135. Fong, J.J., et al., *beta-N-Acetylglucosamine (O-GlcNAc) is a novel regulator of mitosis-specific phosphorylations on histone H3.* J Biol Chem, 2012. **287**(15): p. 12195-203.
136. Sakabe, K., Z. Wang, and G.W. Hart, *Beta-N-acetylglucosamine (O-GlcNAc) is part of the histone code.* Proc Natl Acad Sci U S A, 2010. **107**(46): p. 19915-20.
137. Wang, W., et al., *FOXKs promote Wnt/beta-catenin signaling by translocating DVL into the nucleus.* Dev Cell, 2015. **32**(6): p. 707-18.
138. Okino, Y., et al., *BRCA1-associated protein 1 (BAP1) deubiquitinase antagonizes the ubiquitin-mediated activation of FoxK2 target genes.* J Biol Chem, 2015. **290**(3): p. 1580-91.
139. Panda, D., et al., *The transcription factor FoxK participates with Nup98 to regulate antiviral gene expression.* MBio, 2015. **6**(2).
140. Hannenhalli, S. and K.H. Kaestner, *The evolution of Fox genes and their role in development and disease.* Nat Rev Genet, 2009. **10**(4): p. 233-40.
141. Zaret, K., J. Carroll, and *Pioneer transcription factors: establishing competence for gene expression.* Genes Dev., 2011. **25**: p. 2227-2241.
142. Leung, T.W., et al., *Over-expression of FoxM1 stimulates cyclin B1 expression.* FEBS Lett, 2001. **507**(1): p. 59-66.
143. Ustiyan, V., et al., *Forkhead box M1 transcriptional factor is required for smooth muscle cells during embryonic development of blood vessels and esophagus.* Dev Biol, 2009. **336**(2): p. 266-79.
144. Myatt, S. and E. Lam, *The emerging roles of forkhead box (Fox) proteins in cancer.* Nature Reviews Cancer, 2007. **7**: p. 847-859.
145. Brenkman, A.B., et al., *Mdm2 induces mono-ubiquitination of FOXO4.* PLoS One, 2008. **3**(7): p. e2819.
146. Bader, A.G., et al., *Oncogenic PI3K deregulates transcription and translation.* Nat Rev Cancer, 2005. **5**(12): p. 921-9.
147. Munoz-Fontela, C., et al., *Latent protein LANA2 from Kaposi's sarcoma-associated herpesvirus interacts with 14-3-3 proteins and inhibits FOXO3a transcription factor.* J Virol, 2007. **81**(3): p. 1511-6.
148. Mahajan, A., et al., *Structure and function of the phosphothreonine-specific FHA domain.* Sci Signal, 2008. **1**(51): p. re12.
149. Reinhardt, H.C. and M.B. Yaffe, *Phospho-Ser/Thr-binding domains: navigating the cell cycle and DNA damage response.* Nat Rev Mol Cell Biol, 2013. **14**(9): p. 563-80.
150. Yongkiettrakul, S., I.J. Byeon, and M.D. Tsai, *The ligand specificity of yeast Rad53 FHA domains at the +3 position is determined by nonconserved residues.* Biochemistry, 2004. **43**(13): p. 3862-9.
151. Meeson, A.P., et al., *Sox15 and Fhl3 transcriptionally coactivate Foxk1 and regulate myogenic progenitor cells.* EMBO J, 2007. **26**(7): p. 1902-12.
152. Lee, H.J., et al., *Sox15 is required for skeletal muscle regeneration.* Mol Cell Biol, 2004. **24**(19): p. 8428-36.
153. Shi, X., K.M. Bowlin, and D.J. Garry, *Fhl2 interacts with Foxk1 and corepresses Foxo4 activity in myogenic progenitors.* Stem Cells, 2010. **28**(3): p. 462-9.
154. Garry, D.J., et al., *Myogenic stem cell function is impaired in mice lacking the forkhead/winged helix protein MNF.* Proc Natl Acad Sci U S A, 2000. **97**(10): p. 5416-21.
155. Mauro, A., *Satellite cell of skeletal muscle fibers.* J Biophys Biochem Cytol, 1961. **9**: p. 493-5.
156. Choi, J., et al., *Modulation of lysine methylation in myocyte enhancer factor 2 during skeletal muscle cell differentiation.* Nucleic Acids Res, 2013.

157. Dodou, E., S.M. Xu, and B.L. Black, *mef2c is activated directly by myogenic basic helix-loop-helix proteins during skeletal muscle development in vivo.* Mech Dev, 2003. **120**(9): p. 1021-32.
158. Kumar, R., et al., *Forkhead transcription factors, Fkh1p and Fkh2p, collaborate with Mcm1p to control transcription required for M-phase.* Curr Biol, 2000. **10**(15): p. 896-906.
159. Natesan, S. and M. Gilman, *YY1 facilitates the association of serum response factor with the c-fos serum response element.* Mol Cell Biol, 1995. **15**(11): p. 5975-82.
160. Freddie, C.T., et al., *Functional interactions between the Forkhead transcription factor FOXK1 and the MADS-box protein SRF.* Nucleic Acids Res, 2007. **35**(15): p. 5203-12.
161. Heidenreich, O., et al., *MAPKAP kinase 2 phosphorylates serum response factor in vitro and in vivo.* J Biol Chem, 1999. **274**(20): p. 14434-43.
162. Blaker, A., J. Taylor, and C. Mack, *PKA-dependent Phosphorylation of Serum Response Factor Inhibits Smooth Muscle-Specific Gene Expression.* Arterioscler Thromb Vasc Biol. , 2009. **29**(12): p. 2153-2160.
163. Shi, X. and D.J. Garry, *Sin3 interacts with Foxk1 and regulates myogenic progenitors.* Mol Cell Biochem, 2012. **366**(1-2): p. 251-8.
164. Kadamb, R., et al., *Sin3: Insight into its transcription regulatory functions.* Eur J Cell Biol, 2013.
165. Fulco, M., et al., *Glucose restriction inhibits skeletal myoblast differentiation by activating SIRT1 through AMPK-mediated regulation of Nampt.* Dev Cell, 2008. **14**(5): p. 661-73.
166. Chiurillo, M.A., *Role of the Wnt/beta-catenin pathway in gastric cancer: An in-depth literature review.* World J Exp Med, 2015. **5**(2): p. 84-102.
167. Hart, G.W., *Three Decades of Research on O-GlcNAcylation - A Major Nutrient Sensor That Regulates Signaling, Transcription and Cellular Metabolism.* Front Endocrinol (Lausanne), 2014. **5**: p. 183.
168. Ruan, H.B., et al., *Cracking the O-GlcNAc code in metabolism.* Trends Endocrinol Metab, 2013. **24**(6): p. 301-9.
169. Nagel, A.K. and L.E. Ball, *O-GlcNAc transferase and O-GlcNAcase: achieving target substrate specificity.* Amino Acids, 2014. **46**(10): p. 2305-16.
170. Bullen, J.W., et al., *Cross-talk between two essential nutrient-sensitive enzymes: O-GlcNAc transferase (OGT) and AMP-activated protein kinase (AMPK).* J Biol Chem, 2014. **289**(15): p. 10592-606.
171. Caldwell, S.A., et al., *Nutrient sensor O-GlcNAc transferase regulates breast cancer tumorigenesis through targeting of the oncogenic transcription factor FoxM1.* Oncogene, 2010. **29**(19): p. 2831-42.
172. Fardini, Y., et al., *O-GlcNAcylation: A New Cancer Hallmark?* Front Endocrinol (Lausanne), 2013. **4**: p. 99.
173. Zhang, S., et al., *Modification of histones by sugar beta-N-acetylglucosamine (GlcNAc) occurs on multiple residues, including histone H3 serine 10, and is cell cycle-regulated.* J Biol Chem, 2011. **286**(43): p. 37483-95.
174. Forma, E., et al., *The potential role of O-GlcNAc modification in cancer epigenetics.* Cell Mol Biol Lett, 2014. **19**(3): p. 438-60.
175. Issad, T. and P. Pagesy, *[Protein O-GlcNAcylation and regulation of cell signalling: involvement in pathophysiology].* Biol Aujourdhui, 2014. **208**(2): p. 109-17.
176. Dehennaut, V., D. Leprince, and T. Lefebvre, *O-GlcNAcylation, an Epigenetic Mark. Focus on the Histone Code, TET Family Proteins, and Polycomb Group Proteins.* Front Endocrinol (Lausanne), 2014. **5**: p. 155.
177. Ozcan, S., S.S. Andrali, and J.E. Cantrell, *Modulation of transcription factor function by O-GlcNAc modification.* Biochim Biophys Acta, 2010. **1799**(5-6): p. 353-64.

178. Zhang, Q., et al., *Differential regulation of the ten-eleven translocation (TET) family of dioxygenases by O-linked beta-N-acetylglucosamine transferase (OGT).* J Biol Chem, 2014. **289**(9): p. 5986-96.
179. Yang, X., F. Zhang, and J.E. Kudlow, *Recruitment of O-GlcNAc transferase to promoters by corepressor mSin3A: coupling protein O-GlcNAcylation to transcriptional repression.* Cell, 2002. **110**(1): p. 69-80.
180. Hanover, J.A., *Epigenetics gets sweeter: O-GlcNAc joins the "histone code".* Chem Biol, 2010. **17**(12): p. 1272-4.
181. Arnaudo, A.M. and B.A. Garcia, *Proteomic characterization of novel histone post-translational modifications.* Epigenetics Chromatin, 2013. **6**(1): p. 24.
182. Chen, Q., et al., *TET2 promotes histone O-GlcNAcylation during gene transcription.* Nature, 2013. **493**(7433): p. 561-4.
183. Xu, Q., et al., *AMPK regulates histone H2B O-GlcNAcylation.* Nucleic Acids Res, 2014. **42**(9): p. 5594-604.
184. Ito, R., et al., *TET3-OGT interaction increases the stability and the presence of OGT in chromatin.* Genes Cells, 2014. **19**(1): p. 52-65.
185. Vella, P., et al., *Tet proteins connect the O-linked N-acetylglucosamine transferase Ogt to chromatin in embryonic stem cells.* Mol Cell, 2013. **49**(4): p. 645-56.
186. Isono, T., *O-GlcNAc-specific antibody CTD110.6 cross-reacts with N-GlcNAc2-modified proteins induced under glucose deprivation.* PLoS One, 2011. **6**(4): p. e18959.
187. Ogawa, M., et al., *GTDC2 modifies O-mannosylated alpha-dystroglycan in the endoplasmic reticulum to generate N-acetyl glucosamine epitopes reactive with CTD110.6 antibody.* Biochem Biophys Res Commun, 2013. **440**(1): p. 88-93.
188. Zhang, B.B., G. Zhou, and C. Li, *AMPK: an emerging drug target for diabetes and the metabolic syndrome.* Cell Metab, 2009. **9**(5): p. 407-16.
189. Hammond-Martel, I., et al., *PI 3 kinase related kinases-independent proteolysis of BRCA1 regulates Rad51 recruitment during genotoxic stress in human cells.* PLoS One, 2010. **5**(11): p. e14027.
190. Vassilev, L.T., et al., *Selective small-molecule inhibitor reveals critical mitotic functions of human CDK1.* Proc Natl Acad Sci U S A, 2006. **103**(28): p. 10660-5.
191. Hart, C., et al., *Metabolic labeling and click chemistry detection of glycoprotein markers of mesenchymal stem cell differentiation.* Methods Mol Biol, 2011. **698**: p. 459-84.
192. Haynes, P.A. and R. Aebersold, *Simultaneous detection and identification of O-GlcNAc-modified glycoproteins using liquid chromatography-tandem mass spectrometry.* Anal Chem, 2000. **72**(21): p. 5402-10.
193. Vester-Christensen, M.B., et al., *Mining the O-mannose glycoproteome reveals cadherins as major O-mannosylated glycoproteins.* Proc Natl Acad Sci U S A, 2013. **110**(52): p. 21018-23.
194. Alfaro, J.F., et al., *Tandem mass spectrometry identifies many mouse brain O-GlcNAcylated proteins including EGF domain-specific O-GlcNAc transferase targets.* Proc Natl Acad Sci U S A, 2012. **109**(19): p. 7280-5.
195. Myers, S.A., B. Panning, and A.L. Burlingame, *Polycomb repressive complex 2 is necessary for the normal site-specific O-GlcNAc distribution in mouse embryonic stem cells.* Proc Natl Acad Sci U S A, 2011. **108**(23): p. 9490-5.
196. Vosseller, K., et al., *O-linked N-acetylglucosamine proteomics of postsynaptic density preparations using lectin weak affinity chromatography and mass spectrometry.* Mol Cell Proteomics, 2006. **5**(5): p. 923-34.
197. Trinidad, J.C., et al., *Global identification and characterization of both O-GlcNAcylation and phosphorylation at the murine synapse.* Mol Cell Proteomics, 2012. **11**(8): p. 215-29.

198. Myers, S.A., et al., *Electron transfer dissociation (ETD): the mass spectrometric breakthrough essential for O-GlcNAc protein site assignments-a study of the O-GlcNAcylated protein host cell factor C1.* Proteomics, 2013. **13**(6): p. 982-91.
199. Wysocka, J., et al., *Human Sin3 deacetylase and trithorax-related Set1/Ash2 histone H3-K4 methyltransferase are tethered together selectively by the cell-proliferation factor HCF-1.* Genes Dev, 2003. **17**(7): p. 896-911.
200. Wilson, A.C., et al., *The VP16 accessory protein HCF is a family of polypeptides processed from a large precursor protein.* Cell, 1993. **74**(1): p. 115-25.
201. Wilson, A.C., et al., *HCF-1 amino- and carboxy-terminal subunit association through two separate sets of interaction modules: involvement of fibronectin type 3 repeats.* Mol Cell Biol, 2000. **20**(18): p. 6721-30.
202. Minsky, N. and M. Oren, *The RING domain of Mdm2 mediates histone ubiquitylation and transcriptional repression.* Mol Cell, 2004. **16**(4): p. 631-9.
203. Stoscheck, C.M., *Quantitation of protein.* Methods Enzymol, 1990. **182**: p. 50-68.
204. Comer, F.I., et al., *Characterization of a mouse monoclonal antibody specific for O-linked N-acetylglucosamine.* Anal Biochem, 2001. **293**(2): p. 169-77.
205. Yu, H., et al., *Tumor suppressor and deubiquitinase BAP1 promotes DNA double-strand break repair.* Proc Natl Acad Sci U S A, 2014. **111**(1): p. 285-90.
206. Brown, J.S. and S.P. Jackson, *Ubiquitylation, neddylation and the DNA damage response.* Open Biol, 2015. **5**(4).
207. Gajjala, P.R., et al., *Emerging role of post-translational modifications in chronic kidney disease and cardiovascular disease.* Nephrol Dial Transplant, 2015.
208. Zhu, Y., et al., *The Emerging Link Between O-GlcNAc and Alzheimer's Disease.* J Biol Chem, 2014.
209. Cooper, J.A., T. Kaneko, and S.S. Li, *Cell Regulation by Phosphotyrosine-Targeted Ubiquitin Ligases.* Mol Cell Biol, 2015. **35**(11): p. 1886-1897.
210. Davis, M.E. and M.U. Gack, *Ubiquitination in the antiviral immune response.* Virology, 2015. **479-480c**: p. 52-65.
211. Bogachek, M.V., J.P. De Andrade, and R.J. Weigel, *Regulation of epithelial-mesenchymal transition through SUMOylation of transcription factors.* Cancer Res, 2015. **75**(1): p. 11-5.
212. Zhimin, L. and H. Tony, *Degradation of Activated Protein Kinases by Ubiquitination.* Annual Review of Biochemistry, 2009. **78**(1): p. 435-475.
213. Kerscher, O., R. Felberbaum, and M. Hochstrasser, *Modification of Proteins by Ubiquitin and Ubiquitin-Like Proteins.* Annual Review of Cell and Developmental Biology, 2006. **22**(1): p. 159-180.
214. Tasaki, T., et al., *The N-End Rule Pathway.* Annual Review of Biochemistry, 2012. **81**(1): p. 261-289.
215. Joerger, A.C. and A.R. Fersht, *Structural Biology of the Tumor Suppressor p53.* Annual Review of Biochemistry, 2008. **77**(1): p. 557-582.
216. Hottiger, M.O., *Nuclear ADP-Ribosylation and Its Role in Chromatin Plasticity, Cell Differentiation, and Epigenetics.* Annual Review of Biochemistry, 2015. **84**(1): p. null.
217. Tang, Q.Q. and M.D. Lane, *Adipogenesis: From Stem Cell to Adipocyte.* Annual Review of Biochemistry, 2012. **81**(1): p. 715-736.
218. Kurosaki, T., H. Shinohara, and Y. Baba, *B Cell Signaling and Fate Decision.* Annual Review of Immunology, 2010. **28**(1): p. 21-55.
219. Tajbakhsh, S., P. Rocheteau, and I. Le Roux, *Asymmetric Cell Divisions and Asymmetric Cell Fates.* Annual Review of Cell and Developmental Biology, 2009. **25**(1): p. 671-699.
220. Yu, H., et al., *The Ubiquitin carboxyl hydrolase BAP1 forms a ternary complex with YY1 and HCF-1 and is a critical regulator of gene expression.* Mol Cell Biol, 2010. **30**(21): p. 5071-5085.

221. Machida, Y.J., et al., *The deubiquitinating enzyme BAP1 regulates cell growth via interaction with HCF-1.* J Biol Chem, 2009. **284**(49): p. 34179-88.
222. Misaghi, S., et al., *Association of C-terminal ubiquitin hydrolase BRCA1-associated protein 1 with cell cycle regulator host cell factor 1.* Mol Cell Biol, 2009. **29**(8): p. 2181-92.
223. Mashtalir, N., et al., *Autodeubiquitination protects the tumor suppressor BAP1 from cytoplasmic sequestration mediated by the atypical ubiquitin ligase UBE2O.* Mol Cell, 2014. **54**(3): p. 392-406.
224. Hu, P., S. Shimoji, and G.W. Hart, *Site-specific interplay between O-GlcNAcylation and phosphorylation in cellular regulation.* FEBS Letters, 2010. **584**(12): p. 2526-2538.
225. Hardiville, S., et al., *O-GlcNAcylation/phosphorylation cycling at Ser10 controls both transcriptional activity and stability of delta-lactoferrin.* J Biol Chem, 2010. **285**(25): p. 19205-18.
226. Bond, M.R. and J.A. Hanover, *O-GlcNAc Cycling: A Link Between Metabolism and Chronic Disease.* Annual Review of Nutrition, 2013. **33**(1): p. 205-229.
227. Benhamed, F., et al., *O-GlcNAcylation Links ChREBP and FXR to Glucose-Sensing.* Front Endocrinol (Lausanne), 2014. **5**: p. 230.
228. Ji, Z., et al., *The forkhead transcription factor FOXK2 acts as a chromatin targeting factor for the BAP1-containing histone deubiquitinase complex.* Nucleic Acids Res, 2014. **42**(10): p. 6232-42.
229. Ji, Z., et al., *The forkhead transcription factor FOXK2 promotes AP-1-mediated transcriptional regulation.* Mol Cell Biol, 2012. **32**(2): p. 385-98.
230. Fujii, Y. and M. Nakamura, *FOXK2 transcription factor is a novel G/T-mismatch DNA binding protein.* Journal of Biochemistry, 2010. **147**(5): p. 706-709.
231. Liu, Y., et al., *FOXK2 transcription factor suppresses ERalpha-positive breast cancer cell growth through down-regulating the stability of ERalpha via mechanism involving BRCA1/BARD1.* Sci Rep, 2015. **5**: p. 8796.
232. Shi, X., D.C. Seldin, and D.J. Garry, *Foxk1 recruits the Sds3 complex and represses gene expression in myogenic progenitors.* Biochem J, 2012. **446**(3): p. 349-57.
233. Shi, X., et al., *Foxk1 promotes cell proliferation and represses myogenic differenciation by regulating Foxo4 and Mef2.* Journal of Cell Science, 2012. **125**: p. 5329-5337.
234. Freddie, C., et al., *Functional interactions between the Forkhead transcription factor FOXK1 and the MADS-box protein SRF.* Nucleic Acids Research, 2007. **35**(15): p. 5203-5212.
235. Eletr, Z.M., L. Yin, and K.D. Wilkinson, *BAP1 is phosphorylated at serine 592 in S-phase following DNA damage.* FEBS Lett, 2013. **587**(24): p. 3906-11.
236. Marais, A., et al., *Cell cycle-dependent regulation of the forkhead transcription factor FOXK2 by CDK.cyclin complexes.* J Biol Chem, 2010. **285**(46): p. 35728-39.
237. Gagnon, J., et al., *Undetectable histone O-GlcNAcylation in mammalian cells.* Epigenetics, 2015. **10**(8): p. 677-91.
238. Lea, N.C., et al., *Commitment point during G0-->G1 that controls entry into the cell cycle.* Mol Cell Biol, 2003. **23**(7): p. 2351-61.
239. Dong, P., et al., *Division of labour between Myc and G1 cyclins in cell cycle commitment and pace control.* Nat Commun, 2014. **5**: p. 4750.
240. Sodi, V.L., et al., *mTOR/MYC Axis Regulates O-GlcNAc Transferase Expression and O-GlcNAcylation in Breast Cancer.* Mol Cancer Res, 2015.
241. Garry, D.J., et al., *Persistent expression of MNF identifies myogenic stem cells in postnatal muscles.* Dev Biol, 1997. **188**(2): p. 280-94.
242. Matthews, L.A., et al., *A novel non-canonical forkhead-associated (FHA) domain-binding interface mediates the interaction between Rad53 and Dbf4 proteins.* J Biol Chem, 2014. **289**(5): p. 2589-99.
243. Nott, T.J., et al., *An intramolecular switch regulates phosphoindependent FHA domain interactions in Mycobacterium tuberculosis.* Sci Signal, 2009. **2**(63): p. ra12.

244. Zhao, B., et al., *A coordinated phosphorylation by Lats and CK1 regulates YAP stability through SCF(beta-TRCP).* Genes Dev, 2010. **24**(1): p. 72-85.
245. Jiao, W., et al., *Nucleocytoplasmic shuttling of the retinoblastoma tumor suppressor protein via Cdk phosphorylation-dependent nuclear export.* J Biol Chem, 2006. **281**(49): p. 38098-108.
246. Elrick, L.J. and K. Docherty, *Phosphorylation-dependent nucleocytoplasmic shuttling of pancreatic duodenal homeobox-1.* Diabetes, 2001. **50**(10): p. 2244-52.
247. Hallenborg, P., et al., *PPARgamma ligand production is tightly linked to clonal expansion during initiation of adipocyte differentiation.* J Lipid Res, 2014. **55**(12): p. 2491-500.
248. Qiu, Z., et al., *DNA synthesis and mitotic clonal expansion is not a required step for 3T3-L1 preadipocyte differentiation into adipocytes.* J Biol Chem, 2001. **276**(15): p. 11988-95.
249. Patel, Y.M. and M.D. Lane, *Mitotic clonal expansion during preadipocyte differentiation: calpain-mediated turnover of p27.* J Biol Chem, 2000. **275**(23): p. 17653-60.
250. Affar el, B., et al., *Essential dosage-dependent functions of the transcription factor yin yang 1 in late embryonic development and cell cycle progression.* Mol Cell Biol, 2006. **26**(9): p. 3565-81.
251. Sui, G., et al., *Yin Yang 1 is a negative regulator of p53.* Cell, 2004. **117**(7): p. 859-72.
252. Beltrao, P., et al., *Evolution and functional cross-talk of protein post-translational modifications.* Mol Syst Biol, 2013. **9**: p. 714.
253. Macauley, M.S. and D.J. Vocadlo, *Enzymatic characterization and inhibition of the nuclear variant of human O-GlcNAcase.* Carbohydr Res, 2009. **344**(9): p. 1079-84.
254. Bordeaux, J., et al., *Antibody validation.* Biotechniques, 2010. **48**(3): p. 197-209.
255. Ma, J. and G.W. Hart, *O-GlcNAc profiling: from proteins to proteomes.* Clin Proteomics, 2014. **11**(1): p. 8.
256. Tang, Q.Q., T.C. Otto, and M.D. Lane, *Mitotic clonal expansion: a synchronous process required for adipogenesis.* Proc Natl Acad Sci U S A, 2003. **100**(1): p. 44-9.
257. Guo, L., X. Li, and Q.Q. Tang, *Transcriptional regulation of adipocyte differentiation: a central role for CCAAT/enhancer-binding protein (C/EBP) beta.* J Biol Chem, 2015. **290**(2): p. 755-61.
258. Munekata, K. and K. Sakamoto, *Forkhead transcription factor Foxo1 is essential for adipocyte differentiation.* In Vitro Cell Dev Biol Anim, 2009. **45**(10): p. 642-51.
259. Battaglia, A., *The Importance of Multidisciplinary Approach in Early Detection of BAP1 Tumor Predisposition Syndrome: Clinical Management and Risk Assessment.* Clin Med Insights Oncol, 2014. **8**: p. 37-47.
260. Iurlaro, M., et al., *A screen for hydroxymethylcytosine and formylcytosine binding proteins suggests functions in transcription and chromatin regulation.* Genome Biol, 2013. **14**(10): p. R119.

CHAPITRE 5

5. Annexes

5.1 ANNEXE 1

Statut de l'article: Publié

Référence: Mashtalir N, Daou S, Barbour [illegible], Gagnon J, Hammond-Martel I, Dar HH, Therrien M, Affar el B. Autodeubiquitination protects the tumor suppressor BAP1from cytoplasmic sequestration mediated by the atypical ubiquitin ligase UBE2O.Mol Cell. 2014 May 8;54(3):392-406. doi: 10.1016/j.molcel.2014.03.002. Epub 2014 Apr 3. PubMed PMID: 24703950.

Contribution de l'étudiante:

Pour cet article intitulé *«Autodeubiquitination protects the tumor suppressor BAP1 from cytoplasmic exclusion mediated by the atypical ubiquitin ligase UBE2O»*, j'ai effectué et analysé plusieurs expériences et testé plusieurs hypothèses afin de déterminer le rôle physiologique du mécanisme proposé de l'ubiquitination de BAP1 par l'hybride E2-E3 ligase UBE2O. J'ai planifié et effectué plusieurs traitements cellulaires ciblant différentes voies de signalisation qui pouvaient être impliquées dans ce mécanisme. J'ai effectué des expériences de localisation cellulaire par immunofluorescence et j'ai généré des lignées de cellules C2C12 (murin) et U2OS (humain) exprimant de manière stable des shUBE2O et shBAP1 respectivement sous le contrôle du système inductible tétracycline-ON qui ont été utilisé pour réaliser plusieurs expériences. J'ai également participé aux discussions ainsi qu'à la révision du manuscrit.

Autodeubiquitination protects the tumor suppressor BAP1 from cytoplasmic exclusion mediated by the atypical ubiquitin ligase UBE2O

Nazar Mashtalir[1], Salima Daou[1], Haithem Barbour[1], Nadine N Sen[1], Jessica Gagnon[1], Ian Hammond-Martel[1], Haider H Dar[1], Marc Therrien[2] and El Bachir Affar[1,3]

[1]Maisonneuve-Rosemont Hospital Research Center, Department of Medicine, University of Montréal, QC, Montréal, H1T 2M4, Canada

[2]Institute for Research in Immunology and Cancer, Laboratory of Intracellular Signaling, University of Montréal, Montréal, QC, H3T 1J4, Canada

[3]Correspondence

Conflict of interest

The authors declare no conflict of interest

Running title: UBE2O is a BAP1 E3 ligase.

HIGHLIGHTS

- UBE2O multi-monoubiquitinates BAP1 on its NLS, and regulates its subcellular localization.
- Intramolecular interaction in BAP1 ensures efficient autodeubiquitination and is disrupted by cancer-associated mutations.
- UBE2O and BAP1 have antagonistic roles in cell cycle regulation and differentiation.
- UBE2O targets itself and a subset of chromatin regulators.

Abstract

The tumor suppressor BAP1 interacts with chromatin-associated proteins and regulates cell proliferation, but its mechanism of action and regulation remain poorly defined. We show that the ubiquitin-conjugating enzyme UBE2O multi-monoubiquitinates the nuclear localization signal of BAP1, thereby inducing its cytoplasmic exclusion. This activity is counteracted by BAP1 autodeubiquitination through intramolecular interactions. Significantly, we identified cancer-derived BAP1 mutations that abrogate autodeubiquitination and promote its cytoplasmic retention, indicating that BAP1 autodeubiquitination ensures tumor suppression. The antagonistic relationship between UBE2O and BAP1 is also observed during adipogenesis, whereby UBE2O promotes differentiation and cytoplasmic localization of BAP1. Finally, we established a putative targeting consensus sequence of UBE2O and identified numerous chromatin remodeling factors as potential targets, several of which tested positive for UBE2O-mediated ubiquitination. Thus, UBE2O defines an atypical ubiquitin-signaling pathway that coordinates the function of BAP1 and establishes a paradigm for regulation of nuclear trafficking of chromatin-associated proteins.

Introduction

The covalent attachment of ubiquitin to target proteins, i.e., ubiquitination, regulates both protein stability and function, and is fundamental to diverse biological processes (Hammond-Martel et al., 2012; Jackson and Durocher, 2013). The deubiquitinase (DUB) BAP1 is a transcriptional regulator required for mammalian development (Dey et al., 2012; Yu et al., 2010). BAP1 is also a tumor suppressor inactivated in various cancers, and reconstitution studies in cancer cells harboring BAP1 mutations indicated that both BAP1 catalytic activity and nuclear localization are required for its growth suppressive properties (Carbone et al., 2013; Ventii et al., 2008). Moreover, RNAi-mediated depletion of BAP1 also induces defects in cell-cycle progression indicating that this protein is a key regulator of cell proliferation (Machida et al., 2009). At the molecular level, BAP1 assembles a large multi-protein complex consisting of numerous transcription factors and chromatin-associated proteins including the Host Cell Factor-1 (HCF-1), the Polycomb Group (PcG) proteins Additional Sex Combs Like 1 and 2 (ASXL1/2), the histone demethylase KDM1B, the O-linked N-acetylglucosamine transferase (OGT), the forkhead transcription factors FOXK1/FOXK2, and the zinc finger transcription factor Yin Yang1 (YY1) (Machida et al., 2009; Misaghi et al., 2009; Sowa et al., 2009; Yu et al., 2010).

The *Drosophila* BAP1, calypso, is a PcG protein that interacts with Additional Sex Combs (ASX), localizes at PcG-target gene regulatory regions, and represses HOX gene expression. Calypso/ASX heterodimer, termed PR-DUB (Polycomb repressive DUB), deubiquitinates histone H2A (Scheuermann et al., 2010), a chromatin modification involved in chromatin remodeling and gene silencing (Lanzuolo and Orlando, 2012).

We and others previously identified the ubiquitin-conjugating enzyme UBE2O as a substoichiometric factor that co-purifies with the human BAP1 (Machida et al., 2009; Sowa et al., 2009; Yu et al., 2010), suggesting that it might be involved in the coordination of BAP1 function. UBE2O belongs to the E2 family of ubiquitin-conjugating enzymes, although, unlike most members of this family, it is unusually large (140 kDa) (van Wijk and Timmers, 2010). Pioneering studies from Pickart's group suggested that UBE2O might function as an E2/E3 hybrid (Berleth and Pickart, 1996; Klemperer et al., 1989). This was essentially based on the observation that UBE2O can ubiquitinate free histones in vitro, in the presence of E1 enzyme only. It has been proposed that ubiquitination by UBE2O involves an intramolecular thioester relay mechanism, since this enzyme is inhibited by phenylarsine oxide (PAO) which can

crosslink adjacent cysteines (Klemperer et al., 1989). Otherwise, the physiological substrates of UBE2O are largely unknown. Nonetheless, it was recently shown that UBE2O regulates TRAF6-dependent NF-κB in a catalytic activity-independent manner (Zhang et al., 2013b), monoubiquitinates SMAD6 during bone morphogenetic protein signaling (Zhang et al., 2013a), and coordinates endosomal protein trafficking (Hao et al., 2013) thus implicating UBE2O in numerous cellular processes. In this study, we uncover a novel ubiquitin-signaling pathway, mediated by UBE2O that has important implications for chromatin-associated processes.

Results

The ubiquitin-conjugating enzyme UBE2O interacts with and ubiquitinates BAP1

We previously described the purification of complexes formed by wild-type and catalytic dead BAP1 (C91S) (Yu et al., 2010). The complexes were essentially identical, although when probed with an anti-ubiquitin antibody, the C91S complex exhibited a dramatic increase in signal (Figure 1A). We also routinely observed monoubiquitination of BAP1 in transfected cells, independently of its DUB activity (Figure 1A and Figure S1A-E). This suggests that BAP1 might be functionally regulated by distinct ubiquitination events in DUB activity-dependent and -independent manner. To identify E3 ligases responsible for the ubiquitination of BAP1, we initially considered UBE2O which was more abundant in the C91S versus the wild-type BAP1 complex (Figure 1A). The UBE2O association with BAP1 was not affected by mutation of the HCF-1 Binding Motif (HBM) which eliminates HCF-1, a major component of the complex (Figure 1A). Glycerol density gradient fractionation of nuclear extracts indicated that UBE2O co-sediments with the BAP1 complex (Figure 1B). Next, we cotransfected BAP1 or C91S with UBE2O or its catalytic dead mutant C1040S (hereafter UBE2O CD) and ubiquitin into 293T cells. Strikingly, UBE2O ubiquitinates BAP1, and modified forms were more abundant in the C91S mutant (Figure 1C). Incubation of UBE2O-modified BAP1 C91S with an excess of USP2 DUB catalytic domain resulted in its complete deubiquitination, further demonstrating ubiquitin conjugation (Figure S1F). Of note, deletion of the UCH catalytic domain results in the abolishment of the constitutive monoubiquitination (Figure S1G). On the other hand, a similar UBE2O-dependent ubiquitination pattern could be observed for BAP1 C91S or BAP1 ΔUCH indicating that UBE2O-mediated ubiquitination is distinct from its constitutive monoubiquitination.

Next, to control for the specificity of UBE2O-mediated BAP1 ubiquitination, we evaluated other E2s and none was able to ubiquitinate BAP1 (Figure S1H,I). We also tested two known H2A DUBs, i.e., USP16 and MYSM1, as well as the SUMO protease SENP2, and no UBE2O-mediated ubiquitination could be observed (Figure S1J). Using multiple sequence alignment, we identified three main conserved regions in UBE2O namely CR1 (conserved region 1), CR2 (conserved region 2) and UBC (Ubiquitin-conjugating) (Figure 1D, Figure S1K). Secondary structure prediction analysis revealed all-β domains within CR1 and CR2 and the typical α/β UBC fold. Deletion of either N-terminal (ΔCR1-CR2) or C-terminal (ΔC) regions of UBE2O completely disrupted BAP1 ubiquitination (Figure 1D, E). Moreover, deletion of only the N-terminal CR1 region (ΔCR1-A) was sufficient to abolish UBE2O catalytic activity. Hence, the integrity of multiple domains of UBE2O is required for ubiquitination of BAP1.

UBE2O catalyzes the multi-monoubiquitination of BAP1

To determine the mechanism of UBE2O action on BAP1, we established an *in vitro* assay for BAP1 ubiquitination using wild-type and C91S complexes immobilized on the beads (Figure S2A). UBE2O-mediated ubiquitination appears to be highly specific for the C91S mutant as no modified forms were observed for other BAP1 partners (Figure 2A). Moreover, ubiquitination of the C91S mutant did not disrupt complex integrity, since none of the complex components was released into the soluble fraction in a UBE2O-dependent manner (Figure 2A). Notably, we did not detect ubiquitination of wild-type BAP1 as opposed to C91S, and this ubiquitination was completely abolished by the UBE2O inhibitor PAO (Figure 2A, Figure S2B). We note that UBE2O, purified from HeLa cells under high- or low-salt conditions or from bacteria, ubiquitinates C91S to similar extents (Figure S2C,D). Importantly, although less efficient, ubiquitination was also observed using bacteria-purified BAP1 and UBE2O (Figure S2E). Therefore UBE2O is an atypical E2/E3 enzyme with substrate binding and ubiquitin-conjugating functions.

To further confirm that autodeubiquitination prevents accumulation of ubiquitin on BAP1, the beads-bound wild-type complex was pretreated with N-ethylmaleimide (NEM), which resulted in a significant ubiquitination of BAP1 by UBE2O (Figure S2A, Figure 2B). Next, we used methylated ubiquitin, which is unable to form polyubiquitin or linear chains in the in vitro reaction (Figure 2C). The reaction with methylated ubiquitin was as efficient as with the

unmodified ubiquitin and resulted in a similar ubiquitination pattern, indicating that UBE2O multi-monoubiquitinates BAP1. The same observation was made in vivo when a K0 ubiquitin mutant, incapable of chain formation, was used for co-transfection of 293T cells with the C91S mutant and UBE2O (Figure 2D). Next, 293T cells were co-transfected with wild-type BAP1 or C91S mutant and UBE2O, and then treated with the proteasome inhibitor MG132 (Figure 2E). The typical multi-monoubiquitination pattern of BAP1 was unchanged after proteasome inhibition, indicating that UBE2O is unable to directly catalyze polyubiquitin chain elongation with subsequent degradation of BAP1. Immunodetection of endogenous CDC25A was conducted as a control for proteasome inhibition. Next, we tested several E3s that interact with either UBE2O or BAP1 and no further chain elongation was observed (Figure S2F-I). To further confirm that the stability of BAP1 is not directly regulated by UBE2O, we performed siRNA knockdown of UBE2O in MCF7 cells, which express high protein levels of this enzyme, followed by treatment with cycloheximide (CHX) (Figure 2F). Endogenous BAP1 appears to be highly stable and UBE2O knockdown did not significantly change BAP1 protein levels. We concluded that UBE2O catalyzes BAP1 multi-monoubiquitination without directly promoting its proteasomal degradation under normal growth conditions. Of note, UBE2O depletion also did not affect the constitutive monoubiquitination of BAP1 observed in cells transfected with this DUB (Figure S2J).

The NLS of BAP1 is required for UBE2O-mediated ubiquitination

Using a GST pull down assay, we found that the BAP1 C-terminal region (598-729 aa), which includes the C-terminal domain (CTD) and NLS, is necessary and sufficient for UBE2O binding (Figure 3A). Surprisingly, co-expression of UBE2O with CTD-NLS promoted the latter's degradation by the proteasome, since it could be reversed by MG132 (Figure 3B, left panel and Figure S3A, B). Immunoprecipitation of the CTD-NLS revealed an ubiquitination pattern similar to that of the full length BAP1 (4-5 sites of multi-monoubiquitination), although some high molecular weight smears were also detected (Figure 3B, right panel). Next, we found that both wild-type and K0 ubiquitin mutants promoted UBE2O-mediated multi-monoubiquitination and degradation of the CTD-NLS (Figure S3C). Moreover, knockdown of endogenous UBE2O rescued the degradation of CTD-NLS (Figure 3C). These results confirm that the CTD-NLS represents both the interaction and ubiquitination region for UBE2O. The

degradation of CTD-NLS can be explained by the small size of this region (only 101aa), in line with a recent discovery by Ciechanover's group indicating that monoubiquitinated substrates of less than 150 aa can be degraded without further ubiquitin chain formation (Shabek et al., 2012). Next, we purified the complex of the BAP1ΔCTD mutant that possesses a large deletion of aa 631-693 leaving only the NLS region intact (aa 699-729) (Figure 3D). The abundance of UBE2O was nearly unchanged between the wild-type and the mutant indicating that UBE2O binds the NLS region. BAP1 possesses a complex NLS region (Figure S3D,E). We designed a set of BAP1 NLS mutants in the C91S background to render the ubiquitination analysis more sensitive. We found that both C91SΔ688-716 and C91SΔ711-729 mutants were unable to bind and to be ubiquitinated by UBE2O (Figure 3E). Therefore, the NLS region that includes the RRR (aa 699-701) site, the hydrophobic GVSIGRL patch (aa 703-709) as well as the basic amino acid stretch RRKRSRPYKAKRQ (aa 717-729) is required for binding and ubiquitination by UBE2O. The region of basic amino acids RRKRSR (aa 717-722) is strictly required for binding and ubiquitination by UBE2O (Figures 3E, Figure S3F-G). Thus, multiple determinants of this composite and highly conserved NLS are required for UBE2O-mediated ubiquitination of BAP1 (Figure S3H).

UBE2O ubiquitinates the NLS of BAP1 and regulates its subcellular localization

To identify the UBE2O ubiquitination sites on BAP1, we performed an anti-Flag affinity purification of C91S co-transfected with ubiquitin and UBE2O (Figure 4A). MS peptide analysis revealed 14 unique ubiquitination sites in BAP1, 9 of which were detected more than once (Figure 4B). Analysis of all ubiquitination events revealed that 50 % are located in the area of NLS, which represents only 4 % of the protein. Next, we introduced a series of lysine to arginine mutations in the CTD-NLS region (12 K/R) or in the NLS alone (5 K/R) of C91S (Figure 4C). Mutation of all lysine sites in the CTD-NLS (12 K/R) strongly reduced C91S ubiquitination; moreover, mutation of lysines in the NLS (5 K/R) region had an identical effect on C91S ubiquitination compared with the 12 K/R mutant. Interestingly, the binding of UBE2O to either mutants of C91S was unchanged indicating that K/R mutations do not significantly affect UBE2O binding affinity. Taken together, these results indicate that UBE2O ubiquitinates primarily the NLS of BAP1.

Ubiquitination was reported to promote nuclear export of proteins (Groulx and Lee, 2002; Li et al., 2003). Therefore, we evaluated whether the ubiquitination of BAP1 affects its subcellular localization. BAP1 is prominently nuclear, but displayed strong cytoplasmic staining when co-expressed with UBE2O. This effect depends on the catalytic activity of UBE2O. This effect depends on the catalytic activity of UBE2O. Notably, the effect of UBE2O on the C91S mutant was more pronounced with almost all cells showing cytoplasmic or nucleocytoplasmic localization (Figure 4D). In addition, the C91S mutant usually displayed a more pronounced cytoplasmic localization compared to the wild-type BAP1. Of note, overexpression of UBE2O, but not its catalytic dead form, also promoted cytoplasmic localization of endogenous BAP1 (Figure S4). To probe whether this effect is due to its inability to deubiquitinate its NLS, we compared the nuclear localization of BAP1 and C91S (5 K/R) mutants (Figure 4E). Remarkably, the K/R mutation rescued the C91S mutant from the cytoplasmic sequestration, thus supporting the notion that NLS autodeubiquitination is involved in the regulation of BAP1 nuclear import/export.

Intramolecular interaction in BAP1 is required for efficient NLS autodeubiquitination

UCH37 is highly similar to BAP1 and its crystal structure suggests that an intramolecular interaction occurs between the UCH and the CTD (Figure S5A) (Burgie et al., 2011). Since catalytically dead UCH37 C88A is also strongly ubiquitinated by an unknown E3 ligase (Figure S5B), we reasoned that both BAP1 and UCH37 might use their respective CTD regions for interaction with the UCH domain (Figure S5C). Examination of CTD and UCH flanking sequences of BAP1 revealed putative coiled-coil motifs that can engage in intramolecular interactions (Figure S4D). Next, we used the crystal structure of UCH37 to generate a superimposed model of BAP1 (Figure 5A). This model suggests that the CTD region (containing the CC2) forms an interaction interface with the CC1 and the UCH domain. We note that this model cannot predict the structure of the NLS and NORS regions, which are not present in UCH37. To validate our computational prediction, we designed a series of deletion mutants in the N- terminus of BAP1 including the UCH domain alone and a larger fragment that includes CC1 (UCH-CC1) (Figure 5B). Co-IP between the fragments revealed that both UCH and UCH-CC1 interact with CTD-NLS (Figure 5C). To test whether this interaction can promote deubiquitination of CTD-NLS, we took advantage of the earlier observation that CTD-NLS can

be degraded as a result of ubiquitination by UBE2O. We designed a complementation/rescue system in which the degradation of CTD-NLS would be counteracted by the N-terminus of BAP1. Indeed, the degradation of CTD-NLS was efficiently rescued only by UCH-CC1 but not by UCH alone, and this was dependent on the catalytic activity of BAP1 (Figure 5D). This suggests that despite direct CC2/UCH interaction, the CC1/CC2 interface plays an important role in NLS deubiquitination. To further test the requirement of the CC1/CC2 in the context of the full-length protein, CC1 and CTD deletion mutants were used (Figure 5B). Deletion of the CTD (ΔCTD) or CC2 (ΔCC2) almost completely blocked the autodeubiquitination activity of BAP1 despite the presence of a catalytically proficient UCH domain (Figure 5E). The CC1 deletion mutant had a less pronounced autodeubiquitination defect consistent with the fact that CC2 interacts with both CC1 and UCH. To test whether the deficiency in the ability of BAP1 to autodeubiquitinate the NLS affects its localization, cell lines stably expressing the wild-type or mutants BAP1 were generated. IF analysis revealed that the wild-type BAP1 displayed a typical nuclear localization, whereas the ΔCTD and ΔCC2 mutants had a stronger cytoplasmic localization similar to the C91S mutant (Figure 5J). Notably the ΔHBM mutant displayed normal localization similar to wild-type BAP1. Thus BAP1 autodeubiquitination depends on an intramolecular binding between CC2 and UCH-CC1 and is important to counteract the E3 ligase activity of UBE2O towards the NLS.

BAP1 NLS autodeubiquitination is disrupted by cancer-associated mutations of CTD

Our results suggest that disruption of autodeubiquitination leads to improper BAP1 localization. We thus searched for cancer mutations in BAP1 that may target the UCH-CC1 interaction interface with CC2. We first tested G13V and F660A mutations and none had a noticeable effect on BAP1 autodeubiquitination (Figure S5E,F). Next, we considered two small in frame deletions of CC2 (ΔE631-A634 and ΔK637-C638InsN) (Harbour et al., 2010) (Figure 5B). We conducted complex purification of BAP1, ΔE631-A634 and ΔK637-C638InsN, and strikingly observed in both mutants an intense band around 230 kDa that corresponds to UBE2O (Figure 5F). Other major components of the complex such as OGT and HCF-1 showed no apparent differences (Figure 5F). The CC2 directly interacts with UCH, so mutations in this region may interfere with the catalytic activity of BAP1. To test this, we used *an in vitro* deubiquitination assay using a BAP1 natural substrate, i.e., the nucleosomal histone H2A

ubiquitinated at position K119 (Figure S5G, H, I). The activities of both cancer mutants were very similar to BAP1, whereas the control C91S failed to deubiquitinate H2A (Figure 5G). Next, to evaluate whether these cancer mutations affect the autodeubiquitination activity of BAP1, we exploited the UCH/CTD rescue system and the ability of UBE2O to promote degradation of the BAP1 CTD-NLS. We cloned the CTD-NLS region of ΔK637-C638InsN mutant, and a mutant with a large internal deletion in CC2 (Δ636-655) as a control (Figure 5B). Remarkably, complementation with UCH-CC1 rescued the wild-type CTD-NLS, but not the ΔK637-C638InsN and Δ635-655 (Figure 5H). Next, we sought to investigate these mutations in the context of the full-length protein. The effect of UBE2O on the cancer mutants was almost as dramatic as on the C91S despite their catalytic proficiency (Figure 5I). Finally, ΔE631-A634 and ΔK637-C638InsN mutants displayed increased cytoplasmic localization similar to the C91S mutant (Figure 5J).

UBE2O is regulated by active nucleocytoplasmic transport mechanisms and promotes BAP1 cytoplasmic exclusion during adipocyte differentiation

UBE2O possesses two functional NLS motifs (Figure S6A-D). However, the full-length UBE2O displayed predominant cytoplasmic localization. Next, purification of UBE2O-associated proteins followed by MS analysis revealed numerous components of the nuclear import/export machinery as well as several kinases that might coordinate its nuclear trafficking (Figure 6A). Taking into account that UBE2O is a heavily phosphorylated enzyme (Figure S6F), we sought to determine the impact of kinase inhibition on UBE2O localization. We treated cells with a panel of kinase inhibitors of various specificities and observed a nuclear translocation of UBE2O with the CDK-inhibitors Purvalanol A and RO-3306 (Figure 6B,C). Interestingly, UBE2O catalytic dead form was strongly retained in the nucleus indicating the importance of catalytic activity in coordinating its nucleocytoplasmic transport. Consistent with its potential role in negatively regulating BAP1 function, siRNA-depletion of UBE2O increased cell proliferation whereas siRNA-depletion of BAP1 resulted in decreased cell proliferation (Figure 6D). Of note, no noticeable changes in UBE2O or BAP1 localization were observed in unperturbed cycling cells (Data not shown), suggesting that only very limited pools of UBE2O or BAP1 might be imported or exported respectively. Taking into account that BAP1 tightly coordinate cell proliferation, we reasoned that a substantial change in BAP1 localization might

be observed during permanent cell cycle exit. Since UBE2O was implicated in promoting adipocyte differentiation in the mouse embryo cell line C3H10T1/2, we generated stable cell lines for UBE2O and its catalytic dead form and recapitulated this effect using the 3T3-L1 cellular model of adipocyte differentiation as determined by immunoblotting for aP2 and Perilipin (PLIN) adipogenic markers and Oil Red O staining (Figure 6E,F). Significantly, a fraction of BAP1 become excluded from the nucleus as 3T3-L1 preadipocytes terminally differentiate into adipocytes (Figure 6G). In addition, mutation of the UBE2O-ubiquitination sites in BAP1 resulted in a substantial retention of this DUB in the nucleus. Since BAP1 5K/R mutant still interact with UBE2O and is ubiquitinated on other sites, we also replaced the NLS region of BAP1, containing the UBE2O-interacting motif, with T-large antigen NLS which prominently prevented the cytoplasmic exclusion of this DUB during differentiation.

UBE2O targets a subset of bipartite NLS-containing transcription regulators

UBE2O displays prominent UBC-dependent autocatalytic activity in vitro and in vivo (Figure 7A and Figure 1C), which is inhibited by PAO (Figure S2B, Figure 7A). In addition, a nuclear retention of UBE2O, more pronounced for the catalytic dead form was observed following treatment with CDK inhibitors (Figure 6C). Thus, we sought to determine if NLS sequences within UBE2O may constitute autoubiquitination sites. Strikingly the NLS1/A mutant was completely autoubiquitination deficient similar to UBE2O CD, whereas mutation of NLS2 had no significant effect on UBE2O autoubiquitination (Figure S6A, Figure 7B). In addition, the bipartite NLS regions of UBE2O and BAP1 contain a highly conserved patch of aliphatic hydrophobic amino acids (VLI patch) between the minor and major NLS sites (linker region) (Figure 7C). Mutation of the VLI patch disrupted autoubiquitination (Figure S7A). Of note, the NLS1 architecture is highly conserved between most UBE2O orthologs (Figure S6E). These results prompted us to search whether this subtype of bipartite NLS may serve as a specific signal for UBE2O recognition and ubiquitination in other proteins. Several candidates were identified, notably chromatin-associated proteins, suggesting that UBE2O might exert extensive control over nuclear signaling pathways (Figure S7F). We selected four proteins, i.e., p400, CDT1, INO80 and CXXC1, predicted as potential UBE2O substrates. INO80 and p400 are members of SWI/SNF family of chromatin-remodeling ATPases (Jin et al., 2005; Vassilev et al., 1998) containing the predicted NLS sequences (Figure 7C). CXXC1 is the CpG island binding

protein and component of the SET1 complex (Lee and Skalnik, 2005) that contains two predicted NLS sequences with NLS2 containing the putative UBE2O binding motif. The DNA replication factor CDT1 also harbors a potential binding and ubiquitination site for UBE2O (Nishitani et al., 2000). INO80, p400 and CDT1 were degraded following co-expression with UBE2O in a catalytic-activity-dependent manner, ostensibly as a result of ubiquitin chain extension by unknown E3 ligases (Figure 7D, Figure S7B). CXXC1 showed several slow migrating bands suggesting its ubiquitination without degradation (Figure 7D, right panel). Next, we selected INO80 and CXXC1 as two contrasting examples of UBE2O action for further characterization of their ubiquitination by UBE2O (Figure 7D). When the immunoprecipitated INO80 was loaded in equal amounts, the ubiquitin blot showed a typical polyubiquitin smear in the stacking gel (Figure 7D, left panel). The ubiquitination profile of CXXC1 was similar to that of BAP1 and UBE2O with several distinct multi-monoubiquitin bands (Figure 7D, right panel). Ubiquitination of INO80 and CXXC1 by UBE2O had a pronounced effect on their subcellular localization, as both proteins displayed stronger cytoplasmic localization following co-expression of wild-type but not UBE2O CD mutant (Figure 7E). We also found a potential UBE2O binding consensus in ALC1, another nuclear SWI/SNF family chromatin-remodeling enzyme (Ahel et al., 2009), but UBE2O had no effect on ALC1 ubiquitination and localization (Figure S7C,D,E). This can be explained by the absence of the major NLS stretch in the vicinity of the consensus and/or the location of the consensus in the masked fold of its Macro domain. Therefore, UBE2O targets a subset of chromatin remodeling and modifying factors containing a bipartite NLS with a specific VLI patch in the linker region with the exception of CDT1, which contains the major NLS stretch upstream of the UBE2O consensus. Thus, substrate ubiquitination by UBE2O can induce cytoplasmic exclusion, which might be accompanied by further proteasomal degradation as a consequence of ubiquitin chain extension by other E3 ligases.

Discussion

Regulation of BAP1 by UBE2O-mediated ubiquitination

Here, we define a regulatory mechanism involving the E2/E3 hybrid UBE2O which multi-monoubiquitinates BAP1 in the NLS region. Under normal growth conditions, BAP1 is predominantly nuclear whereas UBE2O is mainly cytoplasmic suggesting that BAP1 ubiquitination is highly regulated. In particular, this compartmentalization raises the question regarding the cellular compartment where the ubiquitination actually occurs. UBE2O could be

imported into the nucleus to ubiquitinate BAP1 and promote its ubiquitin-mediated nuclear export as observed for other proteins (Groulx and Lee, 2002; Li et al., 2003). It is possible that only a small fraction of UBE2O is imported into the nucleus at any given time, consistent with the low abundance of this enzyme in this compartment. Controling UBE2O import itself would provide another level of regulation for the fine-tuning of BAP1 ubiquitination. Indeed, (i) BAP1 and UBE2O exert antagonistic functions during cell proliferation, (ii) CDK inhibitors promoted UBE2O nuclear localization with a stronger effect towards its catalytic dead form, (iii) UBE2O exhibits an autoubiquitination activity towards its own NLS, and (iv) two recent studies revealed that the K521 residue (K516 in mouse), part of UBE2O NLS1, is ubiquitinated in vivo (Figure S6F)**.** Our data do not exclude the possibility that, under specific conditions, BAP1 might be exported to the cytoplasm prior to its ubiquitination, although we did not identify any export signal in BAP1. Further studies are needed to dissect the possible mechanisms of UBE2O nucleocytoplasmic transport including its regulation.

On the other hand, since ubiquitination of BAP1 is counteracted by autodeubiquitination, one can predict that a yet to be identified signal is needed to inactivate BAP1 catalytic activity. This initiating event would render this DUB susceptible to ubiquitination by UBE2O. BAP1 could be modified by other post-translational modifications that inhibit its autodeubiquitination. In fact, several phosphorylation and ubiquitination sites of BAP1 were identified in proteomics studies (Figure S6G), and in this study we identified several ubiquitination sites on UCH, some of which might result from the action of other E3 ligases. Under normal cell growth conditions, UBE2O-mediated ubiquitination of BAP1 might not necessarily lead to a net accumulation of BAP1 in the cytoplasm, since this could be a protracted process that is concomitant with both de novo synthesis of BAP1 and further degradation or re-import of BAP1. We speculate that this could be an editing mechanism that might coordinate the transcriptional competency of BAP1. In contrast, during adipocyte differentiation, we observed a net cytoplasmic redistribution of BAP1 that would drastically impact its transcriptional activity. It is also possible that BAP1 might exert cytoplasmic functions in terminally differentiated adipocytes. We note that, since our conclusion is based on ectopically expressed BAP1, further work is needed to establish this regulation for the endogenous enzyme and to provide insights into the possible concerted action of post-translational modifications in regulating the trafficking and function of this DUB.

Autodeubiquitination of BAP1 and its disruption in cancer

Autodeubiquitination of DUBs was previously observed for UCH-L1, which was able to counteract its own ubiquitination by an unknown E3 ligase (Meray and Lansbury, 2007). Interestingly, in our study, we noticed a similar mechanism regulating UCH37. We also note that UCH37 and BAP1 share a common ancestry. Although vertebrate BAP1 acquired the long NORS region, which contains the HCF-1 interaction motif, the intramolecular interaction between the amino and carboxy termini seems to be evolutionary conserved. It is possible that DUB autodeubiquitination might constitute a regulatory mechanism, which is more widely used than currently appreciated.

Cancer-associated mutations in BAP1 disrupt its function by multiple means. Large deletions in the BAP1 gene result in dysfunctional proteins. Point mutations in the UCH domain of BAP1 often target the catalytic site or its immediate environment resulting in disruption of catalytic activity. The cancer-derived mutations of BAP1 in the catalytic site are predicted to impact both autodeubiquitination as well as DUB activity towards other substrates. Histone H2A is a substrate of BAP1 (Scheuermann et al., 2010; Yu et al., 2014), and other substrates such as HCF-1 and OGT were previously also described (Machida et al., 2009; Misaghi et al., 2009; Ruan et al., 2012). In this study, we identified two cancer-mutations in the coiled-coil motif of the C-terminal region that remarkably did not compromise BAP1 complex assembly, but instead promoted UBE2O association with this DUB. It would be interesting to further determine whether this is a result of structural changes in BAP1 that facilitate UBE2O binding, or rather is a consequence of increased cytoplasmic sequestration of BAP1. Importantly, the two cancer-derived mutations selectively compromised the autodeubiquitination activity of BAP1 without affecting its H2A DUB activity. These cancer-derived mutations also revealed that autodeubiquitination function of the enzyme is important for its proper nuclear localization. Thus, by separating the two activities of BAP1, we provide a biochemical paradigm for testing the involvement of other ubiquitin signaling cascades in regulating BAP1 function.

UBE2O acts as an atypical E2/E3 that ubiquitinates a subset of NLS-containing proteins

The evolution of protein conjugation pathways can be traced back to prokaryotic and archea cells. In eukaryotes, this system diversified resulting in establishment of the classical E1/E2/E3/substrate ubiquitin transfer cascade (Burroughs et al., 2012; Hochstrasser, 2009).

UBE2O is highly conserved in plants and animals suggesting that it evolved from a common ancestor at least 1.6 billion years ago, when the prototypic animal and plant cell types were evolving (Meyerowitz, 2002). UBE2O seems to employ the properties of both E2 and E3 enzymes suggesting that it might recognize a limited number of substrates. In our study, we discovered that UBE2O specifically binds and ubiquitinates a subset of bipartite NLS that contain a VLI patch in their linker. Based on the consensus between two identified UBE2O substrates, i.e. BAP1 and UBE2O itself, we were able to predict the substrate specificity of the enzyme, in turn allowing us to identify more putative UBE2O substrates including proteins involved in RNA processing, transcription, DNA replication, and chromatin remodelling. Thus, UBE2O might be involved in coordinating major signaling pathways in the cytoplasm, organelles, and nucleus that orchestrate cell function during proliferation and differentiation or in response to extracellular stimuli. Although we were able to detect UBE2O expression in multiple cultured cell lines (HeLa, U2OS, MCF-7, 293T and data not shown), its expression seems to be highly regulated. UBE2O levels were previously reported to increase during erythroid differentiation (Wefes et al., 1995). Chromatin of differentiating cells is subjected to multiple epigenetic and structural changes, requiring specific ubiquitin signaling pathways to promote the displacement of chromatin-associated regulators to activate or repress gene expression (Geng et al., 2012). Indeed, UBE2O promotes adipocyte differentiation and is also highly expressed in brain, heart, and skeletal muscle (Nagase et al., 2000; Yokota et al., 2001; Zhang et al., 2013a), all of which comprise post-mitotic cells that must finely coordinate gene expression programs to fulfill metabolically demanding requirements.

Acknowledgments

We thank Elliot Drobetsky, Eric Milot, Dindial Ramotar and Hugo Wurtele for the critical reading of the manuscript. We thank Diana Adjaoud for technical assistance. This work was supported by a grant to EBA from the Canadian Institute of Health Research (CIHR) (MOP115132). EBA is a scholar of the CIHR and Le Fonds de la Recherche en Santé du Québec. MT holds a Tier 1 Canada Research Chair in Intracellular Signaling. NM was supported by a PhD scholarship from the Fonds Québécois de la Recherche sur la Nature et les Technologies. The authors would like to dedicate this paper to the memory of Cecile M. Pickart for her original work that guided us to demonstrate that UBE2O is indeed an E2/E3 hybrid.

Experimental Procedures

Plasmids and Antibodies

UBE2O and RING1B were cloned from HeLa total RNA by reverse transcription and inserted into pENTR D-Topo plasmid (Life Technologies). MYSM1 and USP16 were cloned from HeLa total RNA by reverse transcription and inserted into pEGFP-C1 plasmid. Human RNF10 and RNF219 were cloned from U2OS total RNA by reverse transcription and inserted into p3XFLAG-CMV™-7 expression vector (Sigma-Aldrich). UBE2O expression constructs were generated using LR clonase kit (Life Technologies) in pDEST-Myc, pDEST-His or retroviral pMSCV-Flag/HA-IRES-Puro (Sowa et al., 2009).

For bacterial expression the UBE2O cDNA was cloned into pET30a+ vector (Novagen), to generate N-terminal Flag- and the C- terminal His-tags for the double column purification.

The catalytically inactive UBE2O was generated by site-directed mutagenesis. Non-tagged pCDNA3-BAP1 and C91S were generated by subcloning the cDNA from pOZ-N BAP1 and pOZ-N C91S respectively. BAP1 cancer mutants ΔE631-A634, ΔK637-C638InsN, ΔCC2 and ΔCTD and UBE2O NLS mutants were generated using gene synthesis (BioBasic) and then subcloned into modified pENTR D-Topo plasmid.

BAP1 NLS mutants were generated by subcloning of annealed short adapters containing corresponding mutations in pENTR D-Topo BAP1 and/or C91S. NLS-GFP were generated by subcloning of annealed short adapters containing corresponding BAP1 or UBE2O NLS sequences in pOD35 plasmid provided by Dr. Paul Maddox (Institute for Research in Immunology and Cancer, Canada). All constructs were sequenced.

shRNAs for human UBE2O were from Sigma (#1 NM022066x814s1c1 and #2 NM022066x4103s1c1). The constructs used to produce recombinant full length GST-BAP1 and various deletion fragments, and BAP1 mutant deleted in the NHNY sequence corresponding to the HCF-1 binding domain (ΔHBM) and BAP1 catalytic dead C91S were described (Yu et al., 2010).

Flag-INO80 expression vector was provided by Dr. Yang Shi (Harvard Medical School, USA) (Wu et al., 2007). Flag-p400 was provided by Dr. David M. Livingston (Harvard Medical School, USA) (Chan et al., 2005). Flag-CXXC1 expression vector was provided by Dr. David Skalnik (Indiana University-Purdue University Indianapolis, USA) (Tate et al., 2009). Flag-CDT1 expression vector was provided by Dr. Kevin Struhl (Harvard Medical School, USA) (Miotto and Struhl, 2011). Flag-ALC1 expression vector was provided by Dr. Simon Boulton (London Research Institute, UK) (Ahel et al., 2009). Flag-BRUCE and Flag-BRUCE CD expression vectors were from Dr. Stefan Jentsch (Max Planck Institute of Biochemistry, Germany) (Bartke et al., 2004). HA-UCH37 and HA-UCH37 C88A expression vectors were from Dr. Joan Conaway (Stowers Institute for Medical Research, USA) (Yao et al., 2008). Myc-UBC7 expression vector was provided by Dr. Allan M. Weissman (Center for Cancer Research National Cancer Institute, USA) (Tiwari and Weissman, 2001). Flag-UBCH8 expression vector was provided by Dr. Dong-Er Zhang (UC San Diego, USA) (Kim et al., 2004). GFP-TRIM28 expression vector was provided by Dr. Fanxiu Zhu (Florida State University USA) (Liang et al., 2011). Myc-TRIM27 expression vector was provided by Dr. Patrick R. Potts (UT Southwestern Dallas, USA) (Hao et al., 2013). HA-BRCA1 was generated by subcloning from the GFP-BRCA1 plasmid previously described (Hammond-Martel et al., 2010) into pCDNA3 plasmid. BARD1 expression vector was from Origene (SC119847). HA-wild-type and K0 Ub expression vectors were from Dr. Ted Dawson (John Hopkins University, USA) (Lim et al., 2005).

The siRNA ON-TARGETplus® smart pool for human UBE2O and a non-target control were from Dharmacon (Thermo Scientific).

Rabbit polyclonal anti-UBE2O was from Novus Biologicals (NBP-03336). Mouse monoclonal anti-BAP1 (C4), rabbit polyclonal anti-BAP1 (H300), rabbit polyclonal anti-YY1 (H414), rabbit polyclonal anti-OGT (H300), mouse monoclonal anti-GFP (B2), rabbit polyclonal anti-GFP (FL), mouse monoclonal anti-RING1B (N-32), mouse monoclonal anti-BRCA1 (D-9), mouse monoclonal anti-BARD1 (2059c4a), mouse monoclonal anti-CDC25A (F6), mouse monoclonal anti-Ubiquitin (P4D1) were from Santa Cruz. Rabbit polyclonal anti-HCF-1 (A301-400A) and rabbit polyclonal anti-ASXL2 (A302-037A) were

from Bethyl Laboratories. Mouse monoclonal anti-Flag (M2) was from Sigma. Mouse monoclonal anti-Myc (9E10) and mouse monoclonal anti-HA (HA11) were from Covance. Rabbit polyclonal anti-HA (ab9110) was from Abcam. Rabbit monoclonal anti-Perilipin (PLIN) was from New England BioLabs (D1D8) XP®). Rabbit polyclonal anti-aP2 (FABP4) was from Cayman Chemicals. Mouse polyclonal anti-FOXK1 was provided by Dr. Xiao-Hua Li from Southwestern University of Texas. A rabbit polyclonal anti-FOXK2 was generated using a recombinant fragment of human FOXK2 by Pacific Immunology.

Chemicals and reagents

UBE1, USP2 CD, Ub-VME, Ub-AMC, recombinant Myc-Ub and Ub were from Boston Biochem. Cycloheximide (CHX), N-methylmaleimide (NEM), Phenylarsine oxide (PAO), MG132, Micrococcal nuclease (MNase) where from Sigma. Casein kinase II (CKII) inhibitor TBB (100 μM), Casein kinase I (CKI) inhibitor IC261 (10 μM), protein kinase G inhibitor KT5823 (10 μM), CDK1 inhibitor RO-3306 (10 μM) where purchased from Millipore. The CDK1, CDK2 and CDK5 inhibitor Roscovitine (10 μM), MEK1/2 inhibitor UO126 (20 μM) and the protein kinase A (PKA) inhibitor H-89 (20 μM) were purchased from Cell Signaling. The CDK2 inhibitor Purvalanol A (50 μM) was purchased from Abcam. Protein kinase C inhibitor PKC412 (20 μM) and STK inhibitor GSK 650394 (20 μM) were from Santa Cruz. The PI3-Kinase inhibitor caffeine (10 mM) CDK inhibitor CDKi (100 μM), CDK2 inhibitor GW8510 (20 μM) and JNK inhibitor SP600125 (30 μM) were from Sigma. SU 9516 (5 μM), Chk1 inhibitor SB 218078 (1 μM). Broad spectrum kinase inhibitor Staurosporine (100 nM), tyrosine kinase inhibitor Genistein (20 μM), CDK inhibitor Olomoucine (30 μM), CKII inhibitor Apigenin (20 μM), CKII and CDK inhibitor DRB (50 μM), PI3-Kinase inhibitor LY294002 (20 μM), CKII inhibitor NSC 210902 (15 μM), CKI inhibitor D 4476 (25 μM) and CKII inhibitor CAY10578 (15 μM) where from Cayman chemical.

Cell culture, transfections and western blot

HeLa S3 cervical cancer, MCF7 breast cancer, U2OS osteosarcoma, human embryonic kidney 293T, 293GPG virus-producing cells and 3T3-L1 mouse preadipocytes

and human primary lung fibroblasts LF-1 were cultured in Dulbecco's modified Eagle's medium (DMEM) supplemented with 10% fetal bovine serum and penicillin/streptomycin.

siRNA and plasmid DNA were transfected in MCF7 and U2OS cells, respectively, using Lipofectamine 2000 (Life Technologies). HEK293T (293T) cells were transfected using PEI (Sigma).

Total cell lysates were prepared in buffer containing 25 mM Tris-HCl pH 7.3 and 1% SDS, samples were immediately boiled at 95°C for 10 min and sonicated to break down DNA. Samples were diluted using 2X or 4X Laemmli buffer (Laemmli, 1970). SDS-PAGE and western blotting were conducted according to standard procedures. Images were acquired using ImageQuant™ LAS 4000 biomolecular imager (GE Healthcare, USA). Densitometry quantification of western blot bands was performed using Gel-Pro Analyzer 3.1 (Media Cybernetics)

Stable cell lines

HeLa S3 cell lines stably expressing Flag-HA-BAP1, Flag-HA-C91S, Flag-HA-ΔE631-A634, Flag-HA-ΔK637-C638InsN, Flag-HA-ΔCTD, Flag-HA-ΔCC1 were generated following retroviral infection using pOZ-N-based retroviral constructs and selected using anti-IL2 magnetic beads (Life Technologies) (Yu et al., 2010).

U2OS cell lines stably expressing Flag-HA-BAP1, Flag-HA-C91S, Flag-HA-ΔE631-A634, Flag-HA-ΔK637-C638InsN, Flag-HA-ΔCTD, Flag-HA-ΔCC1 were generated following retroviral infection of pMSCV-Flag/HA-IRES-Puro based constructs and selected with 3 μg/ml of puromycin.

3T3-L1 cell lines stably expressing Flag-HA-BAP1, Flag-HA-BAP1 5 K/R, Flag-HA-BAP1 NLS T1, Flag-HA-UBE2O and Flag-HA-UBE2O CD were generated following retroviral infection of pMSCV-Flag/HA-IRES-Puro based constructs and selected with 3 μg/ml of puromycin.

Stable HeLa S3 Flag-HA-UBE2O cell line was generated following retroviral infection of pMSCV-Flag/HA UBE2O-IRES-Puro and selected with 2 μg/ml of puromycin.

Purification of BAP1 complexes and UBE2O-interacting proteins

HeLa S3 (~12 X 10^9) cells stably expressing Flag-HA-BAP1, Flag-HA-C91S, Flag-HA-ΔE631-A634, Flag-HA-ΔK637-C638InsN, Flag-HA-ΔCTD and Flag-HA-UBE2O were grown in spinner flasks. The cytosolic fraction was used for the purification of UBE2O with Flag and HA immunoaffinity columns essentially as previously described (Groisman et al., 2003) the Flag and HA columns were washed with either low salt buffer containing 100 mM KCl (Flag-HA-UBE2O LS (Figure S2A, C, D) or 300 mM NaCl (Flag-HA-UBE2O LS (Figure S2A, C, D). The BAP1 protein complexes were purified from total soluble protein extracts in EBcom (50 mM Tris-HCl pH 7.5, 150 mM NaCl, 0,5% NP-40, 50 mM NaF, 10 mM β-glycerophosphat, 1mM Na_3VO_4 1 mM DTT, 1mM EDTA, 1 mM PMSF and protease inhibitors cocktail (Sigma)). The extracts were clarified by centrifugation at 30,000g for 1 hour, with subsequent filtration of supernatants through a 0,45 μm pore filter. The extracts were incubated with the anti-Flag M2 resin overnight and extensively washed with EBcom. The resin was eluted three times with EBcom containing 200 ng/ml of Flag peptide. The eluted fractions were incubated with anti-HA resin overnight, and the procedure was repeated as for the previous column. The HA eluted fractions were used for silver stain, western blot and in vitro DUB assay. Mass spectrometric identification of UBE2O-interacting proteins was done at the Taplin Mass Spectrometry facility (Harvard, USA). Identification of additional BAP1-interacting proteins was done at the The Proteomics Platform of the Quebec Genomics Center (CHUQ, Laval University, Canada).

Immunoprecipitation

Cells were lysed in buffer EB150 (50 mM Tris-HCl pH 7.5, 150 mM NaCl, 1% NP-40, 10 mM β-mercaptoethanol, 1 mM PMSF and protease inhibitors cocktail (Sigma)) and the lysates were clarified by centrifugation at 21,000 g for 30 min. The supernatants were incubated with indicated antibodies for 3 hours and then protein-G beads were added and incubated for an additional hour. The samples were extensively washed with EB150 and re-suspended in 2X Laemmli buffer. For an IP under denaturing conditions, the cells were harvested as described for western blot, and diluted in EB300 (50 mM Tris-HCl pH 7.5, 300 mM NaCl, 1% NP-40, 10 mM β-mercaptoethanol). The lysates were incubated overnight

with antibody and protein-G beads. The beads were washed several times with EB300 and resuspended in 2X Laemmli buffer.

Mass spectrometric identification of ubiquitination sites

293T (~1 X 10^9) cells were transfected with HA-Ub, Flag-C91S, and His-UBE2O expression vectors. 96 hours later, the cells were lysed in EB300 containing 20 mM NEM and protease inhibitor cocktail. The extracts were clarified by centrifugation at 30,000g for 1 hour. The extracts were incubated with the anti-Flag M2 resin overnight and extensively washed with EB300. The resin was eluted three times with EB300 containing 200 ng/ml of Flag peptide. The eluted fractions were combined and concentrated using TCA (trichloroacetic acid) precipitation and loaded on the NuPAGE® Bis-Tris Precast Gel (Life Technologies). The gel was stained with Coomassie G-250 and the modified C91S bands were excised and sent for MS analysis at Taplin Mass Spectrometry facility (Harvard, USA).

Glycerol gradient

Molecular mass fractionation of nuclear extract was conduced using a 10-40 % glycerol gradient prepared in 20 mM Tris-HCl, pH 7.9; 100 mM KCl; 5 mM $MgCl_2$; 1 mM PMSF; 0.1% NP40 and 10 mM β-mercaptoethanol. The samples were centrifuged for 12 hours at 50,000 RPM (SW55Ti rotor, Beckman,) at 4 ºC. Individual fractions were then collected from top to bottom and analyzed by western blotting. The BAP1 complex is estimated to have a molecular mass of 1.6 MDa.

***In vitro* interaction assays**

Recombinant GST-BAP1 fusion proteins were purified from bacteria using glutathione agarose beads (Sigma) and 2 to 3 µg of bound proteins were incubated with His-UBE2O for 6 to 8 hours at 4 ºC in pull down buffer (50 mM Tris-HCl, pH 7.5; 50 mM NaCl; 0.02% Tween 20; 1 mM PMSF and 500 µM dithiothreitol). The beads were extensively washed with the same buffer, and bound proteins eluted in 2X Laemmli buffer and subjected to western blotting.

***In vitro* ubiquitination assay**

Ubiquitination reactions were conducted in a total volume of 30 µl containing 25 mM Tris-HCl, pH 7.3, 10 mM $MgCl_2$, 5 mM ATP, 300 ng/µl Ub, 250 ng of human recombinant UBE1 and 1 mM β-mercaptoethanol. Purified Flag-HA-BAP1, Flag-HA-C91S and UBE2O were added as indicated.

Reaction on the beads-immobilized complexes was performed when indicated. Briefly, the anti-Flag M2 beads were incubated with high salt nuclear extracts from HeLa S3 Flag-HA-BAP1 or Flag-HA-C91S for 5 hour and washed 8 times with buffer containing 20 mM Tris-HCl pH 7.5, 100 mM KCl, 1 mM $MgCl_2$, 5 mM EDTA, 0.1% Triton X-100 and 1 mM PMSF. The beads-bound complexes (25 µl) were used for the reaction essentially in the same conditions as for the reaction in solution. Reactions were incubated at 37ºC with constant shaking overnight. Met-Ub was previously described (Kirisako et al., 2006)

Purification of the nucleosomes and *In vitro* nucleosome DUB assay

Preparation of chromatin fractions and digestion with Micrococcal nuclease (MNase Sigma) were conducted as previously described (Groisman et al., 2003), with some modifications. The 293T cellular pellet was resuspended in EB420 (50 mM Tris-HCl pH 7.3, 420 mM NaCl, 1% NP-40, 10 mM β-mercaptoethanol, 20 mM NEM and protease inhibitor cocktail). The soluble fraction was discarded and the pellet was extensively washed with MNase buffer (20 mM Tris-HCl pH 7.5, 100 mM KCl, 2 mM $MgCl_2$, 1 mM $CaCl_2$, 0.3 M sucrose, 0.1% NP-40, and protease inhibitor cocktail). Following MNase treatment (3 U/ml for 10 min at room temperature), the reaction was quenched with 5 mM of EGTA and 5 mM of EDTA. The samples were then centrifuged at 20,000g for 10 min at 4°C to obtain the soluble chromatin fraction. The extract was incubated with anti-Flag resin overnight and washed with EB300 buffer. The beads then were eluted with EB300 containing 200 ng/ml of Flag peptide.

The eluted soluble chromatin fraction was incubated with the indicated Flag/HA purified BAP1 complexes and used for western blotting.

Immunofluorescence

The procedure was carried over essentially as previously described (Daou et al., 2011). Briefly cells were fixed in 3% PFA-PBS and permeabilized using PBS 0.1% NP-40. Anti-mouse Alexa Fluor® 594 and Anti-mouse Alexa Fluor® 488 (Life Technologies) were used as secondary antibodies. Nuclei were stained with 4',6-diamidino-2-phenylindole (DAPI).

Images were acquired using Zeiss. Z2 microscope and Plan Apochrmat 40X/0.95 Korr, Plan Apochrmat 63X/1.4 Oil DIC and Plan Apochrmat 100X/1.4 Oil DIC objectives and AxioCam MRm camera. Images were processed using WCIF-ImageJ program (NIH).

Adipogenic differentiation of 3T3-L1 preadipocytes.

3T3-L1 cell lines stably expressing BAP1 or UBE2O were plated at the same density, upon reaching of confluency the growth media was changed to induction media containing 10% fetal bovine serum, penicillin/streptomycin, 1 μM dexamethasone, 1 μg/ml insulin and 500 μM IBMX (Sigma). Two days post-induction, the media was changed to maintenance media containing 10 % fetal bovine serum, penicillin/streptomycin, 1 μg/ml insulin. The cells were fixed with PFA or harvested for western blotting two to three days post-induction. Lipid droplet content was evaluated using Oil-Red O lipid stain (Sigma).

Protein sequence analysis, and structure modeling

Protein sequences were analyzed and aligned using Geneious 6.1.2 created by Biomatters, available from http://www.geneious.com. NLS consensuses were analyzed using ProSite (Sigrist et al., 2013) and NLStradamus (Nguyen Ba et al., 2009). Coiled-coil regions were predicted using COILS (Lupas et al., 1991). BAP1 3D structure modeling was performed using SWISS-MODEL (Arnold et al., 2006) and crystal structure of UCH37 (Burgie et al., 2011) (PDB code: 3IHR).

References

Ahel, D., Horejsi, Z., Wiechens, N., Polo, S.E., Garcia-Wilson, E., Ahel, I., Flynn, H., Skehel, M., West, S.C., Jackson, S.P., *et al.* (2009). Poly(ADP-ribose)-dependent regulation of DNA repair by the chromatin remodeling enzyme ALC1. Science *325*, 1240-1243.

Berleth, E.S., and Pickart, C.M. (1996). Mechanism of ubiquitin-conjugating enzyme E2-230K: catalysis involving a thiol relay? Biochemistry *35*, 1664-1671.

Burgie, S.E., Bingman, C.A., Soni, A.B., and Phillips, G.N., Jr. (2011). Structural characterization of human Uch37. Proteins.

Burroughs, A.M., Iyer, L.M., and Aravind, L. (2012). The natural history of ubiquitin and ubiquitin-related domains. Frontiers in bioscience : a journal and virtual library *17*, 1433-1460.

Carbone, M., Yang, H., Pass, H.I., Krausz, T., Testa, J.R., and Gaudino, G. (2013). BAP1 and cancer. Nature reviews. Cancer *13*, 153-159.

Daou, S., Mashtalir, N., Hammond-Martel, I., Pak, H., Yu, H., Sui, G., Vogel, J.L., Kristie, T.M., and Affar el, B. (2011). Crosstalk between O-GlcNAcylation and proteolytic cleavage regulates the host cell factor-1 maturation pathway. Proceedings of the National Academy of Sciences of the United States of America *108*, 2747-2752.

Dey, A., Seshasayee, D., Noubade, R., French, D.M., Liu, J., Chaurushiya, M.S., Kirkpatrick, D.S., Pham, V.C., Lill, J.R., Bakalarski, C.E., *et al.* (2012). Loss of the tumor suppressor BAP1 causes myeloid transformation. Science *337*, 1541-1546.

Geng, F., Wenzel, S., and Tansey, W.P. (2012). Ubiquitin and proteasomes in transcription. Annual review of biochemistry *81*, 177-201.

Groisman, R., Polanowska, J., Kuraoka, I., Sawada, J., Saijo, M., Drapkin, R., Kisselev, A.F., Tanaka, K., and Nakatani, Y. (2003). The ubiquitin ligase activity in the DDB2 and CSA complexes is differentially regulated by the COP9 signalosome in response to DNA damage. Cell *113*, 357-367.

Groulx, I., and Lee, S. (2002). Oxygen-dependent ubiquitination and degradation of hypoxia-inducible factor requires nuclear-cytoplasmic trafficking of the von Hippel-Lindau tumor suppressor protein. Molecular and cellular biology *22*, 5319-5336.

Hammond-Martel, I., Yu, H., and Affar el, B. (2012). Roles of ubiquitin signaling in transcription regulation. Cellular signalling *24*, 410-421.

Hao, Y.H., Doyle, J.M., Ramanathan, S., Gomez, T.S., Jia, D., Xu, M., Chen, Z.J., Billadeau, D.D., Rosen, M.K., and Potts, P.R. (2013). Regulation of WASH-Dependent Actin Polymerization and Protein Trafficking by Ubiquitination. Cell *152*, 1051-1064.

Harbour, J.W., Onken, M.D., Roberson, E.D., Duan, S., Cao, L., Worley, L.A., Council, M.L., Matatall, K.A., Helms, C., and Bowcock, A.M. (2010). Frequent mutation of BAP1 in metastasizing uveal melanomas. Science *330*, 1410-1413.

Hochstrasser, M. (2009). Origin and function of ubiquitin-like proteins. Nature *458*, 422-429.

Jackson, S.P., and Durocher, D. (2013). Regulation of DNA Damage Responses by Ubiquitin and SUMO. Molecular cell *49*, 795-807.

Jin, J., Cai, Y., Yao, T., Gottschalk, A.J., Florens, L., Swanson, S.K., Gutierrez, J.L., Coleman, M.K., Workman, J.L., Mushegian, A.*, et al.* (2005). A mammalian chromatin remodeling complex with similarities to the yeast INO80 complex. The Journal of biological chemistry *280*, 41207-41212.

Klemperer, N.S., Berleth, E.S., and Pickart, C.M. (1989). A novel, arsenite-sensitive E2 of the ubiquitin pathway: purification and properties. Biochemistry *28*, 6035-6041.

Lanzuolo, C., and Orlando, V. (2012). Memories from the polycomb group proteins. Annual review of genetics *46*, 561-589.

Lee, J.H., and Skalnik, D.G. (2005). CpG-binding protein (CXXC finger protein 1) is a component of the mammalian Set1 histone H3-Lys4 methyltransferase complex, the analogue of the yeast Set1/COMPASS complex. The Journal of biological chemistry *280*, 41725-41731.

Li, M., Brooks, C.L., Wu-Baer, F., Chen, D., Baer, R., and Gu, W. (2003). Mono- versus polyubiquitination: differential control of p53 fate by Mdm2. Science *302*, 1972-1975.

Machida, Y.J., Machida, Y., Vashisht, A.A., Wohlschlegel, J.A., and Dutta, A. (2009). The deubiquitinating enzyme BAP1 regulates cell growth via interaction with HCF-1. The Journal of biological chemistry *284*, 34179-34188.

Meray, R.K., and Lansbury, P.T., Jr. (2007). Reversible monoubiquitination regulates the Parkinson disease-associated ubiquitin hydrolase UCH-L1. The Journal of biological chemistry *282*, 10567-10575.

Meyerowitz, E.M. (2002). Plants compared to animals: the broadest comparative study of development. Science *295*, 1482-1485.

Misaghi, S., Ottosen, S., Izrael-Tomasevic, A., Arnott, D., Lamkanfi, M., Lee, J., Liu, J., O'Rourke, K., Dixit, V.M., and Wilson, A.C. (2009). Association of C-terminal ubiquitin hydrolase BRCA1-associated protein 1 with cell cycle regulator host cell factor 1. Molecular and cellular biology *29*, 2181-2192.

Nagase, T., Kikuno, R., Hattori, A., Kondo, Y., Okumura, K., and Ohara, O. (2000). Prediction of the coding sequences of unidentified human genes. XIX. The complete sequences of 100 new cDNA clones from brain which code for large proteins in vitro. DNA research : an international journal for rapid publication of reports on genes and genomes *7*, 347-355.

Nishitani, H., Lygerou, Z., Nishimoto, T., and Nurse, P. (2000). The Cdt1 protein is required to license DNA for replication in fission yeast. Nature *404*, 625-628.

Ruan, H.B., Han, X., Li, M.D., Singh, J.P., Qian, K., Azarhoush, S., Zhao, L., Bennett, A.M., Samuel, V.T., Wu, J.*, et al.* (2012). O-GlcNAc transferase/host cell factor C1 complex regulates gluconeogenesis by modulating PGC-1alpha stability. Cell metabolism *16*, 226-237.

Scheuermann, J.C., de Ayala Alonso, A.G., Oktaba, K., Ly-Hartig, N., McGinty, R.K., Fraterman, S., Wilm, M., Muir, T.W., and Muller, J. (2010). Histone H2A deubiquitinase activity of the Polycomb repressive complex PR-DUB. Nature *465*, 243-247.

Shabek, N., Herman-Bachinsky, Y., Buchsbaum, S., Lewinson, O., Haj-Yahya, M., Hejjaoui, M., Lashuel, H.A., Sommer, T., Brik, A., and Ciechanover, A. (2012). The size of the proteasomal substrate determines whether its degradation will be mediated by mono- or polyubiquitylation. Molecular cell *48*, 87-97.

Sowa, M.E., Bennett, E.J., Gygi, S.P., and Harper, J.W. (2009). Defining the human deubiquitinating enzyme interaction landscape. Cell *138*, 389-403.

van Wijk, S.J., and Timmers, H.T. (2010). The family of ubiquitin-conjugating enzymes (E2s): deciding between life and death of proteins. FASEB journal : official publication of the Federation of American Societies for Experimental Biology *24*, 981-993.

Vassilev, A., Yamauchi, J., Kotani, T., Prives, C., Avantaggiati, M.L., Qin, J., and Nakatani, Y. (1998). The 400 kDa subunit of the PCAF histone acetylase complex belongs to the ATM superfamily. Molecular cell *2*, 869-875.

Ventii, K.H., Devi, N.S., Friedrich, K.L., Chernova, T.A., Tighiouart, M., Van Meir, E.G., and Wilkinson, K.D. (2008). BRCA1-associated protein-1 is a tumor suppressor that requires deubiquitinating activity and nuclear localization. Cancer research *68*, 6953-6962.

Wefes, I., Mastrandrea, L.D., Haldeman, M., Koury, S.T., Tamburlin, J., Pickart, C.M., and Finley, D. (1995). Induction of ubiquitin-conjugating enzymes during terminal erythroid differentiation. Proceedings of the National Academy of Sciences of the United States of America *92*, 4982-4986.

Yokota, T., Nagai, H., Harada, H., Mine, N., Terada, Y., Fujiwara, H., Yabe, A., Miyazaki, K., and Emi, M. (2001). Identification, tissue expression, and chromosomal position of a novel gene encoding human ubiquitin-conjugating enzyme E2-230k. Gene *267*, 95-100.

Yu, H., Mashtalir, N., Daou, S., Hammond-Martel, I., Ross, J., Sui, G., Hart, G.W., Rauscher, F.J., 3rd, Drobetsky, E., Milot, E.*, et al.* (2010). The ubiquitin carboxyl hydrolase BAP1 forms a ternary complex with YY1 and HCF-1 and is a critical regulator of gene expression. Molecular and cellular biology *30*, 5071-5085.

Yu, H., Pak, H., Hammond-Martel, I., Ghram, M., Rodrigue, A., Daou, S., Barbour, H., Corbeil, L., Hebert, J., Drobetsky, E.*, et al.* (2014). Tumor suppressor and deubiquitinase BAP1 promotes DNA double-strand break repair. Proceedings of the National Academy of Sciences of the United States of America *111*, 285-290.

Zhang, X., Zhang, J., Bauer, A., Zhang, L., Selinger, D.W., Lu, C.X., and Ten Dijke, P. (2013a). Fine-tuning BMP7 signalling in adipogenesis by UBE2O/E2-230K-mediated monoubiquitination of SMAD6. The EMBO journal *32*, 996-1007.

Zhang, X., Zhang, J., Zhang, L., van Dam, H., and Ten Dijke, P. (2013b). UBE2O negatively regulates TRAF6-mediated NF-kappaB activation by inhibiting TRAF6 polyubiquitination. Cell research *23*, 366-377.

SUPPLEMENTAL REFERENCES

Ahel, D., Horejsi, Z., Wiechens, N., Polo, S.E., Garcia-Wilson, E., Ahel, I., Flynn, H., Skehel, M., West, S.C., Jackson, S.P., *et al.* (2009). Poly(ADP-ribose)-dependent regulation of DNA repair by the chromatin remodeling enzyme ALC1. Science *325*, 1240-1243.

Arnold, K., Bordoli, L., Kopp, J., and Schwede, T. (2006). The SWISS-MODEL workspace: a web-based environment for protein structure homology modelling. Bioinformatics *22*, 195-201.

Bartke, T., Pohl, C., Pyrowolakis, G., and Jentsch, S. (2004). Dual role of BRUCE as an antiapoptotic IAP and a chimeric E2/E3 ubiquitin ligase. Molecular cell *14*, 801-811.

Burgie, S.E., Bingman, C.A., Soni, A.B., and Phillips, G.N., Jr. (2011). Structural characterization of human Uch37. Proteins.

Carbone, M., Yang, H., Pass, H.I., Krausz, T., Testa, J.R., and Gaudino, G. (2013). BAP1 and cancer. Nature reviews. Cancer *13*, 153-159.

Chan, H.M., Narita, M., Lowe, S.W., and Livingston, D.M. (2005). The p400 E1A-associated protein is a novel component of the p53 --> p21 senescence pathway. Genes & development *19*, 196-201.

Conti, E., Uy, M., Leighton, L., Blobel, G., and Kuriyan, J. (1998). Crystallographic analysis of the recognition of a nuclear localization signal by the nuclear import factor karyopherin alpha. Cell *94*, 193-204.

Daou, S., Mashtalir, N., Hammond-Martel, I., Pak, H., Yu, H., Sui, G., Vogel, J.L., Kristie, T.M., and Affar el, B. (2011). Crosstalk between O-GlcNAcylation and proteolytic cleavage regulates the host cell factor-1 maturation pathway. Proceedings of the National Academy of Sciences of the United States of America *108*, 2747-2752.

Groisman, R., Polanowska, J., Kuraoka, I., Sawada, J., Saijo, M., Drapkin, R., Kisselev, A.F., Tanaka, K., and Nakatani, Y. (2003). The ubiquitin ligase activity in the DDB2 and CSA complexes is differentially regulated by the COP9 signalosome in response to DNA damage. Cell *113*, 357-367.

Hamazaki, J., Iemura, S., Natsume, T., Yashiroda, H., Tanaka, K., and Murata, S. (2006). A novel proteasome interacting protein recruits the deubiquitinating enzyme UCH37 to 26S proteasomes. The EMBO journal *25*, 4524-4536.

Hammond-Martel, I., Pak, H., Yu, H., Rouget, R., Horwitz, A.A., Parvin, J.D., Drobetsky, E.A., and Affar el, B. (2010). PI 3 kinase related kinases-independent proteolysis of BRCA1 regulates Rad51 recruitment during genotoxic stress in human cells. PloS one *5*, e14027.

Hao, Y., Sekine, K., Kawabata, A., Nakamura, H., Ishioka, T., Ohata, H., Katayama, R., Hashimoto, C., Zhang, X., Noda, T.*, et al.* (2004). Apollon ubiquitinates SMAC and caspase-9, and has an essential cytoprotection function. Nature cell biology *6*, 849-860.

Hao, Y.H., Doyle, J.M., Ramanathan, S., Gomez, T.S., Jia, D., Xu, M., Chen, Z.J., Billadeau, D.D., Rosen, M.K., and Potts, P.R. (2013). Regulation of WASH-Dependent Actin Polymerization and Protein Trafficking by Ubiquitination. Cell *152*, 1051-1064.

Jensen, D.E., Proctor, M., Marquis, S.T., Gardner, H.P., Ha, S.I., Chodosh, L.A., Ishov, A.M., Tommerup, N., Vissing, H., Sekido, Y.*, et al.* (1998). BAP1: a novel ubiquitin hydrolase which binds to the BRCA1 RING finger and enhances BRCA1-mediated cell growth suppression. Oncogene *16*, 1097-1112.

Joo, H.Y., Zhai, L., Yang, C., Nie, S., Erdjument-Bromage, H., Tempst, P., Chang, C., and Wang, H. (2007). Regulation of cell cycle progression and gene expression by H2A deubiquitination. Nature *449*, 1068-1072.

Kim, K.I., Baek, S.H., Jeon, Y.J., Nishimori, S., Suzuki, T., Uchida, S., Shimbara, N., Saitoh, H., Tanaka, K., and Chung, C.H. (2000). A new SUMO-1-specific protease, SUSP1, that is highly expressed in reproductive organs. The Journal of biological chemistry *275*, 14102-14106.

Kim, K.I., Giannakopoulos, N.V., Virgin, H.W., and Zhang, D.E. (2004). Interferon-inducible ubiquitin E2, Ubc8, is a conjugating enzyme for protein ISGylation. Molecular and cellular biology *24*, 9592-9600.

Kirisako, T., Kamei, K., Murata, S., Kato, M., Fukumoto, H., Kanie, M., Sano, S., Tokunaga, F., Tanaka, K., and Iwai, K. (2006). A ubiquitin ligase complex assembles linear polyubiquitin chains. The EMBO journal *25*, 4877-4887.

Laemmli, U.K. (1970). Cleavage of structural proteins during the assembly of the head of bacteriophage T4. Nature *227*, 680-685.

Lee, B.J., Cansizoglu, A.E., Suel, K.E., Louis, T.H., Zhang, Z., and Chook, Y.M. (2006). Rules for nuclear localization sequence recognition by karyopherin beta 2. Cell *126*, 543-558.

Liang, Q., Deng, H., Li, X., Wu, X., Tang, Q., Chang, T.H., Peng, H., Rauscher, F.J., 3rd, Ozato, K., and Zhu, F. (2011). Tripartite motif-containing protein 28 is a small ubiquitin-related modifier E3 ligase and negative regulator of IFN regulatory factor 7. Journal of immunology *187*, 4754-4763.

Lim, K.L., Chew, K.C., Tan, J.M., Wang, C., Chung, K.K., Zhang, Y., Tanaka, Y., Smith, W., Engelender, S., Ross, C.A.*, et al.* (2005). Parkin mediates nonclassical, proteasomal-independent ubiquitination of synphilin-1: implications for Lewy body formation. The Journal of neuroscience : the official journal of the Society for Neuroscience *25*, 2002-2009.

Lupas, A., Van Dyke, M., and Stock, J. (1991). Predicting coiled coils from protein sequences. Science *252*, 1162-1164.

Markson, G., Kiel, C., Hyde, R., Brown, S., Charalabous, P., Bremm, A., Semple, J., Woodsmith, J., Duley, S., Salehi-Ashtiani, K.*, et al.* (2009). Analysis of the human E2 ubiquitin-conjugating enzyme protein interaction network. Genome research *19*, 1905-1911.

Miotto, B., and Struhl, K. (2011). JNK1 phosphorylation of Cdt1 inhibits recruitment of HBO1 histone acetylase and blocks replication licensing in response to stress. Molecular cell *44*, 62-71.

Nguyen Ba, A.N., Pogoutse, A., Provart, N., and Moses, A.M. (2009). NLStradamus: a simple Hidden Markov Model for nuclear localization signal prediction. BMC bioinformatics *10*, 202.

Nishikawa, H., Wu, W., Koike, A., Kojima, R., Gomi, H., Fukuda, M., and Ohta, T. (2009). BRCA1-associated protein 1 interferes with BRCA1/BARD1 RING heterodimer activity. Cancer research *69*, 111-119.

Pena-Llopis, S., Vega-Rubin-de-Celis, S., Liao, A., Leng, N., Pavia-Jimenez, A., Wang, S., Yamasaki, T., Zhrebker, L., Sivanand, S., Spence, P.*, et al.* (2012). BAP1 loss defines a new class of renal cell carcinoma. Nature genetics *44*, 751-759.

Robbins, J., Dilworth, S.M., Laskey, R.A., and Dingwall, C. (1991). Two interdependent basic domains in nucleoplasmin nuclear targeting sequence: identification of a class of bipartite nuclear targeting sequence. Cell *64*, 615-623.

Sanchez-Pulido, L., Kong, L., and Ponting, C.P. (2012). A common ancestry for BAP1 and Uch37 regulators. Bioinformatics *28*, 1953-1956.

Scheuermann, J.C., de Ayala Alonso, A.G., Oktaba, K., Ly-Hartig, N., McGinty, R.K., Fraterman, S., Wilm, M., Muir, T.W., and Muller, J. (2010). Histone H2A deubiquitinase activity of the Polycomb repressive complex PR-DUB. Nature *465*, 243-247.

Sigrist, C.J., de Castro, E., Cerutti, L., Cuche, B.A., Hulo, N., Bridge, A., Bougueleret, L., and Xenarios, I. (2013). New and continuing developments at PROSITE. Nucleic acids research *41*, D344-347.

Sowa, M.E., Bennett, E.J., Gygi, S.P., and Harper, J.W. (2009). Defining the human deubiquitinating enzyme interaction landscape. Cell *138*, 389-403.

Tate, C.M., Lee, J.H., and Skalnik, D.G. (2009). CXXC finger protein 1 contains redundant functional domains that support embryonic stem cell cytosine methylation, histone methylation, and differentiation. Molecular and cellular biology *29*, 3817-3831.

Tiwari, S., and Weissman, A.M. (2001). Endoplasmic reticulum (ER)-associated degradation of T cell receptor subunits. Involvement of ER-associated ubiquitin-conjugating enzymes (E2s). The Journal of biological chemistry *276*, 16193-16200.

van Wijk, S.J., and Timmers, H.T. (2010). The family of ubiquitin-conjugating enzymes (E2s): deciding between life and death of proteins. FASEB journal : official publication of the Federation of American Societies for Experimental Biology *24*, 981-993.

Ventii, K.H., Devi, N.S., Friedrich, K.L., Chernova, T.A., Tighiouart, M., Van Meir, E.G., and Wilkinson, K.D. (2008). BRCA1-associated protein-1 is a tumor suppressor that requires deubiquitinating activity and nuclear localization. Cancer research *68*, 6953-6962.

Wu, S., Shi, Y., Mulligan, P., Gay, F., Landry, J., Liu, H., Lu, J., Qi, H.H., Wang, W., Nickoloff, J.A.*, et al.* (2007). A YY1-INO80 complex regulates genomic stability through homologous recombination-based repair. Nature structural & molecular biology *14*, 1165-1172.

Wu-Baer, F., Lagrazon, K., Yuan, W., and Baer, R. (2003). The BRCA1/BARD1 heterodimer assembles polyubiquitin chains through an unconventional linkage involving lysine residue K6 of ubiquitin. The Journal of biological chemistry *278*, 34743-34746.

Yao, T., Song, L., Jin, J., Cai, Y., Takahashi, H., Swanson, S.K., Washburn, M.P., Florens, L., Conaway, R.C., Cohen, R.E.*, et al.* (2008). Distinct modes of regulation of the Uch37 deubiquitinating enzyme in the proteasome and in the Ino80 chromatin-remodeling complex. Molecular cell *31*, 909-917.

Yao, T., Song, L., Xu, W., DeMartino, G.N., Florens, L., Swanson, S.K., Washburn, M.P., Conaway, R.C., Conaway, J.W., and Cohen, R.E. (2006). Proteasome recruitment and activation of the Uch37 deubiquitinating enzyme by Adrm1. Nature cell biology *8*, 994-1002.

Yu, H., Mashtalir, N., Daou, S., Hammond-Martel, I., Ross, J., Sui, G., Hart, G.W., Rauscher, F.J., 3rd, Drobetsky, E., Milot, E.*, et al.* (2010). The ubiquitin carboxyl hydrolase BAP1 forms a ternary complex with YY1 and HCF-1 and is a critical regulator of gene expression. Molecular and cellular biology *30*, 5071-5085.

Yu, H., Pak, H., Hammond-Martel, I., Ghram, M., Rodrigue, A., Daou, S., Barbour, H., Corbeil, L., Hebert, J., Drobetsky, E.*, et al.* (2014). Tumor suppressor and deubiquitinase BAP1 promotes DNA double-strand break repair. Proceedings of the National Academy of Sciences of the United States of America *111*, 285-290.

Zhu, P., Zhou, W., Wang, J., Puc, J., Ohgi, K.A., Erdjument-Bromage, H., Tempst, P., Glass, C.K., and Rosenfeld, M.G. (2007). A histone H2A deubiquitinase complex coordinating histone acetylation and H1 dissociation in transcriptional regulation. Molecular cell *27*, 609-621.

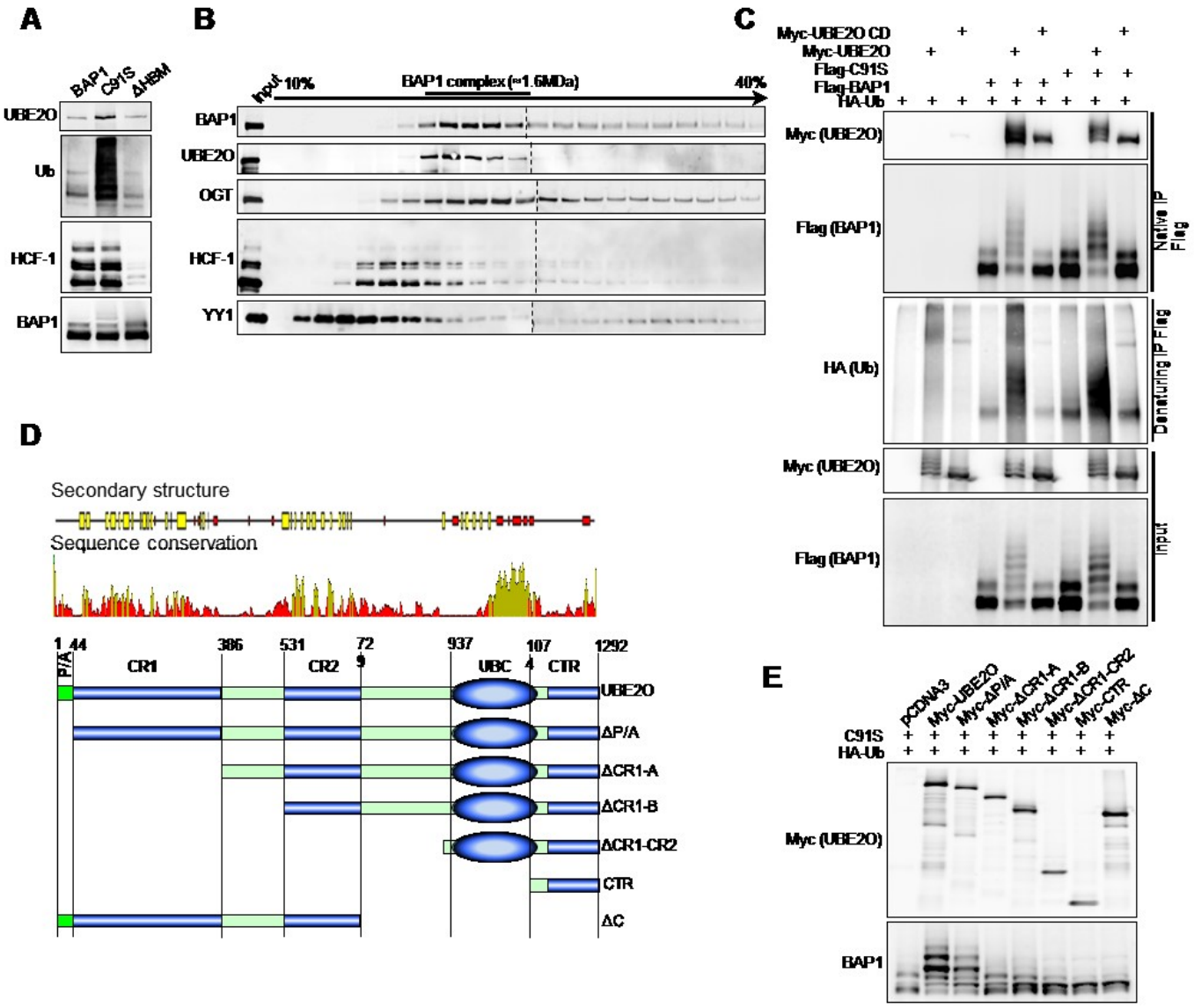

Fig. 1

Figure 1. UBE2O Interacts with and Ubiquitinates BAP1 and This Effect is Actively Counteracted by BAP1 Autodeubiquitination. (**A**) Purified BAP1 complexes were used for western blot. (**B**) HeLa nuclear extract was resolved by glycerol gradient, and used for western blot. (**C**) 293T cells were co-transfected with 2 µg of HA-Ub, 2 µg of Myc-UBE2O (wild-type or CD), and 1 µg of Flag-BAP1 (wild-type or C91S) expression vectors, and cell extracts were used for immunoprecipitation. (**D**) Top, schema representing the human UBE2O with secondary structure prediction (alpha helixes are in red and beta strands are in yellow). The main predicted domains are indicated as CR1 (conserved region 1), CR2 (conserved region 2), UBC (ubiquitin-conjugating) and CTR (C-terminal region). Bottom, schema representing UBE2O deletion mutants used for the ubiquitination assay. (**E**) 293T cells were co-transfected with 2 µg of HA-Ub, 2 µg of Myc-UBE2O fragments, and 1 µg of C91S expression vectors, and cell extracts were used for western blot.

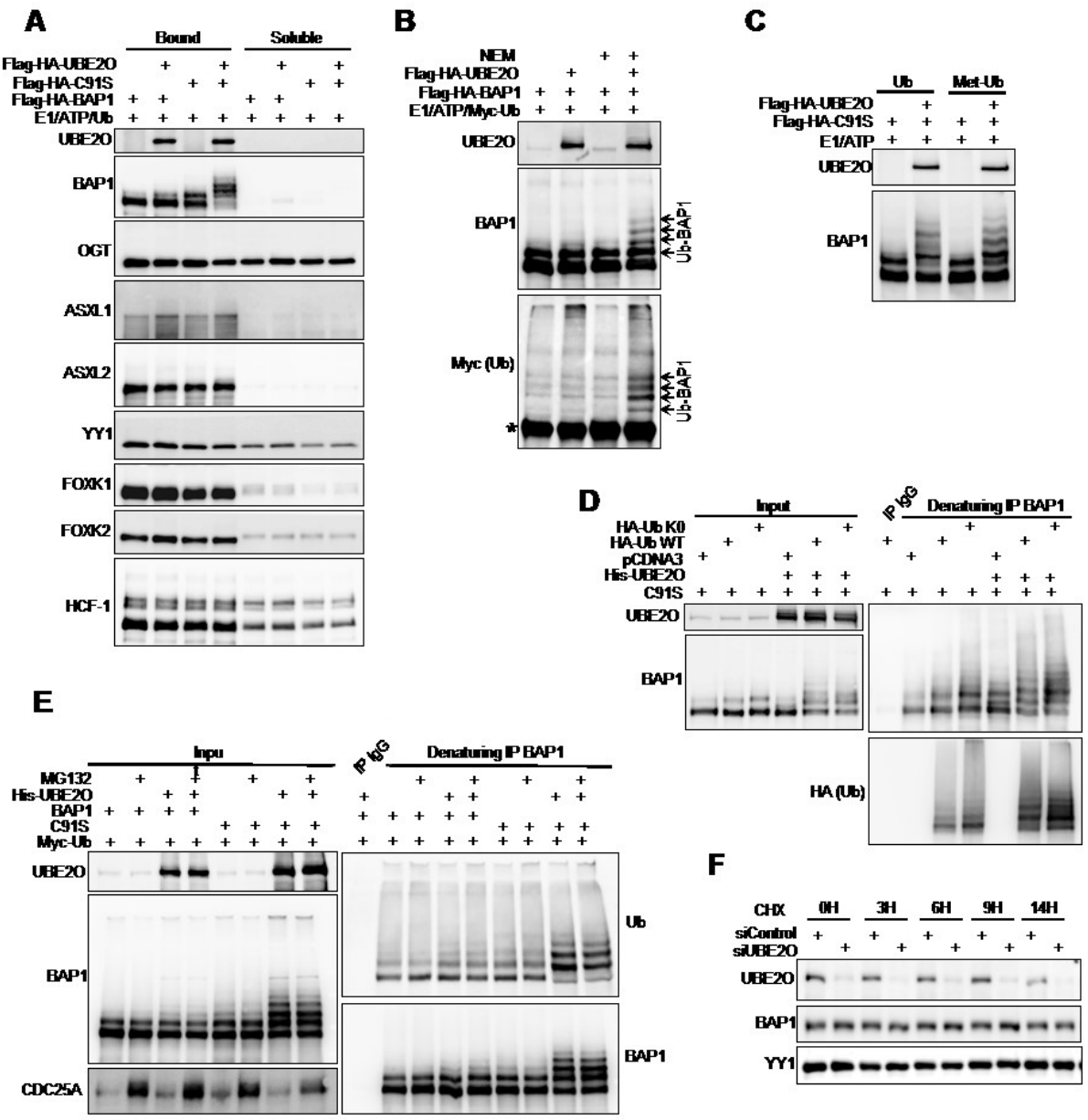

Fig. 2

Figure 2. Characterization of UBE2O-Mediated Ubiquitination of BAP1. (**A**) In vitro ubiquitination reaction with beads-immobilized BAP1 or C91S complexes incubated with immunopurified UBE2O. Fractions were used for western blot detection of components of the BAP1 complex. (**B**) In vitro ubiquitination reaction using the BAP1 complex inhibited with NEM. (**C**) The C91S complex was used for in vitro reaction with UBE2O and either unmodified or methylated ubiquitin. (**D**) 293T cells were co-transfected with 2 μg of wild-type ubiquitin or K0 mutant ubiquitin, 1 μg of BAP1 or C91S and 2 μg of empty vector or His-UBE2O expression vectors, and cell lysates were used for immunoprecipitation. (**E**) 293T cells were co-transfected with 1 μg of HA-Ub, 2 μg of BAP1 or C91S and 1 μg of His-UBE2O expression vectors. Cells were treated with DMSO or 20 μM MG132 for 8 hours before immunoprecipitation. (**F**) MCF7 cells were transfected with non-targeting or UBE2O siRNA for 96 hours, treated with 20 μg/ml of cycloheximide and analyzed by western blot. Asterisk indicates non-specific bands.

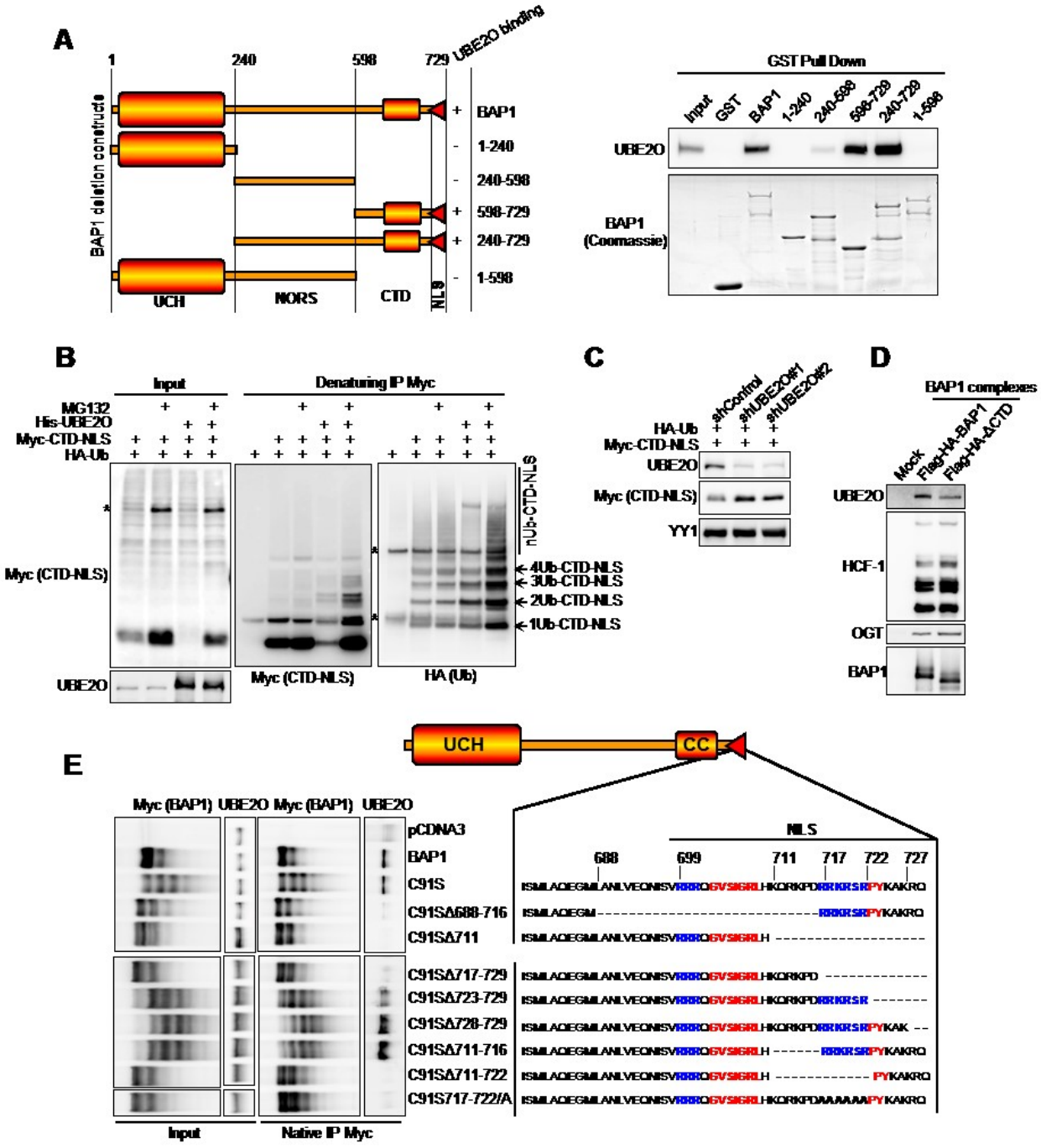
A
1
240
598
729
UBE2O binding
BAP1 deletion constructs
BAP1
1-240
240-598
598-729
240-729
1-598
UCH
NORS
CTD
NLS
GST Pull Down
Input
GST
BAP1
1-240
240-598
598-729
240-729
1-598
UBE2O
BAP1 (Coomassie)
B
Input
Denaturing IP Myc
MG132
His-UBE2O
Myc-CTD-NLS
HA-Ub
Myc (CTD-NLS)
UBE2O
nUb-CTD-NLS
4Ub-CTD-NLS
3Ub-CTD-NLS
2Ub-CTD-NLS
1Ub-CTD-NLS
Myc (CTD-NLS)
HA (Ub)
C
shControl
shUBE2O#1
shUBE2O#2
HA-Ub
Myc-CTD-NLS
UBE2O
Myc (CTD-NLS)
YY1
D
BAP1 complexes
Mock
Flag-HA-BAP1
Flag-HA-ΔCTD
UBE2O
HCF-1
OGT
BAP1
E
UCH
CC
Myc (BAP1)
UBE2O
Myc (BAP1)
UBE2O
pCDNA3
BAP1
C91S
C91SΔ688-716
C91SΔ711
C91SΔ717-729
C91SΔ723-729
C91SΔ728-729
C91SΔ711-716
C91SΔ711-722
C91S717-722/A
NLS
688
699
711
717
722
727
ISMLAQEGMLANLVEQNISVRRRQGVSIGRLHKQRKPDRRKRSRPYKAKRQ
ISMLAQEGM----------RRKRSRPYKAKRQ
ISMLAQEGMLANLVEQNISVRRRQGVSIGRLH----------
ISMLAQEGMLANLVEQNISVRRRQGVSIGRLHKQRKPD----------
ISMLAQEGMLANLVEQNISVRRRQGVSIGRLHKQRKPDRRKRSR-------
ISMLAQEGMLANLVEQNISVRRRQGVSIGRLHKQRKPDRRKRSRPYKAK--
ISMLAQEGMLANLVEQNISVRRRQGVSIGRLH------RRKRSRPYKAKRQ
ISMLAQEGMLANLVEQNISVRRRQGVSIGRLH----------PYKAKRQ
ISMLAQEGMLANLVEQNISVRRRQGVSIGRLHKQRKPDAAAAAAPYKAKRQ
Input
Native IP Myc

Fig. 3

Figure 3. BAP1 NLS is Required for its Ubiquitination by UBE2O. (**A**) Schematic representation of GST-BAP1 fragments used for pull-down assay with His-UBE2O. (**B**) 293T cells were co-transfected with 2 µg of HA-Ub, 2 µg of His-UBE2O, and 1 µg of Myc-CTD-NLS expression vectors, and cell extracts were used for immunoprecipitation. (**C**) U2OS cells were co-transfected with 2 µg of shControl, shUBE2O#1 or shUBE2O#2 and 1 µg of HA-Ub and 0,5 µg of Myc-CTD-NLS expression vectors, and cell extracts were used for western blot. (**D**) Purified complexes of BAP1 or BAP1 ΔCTD were used for western blot detection of components of BAP1 complex. (**E**) 293T cells were co-transfected with 2 µg of HA-Ub, 2 µg of His-UBE2O, and 1 µg of Myc-BAP1 mutants expression vectors, and cell extracts were used for immunoprecipitation. Asterisk indicates non-specific bands.

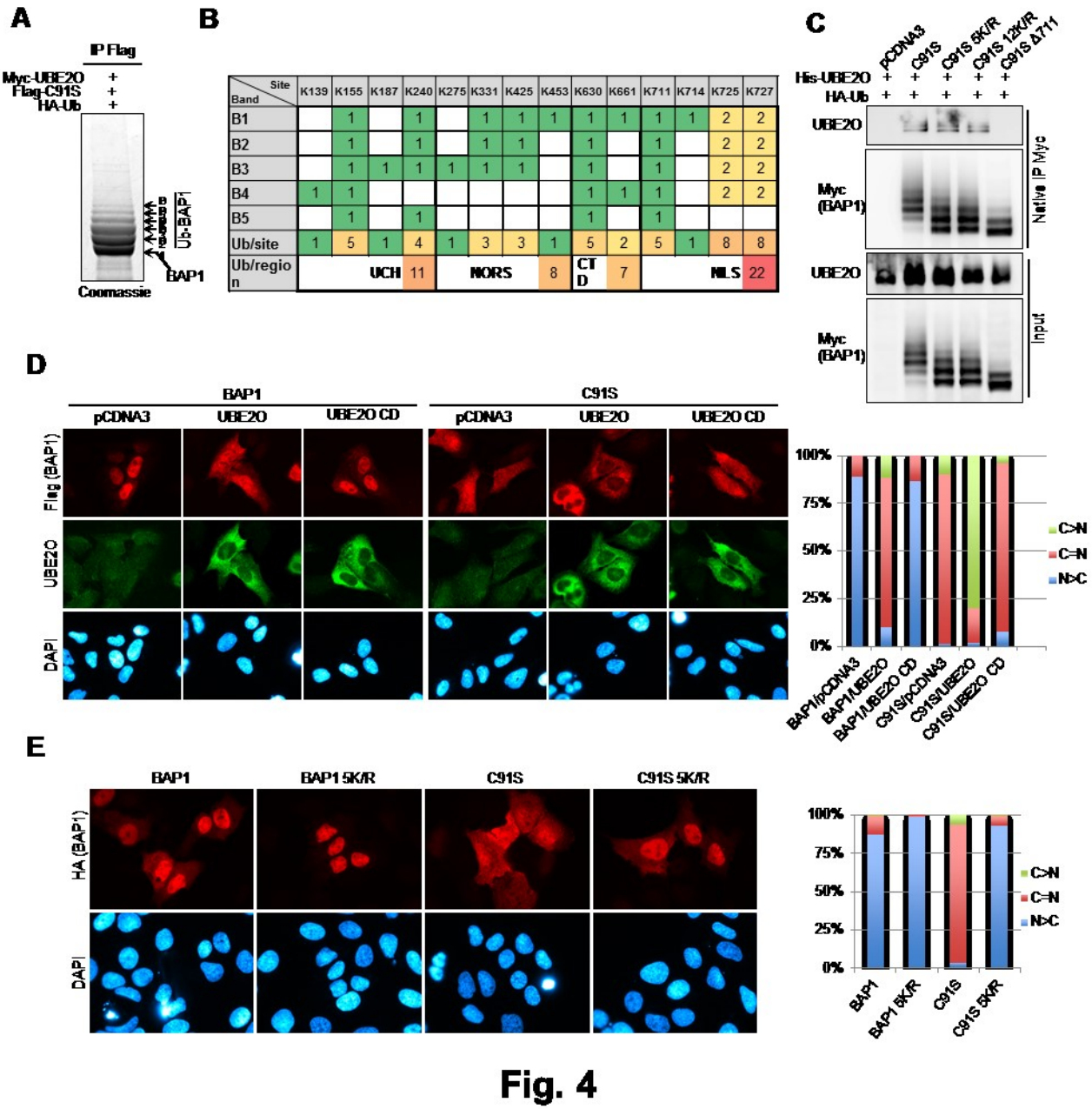

Fig. 4

Figure 4. Ubiquitination of BAP1 NLS by UBE2O promotes its Cytoplasmic Sequestration. (**A**) 293T cells were co-transfected with 2 µg of HA-Ub, 2 µg of Myc-UBE2O, and 1 µg of Flag-C91S, and cell extracts from 40 dishes were used for Flag immunoprecipitation. The indicated bands were excised for MS analysis. (**B**) Table of ubiquitination events detected by MS. (**C**) Cells were co-transfected with 2 µg of HA-Ub, 2 µg of His-UBE2O, and 1 µg of Myc-tagged BAP1 mutants expression vectors, and cell extracts were used for immunoprecipitation. (**D**) U2OS cells were co-transfected with either 2 µg of empty vector, Myc-UBE2O or Myc-UBE2O CD and 3 µg of either Flag-HA-BAP1 or Flag-HA-C91S expression vectors and were used for immunofluorescence analysis. Representative cell counts for BAP1 subcellular localization are shown. C, cytoplasmic; N, nuclear. (**E**) U2OS cells were transfected with Flag-HA-BAP1 mutants expression vectors and used for immunofluorescence analysis as in (**D**).

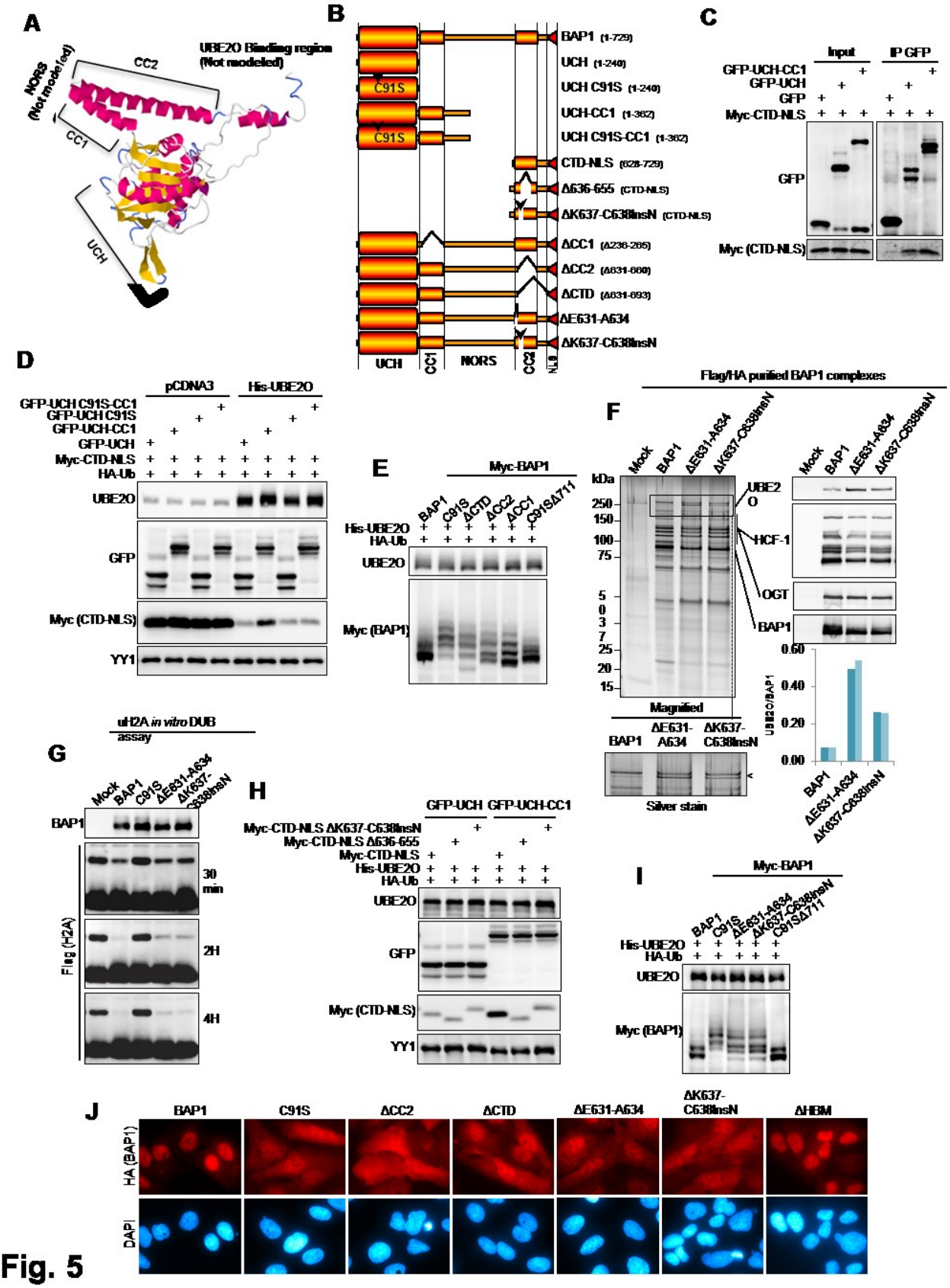
A
UBE2O Binding region (Not modelled)
NORS (Not modelled)
CC2
CC1
UCH
B
BAP1 (1-729)
UCH (1-240)
UCH C91S (1-240)
UCH-CC1 (1-362)
UCH C91S-CC1 (1-362)
CTD-NLS (628-729)
Δ636-655 (CTD-NLS)
ΔK637-C638insN (CTD-NLS)
ΔCC1 (Δ236-265)
ΔCC2 (Δ631-660)
ΔCTD (Δ631-693)
ΔE631-A634
ΔK637-C638insN
C91S
UCH
CC1
NORS
CC2
NLS
C
Input
IP GFP
GFP-UCH-CC1
GFP-UCH
GFP
Myc-CTD-NLS
GFP
Myc (CTD-NLS)
D
pCDNA3
His-UBE2O
GFP-UCH C91S-CC1
GFP-UCH C91S
GFP-UCH-CC1
GFP-UCH
Myc-CTD-NLS
HA-Ub
UBE2O
GFP
Myc (CTD-NLS)
YY1
E
Myc-BAP1
BAP1
C91S
ΔCTD
ΔCC2
ΔCC1
C91SΔ711
His-UBE2O
HA-Ub
UBE2O
Myc (BAP1)
F
Flag/HA purified BAP1 complexes
Mock
BAP1
ΔE631-A634
ΔK637-C638insN
kDa
250
150
100
75
5
0
3
7
25
20
15
UBE2O
HCF-1
OGT
BAP1
Magnified
BAP1
ΔE631-A634
ΔK637-C638insN
Silver stain
UBE2O/BAP1
0.60
0.40
0.20
0.00
G
ul2A in vitro DUB assay
Mock
BAP1
C91S
ΔE631-A634
ΔK637-C638insN
BAP1
Flag (H2A)
30 min
2H
4H
H
GFP-UCH
GFP-UCH-CC1
Myc-CTD-NLS ΔK637-C638insN
Myc-CTD-NLS Δ636-655
Myc-CTD-NLS
His-UBE2O
HA-Ub
UBE2O
GFP
Myc (CTD-NLS)
YY1
I
Myc-BAP1
BAP1
C91S
ΔE631-A634
ΔK637-C638insN
C91SΔ711
His-UBE2O
HA-Ub
UBE2O
Myc (BAP1)
J
BAP1
C91S
ΔCC2
ΔCTD
ΔE631-A634
ΔK637-C638insN
ΔHBM
HA (BAP1)
DAPI

Fig. 5

Figure 5. BAP1 Intramolecular Interaction Promotes Autodeubiquitination, a Mechanism Disrupted by Cancer Mutations. (**A**) Predicted model of BAP1 UCH/CTD interface based on UCH37 crystal structure (PDB: 3IHR). Note that NLS and NORS are not present in UCH37, and thus not included in the model. (**B**) Schematic representation of the mutants used for the complementation assay and the deletion mutants used in the context of full length BAP1. (**C**) 293T cells were co-transfected with 2 μg of the indicated GFP fusion constructs and 2 μg of Myc-CTD-NLS expression vectors, and cell extracts were used for immunoprecipitation. (**D**) 293T cells were co-transfected with 2 μg of HA-Ub and either 2 μg of empty vector or His-UBE2O, 1 μg of the indicated GFP fusion constructs and 1 μg of Myc-CTD-NLS expression vectors. (**E**) 293T cells were co-transfected with 2 μg of HA-Ub, 2 μg of His-UBE2O, and 1 μg of Myc-BAP1 mutants expression vectors. (**F**) Purified BAP1 complexes were analyzed by silver stain and western blotting. Densitometric ratios between UBE2O and BAP1 indicate its relative abundance in the complexes. The histogram shows two independent experiments. (**G**) In vitro nucleosome deubiquitination reaction with purified BAP1 complexes. Samples were incubated at 37°C for the indicated times. (**H**) 293T cells were co-transfected with 2 μg of HA-Ub, 2 μg of His-UBE2O expression vectors, 1 μg of indicated GFP fusion constructs and 1 μg of Myc-tagged constructs. (**I**) 293T cells were co-transfected with 2 μg of HA-Ub, 2 μg of His-UBE2O, and 1 μg of Myc-tagged BAP1 mutants expression vectors. (**J**) U2OS cell lines stably expressing Flag-HA-BAP1 and its mutant forms were used for immunofluorescence analysis.

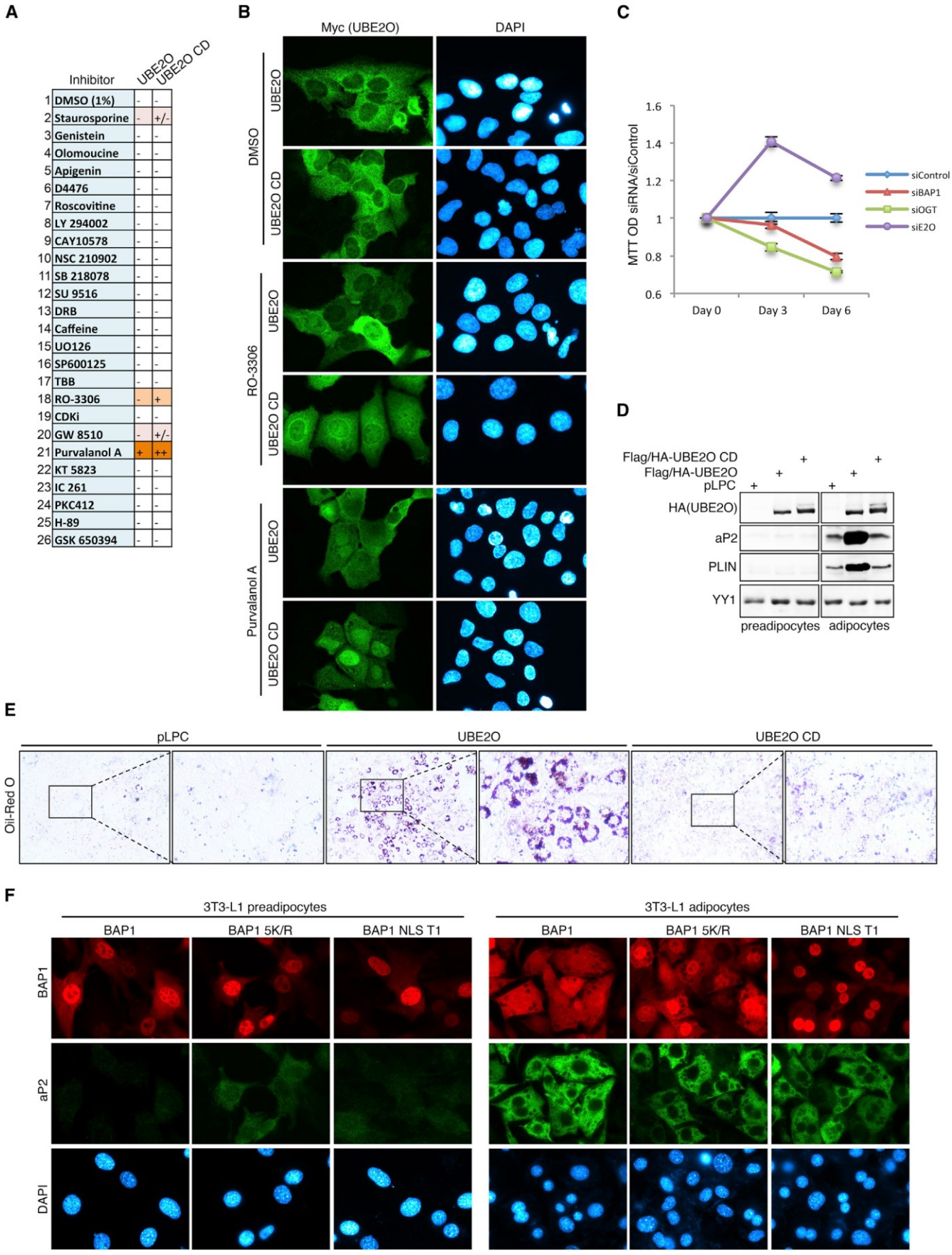
A
Inhibitor
UBE2O
UBE2O CD
1 DMSO (1%) - -
2 Staurosporine - +/-
3 Genistein - -
4 Olomoucine - -
5 Apigenin - -
6 D4476 - -
7 Roscovitine - -
8 LY 294002 - -
9 CAY10578 - -
10 NSC 210902 - -
11 SB 218078 - -
12 SU 9516 - -
13 DRB - -
14 Caffeine - -
15 UO126 - -
16 SP600125 - -
17 TBB - -
18 RO-3306 - +
19 CDKi - -
20 GW 8510 - +/-
21 Purvalanol A + ++
22 KT 5823 - -
23 IC 261 - -
24 PKC412 - -
25 H-89 - -
26 GSK 650394 - -
B
Myc (UBE2O)
DAPI
DMSO
UBE2O
UBE2O CD
RO-3306
UBE2O
UBE2O CD
Purvalanol A
UBE2O
UBE2O CD
C
MTT OD siRNA/siControl
1.6
1.4
1.2
1
0.8
0.6
Day 0
Day 3
Day 6
siControl
siBAP1
siOGT
siE2O
D
Flag/HA-UBE2O CD
Flag/HA-UBE2O
pLPC
HA(UBE2O)
aP2
PLIN
YY1
preadipocytes
adipocytes
E
pLPC
UBE2O
UBE2O CD
Oil-Red O
F
3T3-L1 preadipocytes
3T3-L1 adipocytes
BAP1
BAP1 5K/R
BAP1 NLS T1
BAP1
BAP1 5K/R
BAP1 NLS T1
BAP1
aP2
DAPI

Figure 6. UBE2O Shuttles between the Nucleus and Cytoplasm and Promotes BAP1 Cytoplasmic Localization during Adipocyte Differentiation. (**A**) Effect of kinase inhibition on nuclear localization of UBE2O. U2OS cells were transfected with 4 μg Myc-UBE2O or Myc-UBE2O CD expression vectors and then treated with a panel of kinase inhibitors for 24 hours prior harvesting for IF. + and - indicate the relative intensity in the nuclear staining of UBE2O. (**B**) Representative images of UBE2O localization in U2OS cells treated with CDK inhibitors. (**C**) Effects of siRNA-depletion of UBE2O, BAP1 on cell proliferation, determined by MTT assay. siRNA for OGT is used as a control of decreased proliferation. Note that the values are relative to the non-target control siRNA for each time point. (**D**,**E**) Effects of overexpression of UBE2O wild-type or catalytic dead form on the differentiation of 3T3L1. Immunodetection of differentiation markers (**D**) and Oil-Red O staining (**E**). YY1 is used as a loading control. (**F**) Localization of BAP1 and mutants during adipocyte differentiation. The BAP1 NLST1 corresponds to a mutant in which the NLS region of BAP1 which includes the UBE2O-binding motif is replaced with the T large antigen NLS. The BAP1 K/R mutant is mutated in the UBE2O-ubiquitination sites of the NLS.

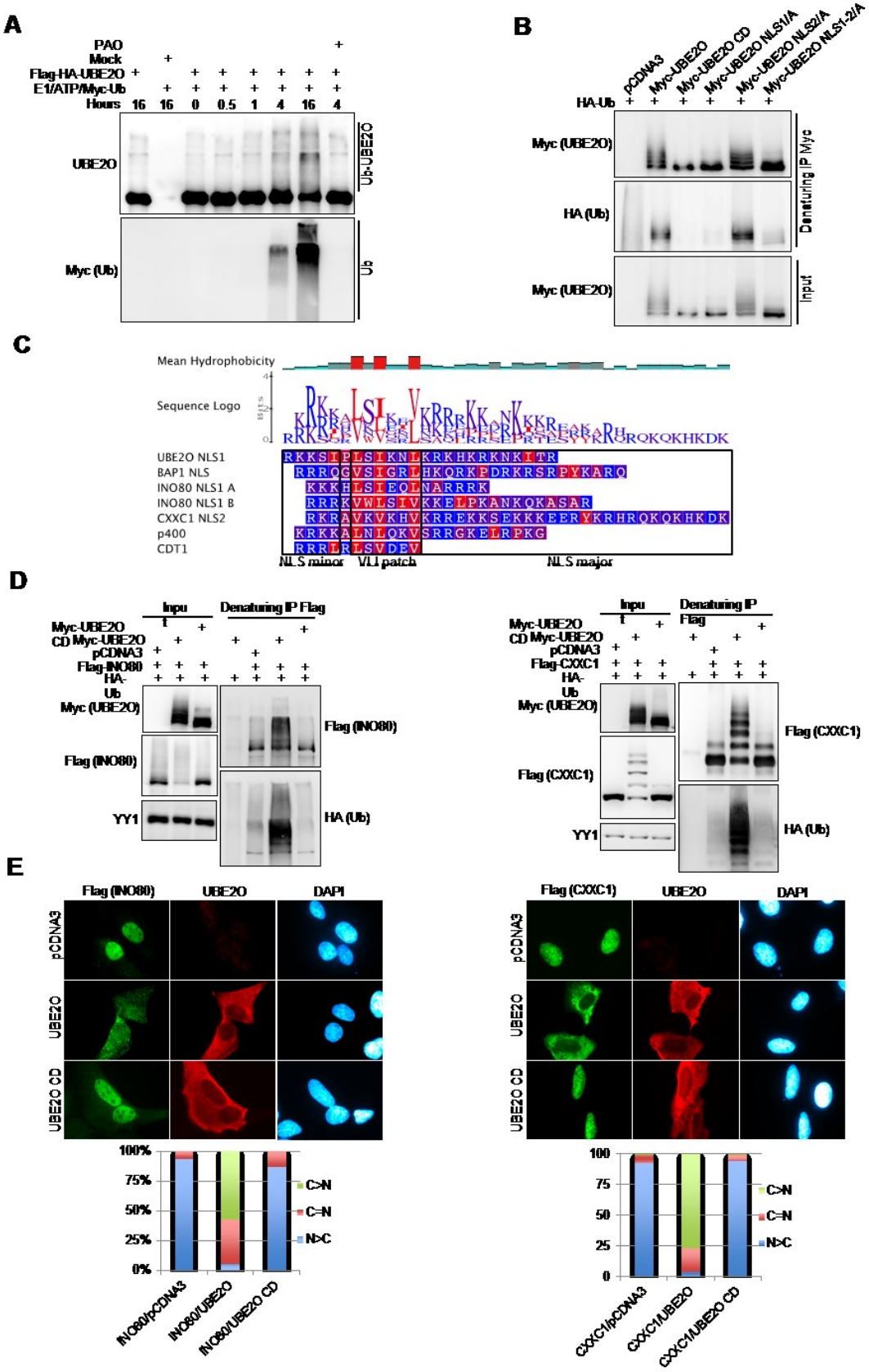
A
PAO
Mock
Flag-HA-UBE2O
E1/ATP/Myc-Ub
Hours 16 16 0 0.5 1 4 16 4
UBE2O
Ub-UBE2O
Myc (Ub)
Ub
B
pCDNA3
Myc-UBE2O
Myc-UBE2O CD
Myc-UBE2O NLS1/A
Myc-UBE2O NLS2/A
Myc-UBE2O NLS1-2/A
HA-Ub
Myc (UBE2O)
HA (Ub)
Myc (UBE2O)
Denaturing IP Myc
Input
C
Mean Hydrophobicity
Sequence Logo
UBE2O NLS1
BAP1 NLS
INO80 NLS1 A
INO80 NLS1 B
CXXC1 NLS2
p400
CDT1
NLS minor
VLI patch
NLS major
D
Input
Denaturing IP Flag
Myc-UBE2O
CD Myc-UBE2O
pCDNA3
Flag-INO80
HA-Ub
Myc (UBE2O)
Flag (INO80)
YY1
HA (Ub)
Denaturing IP Flag
Flag-CXXC1
Flag (CXXC1)
E
Flag (INO80)
UBE2O
DAPI
pCDNA3
UBE2O
UBE2O CD
100%
75%
50%
25%
0%
C>N
C=N
N>C
INO80/pCDNA3
INO80/UBE2O
INO80/UBE2O CD
Flag (CXXC1)
100
75
50
25
0
CXXC1/pCDNA3
CXXC1/UBE2O
CXXC1/UBE2O CD

Fig. 7

Figure 7. UBE2O Targets a Subset of Chromatin-Associated Proteins. (**A**) In vitro ubiquitination reaction with the purified UBE2O. Samples were incubated for the indicated times. (**B**) 293T cells were co-transfected with 2 µg of HA-Ub and 2 µg of indicated Myc-UBE2O mutants, and cell extracts were used for immunoprecipitation. (**C**) Sequence alignment between the UBE2O/BAP1 NLS and a subset of identified UBE2O substrates. Hydrophobic amino acids are in red and polar amino acids are in blue. A large N-terminal extension containing the NLS of CDT1 is not shown. (**D**) 293T cells were co-transfected with 2 µg of HA-Ub and 1 µg of Flag-CXXC1 or 2 µg of Flag-INO80, and either 2 µg of empty vector, Myc-UBE2O or Myc-UBE2O CD expression vectors, and cell extracts were used for immunoprecipitation. (**E**) U2OS cells were co-transfected with 0,5 µg of HA-Ub and either 1 µg of empty vector, Myc-UBE2O, Myc-UBE2O CD and 1 µg of either Flag-INO80 or Flag-CXXC1 expression vectors and used for immunofluorescence analysis. Representative cell counts are shown.

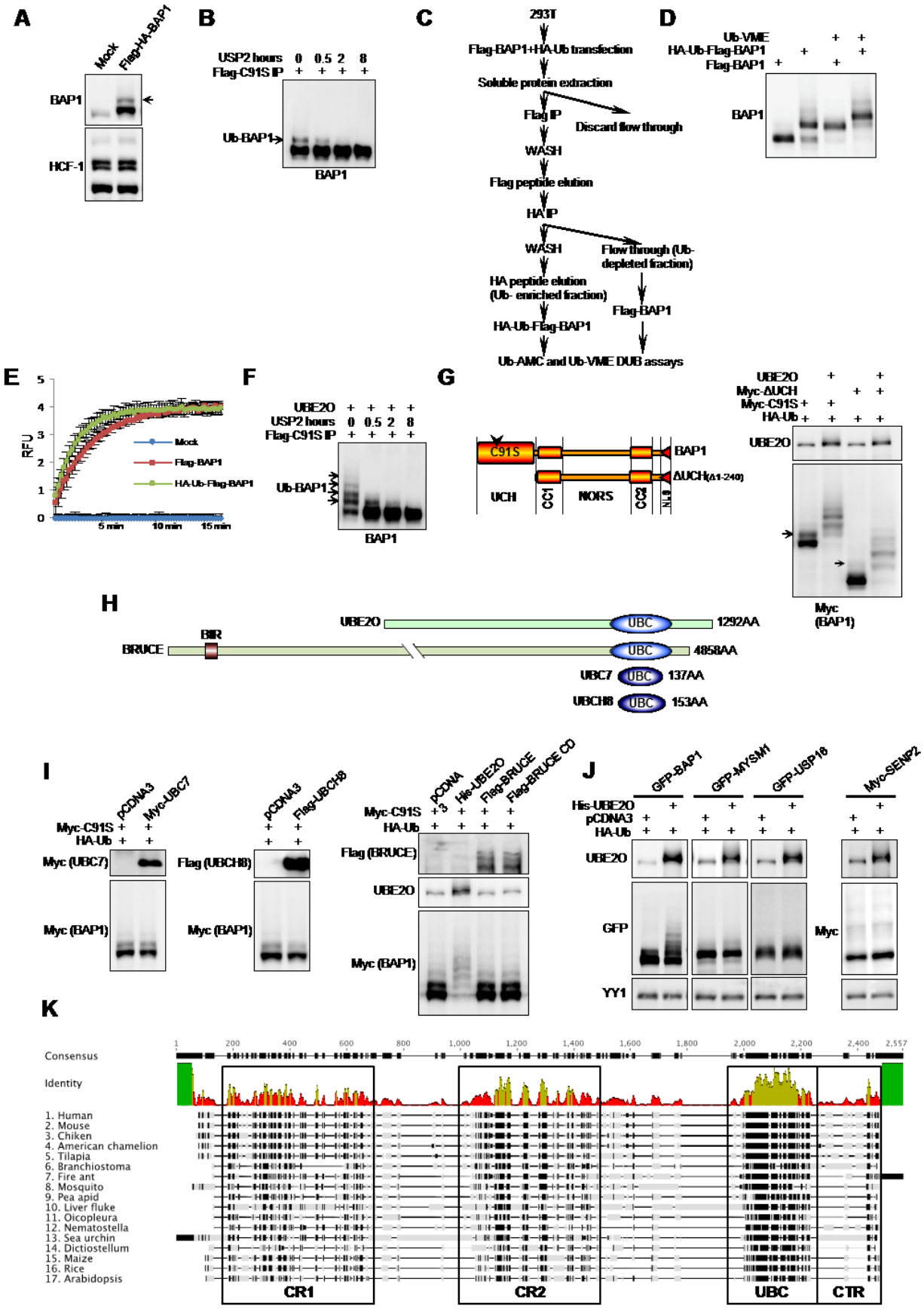
A
Mock
Flag-HA-BAP1
BAP1
HCF-1
B
USP2 hours 0 0.5 2 8
Flag-C91S IP + + + +
Ub-BAP1
BAP1
C
293T
Flag-BAP1+HA-Ub transfection
Soluble protein extraction
Flag IP
Discard flow through
WASH
Flag peptide elution
HA IP
WASH
Flow through (Ub-depleted fraction)
HA peptide elution (Ub- enriched fraction)
Flag-BAP1
HA-Ub-Flag-BAP1
Ub-AMC and Ub-VME DUB assays
D
Ub-VME + +
HA-Ub-Flag-BAP1 + +
Flag-BAP1 + +
BAP1
E
RFU
Mock
Flag-BAP1
HA-Ub-Flag-BAP1
5 min
10 min
15 min
F
UBE2O + + + +
USP2 hours 0 0.5 2 8
Flag-C91S IP + + + +
Ub-BAP1
BAP1
G
C91S
BAP1
ΔUCH(Δ1-240)
UCH
CC1
NORS
CC2
NLS
UBE2O + +
Myc-ΔUCH + +
Myc-C91S + +
HA-Ub + + + +
UBE2O
Myc (BAP1)
H
UBE2O
UBC
1292AA
BRUCE
BIR
UBC
4858AA
UBC7
UBC
137AA
UBCH8
UBC
153AA
I
pCDNA3
Myc-UBC7
Myc-C91S + +
HA-Ub + +
Myc (UBC7)
Myc (BAP1)
pCDNA3
Flag-UBCH8
+ +
Flag (UBCH8)
Myc (BAP1)
pCDNA
His-UBE2O
Flag-BRUCE
Flag-BRUCE CD
Myc-C91S +3 + + +
HA-Ub + + + +
Flag (BRUCE)
UBE2O
Myc (BAP1)
J
GFP-BAP1
GFP-MYSM1
GFP-USP16
Myc-SENP2
His-UBE2O + + +
pCDNA3 + + + +
HA-Ub + + + + + +
UBE2O
GFP
YY1
Myc
K
Consensus
Identity
1. Human
2. Mouse
3. Chiken
4. American chamelion
5. Tilapia
6. Branchiostoma
7. Fire ant
8. Mosquito
9. Pea apid
10. Liver fluke
11. Oicopleura
12. Nematostella
13. Sea urchin
14. Dictiostellum
15. Maize
16. Rice
17. Arabidopsis
1 200 400 600 800 1,000 1,200 1,400 1,600 1,800 2,000 2,200 2,400 2,557
CR1
CR2
UBC
CTR

Fig. S1

Figure S1 (Related to Figure 1). Characterization of the UBE2O-independent mono-ubiquitination of BAP1. (**A**) Detection of the modified form of BAP1 in U2OS cells stably expressing Flag-HA-BAP1. U2OS cells were transduced with empty pOZ-N vector or pOZN-BAP1, selected with anti-IL2 receptor-coupled magnetic beads (4 rounds of selection), as previously described (Yu et al., 2010), and cell lysates were subjected to western blotting with the indicated antibodies. (**B**) 293T cells were transfected with 3 µg of Flag-BAP1 C91S and harvested three days-post-transfection for immunoprecipitation. Anti-Flag column-purified C91S was incubated with 200 nM of recombinant USP2 catalytic domain and collected for western blotting at the indicated time points. Note the decrease of the constitutive ubiquitin modification. (**C**) Schema of the double column purification strategy of ubiquitin-depleted and -enriched fractions of BAP1. (**D**) Analysis of the anti-HA beads-bound and the flow through fractions revealed that the slower migrating band was enriched in the HA-bound fraction and depleted in the flow through fraction proving the monoubiquitination nature of the modification. Monoubiquitination of BAP1 does not influence its ability to incorporate the ubiquitin vinylmethylester (Ub-VME) suicide substrate. HA-Ub-Flag-BAP1 and unmodified Flag-BAP1 fractions where incubated with 1 µM of Ub-VME probe and analyzed by western blot as recently described (Yu et al., 2014). Note the similar efficiency of Ub-VME incorporation that corresponds to the slower migrating form of BAP1. (**E**) Fluorometric analysis of the BAP1 activity towards the Ub-AMC DUB substrate. Adjusted amounts of the HA-Ub-Flag-BAP1 and unmodified Flag-BAP1 fractions where incubated with 100 nM of the Ub-AMC and fluorescence was analyzed in real time. Note that the modified form of BAP1 displays a similar DUB activity as the modified form towards this model substrate. (**F**) The ubiquitinated forms of C91S can be efficiently deubiquitinated by USP2. The procedure was carried out essentially as in panel B except that UBE2O was included in the co-transfection. (**G**) Similar UBE2O-mediated multi-monoubiquitination of BAP1 (C91S or ΔUCH). 293T cells were co-transfected with 1 µg of Myc-C91S or Myc-BAP1 ΔUCH, 2 µg of HA-Ub and 2 µg of either empty vector or UBE2O. Three days later, cell lysates were used for western blotting and probed with the indicated antibodies. Note the decrease of the constitutive BAP1 mono-ubiquitination upon the deletion of the UCH domain indicating that distinct activities modify BAP1.

Characterization of UBE2O specificity towards BAP1. (**H**) Comparison of several members of class I and IV ubiquitin carrier enzymes. (**I**) To control for specificity, we evaluated other E2s (van Wijk and Timmers, 2010) including BRUCE, the closest evolutionary relative of UBE2O which was previously shown to act as an E2/E3 hybrid on other substrates (Bartke et al., 2004; Hao et al., 2004). 293T cells were co-transfected with 1 µg of Myc-C91S, 2 µg of HA-Ub and either 2 µg of empty vector, Myc-UBC7, Flag-UBCH8, 5 µg of Flag-BRUCE or 5 µg Flag-BRUCE CD (C4654S) expression vectors. Three days later, cell lysates were used for western blotting. **J)** We also tested two known H2A DUBs, i.e., USP16 and MYSM1 (Joo et al., 2007; Zhu et al., 2007), as well as the SUMO protease SENP2 (Kim et al., 2000). 293T cells were co-transfected with 2 µg of HA-Ub and either 2 µg of empty vector or 2 µg of His-UBE2O and either 1 µg of GFP-BAP1, GFP-MYSM1, GFP-USP16 or Myc-SENP2 expression vectors. Three days later, cell lysates were used for western blotting. (**K**) Multiple sequence alignment of UBE2O orthologs, conserved regions are highlighted.

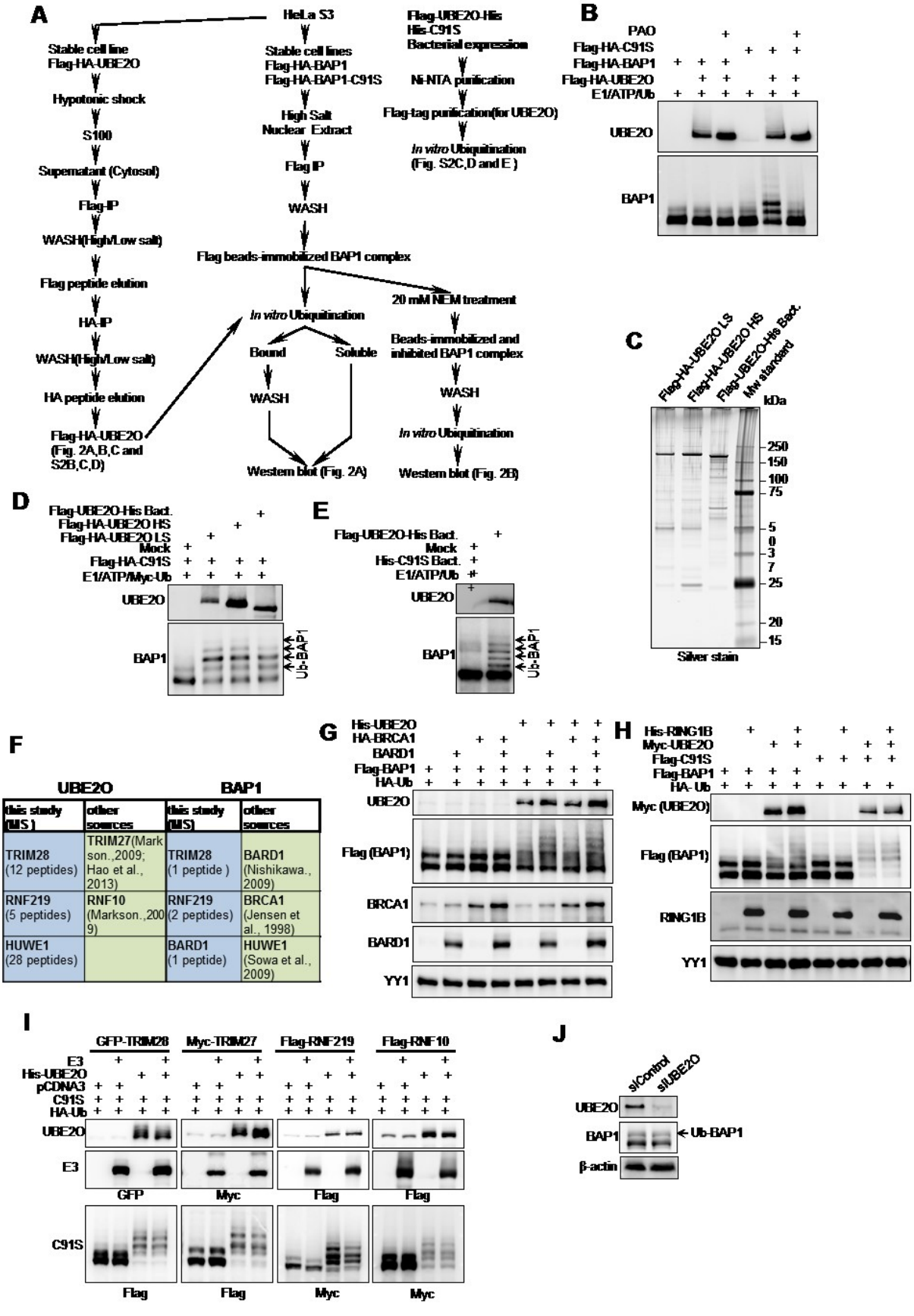

UBE2O

this study (MS)	other sources
TRIM28 (12 peptides)	TRIM27(Markson.,2009; Hao et al., 2013)
RNF219 (5 peptides)	RNF10 (Markson.,2009)
HUWE1 (28 peptides)	

BAP1

this study (MS)	other sources
TRIM28 (1 peptide)	BARD1 (Nishikawa., 2009)
RNF219 (2 peptides)	BRCA1 (Jensen et al., 1998)
BARD1 (1 peptide)	HUWE1 (Sowa et al., 2009)

Fig. S2

Figure S2 (Related to Figure 2). Set up of the *in vitro* ubiquitination reaction. (**A**) Schema of protein purification and *in vitro* ubiquitination reactions for figure **2A**, **2B**, **S2B**, **S2D** and **S2E**. (**B**) Purified BAP1 or C91S complexes were incubated with immunopurified UBE2O in an *in vitro* ubiquitination reaction. Samples were treated with 100 µM PAO as indicated. (**C**) Mammalian Flag/HA or bacterial His/Flag purified UBE2O was loaded on the 4-12% gel and used for silver staining. (**D**) Purified C91S complexes were incubated with UBE2O, purified from human cells or bacteria, in an *in vitro* ubiquitination reaction. Note that UBE2O maintains similar activity towards C91S independently of its origin and method of purification. HS and LS represent high salt and low salt washes, respectively. (**E**) Ubiquitination with recombinant enzymes. His-C91S was purified from bacteria and used for *in vitro* reaction with bacteria purified His/Flag-UBE2O.

BE2O- and BAP1-interacting ubiquitin ligases do not influence UBE2O ubiquitination activity towards BAP1. (**F**) Summary of potential UBE2O- and BAP1-interacting ubiquitin ligases. Our purification and mass spectrometry analysis of UBE2O- or BAP1-interacting proteins revealed additional substoichiometric E3 ligases that might participate in UBE2O-dependent or –independent ubiquitination of BAP1. Other E3 ligases previously reported as potential UBE2O- or BAP1 interacting enzymes were also included. (**G**) 293T cells were transfected with 2 µg of HA-Ub, 1 µg of HA-BRCA1 and/or 0,5 µg of HA-BARD1, 1 µg of BAP1 and either 2 µg of empty vector or Myc-UBE2O expression vectors. Three days later, cell lysates were used for western blotting with the indicated antibodies. We note that BAP1 was described as a partner of the tumor suppressor and RING E3 ligase complex BRCA1/BARD1 that may perform chain elongation (Jensen et al., 1998; Wu-Baer et al., 2003). Nonetheless co-transfection with BRCA1/BARD1 did not significantly affect the pattern of BAP1 ubiquitination by UBE2O. (**H**) Cells were transfected with 2 µg of HA-Ub, 1 µg of His-RING1B, 1 µg of BAP1 or C91S and either 2 µg of empty vector or Myc-UBE2O expression vectors. Three days later, cell lysates were used for western blotting with the indicated antibodies. BAP1 acts in concert with the RING1B E3 ligase to regulate H2A ubiquitination (Carbone et al., 2013; Scheuermann et al., 2010). However, no direct ubiquitination of BAP1 or cooperation between RING1B and UBE2O were observed. (**I**) Cells were transfected with 2 µg of HA-Ub, 0.5 µg of C91S, 2 µg of empty vector or His-UBE2O and 3 µg of GFP-TRIM28, Myc-TRIM27, Flag-RNF219 and Flag-RNF10 expression vectors. Three days later, cell lysates were used for western blotting with the indicated antibodies. Note the similar pattern of the C91S ubiquitination independently of the ubiquitin ligase co-expression. We were unable to express significant levels of HUWE1 (~500 kDa). Thus, we did not conclude about its potential effect alone or on UBE2O-mediated ubiquitination of BAP1. (**J**) U2OS cell line stably expressing Flag-HA-BAP1 was transfected with control siRNA or siUBE2O. Three days later, cell lysates were used for western blotting with the indicated antibodies. Note that the knockdown of UBE2O has no effect on the constitutive monoubiquitination of BAP1 (described in Figure **S1A**, **B**, **C**, **D**, **E**, **G**).

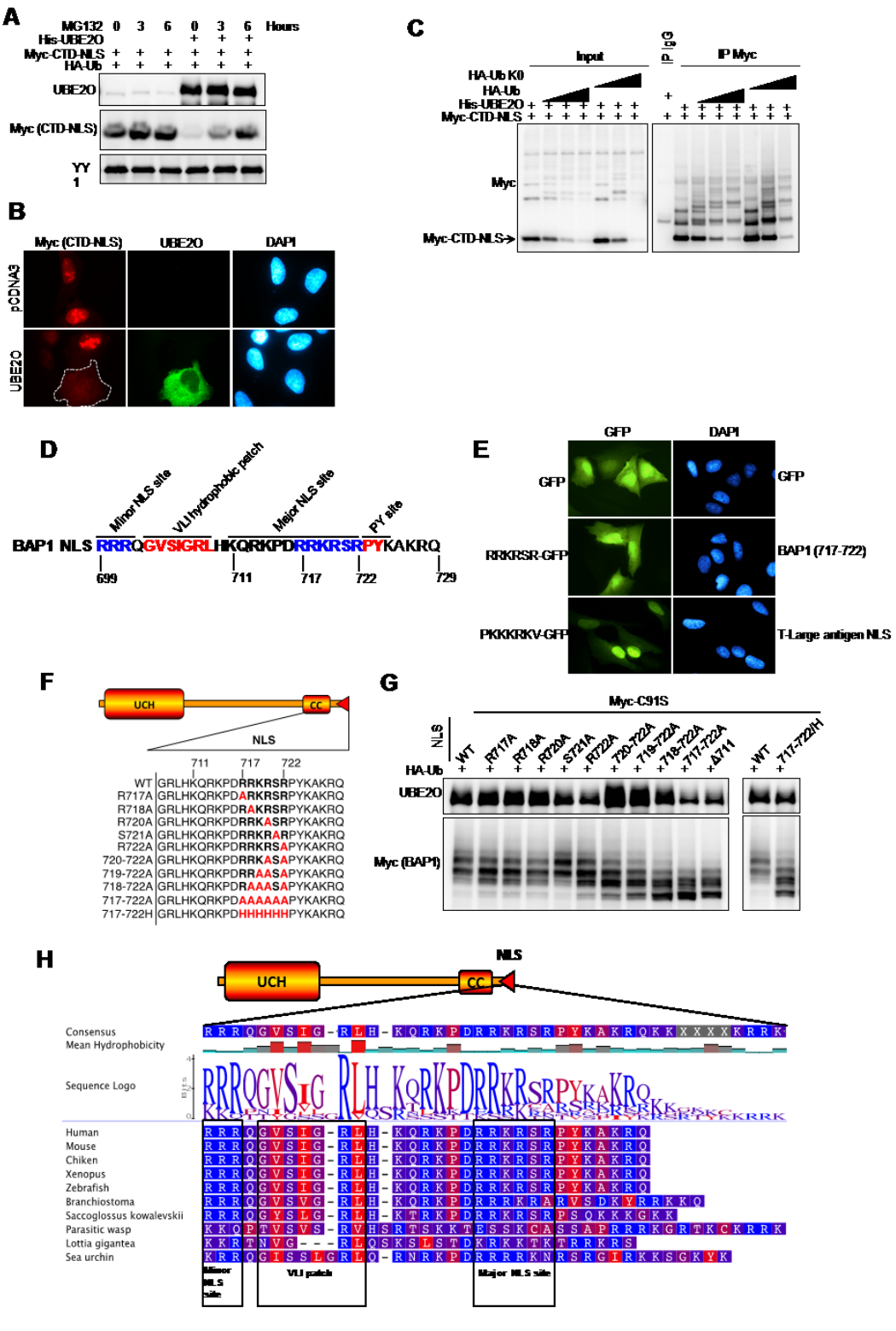
A
MG132 0 3 6 0 3 6 Hours
His-UBE2O + + +
Myc-CTD-NLS + + + + + +
HA-Ub + + + + + +
UBE2O
Myc (CTD-NLS)
YY1
B
Myc (CTD-NLS)
UBE2O
DAPI
pCDNA3
UBE2O
C
Input
IP Myc
HA-Ub K0
HA-Ub
His-UBE2O
Myc-CTD-NLS
Myc
Myc-CTD-NLS
D
Minor NLS site
VLI hydrophobic patch
Major NLS site
PY site
BAP1 NLS RRRQGVSIGRLHKQRKPDRRKRSRPYKAKRQ
699
711
717
722
729
E
GFP
DAPI
GFP
RRKRSR-GFP
BAP1 (717-722)
PKKKRKV-GFP
T-Large antigen NLS
F
UCH
CC
NLS
711 717 722
WT GRLHKQRKPDRRKRSRPYKAKRQ
R717A GRLHKQRKPDARKRSRPYKAKRQ
R718A GRLHKQRKPDRAKRSRPYKAKRQ
R720A GRLHKQRKPDRRKASRPYKAKRQ
S721A GRLHKQRKPDRRKRARPYKAKRQ
R722A GRLHKQRKPDRRKRSAPYKAKRQ
720-722A GRLHKQRKPDRRKASAPYKAKRQ
719-722A GRLHKQRKPDRRAASAPYKAKRQ
718-722A GRLHKQRKPDRAAASAPYKAKRQ
717-722A GRLHKQRKPDAAAAAAPYKAKRQ
717-722H GRLHKQRKPDHHHHHHPYKAKRQ
G
Myc-C91S
NLS
WT R717A R718A R720A S721A R722A 720-722A 719-722A 718-722A 717-722A Δ711 WT 717-722H
HA-Ub
UBE2O
Myc (BAP1)
H
UCH
CC
NLS
Consensus
Mean Hydrophobicity
Sequence Logo
Human
Mouse
Chiken
Xenopus
Zebrafish
Branchiostoma
Saccoglossus kowalevskii
Parasitic wasp
Lottia gigantea
Sea urchin
Minor NLS site
VLI patch
Major NLS site

Fig. S3

U

Figure S3 (Related to Figure 3). UBE2O promotes degradation of BAP1 CTD-NLS. (**A**) 293T cells were co-transfected with 2 µg of HA-Ub, 2 µg of His-UBE2O, and 1 µg of Myc-CTD-NLS expression vectors. Three days later, cells were treated with 20 µM of MG132 for the indicated time points and harvested for western blotting. (**B**) U2OS cells were co-transfected with 0,5 µg of HA-Ub, 1 µg of His-UBE2O and 1 µg of Myc-CTD-NLS expression vectors and plated on coverslips. Three days later, cells were fixed and used for immunofluorescence. (**C**) 293T cells were co-transfected with increasing amounts of HA-Ub or HA-Ub K0 (0.5 µg, 1.5 µg and 4 µg), 2 µg of His-UBE2O, and 1 µg of Myc-CTD-NLS expression vectors. Three days later, cells extracts were analyzed by western blotting. Note that UBE2O promotes the Myc-CTD-NLS degradation in ubiquitin-dependent manner, and a similar degradation profile is obtained with either wild-type or K0 ubiquitin mutant.

Characterization of the BAP1 NLS region. (**D**) Representation of the predicted BAP1 NLS. The basic regions are in blue and hydrophobic regions are in red. BAP1 possesses a complex NLS region that shares similarities with classical monopartite (Conti et al., 1998), bipartite (Robbins et al., 1991) and the atypical hydrophobic/basic PY NLS (Lee et al., 2006). (**E**) U2OS cells were transfected with 0,5 µg of the indicated GFP fusion NLS. Three days later, cells were fixed and used for fluorescence microscope imaging. The region spanning a short stretch of basic amino acids RRKRSR (aa 717-722) is necessary for proper nuclear localization of BAP1 (Ventii et al., 2008). However, when fused to GFP, this motif was not sufficient to promote nuclear localization, i.e., additional sequences are required for NLS function. Therefore, we considered the entire aa 699-729 region as BAP1 NLS for further characterization.

Requirement of the major NLS site of BAP1 for UBE2O-mediated ubiquitination. (**F**) Schematic representation of the alanine screen mutants, mutations are indicated in red. (**G**) 293T cells were co-transfected with 2 µg of HA-Ub, 2 µg of His-UBE2O, and 1 µg of Myc-tagged BAP1 mutants expression vectors. Three days later, cell extracts were used for western blotting and probed with the indicated antibodies. Single point mutations in the region did not cause significant reduction of C91S ubiquitination, but cumulative alanine mutations were able to gradually decrease the efficiency of ubiquitination. The substitution of RRKRSR to a similarly positively charged histidine stretch also strongly reduced the ubiquitination by UBE2O indicating that the arginine/lysine residues are critical

Sequence comparison of the NLS region from different BAP1 orthologs. (**H**) Multiple sequence alignment of the NLS regions of BAP1 from metazoan species using the Geneious tool, polar amino acids are in blue, hydrophobic amino acids are in red.

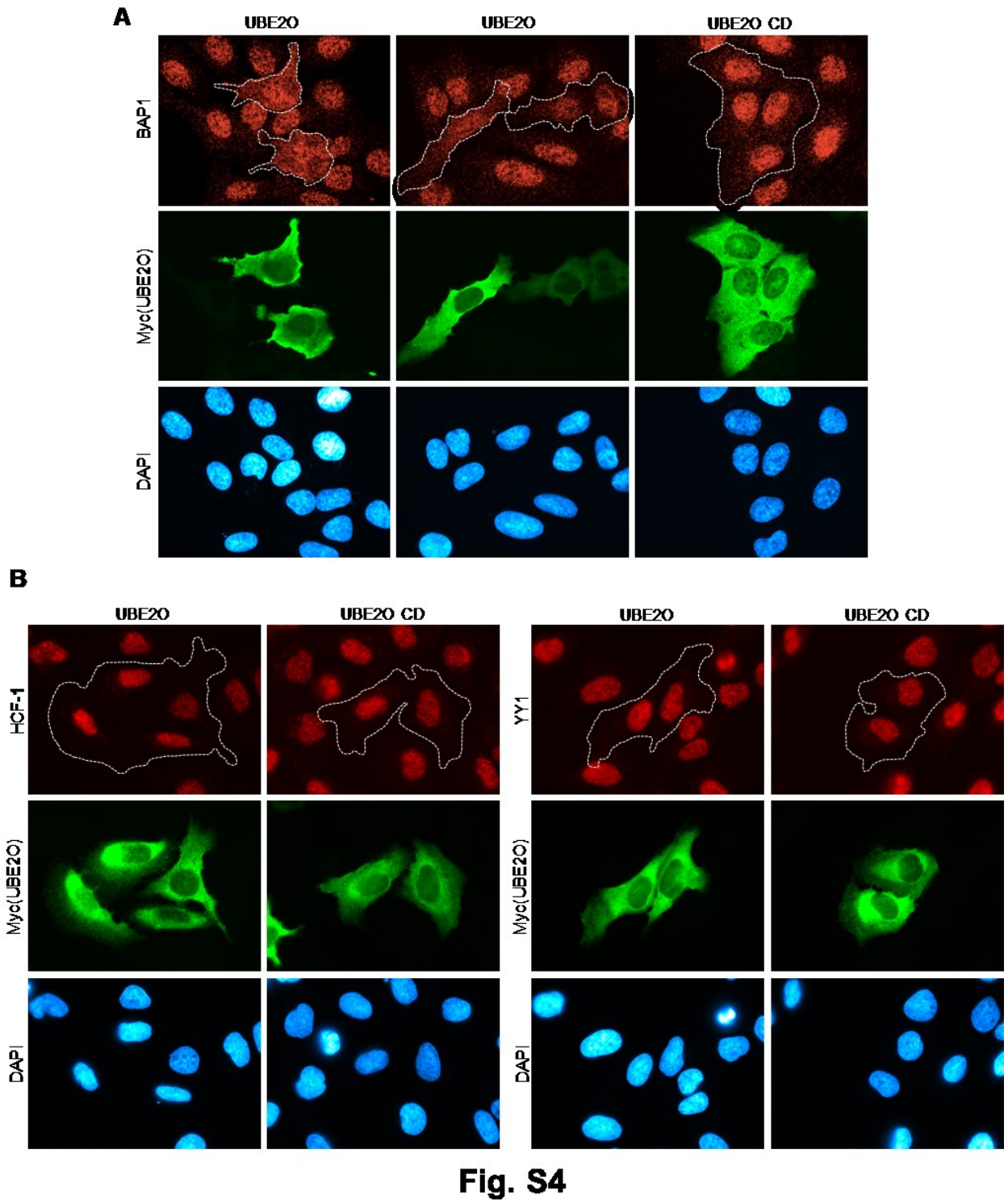

Fig. S4

Figure S4 (Related to Figure 4). Overexpression of UBE2O promotes cytoplasmic localization of endogenous BAP1. U2OS cells were transfected with 4 μg of the Myc-UBE2O or Myc-UBE2O CD. Three days later, cells were fixed and used for Immunofluorescence for BAP1 (**A**) or HCF-1 and YY1 (**B**). UBE2O promoted cytoplasmic localization of BAP1 but had no visible effect on YY1 and HCF-1.

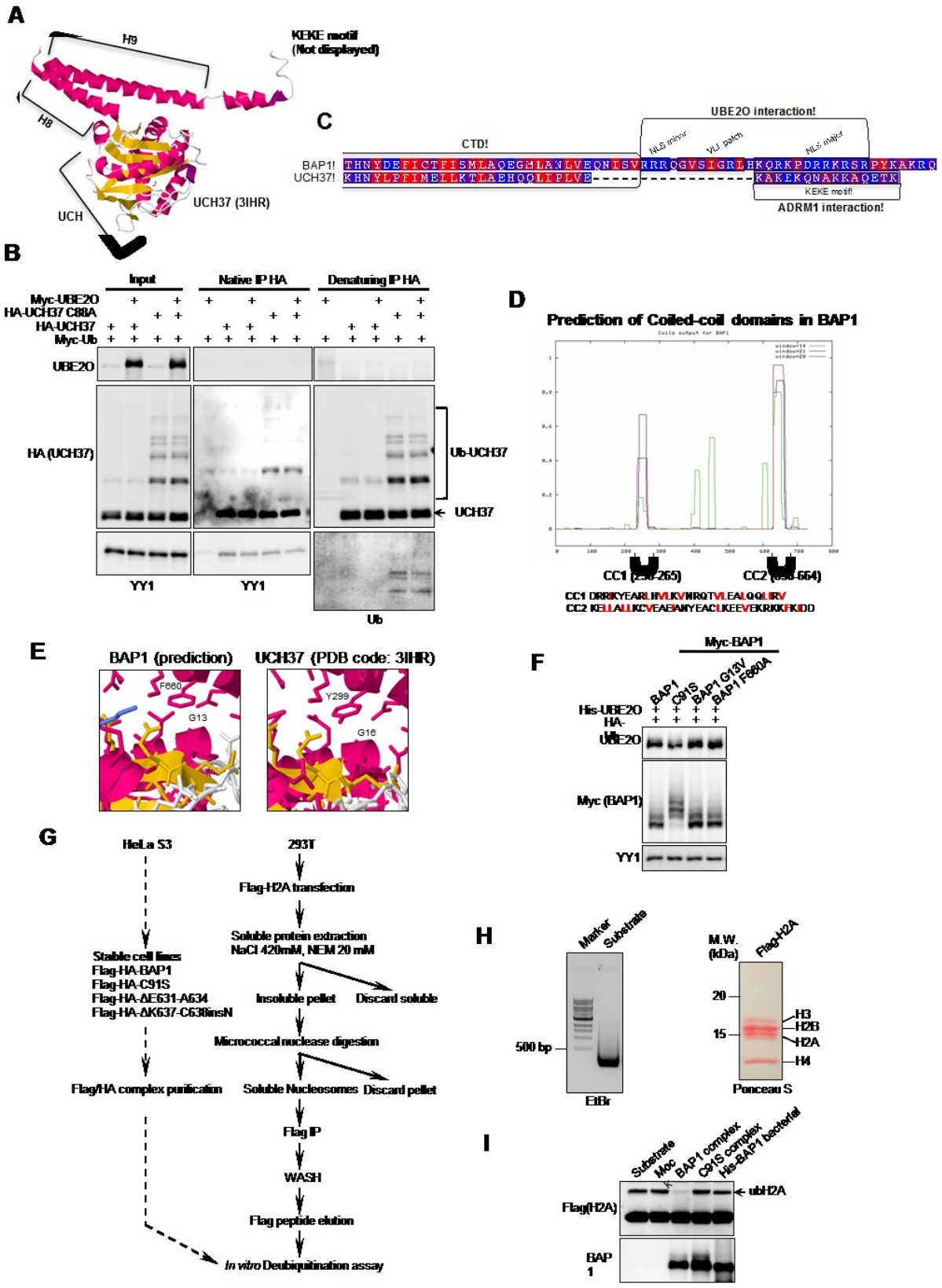
A
H9
KEKE motif
(Not displayed)
H8
UCH37 (3IHR)
UCH
C
UBE2O interaction!
CTD!
NLS minor
VLI patch
NLS major
BAP1!
UCH37!
KEKE motif!
ADRM1 interaction!
B
Input
Native IP HA
Denaturing IP HA
Myc-UBE2O
HA-UCH37 C88A
HA-UCH37
Myc-Ub
UBE2O
HA (UCH37)
Ub-UCH37
UCH37
YY1
YY1
Ub
D
Prediction of Coiled-coil domains in BAP1
CC1
CC2
E
BAP1 (prediction)
UCH37 (PDB code: 3IHR)
F660
G13
Y299
G16
F
Myc-BAP1
BAP1
C91S
BAP1 G13V
BAP1 F660A
His-UBE2O
HA-Ub
UBE2O
Myc (BAP1)
YY1
G
HeLa S3
293T
Flag-H2A transfection
Soluble protein extraction
NaCl 420mM, NEM 20 mM
Stable cell lines
Flag-HA-BAP1
Flag-HA-C91S
Flag-HA-ΔE631-A634
Flag-HA-ΔK637-C638insN
Insoluble pellet
Discard soluble
Micrococcal nuclease digestion
Flag/HA complex purification
Soluble Nucleosomes
Discard pellet
Flag IP
WASH
Flag peptide elution
In vitro Deubiquitination assay
H
Marker
Substrate
500 bp
EtBr
M.W. (kDa)
Flag-H2A
20
15
H3
H2B
H2A
H4
Ponceau S
I
Substrate
Mock
BAP1 complex
C91S complex
His-BAP1 bacterial
Flag(H2A)
ubH2A
BAP 1

Fig. S5

Figure S5 (Related to Figure 5). BAP1 and UCH37 may employ a similar autodeubiquitination mechanism. (**A**) Crystal structure of UCH37 (3IHR) (Burgie et al., 2011). (**B**) UCH37 (UCHL5) is highly similar to BAP1 with respect to domain architecture (Sanchez-Pulido et al., 2012). Crystal structure of UCH37 suggests that an intramolecular interaction occurs between the UCH and the CTD. Therefore, we evaluated the possibility that UCH37 might also be regulated by UBE2O. 293T cells were co-transfected with 1 µg of Myc-Ub, 1 µg of HA-UCH37 WT or HA-UCH37 C88A and either 2 µg of empty vector or Myc-UBE2O expression vectors. Three days later, cells lysates were used for IP with HA antibodies under native or denaturing conditions. Western blots were probed with the indicated antibodies. We detected ubiquitination of UCH37, which was more pronounced for its catalytic dead mutant (C88A), but this effect was independent of UBE2O. UCH37 also failed to interact with UBE2O in co-IP. Nonetheless, this result suggests that UCH37 may employ the same autodeubiquitination mechanism as BAP1 to counteract the action of another, yet to be identified E3 ligase. Note that UCH37 co-immunoprecipitates endogenous YY1 providing an indication of IP validity (Yao et al., 2008). (**C**) Alignment of human BAP1 and human UCH37 C-terminal regions, polar amino acids are in blue, hydrophobic amino acids are in red. Note the difference in the C-terminal region of both proteins, NLS in BAP1 and ADRM1-interacting region (KEKE) in UCH37 (Hamazaki et al., 2006; Yao et al., 2006). (**D**) Prediction of coiled-coil domains in BAP1 using COILS program (Lupas et al., 1991). The amino acid sequences of CC1 and CC2 are presented. The hydrophobic amino acids are indicated in red.

G13V cancer mutant of BAP1 does not impair auto-deubiquitination of NLS. We initially tested the G13V mutation recently described in renal carcinoma patient (Pena-Llopis et al., 2012). (**E**) Prediction for the G13/F660 intra-molecular interaction (left) based on the crystal structure of UCH37 (3IHR)(right). (**F**) 293T Cells were co-transfected with 2 µg of HA-Ub, 2 µg of His-UBE2O, and 1 µg of Myc-BAP1 expression vectors. Three days later, samples were used for western blotting and probed with the indicated antibodies. The G13 residue in UCH is predicted to interact with the F660 residue of the CC2; nonetheless G13V and F660A mutations did not have a noticeable effect on the autodeubiquitination activity of BAP1.

Establishment of the *in vitro* nucleosome deubiquitination assay. (**G**) Schema representing the steps for the preparation of nucleosomes containing H2A mono-ubiquitinated on lysine 119 and the *in vitro* DUB assays. (**H**) DNA from nucleosomal Flag elution was purified using phenol/chloroform separation and loaded on EtBr agarose gel (left). The Ponceau S staining of the nucleosomal Flag elution indicates the presence of all four histone types (right panel). (**I**) *In vitro* nucleosome deubiquitination reaction with purified BAP1 complexes and bacteria purified BAP1. Samples were incubated at 37°C for 4 hours, reactions were stopped with 2X Laemmli buffer, and used for western blot with the indicated antibodies. Note that recombinant BAP1 (not assembled into its complex) does not deubiquitinate H2A .

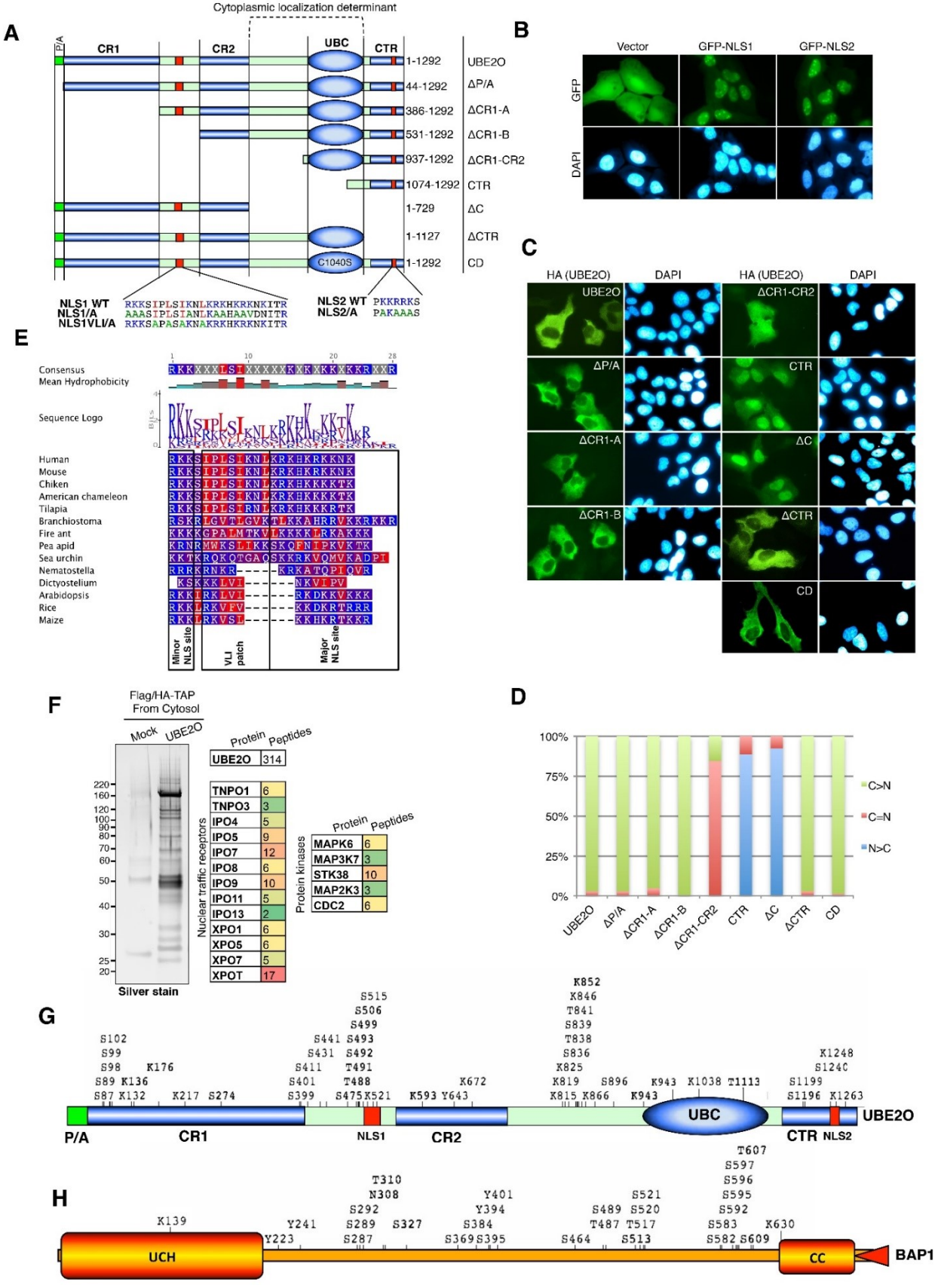
A
Cytoplasmic localization determinant
P/A
CR1
CR2
UBC
CTR
1-1292 UBE2O
44-1292 ΔP/A
386-1292 ΔCR1-A
531-1292 ΔCR1-B
937-1292 ΔCR1-CR2
1074-1292 CTR
1-729 ΔC
1-1127 ΔCTR
C1040S
1-1292 CD
NLS1 WT RKKSIPLSIKNLKRKHKRKNKITR
NLS1/A AAASIPLSIANLKAAHAAVDNITR
NLS1VLI/A RKKSAPASAKNAKRKHKRKNKITR
NLS2 WT PKKRRKS
NLS2/A PAKAAAS
B
Vector
GFP-NLS1
GFP-NLS2
GFP
DAPI
C
HA (UBE2O)
DAPI
UBE2O
ΔCR1-CR2
ΔP/A
CTR
ΔCR1-A
ΔC
ΔCR1-B
ΔCTR
CD
D
100%
75%
50%
25%
0%
C>N
C=N
N>C
UBE2O
ΔP/A
ΔCR1-A
ΔCR1-B
ΔCR1-CR2
CTR
ΔC
ΔCTR
CD
E
Consensus
Mean Hydrophobicity
Sequence Logo
Human
Mouse
Chiken
American chameleon
Tilapia
Branchiostoma
Fire ant
Pea apid
Sea urchin
Nematostella
Dictyostelium
Arabidopsis
Rice
Maize
Minor NLS site
VLI patch
Major NLS site
F
Flag/HA-TAP From Cytosol
Mock
UBE2O
Silver stain
Protein Peptides
UBE2O 314
Nuclear traffic receptors
TNPO1 6
TNPO3 3
IPO4 5
IPO5 9
IPO7 12
IPO8 6
IPO9 10
IPO11 5
IPO13 2
XPO1 6
XPO5 6
XPO7 5
XPOT 17
Protein kinases
MAPK6 6
MAP3K7 3
STK38 10
MAP2K3 3
CDC2 6
G
P/A
CR1
NLS1
CR2
UBC
CTR
NLS2
UBE2O
H
UCH
CC
BAP1

Figure S6 (Related to Figure 6). Subcellular localization of UBE2O deletion mutants reveals nuclear and cytoplasmic targeting regions. (**A**) Schema of UBE2O mutants used to study its subcellular localization**.** (**B**) U2OS cells were transfected with 1 µg of GFP fusion expression vectors of UBE2O NLS regions or empty vector and plated on coverslips. Two day later, cells were fixed and used for fluorescence microscopy analysis. (**C**) U2OS cells were transfected with 3 µg of Flag-HA tagged expression vectors of UBE2O mutants and plated on coverslips. Two days later, cells were fixed and used for the immunofluorescence analysis with HA antibody. (**D**) Representative cell counts for UBE2O subcellular localization are shown.

Multiple sequence alignment of NLS1 region from different UBE2O orthologs. (**E**) Multiple sequence alignment of NLS regions in UBE2O orthologs, polar amino acids are in blue, hydrophobic amino acids are in red.

Post-translational modifications of UBE2O and BAP1 (**F**) Schema of known UBE2O phosphorylation sites (modified from http://www.phosphosite.org/) (**G**) Schema of known BAP1 phosphorylation sites (modified from http://www.phosphosite.org/)

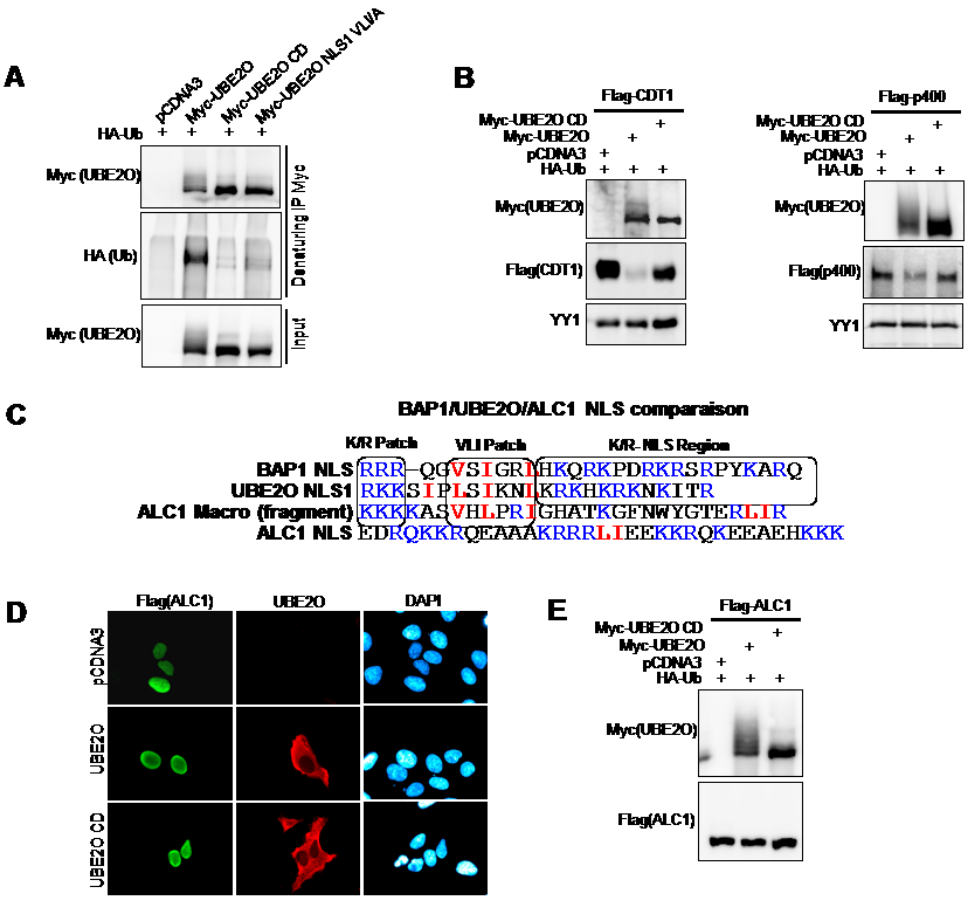

F

UniProt ID[a]	Name[b]	position[c]	Consensus sequence[d]	UBE2O substrate[e]
Q92560	BAP1	699-709	RRRqgVsIgrL	Yes
Q9C0C9	UBE2O	512-523	RKKsipLsIknL	Yes
Q9ULG1	INO80	264 - 273; 276 - 285	KKKh.LsIeqL; RRRk.VwLsiV	Yes
Q9H211	CDT1	67 - 77	RRRlrLsVdeV	Yes
Q9NS56	TOPORS	859 - 870	KRKtrsLsVeiV	unknown
Q9BRD0	BUD13	469 - 478	RKRn.LkLerL	unknown
Q5T5N4	C6orf118	172 - 182	RRReeLrLpdL	unknown
Q86WJ1	ALC1	833 - 843	KKKasVhLprI	NO
O43889	CREB3	192 - 202	RRKkkVyVggL	unknown
Q9P0U4	CXXC1	321 - 330	RKRa.VkVkhV	Yes
Q96L91	EP400	899 - 909	KRKkaLnLqkV	Yes
Q9NSI2	FAM207A	134 - 144	RRRatVvVgdL	unknown
O94915	FRYL	974 - 984	RRRdiLrVqlV	unknown
P5419	HIRA	628 - 638	KRKleLeVetV	unknown
Q32MZ4	LRRF1	578 - 588	KKKspVpVetL	unknown
O60942	MCE1	221 - 231	RRKerLkLgaI	unknown
O00566	MPP10	669 - 679	KKRqdIsVhkL	unknown
P35228	NOS2	509 - 518	KRRe.IpLkvL	unknown
Q86V59	PNMAL1	362 - 372	RKKkkVsLgpV	unknown
O60216	RAD21	319 - 329	KRKrkLiVdsV	unknown
P62979	RS27A	94 - 103	KRKk.VkLavL	unknown
P15822	ZEP1	1280 - 1289	KKKr.LrLaeI	unknown
Q9NQ69	LHX9	220 - 231	KRKspaLgVdiV	unknown
Q96NK8	NEUROD6	81 - 92	KKKttkLrLerV	unknown
Q96C28	ZNF707	166 - 177	RRKqraVeLsfI	unknown

Fig. S7

Figure S7 (Related to Figure 7). NLS1 hydrophobic VLI patch is required for autocatalytic UBE2O targeting. (**A**) 293T cells were co-transfected with 2 µg of HA-Ub and 2 µg of indicated Myc-tagged UBE2O mutants, and cell extracts were used for immunoprecipitation.

UBE2O promotes degradation of p400 and CDT1. (**B**) 293T cells were co-transfected with 2 µg of HA-Ub and 2 µg of empty vector, Myc-UBE2O or Myc-UBE2O CD and either 1 µg of Flag-CDT1 or 5 µg Flag-p400 expression vectors. Three days later, samples were used for western blotting and probed with the indicated antibodies.

UBE2O does not ubiquitinate or promote localization change of ALC1, protein with unrelated NLS and the predicted consensus within Macro domain. (**C**) Sequence alignment between the UBE2O/BAP1 in comparison to ALC1 NLS. VLI patch is in red, and basic amino acids are in blue. Note that the K/R NLS region is absent downstream of the UBE2O consensus found in ALC1. The previously defined NLS sequence of ALC1 does not show similarities with the UBE2O consensus. (**D**) U2OS cells were co-transfected with 0,5 µg of HA-Ub and either 1 µg of empty vector Myc-UBE2O, Myc-UBE2O CD and 1 µg of Flag-ALC1 expression vectors and plated on coverslips. Three days later, cells were fixed and used for immunofluorescence analysis with the indicated antibodies. (**E**) 293T cells were co-transfected with 2 µg of HA-Ub and 2 µg of empty vector, Myc-UBE2O or Myc-UBE2O CD and 1µg of Flag-ALC1 expression vectors. Three days later, samples were used for western blotting and probed with the indicated antibodies.

Identification of potential UBE2O substrates (**F**) Prediction of UBE2O substrates based on BAP1/UBE2O NLS consensus

[a]UniProt accession number.

[b]protein name.

[c]protein positions of the *[KR][KR][KR]-X(1,3)-[VLI]-X-[VLI]-X-X-[VLI]* UBE2O binding consensus.

[d]consensus sequence (consensus-defined amino acids are capital).

[e]experimental evidence of the predicted UBE2O-mediated substrate ubiquitination (see Figures **7** and figure **S7**).

5.2 ANNEXE 2

Statut de l'article : Publié

Référence : Daou S, Hammond-Martel I, Mashtalir N, Barbour H, Gagnon J, Iannantuono NV,Sen Nkwe N, Motorina A, Pak H, Yu H, Wurtele H, Milot E, Mallette FA, Carbone M, Affar EB. The BAP1/ASXL2 Histone H2A Deubiquitinase Complex Regulates Cell Proliferation and is Disrupted in Cancer. J Biol Chem. 2015 Sep 28. pii:jbc.M115.661553. [Epub ahead of print] PubMed PMID: 26416890.

Contributions des co-auteurs :

Pour cet acrticle intitulé «The BAP1/ASXL2 Histone H2A Deubiquitinase Complex Regulates Cell Proliferation and is Disrupted in Cancer» J'ai effectué et analysé plusieurs expériences importantes à la caractérisation du mécanisme présenté, incluant des expériences de compétitions, d'immunoprécipitation, de localisation cellulaire (immunofluorescence), de prolifération (BrdU), de croissance, de sénescence et de stress cellulaires. J'ai également généré des lignées de cellules H226 exprimant de manière stable divers mutants de BAP1 et effectué des expériences de qRT-PCR des gènes cibles d'E2F après déplétion par RNAi de BAP1, ASXL1 et ASXL2.

Plus spécifiquement, tel qu'indiqué dans la version publiée de l'article, Salima Daou et El Bachir Affar ont fait le design de l'étude. Salima Daou, Ian Hammond-Martel et El Bachir affar ont écrit le manuscript. Salima Daou et Ian Hammond-Martel ont performé et analysé les résultats présentés aux figures 1, 2, 3, 4, 5 et 10. Salima Daou a conduit les expériences liées aux figures 8 et 9. Salima Daou et Nazar Mashtalir ont performé les expériences présentées aux figures 6 et 7. Nazar Mashtalir a réalisé les expériences présentées aux figures 5A et 5F. Haithem Barbour et Nazar Mashtalir ont performé les analyses d'alignements présentées aux figures 6C et 8A respectivement. Haithem Barbour a effectué les expériences liées aux figures 5D et 8C. **Jessica Gagnon** a conduit les expériences présentées aux figures 1E et 2H. Salima Daou, Frédérick A. Mallette, Alena Motorina, **Jessica Gagnon** et Nicholas VG Iannantuono ont fait le design et ont performé les expériences liées à la figure 11. Helen Pak a réalisé l'expérience présentée à la figure 3B. Helen Yu a performé l'expérience présentée à la figure 2F. Nadine S. Nkwe a aide à générer les constructions des vecteurs d'expression chez les mammifères pour ASXL1, ASXL2, ASXL1 ΔASXM et ASXL2 ΔASXM. Salima Daou et Nazar Mashtalir ont fait le design et ont généré les vecteurs d'expression des différentes formes mutantes de BAP1, ASXM2 et de l'ubiquitine utilisé pour les expériences liées aux figures 6, 7, 8 et 9. Tous les auteurs ont révisé et interprété les résultats expérimentaux et édité le manuscrit.

The BAP1/ASXL2 Histone H2A Deubiquitinase Complex Regulates Cell Proliferation and is Disrupted in Cancer

Salima Daou[1], Ian Hammond-Martel[1], Nazar Mashtalir[1], Haithem Barbour[1], Jessica Gagnon[1], Nicholas V.G. Ianantuono[1], Nadine S. Nkwe[1], Alena Motorina[1], Helen Pak[1], Helen Yu[1], Hugo Wurtele[1], Eric Milot[1], Frédérick A. Mallette[1], Michele Carbone[2] and El Bachir Affar[1]

[1]Maisonneuve-Rosemont Hospital Research Center and Department of Medicine, University of Montréal, Montréal H3C 3J7, Québec, Canada

[2]University of Hawaii Cancer Center, BSB200, 701 Ilalo Street, Honolulu, Hawaii 96813, USA.

***Running title**: Inactivation of BAP1/ASXL DUB activity in cancer.

To whom correspondence should be addressed: EL Bachir Affar, Maisonneuve-Rosemont Hospital Research Center and Department of Medicine, University of Montréal, Montréal H3C 3J7, Québec, Canada, Tel.: (1) 514 252 3400 (EXT: 3343); Fax: (1) 514 252 3430;

Keywords: Histone H2A ubiquitination; epigenetics; deubiquitylation (deubiquitination); Polycomb Group Proteins; BAP1; Calypso; ASXL; cancer biology; cell proliferation; cellular senescence

[2]The abbreviations used are: DUB, Deubiquitinase; H2Aub, H2A K119 ubiquitination; CTD, C-Terminal domain; CUBI, Composite Ubiquitin Binding Interface; UCH, Ubiquitin Carboxyl Hydrolase; CC1, Coiled Coil motif 1; CC2, Coiled Coil motif 2; ULD, C-Terminal Domain of UCH37; UBD, Ubiquitin Binding domains; PR-DUB, Polycomb Repressive-DUB, PRC1, Polycomb Repressive Complex 1; PcG, Polycomb Group Proteins; TrxG, Trithorax Group Proteins; PHD, Plant Homeo Domain.

Abstract

The deubiquitinase (DUB) and tumor suppressor BAP1 catalyzes ubiquitin removal from histone H2A K119 and coordinates cell proliferation, but how BAP1 partners modulate its function remains poorly understood. Here, we report that BAP1 forms two mutually exclusive complexes with the transcriptional regulators ASXL1 and ASXL2, which are necessary for maintaining proper protein levels of this DUB. Conversely, BAP1 is essential for maintaining ASXL2, but not ASXL1 protein stability. Notably, cancer-associated loss of BAP1 expression results in ASXL2 destabilization and hence loss of its function. ASXL1 and ASXL2 use their ASXM domains to interact with the C-terminal domain (CTD) of BAP1 and these interactions are required for ubiquitin binding and H2A deubiquitination. The deubiquitination promoting effect of ASXM requires intramolecular interactions between catalytic and non-catalytic domains of BAP1 which generate a composite ubiquitin binding interface (CUBI). Notably, the CUBI engages multiple interactions with ubiquitin involving, (i) the ubiquitin carboxyl hydrolase (UCH) catalytic domain of BAP1 which interacts with the hydrophobic patch of ubiquitin and (ii) the CTD domain which interacts with a charged patch of ubiquitin. Significantly, we identified cancer-associated mutations of *BAP1* that disrupt the CUBI, and notably an in frame deletion in the CTD that inhibits its interaction with ASXL1/2, DUB activity and deregulates cell proliferation. Moreover, we demonstrated that BAP1 interaction with ASXL2 regulates cell senescence and that *ASXL2* cancer-associated mutations disrupt BAP1 DUB activity. Thus BAP1 orchestrates tumor suppression function via a unique mechanism of deubiquitination and inactivation of BAP1/ASXL2 axis contributes to cancer development.

Introduction

Covalent attachment of ubiquitin on lysine or N-terminal residues of target proteins can influence substrate stability and function, and as such exerts major roles in diverse cellular processes including intracellular trafficking, protein quality control, cell cycle progression, transcription, DNA replication and repair (1-5). Ubiquitination is catalyzed by the concerted action of E1-ubiquitin activating, E2-ubiquitin conjugating and E3-ubiquitin ligases and generally results in the attachment of one or several ubiquitin molecules, i.e. mono- or poly-ubiquitination, respectively (3,6). Ubiquitination events are tightly coordinated by DUBs, which are responsible for reversing this modification (7,8).

Proteins containing ubiquitin-binding domains (UBDs) are responsible for the specific and non-covalent recognition of free ubiquitin and of mono- or poly-ubiquitinated substrates. UBDs can be categorized into several families based on structural characteristics such as the presence of single or multiple α-helices, zinc fingers or pleckstrin-homology fold, which constitute interfaces of low affinity interaction with one or multiple molecules of ubiquitin. UBD-containing proteins are thus widely involved in the proper and timely initiation, propagation or termination of ubiquitin-mediated signaling events (3,9).

The nuclear DUB BAP1 is a tumor suppressor deleted and mutated in an increasing number of cancers of diverse origins (10,11). Indeed, somatic or germinal inactivating mutations in BAP1 are found in mesothelioma, uveal melanoma, cutaneous melanocytic tumors, clear cell renal cell carcinoma, breast and lung cancers, thereby making BAP1 the most frequently and widely mutated DUB-encoding gene in cancer (12-20). Previous studies indicated that BAP1 tumor suppressor function requires DUB activity and nuclear localization (21). Consistent with its role in tumor suppression, BAP1 was shown to act as a positive or a negative regulator of cell proliferation (21-24). Moreover, genetic ablation of BAP1 in mice inhibits embryonic development, while selective inactivation of BAP1 in the hematopoietic system induces severe defects in the myeloid cell lineage, recapitulating key features of myelodysplastic syndrome (19). At the molecular level, BAP1 acts as a chromatin-associated protein that is assembled into large multi-protein complexes containing several transcription factors and co-factors including the Host Cell Factor 1 (HCF-1), the O-linked N-acetyl-Glucosamine Transferase (OGT), the Lysine Specific Demethylase KDM1B/LSD2/AOF1, the Additional Sex Comb Like proteins ASXL1 and ASXL2 (ASXL1/2), the Forkhead transcription factors FOXK1 and FOXK2 as well as the zinc

finger transcription factor Yin Yang 1 (YY1) (22,25,26). BAP1 is recruited at gene promoter regions to activate transcription, and has been shown to regulate the expression of genes involved in cell proliferation (15,26,27). BAP1 is also recruited to sites of DNA double strand breaks to promote repair by homologous recombination (24,28), and is implicated in DNA replication-associated processes (29,30). Importantly, BAP1 functions appear to be regulated by post-translational modifications including phosphorylation and ubiquitination (24,30,31). Nonetheless, the mechanism by which BAP1 function is coordinated by its partners remains poorly defined.

Calypso, the *Drosophila* ortholog of BAP1 is a Polycomb Group (PcG) protein that interacts with the transcriptional regulator ASX and assembles the Polycomb Repressive-DUB (PR-DUB) complex which deubiquitinates histone H2A K118 (H2A K119 in vertebrates, hereafter H2Aub) and promotes PcG target gene repression (32). While the exact mechanism of repression remains unknown, it is interesting to note that the Polycomb Repressive Complex 1 (PRC1), which catalyzes H2A ubiquitination, is also required for PcG target gene repression (33). *Drosophila* ASX protein is an atypical PcG factor, since it is involved in both transcriptional silencing and activation (34,35). ASXL1 and ASXL2 (hereafter ASXL1/2) are paralogs that appear to have diverged from ASX during evolution, and are reported to function with a number of co-repressors and co-activators, notably the Lysine-Specific Demethylase KDM1A/LSD1, the PcG complex PRC2 and the Trithorax Group (TrxG) epigenetic regulators (36-39). Similar to PR-DUB complex, a minimal complex containing mammalian BAP1 and the N-terminal region of ASXL1 was shown to efficiently deubiquitinate H2A *in vitro,* indicating the requirement of ASX or ASXL1 for DUB activity (32). The DUB activity of BAP1 toward histone H2A K119 was also observed in vivo (20,24,27,40). BAP1 was also shown to deubiquitinate and stabilise some of its interacting partners including HCF-1 and OGT indicating the functional importance of its catalytic activity (19,22,23). Interestingly, the DUB activity of a BAP1 family member, UCH37, is stimulated by RPN13 (ADRM1) 19S proteasome subunit (42-44), and phylogenetic studies suggest that RPN13 and ASXL1/2 share a conserved domain termed the DEUBiquitinase ADaptor (DEUBAD) domain corresponding to ASXM (45). This suggests that BAP1/ASXL1/2 might use a similar mechanism of DUB activation as UCH37/RPN13.

The genes encoding ASXL1/2 are involved in chromosomal translocations and are frequently truncated in various cancer types (46). ASXL1 is frequently mutated in myeloid malignancies. Most of these mutations generate truncated ASXL1 proteins that retain the N-terminal region required for interaction with BAP1 (32). Although, ASXL1 interaction with BAP1 was initially revealed dispensable for leukemia development (39), it was recently shown that leukemia-associated mutations of ASXL1, lead to an aberrant enhancement of BAP1 DUB activity (47). Moreover, expression of these ASXL1 constructs

in hematopoietic precursor cell line causes an overall depletion of H2Aub associated with defects in myeloid differentiation (47). However, the involvement of this interaction in other cancers remains unknown. In addition, the specific contribution of ASXL1 and ASXL2 to BAP1 function remains undefined. Here, we sought to determine how ASXL1/2 modulates the H2A DUB activity of BAP1, and the relevance of these factors for BAP1 tumor suppressor function. We mapped the exact interaction domains and motifs between BAP1 and ASXL1/2 and demonstrated that ASXL1/2 form two mutually exclusive complexes with BAP1, both of which are competent in deubiquitinating H2A. Furthermore, we showed that the loss of BAP1 expression in cancer is concomitant with a destabilization of ASXL2. We also found that the ASXM domain of ASXL1/2 is prerequisite for ubiquitin binding and deubiquitination by BAP1. Moreover, we found that BAP1 catalytic and non-catalytic domains form, along with the ASXM domain, a composite ubiquitin binding interface (CUBI) required for promoting BAP1 DUB activity by ASXL1/2 and coordination of cell proliferation. Finally, we identified a cancer-derived mutation of BAP1 CTD, □R606-H609, which results in a selective loss of interaction with ASXL1/2 and inhibition of H2A DUB activity. The □R606-H609 mutation also abolishes the ability of BAP1/ASXL2 axis to regulate cell proliferation and cellular senescence, thus providing a link between BAP1 function and mechanisms of tumor suppression.

Results

ASXL1 and ASXL2 compete for their interaction with BAP1

ASXL1 and ASXL2 compete for their interaction with BAP1-ASXL1 and ASXL2 factors co-purified with BAP1 (25,26), and mass spectrometry peptide counts suggest that they are associated with BAP1 at similar levels (Fig. 1A). BAP1 interaction with ASXL1/2 was not affected by the loss of HCF-1, a major subunit of the BAP1 core complexes associated through its HCF-1 binding motif (HBM). We also note that the interaction between BAP1 and OGT is strongly reduced in the context of BAP1□HBM complexes, indicating that HCF-1 bridges OGT and BAP1. (Fig.1B). We sought to further investigate the functional relationship between these factors. Immunoprecipitation (IP) of ASXL2 from purified BAP1 complexes did not show interaction with ASXL1 (Fig. 1C), and ASXL1 and ASXL2 failed to interact with each other following overexpression (Fig. 1D). We noted that BAP1 interaction with ASXL2 was reduced following expression of ASXL1 (Fig. 1D), suggesting that ASXL1 might compete with ASXL2 for BAP1 binding. To further confirm that ASXL1 and ASXL2 compete for interaction with BAP1, we overexpressed increasing amounts of ASXL1 with constant amounts of BAP1 and ASXL2 in 293T cells and conducted immunoprecipitation. Interestingly, although ASXL2 and BAP1 protein levels also increased following ASXL1 overexpression, we observed that ASXL2 was displaced from BAP1-

containing protein complexes (Fig. 1E) indicating that ASXL1 and ASXL2 form two distinct complexes with BAP1.

BAP1 and ASXL1/2 are co-regulated and loss of BAP1 in cancer is concomitant with ASXL2 destabilization

To further investigate the relevance of ASXL1 and ASXL2 in regulating BAP1 function, we transfected 293T cells with BAP1 and increasing amounts of Myc-tagged ASXL1/2-expressing constructs. We found that BAP1 protein levels increased with ASXL1/2 expression in a dose-dependent manner (Fig. 2A). Conversely, ASXL1/2 protein levels were also increased following overexpression of BAP1 (Fig. 2B). siRNA knockdown of either ASXL1 or ASXL2 in U2OS osteosarcoma cells or primary human fibroblasts resulted in a significant decrease of BAP1 protein levels (Fig. 2C,D), while combined knockdown of ASXL1/2 caused an even stronger decrease of BAP1 levels than depletion of individual proteins (Fig. 2C). This indicates that ASXL1/2 are necessary for maintaining proper protein levels of this DUB. We also observed that depletion of ASXL1 resulted in a noticeable decrease of ASXL2, while knockdown of ASXL2 caused an increase of ASXL1 (Fig. 2C,D). Knockdown of BAP1 strongly reduced ASXL2 levels. This effect is independent of BAP1 DUB activity, as the decrease of ASXL2 protein in U2OS cells was prevented by re-expression of siRNA-resistant forms of BAP1, either wild type or catalytically dead mutant, BAP1C91S (Fig. 2E). The dependency of ASXL2 protein levels on BAP1 abundance suggests that ASXL2/BAP1 may form an obligate complex. Consistently, immunodepletion of endogenous proteins from HeLa nuclear extracts revealed that the majority of ASXL2 is associated with BAP1 (Fig. 2F). However, only about half the amount of BAP1 is in complex with ASXL2. PARP1 was used as a control which remained in the flow through fraction. Significantly, ASXL2 was downregulated in BAP1-deficient H28 mesothelioma and H226 lung carcinoma cells, and re-expression of BAP1 or BAP1C91S restored ASXL2 protein levels in these cells, without affecting its mRNA levels (Fig. 2G,H). These data suggest that BAP1/ASXL1/2 interactions are regulated and that loss of BAP1 during cancer development results in concomitant loss of ASXL2 protein and function.

The ASXM domain of ASXL1/2 is required for interaction with the CTD of BAP1

BAP1 was shown to interact with the N-terminal region of ASXL1 (1-337 a.a.) (32). To identify the exact domain of ASXL1/2 responsible for this interaction, we conducted GST-pull down assays and found that in vitro-translated ASXM domain (ASXM1: 253-391 a.a., ASXM2: 253-411 a.a. of ASXL1 and ASXL2 respectively) interacted with GST-BAP1 (Fig. 3A, B). To gain insights into the significance of the BAP1/ASXL1/2 interactions, we generated ASXL1/2 expression constructs lacking the BAP1-interacting domain (ASXL1/2□ASXM). As expected, following transfection, protein levels of ASXL2□ASXM, but

not ASXL1□ASXM, were reduced in comparison to their wild type counterparts (Fig. 3C). Of note, the polypeptides encoded by the ASXL1/2 constructs were essentially nuclear (Fig. 3D). GFP-PAR-4 fusion protein which localizes in both the cytoplasm and the nucleus was included as a control (51). Next, after adjusting the amounts of transfected plasmids to obtain comparable expression of the wild type and mutant forms of ASXL1/2, we found that the ability of ASXL1/2 mutants, lacking their respective ASXM domain, to interact with BAP1 and to form protein complexes in vivo was strongly reduced (Fig. 3E).

BAP1 contains an Ubiquitin Carboxyl Hydrolase (UCH) catalytic domain and a Coiled-Coil motif (CC1) in the N-terminal region, as well as a C-Terminal Domain (CTD) containing a second Coiled-Coil motif (CC2) (12,23,31) (Fig. 4A). This DUB also possesses a big middle region (MR), that contain the HBM and other protein interaction motifs, separating UCH/CC1 from the CTD, (12,23,40,52). We found that only GST-tagged fragments of BAP1 containing an intact CTD interacted with ASXM domains of ASXL1/2 (Fig. 4B). These results indicate that ASXL1/2 use the ASXM domain to interact with the CTD of BAP1. To provide further insights into ASXL1/2/BAP1 interactions, we constructed BAP1 mutants disrupted in the CTD region (Fig. 4C). The BAP1□CTD1 represents a deletion of CTD except for the KRKKFK putative nuclear localization signal (21). The BAP1□CTD and BAP1□CC2 represent a complete deletion of the CTD and CC2, respectively. Supporting our finding reported above, we noticed that disruption of CTD resulted in decreased BAP1 protein levels (Fig. 4D). We also generated HeLa cell lines stably expressing BAP1wild type or its mutant form lacking most of the CTD, BAP1□CTD1, and use for complex purification. To enable meaningful comparisons, the eluted complexes were adjusted by immunoblotting for similar amounts of BAP1 protein prior to silver staining. This revealed that BAP1 and BAP1□CTD1 complexes were quite similar in protein composition (Fig. 4E). However, immunoblotting analysis showed that the interaction between BAP1□CTD1 and ASXL1/2 was abolished (Fig. 4E). In contrast, association of BAP1□CTD1 with HCF-1/OGT remained unchanged in comparison to the wild type variant. Altogether, these results indicate that CTD and ASXMdomains are necessary and sufficient for assembly of BAP1/ASXL1/2 complexes

BAP1 is a major DUB for H2Aub K119 and its enzymatic activity is ASXM-dependent

Several DUBs including BAP1 were reported to target H2Aub K119 in mammals (4,53). However, the relative contribution of each enzyme in H2A deubiquitination in vivo remained unknown. We conducted an siRNA screen using a library that covers the human DUB repertoire by analyzing the global increase of H2Aub using an in-cell western assay. Depletion of BAP1 produced the most significant increase of H2Aub, indicating that this enzyme is a major DUB for this histone modification under normal growth conditions (Fig. 5A). To investigate how ASXL1/2 regulate mammalian BAP1 DUB activity in vivo, we

conducted RNAi-mediated depletion of these factors, and found that neither ASXL1 nor ASXL2 individual knockdown induced noticeable changes in global H2Aub levels (Fig. 5B, 5C). However, combined knockdown of ASXL1 and ASXL2 resulted in significant increase of H2Aub, similar to the effect induced by BAP1 depletion (Fig. 5B). This prompted us to determine the respective contribution of ASXL1 and ASXL2 to the H2A DUB activity of BAP1. A striking BAP1-mediated deubiquitination of H2A was observed upon its co-expression with either ASXL1 or ASXL2, and this effect was dependent on BAP1 catalytic activity (Fig. 5D). Consistent with our mapping analysis, ASXL1 and ASXL2 lacking ASXM were unable to stimulate H2A deubiquitination (Fig. 5E). In addition, we purified monoubiquitinated nucleosomal Flag-H2A, from 293T cells, that we used for in vitro DUB assay and found that ASXM1 or ASXM2, but not GST-CTD used as a control, are sufficient for stimulating BAP1-mediated deubiquitination of H2A (Fig. 5F). Based on these results, we concluded that interaction between ASXL1/2 and BAP1 require ASXM, and the latter is necessary and sufficient for promoting BAP1-mediated deubiquitination of its physiological substrate H2Aub K119.

Identifications of domains and motifs in ASXM required for promoting ubiquitin binding and DUB activity towards histone H2A of BAP1

To further dissect the mechanism of H2A deubiquitination by BAP1, we conducted ubiquitin pull down assays and found that ASXM2 strongly enhanced BAP1 binding to ubiquitin (Fig.6A). ASXM2 alone can directly bind ubiquitin, but this interaction was weak as an enrichment of about two-folds above the background was observed (Fig. 6A). ASXM1 also promoted BAP1 binding to ubiquitin in a similar manner as ASXM2 (Fig. 6B). Since ASXM1 and ASXM2 domains acted similarly in promoting BAP1 binding to ubiquitin and DUB activity, we selected ASXM2 for further studies. Sequence alignment of ASXL proteins indicated that the ASXM domain is highly conserved (Fig. 6C). We generated several constructs encompassing several regions and conserved motifs of ASXM2 (Fig. 6C). We found that the 246-347 a.a. region interacted with BAP1 as efficiently as the full length ASXM2 (246-401 a.a.), while no interaction was observed for the 316-401 a.a. region (Fig. 6D). The 246-313 a.a. and 300-401 a.a. regions interacted only poorly with BAP1. These results suggest that critical interaction motifs are located within or overlapping with the 300-347 a.a. region (Fig. 6D). Only the full length ASXM2 and the 246-347 a.a. fragment, that strongly interacted with BAP1, promoted its binding to ubiquitin and DUB activity. Nonetheless, we noted that the 246-347 a.a. fragment was significantly less competent in promoting BAP1 binding to ubiquitin which could explain its weakness in promoting deubiquitination (Fig. 6D,E). Next, we generated discrete mutations of

several highly conserved residues of ASXM2 (Fig. 6C), and found that ASXM2 interaction with BAP1 and ubiquitin binding are maintained for most mutants except for the LLLL303-306AAAA hydrophobic stretch mutant which essentially lost its interaction with BAP1 (Fig. 6F,G). As expected, the LLLL303-306AAAA mutant failed to stimulate DUB activity (Fig. 6H). Interestingly, while the L286A and NN328-329AA mutants were essentially equally efficient in promoting BAP1 binding to ubiquitin, their ability to deubiquitinate H2A was significantly different (Fig. 6G,H).

Intramolecular interactions in BAP1 create an ASXM-dependent Composite Ubiquitin Binding Interface (CUBI) and enable DUB activity

The CTD of BAP1 is necessary and sufficient for the interaction between BAP1 and ASXL1/2 (Fig. 4). This domain also engages an intramolecular interaction with both the CC1 and the UCH domains in order to ensure BAP1 auto-deubiquitination and proper nuclear localization (31). Hence, we sought to test whether this intramolecular interaction in BAP1 is necessary for ASXM stimulation of ubiquitin binding and DUB activity. Indeed, as is the case for BAP1□UCH or BAP1C91S, BAP1□CTD was unable to deubiquitinate H2A following incubation with ASXM2 (Fig. 7A,B). BAP1□CTD or BAP1□CC2 mutants were also incapable of deubiquitinating H2A in the context of BAP1 protein complexes in vitro (Fig. 7C), As a control, BAP1□HBM complexes were competent in promoting DUB activity (Fig. 7D), as previously shown (20). BAP1□CTD was also unable to promote BAP1 DUB activity in vivo when expressed with either ASXL1 or ASXL2 (Fig. 7E). In addition, while ASXM2 promoted binding to ubiquitin of both BAP1 and BAP1C91S, this domain failed to enhance ubiquitin binding of BAP1□CTD or BAP1□UCH (Fig. 7F). ASXM2 only partially promoted BAP1□CC1 binding to ubiquitin (Fig. 7A,F), and this mutant is completely inactive in H2A deubiquitination (Fig. 7B). Thus, ASXM2 requires intramolecular interactions between multiple domains of BAP1 to promote ubiquitin binding and catalysis.

In contrast to the CC1 and CTD in BAP1, the corresponding domains in UCH37, helix α7 and ULD respectively, are contiguous (Fig. 8A, left panel) (54). Nonetheless, co-crystallization of UCH37 of the worm Trichinella spiralis (tsUCH37) with ubiquitin indicated an intramolecular interaction similar to the one observed in BAP1 (54). In addition, R261 and Y262 a.a. residues of the ULD establish direct contacts with ubiquitin K48 and Q49/R72, respectively (54). Molecular dynamics simulation suggested that E265 and N272, part of a non-crystalized extension of the ULD, might also bind R42 and D52 of ubiquitin, respectively (54). R261, Y262, E265 and N272 are essentially conserved in BAP1 and correspond to K659, F660, D663 and N670, respectively (Fig. 8A, right panel). Thus, we were prompted to test whether

the CTD is sufficient for binding ubiquitin in solution. We found that the CTD weakly interacted with ubiquitin, as a signal above the background was consistently observed (Fig. 8B). Importantly, mutation of ubiquitin R42/Q49/D52/R72 residues (we termed the RQDR charged patch), involved in binding the tsUCH37 ULD, reduced this interaction (Fig. 8B,C). Moreover, mutation of the RQDR patch also abolished ubiquitin binding by the BAP1/ASXM2 complex (Fig. 8D). Also, ubiquitin binding by BAP1/ASXM2 is completely abrogated by mutating the VLI, Ile36 and Il44 hydrophobic patches of ubiquitin, which are involved in binding by the UCH domain (54-56) (Fig. 8C,D). These data indicate that the hydrophobic and the charged RQDR patches are necessary to ensure strong ubiquitin binding by the BAP1/ASXM2 complex. Finally, mutation of the TEK box, Phe4 patch or D58 did not affect ubiquitin binding by BAP1/ASXM2 (Fig. 8C,D). We concluded that ASXM induces the assembly of a composite ubiquitin binding interface (CUBI) that requires catalytic and non-catalytic domains of BAP1 and involves multiple patches of ubiquitin.

Cancer-derived mutations abolish BAP1 interaction with ASXL1/2, ubiquitin binding and DUB activity

We asked whether tumor-associated mutations of BAP1 result in selective loss of interaction with ASXL1/2 and ubiquitin binding and catalysis. Based on our data and tsUCH37-ubiquitin co-crystal structure (54), we analyzed the previously reported cancer mutation landscape of BAP1 (cBioPortal for Cancer Genomics and COSMIC cancer databases), notably in solid tumors (e.g. uveal melanoma and renal cell carcinoma) and selected several mutations within or near its UCH (E31K, Y33D), CC1 (L230Q, Q253K) and CTD (K656N, K658R, D663H, R666-H669) domains (13,20) (Fig. 8A). We also included additional mutations, not found in cancer, but corresponding to highly conserved amino acids in the vicinity of these cancer mutations (F228A, N670A) (Fig. 8A). We co-expressed these BAP1 mutants with ASXL2 and found that most mutations did not significantly affect protein interactions except for the R666-H669 mutant whose interaction with ASXL2 is strongly reduced (Fig. 9A). It is worth mentioning that although BAP1 and ASXL2 are overexpressed in 293T cells, reduced protein levels of R666-H669 mutant are still observed (Fig. 9A). In vitro ubiquitin pull down interaction assays revealed that E31K and Y33D mutations in the UCH domain result in a reduced binding of BAP1/ASXM2 to ubiquitin (Fig. 9B). Significantly, several mutants in other domains, e.g., F228A, L230Q, K658R and R666-H669 strongly affected BAP1/ASXM2 ability to bind ubiquitin (Fig. 9B). Most BAP1 mutants were also significantly disrupted in their ability to deubiquitinate H2A (Fig. 9B). Interestingly, the D663H mutant was essentially efficient in binding ASXM2 and ubiquitin but failed to promote efficient DUB activity. Since the deletion of amino acids R666-H669 (hereafter BAP1R666-H669) abolished interaction with ASXL2, ubiquitin binding and DUB activity, we selected this mutant for further biochemical and functional studies. Of note,

BAP1R666-H669 is expressed predominantly in the nucleus (Fig. 9C). We generated HeLa cells stably expressing Flag-HA-BAP1R666-H669 and conducted immuno-affinity purification of DUB complexes. After adjusting for similar amounts of immunopurified BAP1 we conducted silver staining of the eluted material. This indicated that R666-H669 mutation did not change the overall composition of BAP1 complexes as compared to the wild type, except for missing ASXL2 band in the purified BAP1R666-H669 complexes (Fig. 9D, left panel). ASXL1 co-migrates with other high M.W. proteins, and could not be discerned as a distinct band. Strikingly, western blot analysis of the complexes indicated that BAP1R666-H669 does not interact with ASXL1/2, whereas interaction with HCF-1/OGT were not affected (Fig. 9D, right panel). Moreover, the purified BAP1R666-H669 complex was unable to deubiquitinate nucleosomal histone H2A (Fig. 9E, left panel), or to bind ubiquitin in vitro (Fig. 9E, right panel). Concordant with this data, neither full length ASXL1 nor ASXL2 are capable of stimulating DUB activity by BAP1R666-H669 in vivo (Fig. 9F). To further investigate the disruption of BAP1/ASXL2 DUB activity in cancer, we selected several reported cancer-associated point mutations in ASXM2 (Fig. 6C), especially in solid tumors (e.g. breast carcinoma and colorectal adenocarcinoma), and found that these mutations did not disrupt ASXM2 interaction with BAP1 (Fig. 9G). The BAP1/ASXM2 complex with P274L mutation showed reduced binding to ubiquitin, while the ability of other mutants to bind ubiquitin was essentially unaffected (Fig. 9H). Finally, three of these mutants (P274L, E330Q, F331L) showed reduced DUB activity toward H2A indicating that ASXL2 is also targeted by mutations that inhibit the enzymatic activity of the complex (Fig. 9I). Altogether, these results indicate that several cancer-associated mechanisms target the BAP1/ASXL2 complexes inducing loss of ubiquitin binding and DUB activity.

BAP1/ASXL1/2 axis is required for proper cell cycle progression

We enquired to determine the biological significance of BAP1/ASXL1/2 interactions. Since BAP1 knockdown delays cell proliferation in multiple cell types (22,23,57), we sought to determine whether ASXL1/2 and BAP1 interactions influence cell cycle progression. We generated U2OS cells stably expressing comparable levels of siRNA-resistant BAP1, BAP1C91S or BAP1R666-H669 (Fig. 10A), and conducted RNAi depletion of endogenous BAP1. Cells were then synchronized in early S phase using double thymidine block and released in the cell cycle. As expected, in the empty vector cells, depletion of endogenous BAP1 delayed S phase progression. While re-expression of BAP1 rescued the defect induced by knockdown of endogenous BAP1, this was not observed with BAP1C91S nor BAP1R666-H669 (Fig. 10B). In addition, expression of BAP1C91S or BAP1R666-H669 significantly affected the ability of U2OS cells to be synchronized (Fig. 10B). Similar cell cycle defects were also observed following expression of BAP1 lacking CTD, BAP1ΔCTD (Fig. 10C). The increase of H2Aub levels following

knockdown of BAP1, was prevented by re-expression of wild type BAP1, but not by BAP1R666-H669 or BAP1C91S mutants (Fig. 10A). We note that the higher levels of H2Aub in U2OS expressing BAP1C91S might result from a dominant negative effect on endogenous BAP1. Next, re-introduction of BAP1, but not the BAP1R666-H669 nor the BAP1C91S in the BAP1-deficent lung carcinoma cell line H226 promoted substantial H2A deubiquitination (Fig. 10D, top panel). In addition, unlike the wild type BAP1, which strongly inhibited cell proliferation as previously observed (21), the BAP1R666-H669 mutant only partially inhibited cell proliferation (Fig. 10D, bottom panel). Thus, physical interaction between ASXL1/2 and BAP1 and DUB activity are required for proper coordination of cell cycle progression.

Enforced expression of BAP1 or ASXL2 induce cellular senescence and the p53/p21 tumor suppressor pathway in CTD/ASXM-dependent manner

Cellular senescence-associated cell cycle exit is a potent tumor suppressor mechanism. Since we established that BAP1 function is coordinated with ASXL1 and ASXL2 in regulating cell cycle progression, we were prompted to determine if BAP1/ASXL1/2 might influence cellular senescence. Of note, PcG proteins, notably BMI1, are known to be involved in senescence (58-60). Therefore, we evaluated whether enforced expression of BAP1, trigger senescence in the normal diploid human fibroblasts IMR90 cell line model. Strikingly, retroviral overexpression of BAP1 reduced cell proliferation and induced senescence-associated β-galactosidase (SA-β-gal) activity (Fig. 11A,B). Interestingly, overexpression of BAP1C91S mutant also induced senescence with a more pronounced effect than the wild type form (Fig.11A,B). To probe whether this effect is due to BAP1 ability to interact with ASXL1/2, we evaluated the effect of BAP1ΔCTD and BAP1R666-H669 on cellular senescence. Indeed, these mutations significantly reduced the ability of BAP1 to induce senescence (Fig 11A,B). Similar effects were observed for the double mutants BAP1C91S-ΔCTD, although a complete rescue was observed for BAP1C91S-R666-H669 (Fig. 11A,B). On the other hand, overexpression of ASXL2, but not ASXL1, also strongly induced senescence and reduced cell proliferation (Fig. 11A,B). Moreover, deletion of ASXM (ASXL2□ASXM) inhibited the senescence-inducing ability of ASXL2, indicating the importance of ASXL2-BAP1 interaction in coordinating cellular senescence. To provide further insights into the molecular mechanism that orchestrate BAP1/ASXL2-mediated senescence, we evaluated the expression levels of known proteins that induce cellular senescence upon overexpression of BAP1, BAP1C91S and corresponding mutants (Fig. 11C). We found that, although the effect of BAP1 was less pronounced than the BAP1C91S form, overexpression of this DUB induced the p53/p21 tumor suppressor pathway. Overexpression of BAP1ΔCTD, BAP1R666-H669, BAP1C91S-ΔCTD or BAP1C91S-R666-H669 did not upregulate p53/p21 indicating the requirement for ASXL1/2 in BAP1-mediated senescence (Fig. 11C). We also observed a concomitant decrease of CDC6 and pRB following

overexpression of BAP1 or BAP1C91S, and these effects required interaction with ASXL1/2. In contrast, no significant changes were observed on p16INK4a cell cycle inhibitor and the p53 E3 ligase MDM2.

Altogether, these results indicate that the fine balance between ASXL1/2 complexes and their coordination of BAP1 DUB activity are required for the proper progression of cell cycle and tumor suppression.

Discussion

We provided novel insights into the mechanisms by which the DUB activity and function of the tumor suppressor BAP1 are coordinated. First, we revealed that BAP1 and ASXL1/2 protein levels are tightly regulated by each other. Notably, BAP1 protein levels are nearly completely reduced following concomitant depletion of ASXL1 and ASXL2. This regulation is highly conserved since, in drosophila, deletion of ASX also destabilized dBAP1/Calypso (32). The fact that relatively similar protein amounts of ASXL1 and ASXL2 co-purified with mammalian BAP1 and that siRNA depletion of either ASXL1 or ASXL2 reduced BAP1 protein levels by approximately half, it is likely that BAP1/ASXL1 and BAP1/ASXL2 complexes coexist in the cells with a similar abundance. These complexes might exert distinct functions and/or compete for gene regulatory regions. We also found that depletion or loss of BAP1 destabilized ASXL2, but not ASXL1. These findings demonstrate for the first time the importance of complex assembly in maintaining proper protein levels of ASXL2, and hence its function in vivo. Thus, developmental or disease-associated inactivation or loss of expression of one component would result in a profound functional impact on the other partners. Indeed, loss of BAP1 in two tumor types of different histological origins, i.e., mesothelioma and non-small lung carcinoma, caused a severe reduction of ASXL2 protein levels. A survey of mutations in several cancers shows truncating mutations and deletions of BAP1 that would often result in the loss of the CTD and consequently ASXL1/2 interaction. Therefore, loss of ASXL2 function is a prevalent event in cancers with BAP1 mutations.

Similar to other post-translational modifications, ubiquitin recognition important roles in ubiquitin-dependent signaling (9). Often, UBDs involve distinct protein domains that engage interactions with the hydrophobic patches or other surfaces of ubiquitin and act as signal readers (9). Our study revealed that the CTD domain of BAP1 plays a central role in coordinating ubiquitin binding and catalysis by BAP1/ASXL1/2 complexes. First, the CTD is sufficient for binding a RQDR charged patch of ubiquitin and can be qualified as a bona fide UBD. Second, the CTD interacts with the CC1 and the UCH domains (31), and acts to stabilize the interaction of the ubiquitin with the catalytic domain. Third,

the CTD also strongly interacts with ASXM domain, and the latter induces ubiquitin binding by the CUBI and is required for catalysis. We also found that ASXM itself weakly bind ubiquitin, and hence probably participate in ubiquitin positioning. Thus, our data support a model whereby UCH, CC1, CTD and ASXM domains cooperate in order to generate an interface for stable binding with multiple ubiquitin patches, thus facilitating recruitment and specific substrate deubiquitination (Fig. 12). In support of our findings on BAP1/ASXL1/2, recent crystallography and molecular studies characterized the mechanism of activation of UCH37 by RPN13 (55,56). The most remarkable similarities with BAP1 are the conserved intramolecular interaction between the DEUBAD of RPN13 and the ULD of UCH37 and the stimulatory effect of RPN13 at the level of substrate binding. Moreover, highly conserved amino acid residues in BAP1 and UCH37, are required for the interaction with the hydrophobic patch of ubiquitin. Finally, similar to ASXM, the DEBUAD of RPN13 also establishes a weak interaction with ubiquitin (55,56). Thus, BAP1 and UCH37 share a highly conserved mechanism of cofactor-mediated DUB activation. Interestingly, INO80 chromatin remodeling factor also possesses a DEUBAD, and through molecular mimicry, this domain associates with and inhibits UCH37 (55,56). Of note, BAP1 also interacts with INO80 ATPase, a component of the INO80 chromatin remodeling complex, and promotes its deubiquitination (29). As INO80G (NFRKB) subunit of the complex inhibits UCHL5 through its DEUBAD, it will be interesting to determine whether, in specific contexts, this factor could also negatively regulate the DUB activity of BAP1.

Our protein complex purification studies indicated that deletion of BAP1 HBM domain does not interfere with BAP1 interaction with ASXL1/2. Conversely, mutation in CTD does not impact the interaction of BAP1 with HCF-1/OGT. Moreover, BAP1 complexes lacking HCF-1/OGT are competent in deubiquitinating nucleosomal histone H2A indicating that these components do not directly participate in ubiquitin binding and catalysis. Taking into account that dBAP1/Calypso does not possess the middle region which was acquired later in vertebrate evolution (32), HCF1/OGT and ASXL1/2 appear to define two functional axes of the BAP1 complexes. Notably, HCF-1 recruits chromatin modifying complexes including MLL family of histone H3K4 methyltransferases and Sin3/HDAC deacetylase complexes at gene regulatory regions (61,62). Thus, HCF1/OGT and ASXL1/2 exert distinct, but likely concerted, functions tethered by BAP1. Indeed, similar to HCF-1 interactions with BAP1 (22), ASXL1/2 association with this DUB also regulates cell proliferation.

To establish the significance of BAP1/ASXL1/2 complexes for tumor suppression, we conducted RNAi rescue studies, and showed that cancer-derived mutations that directly target BAP1/ASXL1/2 interaction result in a loss of DUB activity, increased H2Aub levels and deregulation of cell cycle progression. In addition, mutations that directly target the BAP1 catalytic site are frequently found in

cancer (11,13,20), and these mutations also result in increased H2Aub levels and deregulation of cell cycle control. These findings highlight the importance of the catalytic activity of BAP1/ASXL1/2 complexes for tumor suppression. Interestingly, overexpression of BAP1 or its catalytically dead form in primary human fibroblasts induced cellular senescence and up regulation of the p53/p21 DNA damage response in CTD-dependent manner, although more pronounced effects were observed for the catalytic inactive form of BAP1. It is currently unclear how both catalytically competent and inactive BAP1 promote cellular senescence. Nonetheless, as the catalytic dead BAP1 binds ubiquitin, it is possible that these effects are associated mostly with BAP1/ASXL1/2 binding to H2Aub rather than catalysis. Deregulation of H2Aub levels or its recognition might cause defects in transcriptional events (26), DNA double strand break repair (24) or replication fork progression (29), all of which could promote the induction of DNA damage and the p53 response and lead to genomic instability and cancer development. While further studies are needed to address these possibilities, our findings, nonetheless, suggest that the proper balance of BAP1/ASXL1/2 complexes and their coordinated binding to ubiquitinated substrates and/or DUB activity are essential for normal control of cell proliferation. Another interesting finding is that, overexpression of ASXL2, but not ASXL1, induces senescence in ASXM-dependent manner. Taking into account that ASXL2 and BAP1 form an obligate complex, our study delineates that ASXL2 plays an important role in regulating BAP1 function in cell proliferation. Moreover, a cancer-derived mutation of BAP1 that abolishes its interaction with ASXL1/2 prevents cellular senescence, further supporting the notion that the BAP1/ASXL2 signaling axis is important for tumor suppression.

Although, we cannot exclude that BAP1/ASXL1/2 target other known substrates such HCF-1 and OGT (19,23), our study and others provide strong support for the role of this DUB in the regulation of H2Aub levels and tumor suppression. Indeed (i) BAP1 was revealed as a major DUB for H2A in mammalian cells, (ii) several cancer mutations of BAP1 and ASXL2 target the UCH/CC1/CTD/ASXM platform, which is critical for ubiquitin binding and H2A deubiquitination, (iii) BAP1 null cancer cells display high H2Aub levels that could be reduced following reintroduction of BAP1, but not ASXL1/2 interaction-deficient mutants, (iv) both PcG proteins Ring1B and BMI1, two critical components of the PRC1 complex that catalyze H2A ubiquitination, regulate cell proliferation and are overexpressed in cancer (63-65). Thus, our study provides further insights into the potential involvement of H2Aub in tumorigenesis.

References

1. MacGurn, J. A., Hsu, P. C., and Emr, S. D. (2012) Ubiquitin and membrane protein turnover: from cradle to grave. Annual review of biochemistry 81, 231-259

2. Nakayama, K. I., and Nakayama, K. (2006) Ubiquitin ligases: cell-cycle control and cancer. Nature reviews. Cancer 6, 369-381

3. Komander, D., and Rape, M. (2012) The ubiquitin code. Annu Rev Biochem 81, 203-229

4. Hammond-Martel, I., Yu, H., and Affar el, B. (2012) Roles of ubiquitin signaling in transcription regulation. Cellular signalling 24, 410-421

5. Jackson, S. P., and Durocher, D. (2013) Regulation of DNA damage responses by ubiquitin and SUMO. Molecular cell 49, 795-807

6. Metzger, M. B., Hristova, V. A., and Weissman, A. M. (2012) HECT and RING finger families of E3 ubiquitin ligases at a glance. Journal of cell science 125, 531-537

7. Reyes-Turcu, F. E., Ventii, K. H., and Wilkinson, K. D. (2009) Regulation and cellular roles of ubiquitin-specific deubiquitinating enzymes. Annu Rev Biochem 78, 363-397

8. Eletr, Z. M., and Wilkinson, K. D. (2014) Regulation of proteolysis by human deubiquitinating enzymes. Biochimica et biophysica acta 1843, 114-128

9. Husnjak, K., and Dikic, I. (2012) Ubiquitin-binding proteins: decoders of ubiquitin-mediated cellular functions. Annu Rev Biochem 81, 291-322

10. Murali, R., Wiesner, T., and Scolyer, R. A. (2013) Tumours associated with BAP1 mutations. Pathology 45, 116-126

11. Carbone, M., Yang, H., Pass, H. I., Krausz, T., Testa, J. R., and Gaudino, G. (2013) BAP1 and cancer. Nature reviews. Cancer 13, 153-159

12. Jensen, D. E., Proctor, M., Marquis, S. T., Gardner, H. P., Ha, S. I., Chodosh, L. A., Ishov, A. M., Tommerup, N., Vissing, H., Sekido, Y., Minna, J., Borodovsky, A., Schultz, D. C., Wilkinson, K. D., Maul, G. G., Barlev, N., Berger, S. L., Prendergast, G. C., and Rauscher, F. J., 3rd. (1998) BAP1: a novel ubiquitin hydrolase which binds to the BRCA1 RING finger and enhances BRCA1-mediated cell growth suppression. Oncogene 16, 1097-1112

13. Harbour, J. W., Onken, M. D., Roberson, E. D., Duan, S., Cao, L., Worley, L. A., Council, M. L., Matatall, K. A., Helms, C., and Bowcock, A. M. (2010) Frequent mutation of BAP1 in metastasizing uveal melanomas. Science 330, 1410-1413

14. Abdel-Rahman, M. H., Pilarski, R., Cebulla, C. M., Massengill, J. B., Christopher, B. N., Boru, G., Hovland, P., and Davidorf, F. H. (2011) Germline BAP1 mutation predisposes to uveal melanoma, lung adenocarcinoma, meningioma, and other cancers. J Med Genet

15. Bott, M., Brevet, M., Taylor, B. S., Shimizu, S., Ito, T., Wang, L., Creaney, J., Lake, R. A., Zakowski, M. F., Reva, B., Sander, C., Delsite, R., Powell, S., Zhou, Q., Shen, R., Olshen, A., Rusch, V., and Ladanyi, M. (2011) The nuclear deubiquitinase BAP1 is commonly inactivated by somatic mutations and 3p21.1 losses in malignant pleural mesothelioma. Nature genetics 43, 668-672

16. Goldstein, A. M. (2011) Germline BAP1 mutations and tumor susceptibility. Nature genetics 43, 925-926

17. Testa, J. R., Cheung, M., Pei, J., Below, J. E., Tan, Y., Sementino, E., Cox, N. J., Dogan, A. U., Pass, H. I., Trusa, S., Hesdorffer, M., Nasu, M., Powers, A., Rivera, Z., Comertpay, S., Tanji, M., Gaudino, G., Yang, H., and Carbone, M. (2011) Germline BAP1 mutations predispose to malignant mesothelioma. Nature genetics 43, 1022-1025

18. Wiesner, T., Obenauf, A. C., Murali, R., Fried, I., Griewank, K. G., Ulz, P., Windpassinger, C., Wackernagel, W., Loy, S., Wolf, I., Viale, A., Lash, A. E., Pirun, M., Socci, N. D., Rutten, A., Palmedo, G., Abramson, D., Offit, K., Ott, A., Becker, J. C., Cerroni, L., Kutzner, H., Bastian, B. C., and Speicher, M. R. (2011) Germline mutations in BAP1 predispose to melanocytic tumors. Nature genetics 43, 1018-1021

19. Dey, A., Seshasayee, D., Noubade, R., French, D. M., Liu, J., Chaurushiya, M. S., Kirkpatrick, D. S., Pham, V. C., Lill, J. R., Bakalarski, C. E., Wu, J., Phu, L., Katavolos, P., LaFave, L. M., Abdel-Wahab, O., Modrusan, Z., Seshagiri, S., Dong, K., Lin, Z., Balazs, M., Suriben, R., Newton, K., Hymowitz, S., Garcia-Manero, G., Martin, F., Levine, R. L., and Dixit, V. M. (2012) Loss of the tumor suppressor BAP1 causes myeloid transformation. Science 337, 1541-1546

20. Pena-Llopis, S., Vega-Rubin-de-Celis, S., Liao, A., Leng, N., Pavia-Jimenez, A., Wang, S., Yamasaki, T., Zhrebker, L., Sivanand, S., Spence, P., Kinch, L., Hambuch, T., Jain, S., Lotan, Y., Margulis, V., Sagalowsky, A. I., Summerour, P. B., Kabbani, W., Wong, S. W., Grishin, N., Laurent, M., Xie, X. J., Haudenschild, C. D., Ross, M. T., Bentley, D. R., Kapur, P., and Brugarolas, J. (2012) BAP1 loss defines a new class of renal cell carcinoma. Nature genetics 44, 751-759

21. Ventii, K. H., Devi, N. S., Friedrich, K. L., Chernova, T. A., Tighiouart, M., Van Meir, E. G., and Wilkinson, K. D. (2008) BRCA1-associated protein-1 is a tumor suppressor that requires deubiquitinating activity and nuclear localization. Cancer research 68, 6953-6962

22. Machida, Y. J., Machida, Y., Vashisht, A. A., Wohlschlegel, J. A., and Dutta, A. (2009) The deubiquitinating enzyme BAP1 regulates cell growth via interaction with HCF-1. The Journal of biological chemistry

23. Misaghi, S., Ottosen, S., Izrael-Tomasevic, A., Arnott, D., Lamkanfi, M., Lee, J., Liu, J., O'Rourke, K., Dixit, V. M., and Wilson, A. C. (2009) Association of C-terminal ubiquitin hydrolase BRCA1-associated protein 1 with cell cycle regulator host cell factor 1. Molecular and cellular biology 29, 2181-2192

24. Yu, H., Pak, H., Hammond-Martel, I., Ghram, M., Rodrigue, A., Daou, S., Barbour, H., Corbeil, L., Hebert, J., Drobetsky, E., Masson, J. Y., Di Noia, J. M., and Affar el, B. (2014) Tumor suppressor and deubiquitinase BAP1 promotes DNA double-strand break repair. Proceedings of the National Academy of Sciences of the United States of America 111, 285-290

25. Sowa, M. E., Bennett, E. J., Gygi, S. P., and Harper, J. W. (2009) Defining the human deubiquitinating enzyme interaction landscape. Cell 138, 389-403

26. Yu, H., Mashtalir, N., Daou, S., Hammond-Martel, I., Ross, J., Sui, G., Hart, G. W., Rauscher, F. J., 3rd, Drobetsky, E., Milot, E., Shi, Y., and Affar, E. B. (2010) The Ubiquitin Carboxyl Hydrolase BAP1 Forms a Ternary Complex with YY1 and HCF-1 and is a Critical Regulator of Gene Expression. Molecular and cellular biology

27. Pan, H., Jia, R., Zhang, L., Xu, S., Wu, Q., Song, X., Zhang, H., Ge, S., Leon Xu, X., and Fan, X. (2015) BAP1 regulates cell cycle progression through E2F1 target genes and mediates transcriptional silencing via H2A monoubiquitination in uveal melanoma cells. The international journal of biochemistry & cell biology 60C, 176-184

28. Ismail, I. H., Davidson, R., Gagne, J. P., Xu, Z. Z., Poirier, G., and Hendzel, M. J. (2014) Germline Mutations in BAP1 Impair its Function in DNA Double-Strand break Repair. Cancer research

29. Lee, H. S., Lee, S. A., Hur, S. K., Seo, J. W., and Kwon, J. (2014) Stabilization and targeting of INO80 to replication forks by BAP1 during normal DNA synthesis. Nature communications 5, 5128

30. Eletr, Z. M., Yin, L., and Wilkinson, K. D. (2013) BAP1 is phosphorylated at serine 592 in S-phase following DNA damage. FEBS letters 587, 3906-3911

31. Mashtalir, N., Daou, S., Barbour, H., Sen, N. N., Gagnon, J., Hammond-Martel, I., Dar, H. H., Therrien, M., and Affar el, B. (2014) Autodeubiquitination protects the tumor suppressor BAP1 from cytoplasmic sequestration mediated by the atypical ubiquitin ligase UBE2O. Molecular cell 54, 392-406

32. Scheuermann, J. C., de Ayala Alonso, A. G., Oktaba, K., Ly-Hartig, N., McGinty, R. K., Fraterman, S., Wilm, M., Muir, T. W., and Muller, J. (2010) Histone H2A deubiquitinase activity of the Polycomb repressive complex PR-DUB. Nature 465, 243-247

33. Wang, H., Wang, L., Erdjument-Bromage, H., Vidal, M., Tempst, P., Jones, R. S., and Zhang, Y. (2004) Role of histone H2A ubiquitination in Polycomb silencing. Nature 431, 873-878

34. Milne, T. A., Sinclair, D. A., and Brock, H. W. (1999) The Additional sex combs gene of Drosophila is required for activation and repression of homeotic loci, and interacts specifically with Polycomb and super sex combs. Molecular & general genetics : MGG 261, 753-761

35. Gildea, J. J., Lopez, R., and Shearn, A. (2000) A screen for new trithorax group genes identified little imaginal discs, the Drosophila melanogaster homologue of human retinoblastoma binding protein 2. Genetics 156, 645-663

36. Cho, Y. S., Kim, E. J., Park, U. H., Sin, H. S., and Um, S. J. (2006) Additional sex comb-like 1 (ASXL1), in cooperation with SRC-1, acts as a ligand-dependent coactivator for retinoic acid receptor. The Journal of biological chemistry 281, 17588-17598

37. Lee, S. W., Cho, Y. S., Na, J. M., Park, U. H., Kang, M., Kim, E. J., and Um, S. J. (2010) ASXL1 represses retinoic acid receptor-mediated transcription through associating with HP1 and LSD1. The Journal of biological chemistry 285, 18-29

38. Park, U. H., Yoon, S. K., Park, T., Kim, E. J., and Um, S. J. (2011) Additional sex comb-like (ASXL) proteins 1 and 2 play opposite roles in adipogenesis via reciprocal regulation of peroxisome proliferator-activated receptor {gamma}. The Journal of biological chemistry 286, 1354-1363

39. Abdel-Wahab, O., Adli, M., LaFave, L. M., Gao, J., Hricik, T., Shih, A. H., Pandey, S., Patel, J. P., Chung, Y. R., Koche, R., Perna, F., Zhao, X., Taylor, J. E., Park, C. Y., Carroll, M., Melnick, A., Nimer, S. D., Jaffe, J. D., Aifantis, I., Bernstein, B. E., and Levine, R. L. (2012) ASXL1 mutations promote myeloid transformation through loss of PRC2-mediated gene repression. Cancer cell 22, 180-193

40. Okino, Y., Machida, Y., Frankland-Searby, S., and Machida, Y. J. (2015) BRCA1-associated protein 1 (BAP1) deubiquitinase antagonizes the ubiquitin-mediated activation of FoxK2 target genes. The Journal of biological chemistry 290, 1580-1591

41. Fisher, C. L., Randazzo, F., Humphries, R. K., and Brock, H. W. (2006) Characterization of Asxl1, a murine homolog of Additional sex combs, and analysis of the Asx-like gene family. Gene 369, 109-118

42. Yao, T., Song, L., Xu, W., Demartino, G. N., Florens, L., Swanson, S. K., Washburn, M. P., Conaway, R. C., Conaway, J. W., and Cohen, R. E. (2006) Proteasome recruitment and activation of the Uch37 deubiquitinating enzyme by Adrm1. Nature cell biology

43. Qiu, X. B., Ouyang, S. Y., Li, C. J., Miao, S., Wang, L., and Goldberg, A. L. (2006) hRpn13/ADRM1/GP110 is a novel proteasome subunit that binds the deubiquitinating enzyme, UCH37. The EMBO journal 25, 5742-5753

44. Hamazaki, J., Iemura, S., Natsume, T., Yashiroda, H., Tanaka, K., and Murata, S. (2006) A novel proteasome interacting protein recruits the deubiquitinating enzyme UCH37 to 26S proteasomes. The EMBO journal 25, 4524-4536

45. Sanchez-Pulido, L., Kong, L., and Ponting, C. P. (2012) A common ancestry for BAP1 and Uch37 regulators. Bioinformatics 28, 1953-1956

46. Katoh, M. (2013) Functional and cancer genomics of ASXL family members. British journal of cancer

47. Balasubramani, A., Larjo, A., Bassein, J. A., Chang, X., Hastie, R. B., Togher, S. M., Lahdesmaki, H., and Rao, A. (2015) Cancer-associated ASXL1 mutations may act as gain-of-function mutations of the ASXL1-BAP1 complex. Nature communications 6, 7307

48. Minsky, N., and Oren, M. (2004) The RING domain of Mdm2 mediates histone ubiquitylation and transcriptional repression. Molecular cell 16, 631-639

49. Hammond-Martel, I., Pak, H., Yu, H., Rouget, R., Horwitz, A. A., Parvin, J. D., Drobetsky, E. A., and Affar el, B. (2010) PI 3 kinase related kinases-independent proteolysis of BRCA1 regulates Rad51 recruitment during genotoxic stress in human cells. PloS one 5, e14027

50. Daou, S., Mashtalir, N., Hammond-Martel, I., Pak, H., Yu, H., Sui, G., Vogel, J. L., Kristie, T. M., and Affar el, B. (2011) Crosstalk between O-GlcNAcylation and proteolytic cleavage regulates the host cell factor-1 maturation pathway. Proceedings of the National Academy of Sciences of the United States of America 108, 2747-2752

51. Lee, J. W., Lee, K. F., Hsu, H. Y., Hsu, L. P., Shih, W. L., Chu, Y. C., Hsiao, W. T., and Liu, P. F. (2007) Protein expression and intracellular localization of prostate apoptosis response-4 (Par-4) are associated with apoptosis induction in nasopharyngeal carcinoma cell lines. Cancer letters 257, 252-262

52. Ji, Z., Mohammed, H., Webber, A., Ridsdale, J., Han, N., Carroll, J. S., and Sharrocks, A. D. (2014) The forkhead transcription factor FOXK2 acts as a chromatin targeting factor for the BAP1-containing histone deubiquitinase complex. Nucleic acids research 42, 6232-6242

53. Belle, J. I., and Nijnik, A. (2014) H2A-DUBbing the mammalian epigenome: expanding frontiers for histone H2A deubiquitinating enzymes in cell biology and physiology. The international journal of biochemistry & cell biology 50, 161-174

54. Morrow, M. E., Kim, M. I., Ronau, J. A., Sheedlo, M. J., White, R. R., Chaney, J., Paul, L. N., Lill, M. A., Artavanis-Tsakonas, K., and Das, C. (2013) Stabilization of an unusual salt bridge in ubiquitin by the extra C-terminal domain of the proteasome-associated deubiquitinase UCH37 as a mechanism of its exo specificity. Biochemistry 52, 3564-3578

55. Sahtoe, D. D., van Dijk, W. J., El Oualid, F., Ekkebus, R., Ovaa, H., and Sixma, T. K. (2015) Mechanism of UCH-L5 activation and inhibition by DEUBAD domains in RPN13 and INO80G. Molecular cell 57, 887-900

56. VanderLinden, R. T., Hemmis, C. W., Schmitt, B., Ndoja, A., Whitby, F. G., Robinson, H., Cohen, R. E., Yao, T., and Hill, C. P. (2015) Structural basis for the activation and inhibition of the UCH37 deubiquitylase. Molecular cell 57, 901-911

57. Nishikawa, H., Wu, W., Koike, A., Kojima, R., Gomi, H., Fukuda, M., and Ohta, T. (2009) BRCA1-associated protein 1 interferes with BRCA1/BARD1 RING heterodimer activity. Cancer research 69, 111-119

58. Jacobs, J. J., Kieboom, K., Marino, S., DePinho, R. A., and van Lohuizen, M. (1999) The oncogene and Polycomb-group gene bmi-1 regulates cell proliferation and senescence through the ink4a locus. Nature 397, 164-168

59. Dietrich, N., Bracken, A. P., Trinh, E., Schjerling, C. K., Koseki, H., Rappsilber, J., Helin, K., and Hansen, K. H. (2007) Bypass of senescence by the polycomb group protein CBX8 through direct binding to the INK4A-ARF locus. The EMBO journal 26, 1637-1648

60. Luis, N. M., Morey, L., Mejetta, S., Pascual, G., Janich, P., Kuebler, B., Cozutto, L., Roma, G., Nascimento, E., Frye, M., Di Croce, L., and Benitah, S. A. (2011) Regulation of human epidermal stem cell proliferation and senescence requires polycomb- dependent and -independent functions of Cbx4. Cell stem cell 9, 233-246

61. Wysocka, J., Myers, M. P., Laherty, C. D., Eisenman, R. N., and Herr, W. (2003) Human Sin3 deacetylase and trithorax-related Set1/Ash2 histone H3-K4 methyltransferase are tethered together selectively by the cell-proliferation factor HCF-1. Genes & development 17, 896-911

62. Tyagi, S., Chabes, A. L., Wysocka, J., and Herr, W. (2007) E2F activation of S phase promoters via association with HCF-1 and the MLL family of histone H3K4 methyltransferases. Molecular cell 27, 107-119

63. Leung, C., Lingbeek, M., Shakhova, O., Liu, J., Tanger, E., Saremaslani, P., Van Lohuizen, M., and Marino, S. (2004) Bmi1 is essential for cerebellar development and is overexpressed in human medulloblastomas. Nature 428, 337-341

64. Xu, F., Li, X., Wu, L., Zhang, Q., Yang, R., Yang, Y., Zhang, Z., He, Q., and Chang, C. (2011) Overexpression of the EZH2, RING1 and BMI1 genes is common in myelodysplastic syndromes: relation to adverse epigenetic alteration and poor prognostic scoring. Annals of hematology 90, 643-653

65. Bosch, A., Panoutsopoulou, K., Corominas, J. M., Gimeno, R., Moreno-Bueno, G., Martin-Caballero, J., Morales, S., Lobato, T., Martinez-Romero, C., Farias, E. F., Mayol, X., Cano, A., and Hernandez-Munoz, I. (2014) The Polycomb group protein RING1B is overexpressed in ductal breast carcinoma and is required to sustain FAK steady state levels in breast cancer epithelial cells. Oncotarget 5, 2065-2076.

Acknowledgements

We thank Yang Shi for support, Haider Dar, Sarah Hadj-Mimoune, Diana Adjaoud and Marie-Anne Germain for technical assistance. *This work was supported by grants from the Canadian Institutes of Health Research (CIHR) (MOP-115132) and the Natural Sciences and Engineering Research Council of Canada (355814-2010) to E.B.A, and CIHR to F.A.M (MOP-133442). E.B.A. is a scholar of the Fonds de la Recherche du Québec - Santé (FRQ-S)

and the CIHR. H.W. and F.A.M. are Scholars of the FRQ-S. S.D. had a PhD scholarship from the Islamic Bank for Development. H.Y. had a PhD scholarship from the CIHR. H.B has a PhD scholarship from the Ministry of Higher Education and from Scientific Research of Tunisia and the Cole Foundation. J.G has a M.Sc. scholarship from the FRQ-S. H.Y. had a PhD scholarship from the CIHR.

[1]To whom correspondence may be addressed**:** Maisonneuve-Rosemont Hospital Research Center and Department of Medicine, University of Montréal, Montréal H3C 3J7, Québec, Canada, Tel.: (1) 514 252 3400 (EXT: 3343); Fax: (1) 514 252 3430;

Experimental Procedures

Plasmids

Plasmids-Retroviral constructs pOZ-N-Flag-HA-BAP1, pOZ-N-Flag-HA-BAP1 C91S (catalytic dead) and pOZ-N-Flag-HA-BAP1ΔHBM (BAP1 mutant deleted in the NHNY sequence corresponding to the HCF-1 binding motif); constructs to produce recombinant full-length GST-BAP1 and various deleted forms; pET30a+ BAP1 for production of His-tagged BAP1 were previously described (26). pCDNA3-Flag-H2A was obtained from Moshe Oren (48). pOZ-N-Flag-HA-BAP1 ΔCTD1 and pOZ-N-Flag-HA-BAP1 ΔCC2 were generated by PCR-based subcloning. Non-tagged pCDNA3-BAP1 and pCDNA3-BAP1-C91S were generated by subcloning the cDNAs from pOZ-N-Flag-HA-BAP1 and pOZ-N-Flag-HA-BAP1-C91S respectively. siRNA resistant constructs for BAP1, BAP1-C91S, BAP1 ΔCTD, BAP1R666-H669 were generated using gene synthesis (BioBasic) and then subcloned into modified pENTR D-Topo plasmid (Life Technologies). Expression constructs of siRNA resistant BAP1, BAP1 C91S, BAP1 ΔCTD and BAP1 ΔR666-H669 were generated by recombination using LR clonase kit (Life Technologies) into pMSCV-Flag-HA-IRES-Puro or pDEST-Myc constructs (25). BAP1ΔUCH, BAP1ΔCC1 and BAP1ΔCTD were described (31), and were sub-cloned by PCR into pENTR. Ubiquitin constructs (Ub wild type, Ub VLI (V70A/L8A/I44A), Ub I36A, Ub I44A, Ub D58A) flanked by att-B and att-P recombination sites were generated by gene synthesis (Life technologies) directly into pMK-Rq plasmid and bacterial expression constructs were generated by recombination into pDEST-GST. Other Ubiquitin mutants constructs (Ub TEK (K6A/L11A/T12A/T14A/E34A), Ub Il36 patch (L8A/I36A/L71A/L73A), Ub IL44 patch (L8A/L44A/H68A/V70A), Ub Phe4 patch (Q2A/F4A/T14A), Ub (Q49A/R72A), Ub (R42A/Q49A/D52A/R72A)) flanked by att-B and att-P recombination sites were generated by gene synthesis (Biobasic) directly into pUC57-Kan Vector and bacterial expression constructs were generated by recombination into pDEST-GST. Human cDNA

ASXL1 (NCBI: NM_015338.5) and ASXL2 (NCBI: NM_018263.4) were cloned from HeLa total RNA by reverse transcription and inserted into pENTR D-Topo plasmid. BAP1 point mutations constructs were generated by site direct mutagenesis in pENTR D-Topo BAP1 using PfuUltra High-Fidelity DNA Polymerase. Human Myc-ASXL1 ΔASXM and Myc-ASXL2 ΔASXM constructs were generated by PCR-based subcloning of 2 fragments each ligated in frame into pENTR D-Topo. Expression constructs of ASXL1, ASXL2 and corresponding vectors with deletions of ASXM were generated in pDEST-Myc and pDEST-Flag. Other expression constructs for BAP1 and corresponding mutants forms, were generated using LR clonase in pDEST-Myc, pDEST-Flag and bacterial pDEST-His. Full length ASXM1 and ASXM2 and deletions mutants forms of ASXM2 (ASXM2 246-313, ASXM2 300-401, ASXM2 316-401, ASXM2 246-347) were sub-cloned by PCR and inserted into pENTR D-Topo plasmid. ASXM2 point mutations constructs were generated by site direct mutagenesis in pENTR D-Topo ASXM2. Bacterial expression vectors of ASXM1, ASXM2 and respective mutant forms were generated in pDEST-GST and pDEST-MBP vectors. Human PAR-4 was cloned in-frame with GFP in pCDNA3 using PCR.

Cell culture and cell transfection

Primary human skin fibroblasts (LF1), BAP1-deficient human lung squamous carcinoma NCI-H226, BAP1-deficient human mesothelioma NCI-H28, U2OS osteosarcoma, human embryonic kidney HEK293T (293T), Cervical cancer HeLa, normal Human Lung Fibroblasts (IMR90), phoenix ampho and 293-GPG packaging cells were cultured in Dulbecco's modified Eagle's medium (DMEM) supplemented with foetal bovine serum (FBS), L-glutamine and penicillin/streptomycin. HeLa S3 cells were cultured in Minimum Essential Media (MEM) supplemented with FBS, L-glutamine and penicillin/streptomycin.

293T cells were transfected with the mammalian expressing vectors using polyethylenimine (PEI) (Sigma-Aldrich). Three days post-transfection, cells were harvested for immunoblotting, immunoprecipitation or immunostaining.

Similar numbers of H226 BAP1-null cells stably expressing BAP1, BAP1C91S or BAP1R666-H669 were seeded on the plates and cultured for 5 days. The clonogenic survival assay was essentially done as described before (24).

U2OS or LF1 cells were transfected using Lipofectamine 2000 (Life technologies) with 200 pmol of either ON-TARGET plus Non-targeting pool (D-001810) or ON-TARGET plus SMARTpool BAP1 (L-005791) (Thermo Scientific, Dharmacon) or with a pool of siRNA

sequences purchased from Sigma-Aldrich targeting ASXL1 (pool of 4 oligonucleotides, SASI_Hs02_00347642, SASI_Hs01_00200507, SASI_Hs01_00200508, SASI_Hs01_00200509) and ASXL2 (2 pools of 4 oligonucleotides, SASI_Hs01_00202197, SASI_Hs01_00202198, SASI_Hs01_00202199, SASI_Hs01_00202200 and SASI_Hs01_00202197, SASI_Hs01_00202200, SASI_Hs01_00202203, SASI_Hs01_00202201). Four days post-transfection, cells were harvested for immunoblotting

siRNA DUB screen

HeLa cells were transfected with individual siRNA pool targeting DUBs (ON-TARGETplus® SMARTpool® siRNA Library-Human Deubiquitinating Enzymes) using Lipofectamine 2000 (Life Technologies). Three days post-transfection, cells were fixed and used for immunostaining with H2Aub antibody and the fluorescence signals were detected with a Fluoroskan Ascent™ Microplate Fluorometer (Thermo Scientific), and the obtained values were used to derive the Z-scores. The screen was done in duplicate and the values of H2Aub signals were normalized to DAPI staining.

qRT-PCR analysis of mRNA expression

Total RNA was used to prepare the cDNAs as described (26). The cDNAs were analyzed by Real time PCR using SYBR Green detection DNA quantification kit (Life technologies) to determine levels of gene mRNAs. PCR was conducted on an Applied Biosystems® 7500 Real-Time PCR Systems (Life Technologies). To ensure accurate quantification of mRNA, similar amounts of total RNA were spiked with an in vitro synthesized GAL4 mRNA, which was performed following the manufacturer procedure (MAXIscript Kit Procedure, Life Technologies). The transcript was synthesized from pcDNA.3-GAL4 construct with T7 promoter. The primers used are listed below. hASXL2-F: GAATCCAGGTGCGAAAAGTAC and hASXL2-R: GATGGAGACTGGAAAACGAGC and GAL4-F: CAACTGGGAGTGTCGCTACT, and GAL4-R: AATCATGTCAAGGTCTTCTCGA

Immunoblotting and antibodies

Total cell extracts were used for SDS-PAGE and immunoblotting was done according to standard procedures (26). The band signals were acquired with a LAS-3000 LCD camera coupled to MultiGauge software (Fuji, Stamford, CT, USA). Anti-FOXK2 rabbit polyclonal

antibody was previously described (31). The rabbit polyclonal antibody anti-ASXL1 was generated using bacteria-expressed fragment (700-950 amino acids of the human protein) with Pacific Immunology. Mouse monoclonal anti-BAP1 (C4, sc-28383), rabbit polyclonal anti-BAP1 (H300, sc-28236), rabbit polyclonal anti-YY1 (H414, sc-1703), rabbit polyclonal anti-OGT (H300, sc-32921), mouse monoclonal anti-CDC6 (180.2, sc-9964), mouse monoclonal anti-MCM6, mouse monoclonal anti-tubulin (B-5-1-2, sc-SC-23948), mouse monoclonal anti-p53 (DO-1, sc-126), mouse monoclonal anti-p16 (JC8, sc-56330), mouse monoclonal anti-MDM2 (SMP14, sc-965), rabbit polyclonal anti-FOXK1 (H-140, sc-134550), and mouse monoclonal anti-PARP1 (F2, sc-8007) were from Santa Cruz. Rabbit polyclonal anti-HCF-1 (A301-400A) and rabbit polyclonal anti-ASXL2 (A302-037A) were from Bethyl Laboratories. Mouse monoclonal anti-p21 (55643) was from BD Pharmigen. Mouse monoclonal anti-Flag (M2) and rabbit polyclonal anti-GST (G7781) were from Sigma-Aldrich. Mouse monoclonal anti-MYC (9E10) was from Covance. Rabbit polyclonal anti-H2Aub K119 (D27C4) rabbit polyclonal anti-H2Bub K120 (D11 XP), mouse monoclonal anti-RB (4H1), rabbit polyclonal anti-pRB (S807/811) and mouse monoclonal (HRP conjugated) anti-MBP (E8038) were from Cell Signaling. Mouse monoclonal anti-H2Bub antibody (NRO3) was from MEDIMABS. Mouse monoclonal anti-Phospho-H2AX (ser139) (clone JBW301, 05-636), Mouse monoclonal anti-H2Bub antibody clone 56 (05-1312), Mouse monoclonal anti-H2Aub K119 antibody clone E6C5 (05-678) and mouse monoclonal anti-□-Actin (MAB1501, clone C4) were from Millipore.

Immunodepletion and Immunoprecipitation

Immunodepletion experiments were done as described (26). Reciprocal immunoprecipitation from the BAP1 complexes was conducted essentially as described (31). Briefly, the purified BAP1 complexes were incubated with the indicated antibodies overnight at 4 ºC. The immuno-depleted complexes were recovered next day with protein G sepharose beads saturated with 1% BSA. Co-immunoprecipitation was conducted as described (26).

Cell lines with stable expression and protein complex purification

HeLa S3 cell lines stably expressing Flag-HA-BAP1, Flag-HA-BAP1ΔCTD1, or Flag-HA-BAP1R666-H669, H28 cell lines stably expressing Flag-HA-BAP1 and Flag-HA-BAP1C91S, as well as H226 cell lines stably expressing Flag-HA-BAP1, Flag-HA-BAP1C91S and Flag-HA- BAP1R666-H669 were generated following retroviral infection using pOZ-N-Flag-HA-

IRES-IL2R retroviral constructs and selection using anti-IL2 magnetic beads (Life Technologies) (26). U2OS expressing siRNA resistant Flag-HA-BAP1, Flag-HA-BAP1C91S, Flag-HA-BAP1 ΔCTD and Flag-HA- BAP1R666-H669 were generated following retroviral infection using pMSCV-Flag-HA-IRES-Puro based constructs and selection with 3 μg/ml of puromycin. Around 3 X 109 of HeLa S3 cells were used for the immunoaffinity purification of the different BAP1 complexes. The purification was done as previously described (31). Eluted complexes were used for silver stain, western blot analysis and in vitro ubiquitin pulldown and DUB assays.

In vitro interaction assays

Protein interaction pull down assays were conducted as previously described (26).

Ubiquitin pull down interaction assays

GST-ubiquitin immobilized beads and its corresponding mutant forms were purified using glutathione agarose beads. For the Ubiquitin-Agarose pull down interaction assays, His-BAP1 or the corresponding mutant forms (1.6 μg, 20 nM) were pre-incubated for 30 min to 1 hour with GST-ASXM1 or GST-ASXM2 (2 μg each, 50 nM) or GST-ASXM2 deletion mutant forms at 4 ºC in 50 mM Tris, pH 7.5; 150 mM NaCl; 1% Triton; 1 mM PMSF, protease inhibitors cocktail and 2 mM DTT. The mix was incubated for 3 hours with Ubiquitin-Agarose beads (Boston Biochem) which were then washed 6 times with the same buffer. The associated proteins were eluted in Laemmli buffer and subjected to western blotting. For the GST-Ubiquitin (GST-Ub) pull down interaction assays, His-BAP1 or His-BAP1 C91S or the recombinant BAP1 deletion mutants (1.6 μg, 20 nM) were pre-incubated for 30 min to 1 hour with either MBP-ASM2 or its corresponding mutant forms (2 μg, 30 nM). The mix was then incubated overnight with either GST-Ubiquitin immobilized beads or mutant forms (3 μg, 80 nM). The beads were washed 6 times with the same buffer and the associated proteins were subjected to western blotting. For the GST-Ubiquitin (GST-Ub) pull down interaction assays using MBP-ASXM2 (2 μg, 30 nM) or MBP-CTD (3 μg, 40 nM), the purified proteins were incubated for 16 hours with GST-Ubiquitin immobilized beads (3 μg, 80 nM). The beads were washed 6 times with the same buffer and the associated proteins were subjected to western blotting.

Purification of the nucleosomes and in vitro DUB assay

Native nucleosomes were purified as described (24). The purified nucleosomes were used for the in vitro DUB assay using either Flag-HA purified BAP1 complexes or bacteria-purified His-BAP1 (8 ng, 2 pM) with or without bacteria purified GST-ASXM1/2 (10 ng, 4 pM) or MBP-ASXM2 (10 ng, 2,8 pM) as described (24). The DUB reaction was carried out in the reaction buffer (50 mM Tris-HCl, pH 7.3; 1 mM MgCl2; 50 mM NaCl; 1 mM DTT) for the indicated times at 37°C. The in vitro reaction was stopped by adding Laemmli buffer and analyzed by immunoblotting.

Synchronization and cell cycle analysis

U2OS cells were synchronized at the G1/S border using the method of thymidine (2 mM) double block and analyzed by flow cytometry as described previously (49).

Immunofluorescence

The immunostaining procedure was carried as previously described (50).

Protein sequence analysis and structure modeling-Conservation of protein sequences was determined using Geneious 6.1.2 (Biomatters, http://www.geneious.com). The ubiquitin resolved 3D structure PDB file (1UBQ) was downloaded from the PDB database (http://www.rcsb.org/pdb/home/home.do). We used the Chimera software (UCSF Chimera V 1.10) to visualize the 3D structure and to highlight different ubiquitin interfaces.

Statistical Analysis

Most experiments were conducted at least three times. Quantifications were done for a representative experiment. DUB RNAi screen was conducted once. Cell counts for senescence studies were derived from one representative experiment and are shown as average with standard deviation.

A

ASXL1	ASXL2
Peptides sequences	Peptides sequences
18 RLVLENYSDAPMTPKQ 33	32 KEILQVKQRE 41
32 KQILQVIEAEGLKEMRF 47	237 KVENTLLGLGKK 248
65 RGGEGLFYKLPGRI 78	302 RLLLLLPEVDRQ 313
77 RISLFTLKKD 86	342 RLSEGEFTPEMQVRI 356
218 RGQAEVTQDPAPLLRG 233	410 KSMPVSEASLIR1 422
244 RNRGEEIDFETPGSILVNTNLRA 266	639 RARFPVSITSPNRT 652
323 RLADGEFTHEMQVRI 337	978 KTVPLTAKEERG 989
362 KLGLTKEESLQQNVGQEEAEIKS 384	988 RGMGALIATNTTENSTRE 1005
489 RIQAEPDNLARA 500	1060 KATQDQILQTLIQRV 1074
1247 RAMSQDSNSNAAPGKSPGDLTTSRT 1271	1217 RETLSTSDCLASKN 1230
1273 RFSSPNMSFGPEQTGRA 1290	1259 KTLARDLIQAAQKQ 1272
1337 KLGPSTNSMSGGVQTPRE 1354	1315 KLYGSPTQIGPSYRG 1329
1419 KGLSEPLEPSSLPSQLSIKQ 1438	1426 KLCVSCLWR 1435
1446 KLQLSSTSFNYSSSSPTFPKG 1466	

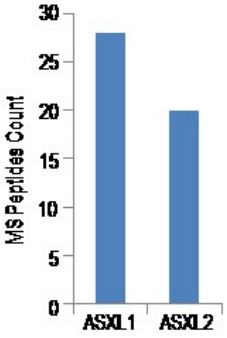

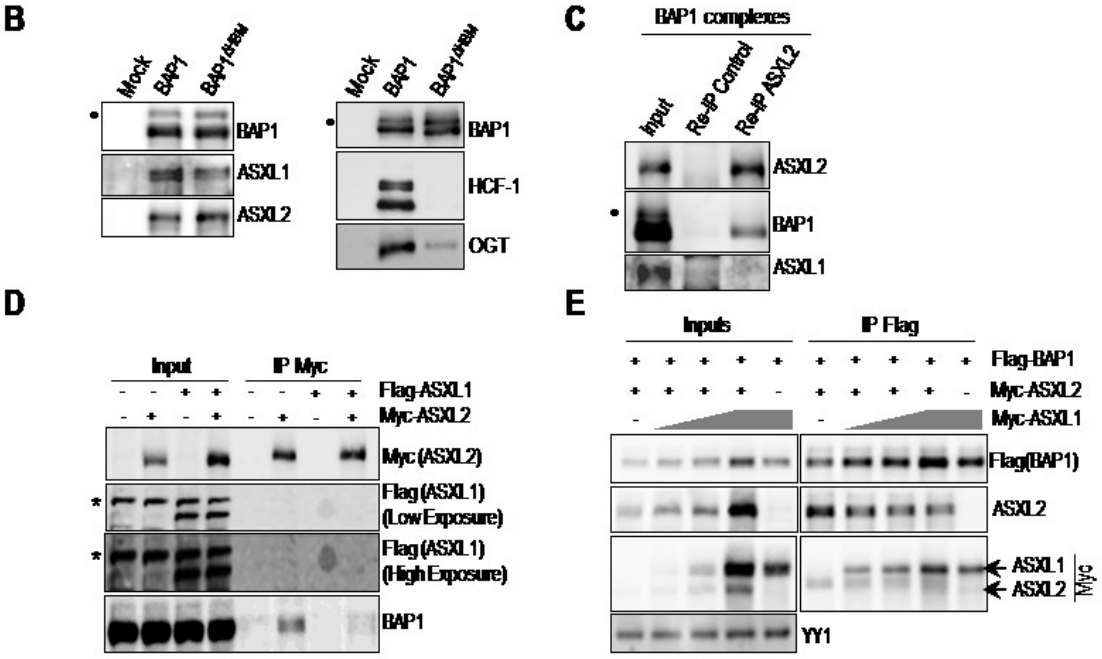

Figure 1

Figure 1. BAP1 interacts with either ASXL1 or ASXL2.

A) BAP1 complexes contain relatively similar amounts of ASXL1/2 proteins. ASXL1/2 peptides identified by mass spectrometry following the purification of BAP1 complexes from HeLa S3 cells. The amino acid positions of the peptides are indicated. B) HCF-1 is not required to maintain the interaction between BAP1 and ASXL1/2. Purification of BAP1 or BAP1ΔHBM (lacking the HCF-1-binding motif) complexes and detection of ASXL1/2 and BAP1 by immunoblotting (left panel). The immunopurifed proteins were also analyzed by immunoblotting to detect the two major components of the BAP1 complexes, HCF-1 and OGT (right panel). Note that OGT is greatly reduced in the BAP1ΔHBM complexes due to the absence of HCF-1. C) Reciprocal immunoprecipitation (Re-IP) of ASXL2 from the purified BAP1 complexes. D) 293T cells were transfected with Myc-ASXL2 (6 μg) with or without Flag-ASXL1 (4 μg) expression vectors and harvested, three days later, for IP of Myc (ASXL2). E) 293T cells were transfected with Flag-BAP1 (0.1 μg) and Myc-ASXL2 (3 μg) constructs in the presence of increasing amounts of Myc-ASXL1 construct (1, 2 and 5 μg) and harvested, three days later, for IP of BAP1 using anti-Flag. Overexpressed Myc-ASXL2 was detected with anti-ASXL2 and anti-Myc antibodies. ASXL1 was detected with anti-Myc antibody. The difference in M.W. allows discrimination between ASXL1 and ASXL2 bands. YY1 is used as a loading control. Quantification of band intensity for each protein was conducted relative to the lowest amount of transfected plasmid. The dot and the star indicate a monoubiquitinated form of BAP1 (31), and non-specific bands respectively (panels B, C, D).

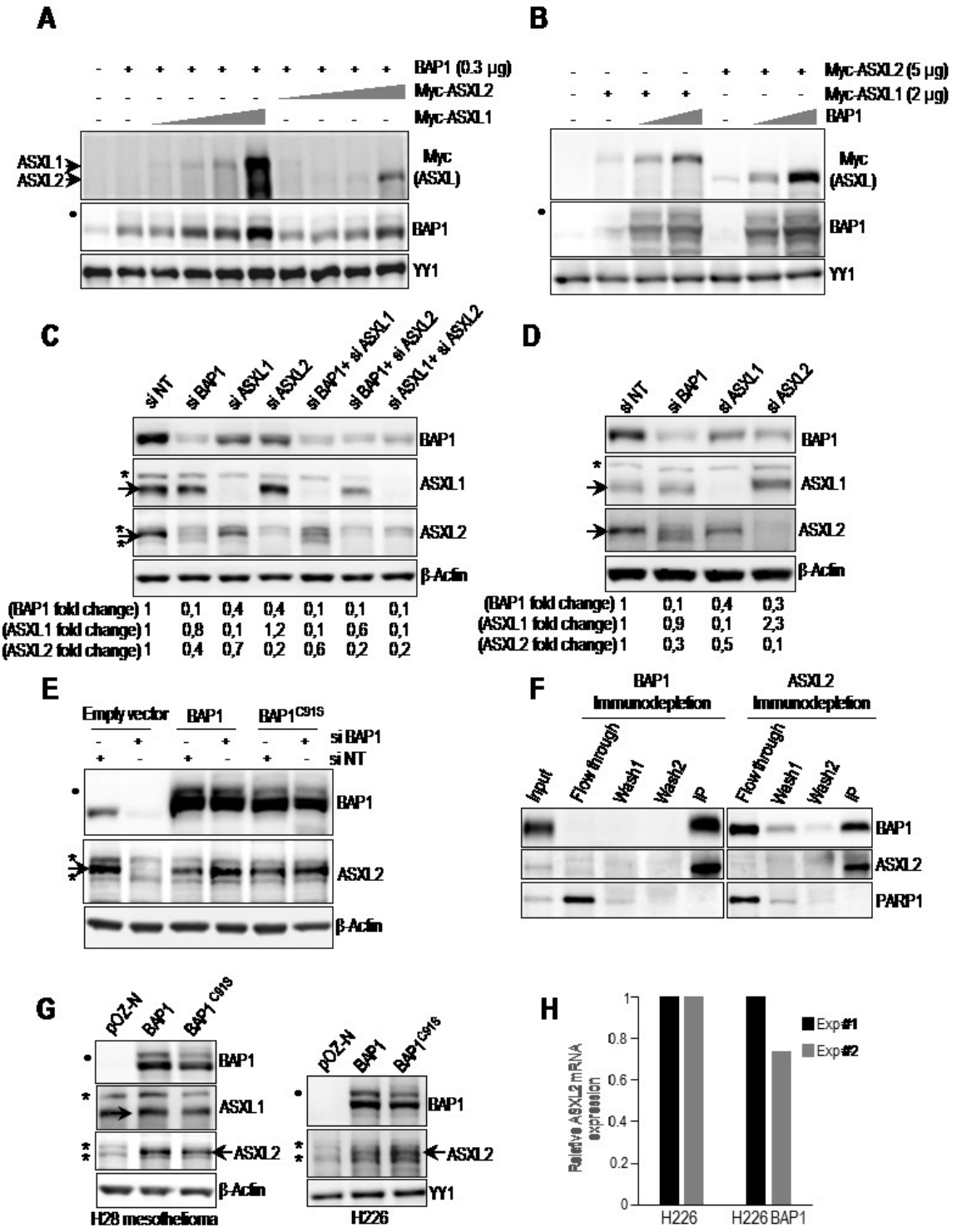
A
BAP1 (0.3 µg)
Myc-ASXL2
Myc-ASXL1
ASXL1
ASXL2
Myc (ASXL)
BAP1
YY1
B
Myc-ASXL2 (5 µg)
Myc-ASXL1 (2 µg)
BAP1
Myc (ASXL)
BAP1
YY1
C
si NT
si BAP1
si ASXL1
si ASXL2
si BAP1+ si ASXL1
si BAP1+ si ASXL2
si ASXL1+ si ASXL2
BAP1
ASXL1
ASXL2
β-Actin
(BAP1 fold change) 1 0,1 0,4 0,4 0,1 0,1 0,1
(ASXL1 fold change) 1 0,8 0,1 1,2 0,1 0,6 0,1
(ASXL2 fold change) 1 0,4 0,7 0,2 0,6 0,2 0,2
D
si NT
si BAP1
si ASXL1
si ASXL2
BAP1
ASXL1
ASXL2
β-Actin
(BAP1 fold change) 1 0,1 0,4 0,3
(ASXL1 fold change) 1 0,9 0,1 2,3
(ASXL2 fold change) 1 0,3 0,5 0,1
E
Empty vector
BAP1
BAP1C91S
si BAP1
si NT
BAP1
ASXL2
β-Actin
F
BAP1 Immunodepletion
ASXL2 Immunodepletion
Input
Flow through
Wash1
Wash2
IP
BAP1
ASXL2
PARP1
G
pOZ-N
BAP1
BAP1 C91S
BAP1
ASXL1
ASXL2
β-Actin
H28 mesothelioma
YY1
H226
H
Relative ASXL2 mRNA expression
Exp#1
Exp#2
H226
H226 BAP1

Figure 2

Figure 2. BAP1 and ASXL1/2 are co-regulated and loss of BAP1 in cancer is concomitant with ASXL2 depletion.
A) 293T cells were transfected with BAP1 and increasing amounts of either Myc-ASXL1 (0.5, 1, 2 and 5 μg) or Myc-ASXL2 (0.5, 1, 2 and 5 μg) expression vectors and harvested, three days later, for immunoblotting. B) 293T cells were transfected with Myc-ASXL1 or Myc-ASXL2 with increasing amounts of BAP1 (0.3 and 1 μg) vectors and harvested, three days later, for immunoblotting. Quantification of band intensity for each protein was conducted relative to the lowest amount of transfected plasmid (panels, A, B). C) Protein levels following siRNA depletion of BAP1 and/or ASXL1/2 in U2OS cells. D) Protein expression following siRNA depletion of BAP1, ASXL1 and ASXL2 in LF1 human fibroblasts. E)Depletion of endogenous BAP1 using siRNA in U2OS cells stably expressing empty vector, siRNA-resistant BAP1 wild-type or siRNA-resistant BAP1 catalytic dead mutant (C91S). Protein levels of BAP1 and ASXL2 were detected by immunoblotting. Quantification of band intensity was conducted relative to the non-target siRNA control (panels C, D, E). F) Immunodepletion of BAP1 or ASXL2 from HeLa nuclear extracts. The nuclear DNA damage signaling enzyme, PARP1, was used as a control, which mostly remained in the flow through fraction. G) Reconstitution by retroviral infection of H28 mesothelioma and H226 non-small lung carcinoma BAP1-deficient cells with BAP1 or BAP1C91S. Protein levels of BAP1 and mutants were detected by immunoblotting. H) mRNA of ASXL2 in reconstituted H226 cells was quantified by qPCR. The data represent two independent experiments. β-Actin or YY1 are used as protein loading controls. Quantification of band intensity was conducted relative to BAP1 transfected samples (panels G). The dot and stars indicate a monoubiquitinated form of BAP1 (31), and non-specific bands respectively (panels, A, B, C, D, E, G).

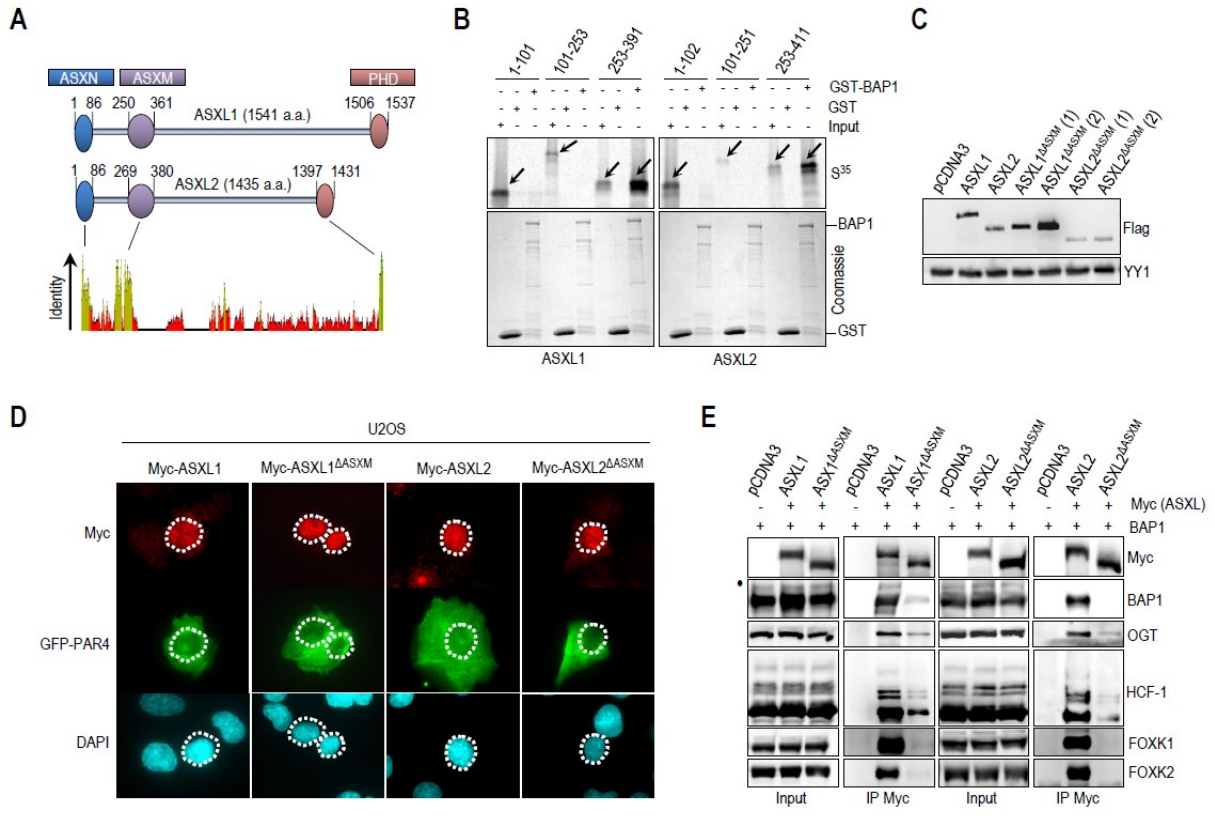

Figure 3

Figure 3. ASXM of ASXL1/2 is required for interaction with BAP1.

A) Schematic representation and conservation of ASXL1/2. B) GST-pull down assay using GST-BAP1 and methionine S35-labeled ASXL1 or ASXL2 fragments. The arrows indicate the full length forms of the fragments. C) ASXM is required for ASXL2, but not ASXL1, stability. Flag-ASXL1/2 and their respective Flag-ASXL1/2 ΔASXM mutants (3 μg each) were transfected in 293T cells which were harvested, three days post-transfection, for immunoblotting. A duplicate of transfection is shown for Flag-ASXL1/2 ΔASXM mutants. D) U2OS cells were transfected with either Myc-ASXL1 (4 μg), Myc-ASXL1 ΔASXM (4 μg), Myc-ASXL2 (4 μg), or Myc-ASXL2 ΔASXM (4 μg) along with GFP-PAR4 (0.5 μg). Three days post-transfection, cells were harvested for Immunostaining using the indicated antibodies. The cells overexpressing the different forms of ASXL1/2 were encircled. E) 293T cells were transfected with Myc-ASXL1 (4 μg), Myc-ASXL1 ΔASXM (4 μg), Myc-ASXL2 (4 μg), or Myc-ASXL2 ΔASXM (6 μg), along with BAP1 (1 μg) vectors and harvested, three days post-transfection, for IP with anti-Myc. The dot indicates a monoubiquitinated form of BAP1 (panel E) (31).

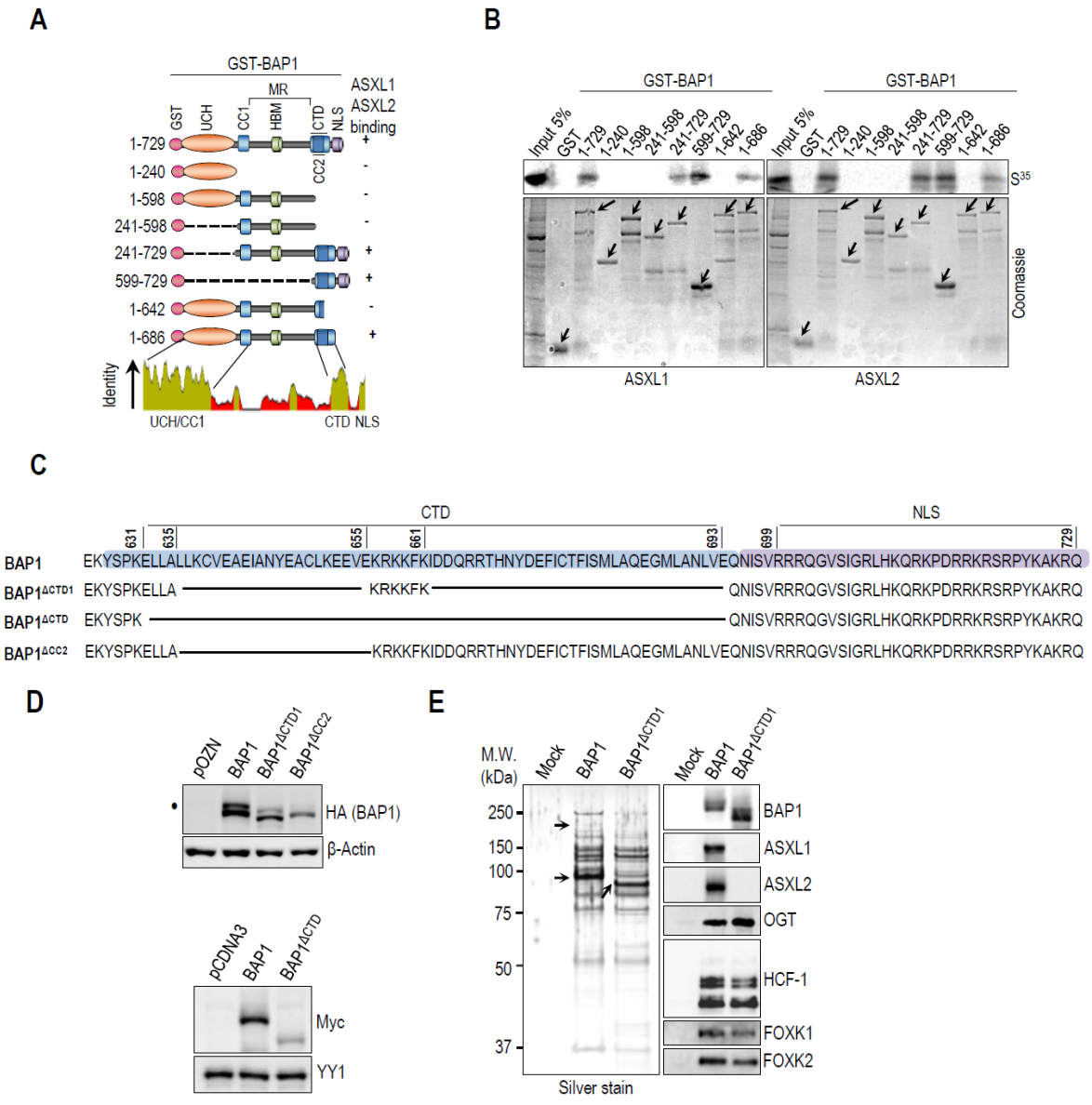
A
GST-BAP1
MR
GST
UCH
CC1
HBM
CTD
NLS
CC2
ASXL1
ASXL2
binding
1-729 +
1-240 -
1-598 -
241-598 -
241-729 +
599-729 +
1-642 -
1-686 +
Identity
UCH/CC1
CTD NLS
B
GST-BAP1
GST-BAP1
Input 5%
GST
1-729
1-240
1-598
241-598
241-729
599-729
1-642
1-686
S35
Coomassie
ASXL1
ASXL2
C
CTD
NLS
631
635
655
661
693
699
729
BAP1 EKYSPKELLALLKCVEAEIANYEACLKEEVEKRKKFKIDDQRRTHNYDEFICTFISMLAQEGMLANLVEQNISVRRRQGVSIGRLHKQRKPDRRKRSRPYKAKRQ
BAP1ΔCTD1 EKYSPKELLA KRKKFK QNISVRRRQGVSIGRLHKQRKPDRRKRSRPYKAKRQ
BAP1ΔCTD EKYSPK QNISVRRRQGVSIGRLHKQRKPDRRKRSRPYKAKRQ
BAP1ΔCC2 EKYSPKELLA KRKKFKIDDQRRTHNYDEFICTFISMLAQEGMLANLVEQNISVRRRQGVSIGRLHKQRKPDRRKRSRPYKAKRQ
D
pOZN
BAP1
BAP1ΔCTD1
BAP1ΔCC2
HA (BAP1)
β-Actin
pCDNA3
BAP1
BAP1ΔCTD
Myc
YY1
E
M.W. (kDa)
Mock
BAP1
BAP1ΔCTD1
250
150
100
75
50
37
Silver stain
BAP1
ASXL1
ASXL2
OGT
HCF-1
FOXK1
FOXK2

Figure 4

Figure 4. BAP1 interacts with ASXL1/2 via its CTD domain.
A) Schematic representation of the BAP1 fragments used for in vitro pull down in panel B. B) GST-pull down assay using GST-BAP1 fragments and methionine S35-labeled ASXM domains of ASXL1 or ASXL2. The arrows indicate the full length forms of the fragments. C) Schema of the different deletions in the CTD domain used to generate BAP1 mutants. BAP1ΔCTD1 represents a deletion of the CTD from 635 up to 693 amino acids except the KRKKFK motif which is suggested to function as an NLS (21). We also generated a BAP1ΔCTD which represents a mutant with a deletion of the CTD domain (Δ631-693 amino acids). BAP1ΔCC2 represents a mutant with a smaller deletion within the CTD domain (Δ635-655 amino acids). D) A functional CTD is required for proper protein stability of BAP1. Protein expression levels of BAP1 and its CTD deletion mutant form in stable HeLa S cell lines (Top panel). Myc-BAP1, Myc-BAP1 ΔCTD expression constructs (3 μg each) were transfected in 293T cells, which were harvested, three days post-transfection, for immunoblotting (Bottom panel). E) Left panel, silver stain of the immunopurified BAP1 and BAP1□CTD1 complexes. Right panel, western blot detection of components of the BAP1 complexes. The high and low arrows indicate the position of ASXL2 and BAP1 (WT and BAP1□CTD1) respectively. β-Actin or YY1 are used as protein loading controls. The dot indicates a monoubiquitinated form of BAP1 (panel D) (31).

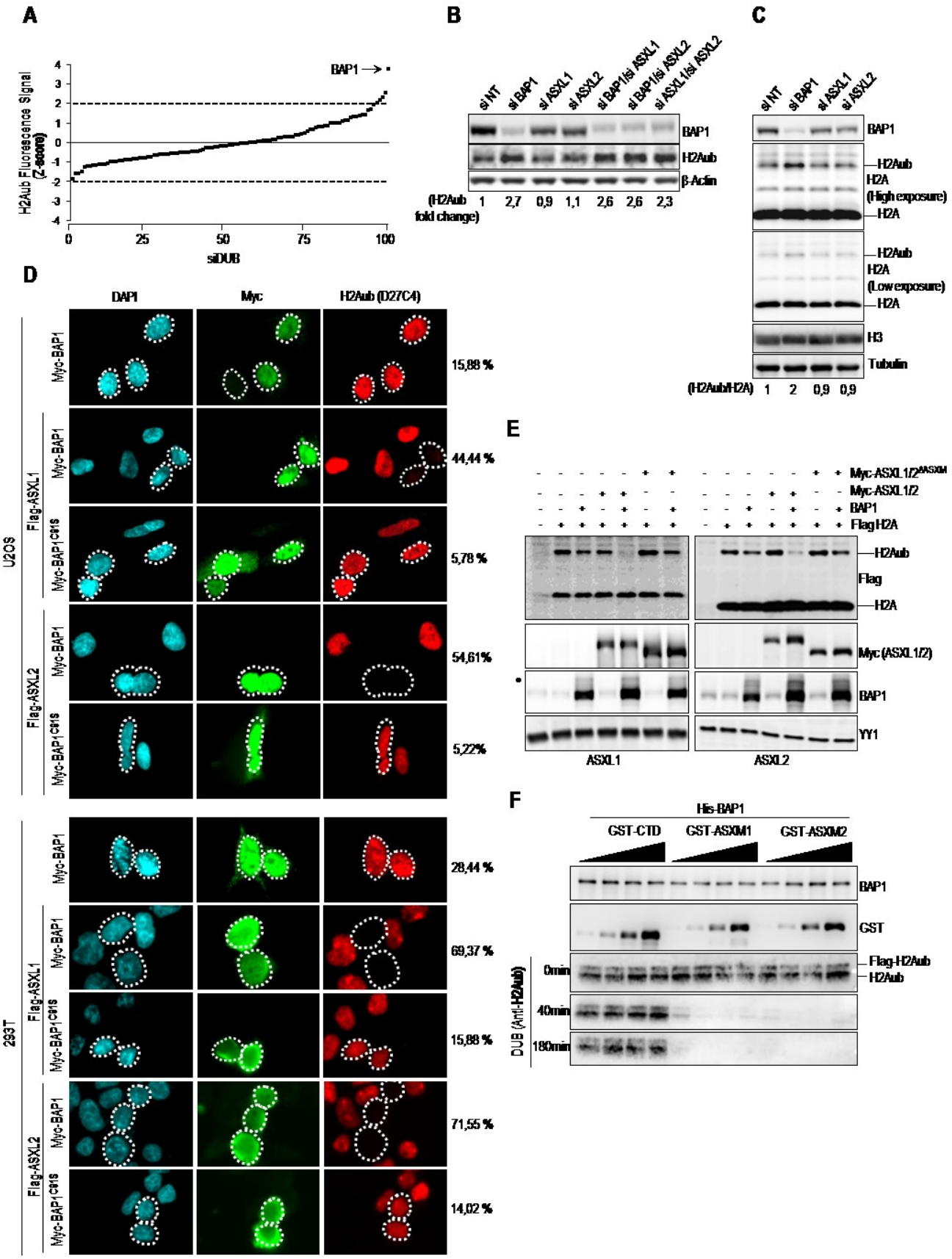
A
H2Aub Fluorescence Signal (Z-score)
BAP1
siDUB
B
si NT
si BAP1
si ASXL1
si ASXL2
si BAP1/si ASXL1
si BAP1/si ASXL2
si ASXL1/si ASXL2
BAP1
H2Aub
β-Actin
(H2Aub fold change) 1 2,7 0,9 1,1 2,6 2,6 2,3
C
si NT
si BAP1
si ASXL1
si ASXL2
BAP1
H2Aub
H2A
(High exposure)
H2A
H2Aub
H2A
(Low exposure)
H2A
H3
Tubulin
(H2Aub/H2A) 1 2 0,9 0,9
D
DAPI
Myc
H2Aub (D27C4)
U2OS
293T
Flag-ASXL1
Flag-ASXL2
Myc-BAP1
Myc-BAP1C/S
15,88 %
44,44 %
5,78 %
54,61%
5,22%
28,44 %
69,37 %
15,88 %
71,55 %
14,02 %
E
Myc-ASXL1/2ΔASXM
Myc-ASXL1/2
BAP1
Flag H2A
H2Aub
Flag
H2A
Myc (ASXL1/2)
BAP1
YY1
ASXL1
ASXL2
F
His-BAP1
GST-CTD
GST-ASXM1
GST-ASXM2
BAP1
GST
DUB (Anti-H2Aub)
0min
40min
180min
Flag-H2Aub
H2Aub

Figure 5

Figure 5. ASXM of ASXL1/2 stimulates BAP1 DUB activity.
A) siRNA screen for DUBs that coordinate H2Aub levels. Following transfection with siRNA DUB library, HeLa cells were fixed and immunostained for H2Aub K119 (H2Aub). The fluorescence signal was determined and the values used to derive the Z-scores. B) Knockdown of BAP1 or concomitant Knockdown of ASXL1 and ASXL2 induces a significant increase of the global level of H2Aub. U2OS cells were transfected with siRNA as indicated and harvested four days post-transfection for immunoblotting using the indicated antibodies. Quantification of band intensity for H2Aub was conducted relative to the non-target siRNA control (siNT). C) Increase of H2Aub levels following BAP1 depletion is not due to a global increase of H2A. U2OS cells were transfected with siRNA of BAP1, ASXL1 and ASXL2 and harvested, four days post-transfection, for immunoblotting using the respective antibodies. Tubulin was used a loading control for soluble proteins and histone H3 as a loading control for histones levels. Quantification of band intensity for H2Aub was conducted relative to the non-modified histone H2A and the values were then normalized to the non-target siRNA control (siNT). D) ASXL1/2 promote BAP1 DUB activity toward H2Aub in vivo. U2OS cells (top panel) or 293T cells (bottom panel) were transfected with either Myc-BAP1 (0.5 μg) or Myc-BAP1 C91S (0.5 μg) expression constructs in the presence or absence of Flag-ASXL1/2 (4 μg) expression constructs. Three days post-transfection, cells were harvested for Immunostaining using the indicated antibodies. The cells overexpressing BAP1 and BAP1C91S were encircled. Note that the transfections were conducted with plasmid ratios optimized to ensure that most BAP1 transfected cells also express ASXL1 or ASXL2. Cells overexpressing BAP1 were counted for change in H2Aub signal. The percentages at the right of the panel represent the number of cells showing very low signal of H2Aub versus the total number of BAP1 expressing cells. E) 293T cells were transfected as indicated using Flag H2A (0.2 μg), BAP1 (1 μg), Myc-ASXL1 (4 μg) or Myc-ASXL1 ΔASXM (4 μg) vectors (left panel); Myc-ASXL2 (4 μg) or Myc-ASXL2 ΔASXM (6 μg) vectors (right panel) and harvested, three days later, for immunoblotting. F) In vitro DUB assay of nucleosomal H2A using recombinant His-BAP1 (8 ng, 2 pM) in presence of increasing amounts of recombinant GST-CTD, GST-ASXM1 or GST-ASXM2 (0.6 pM, 1.2 pM, 2 pM and 4 pM). β-Actin, Tubulin or YY1 were used as loading controls.

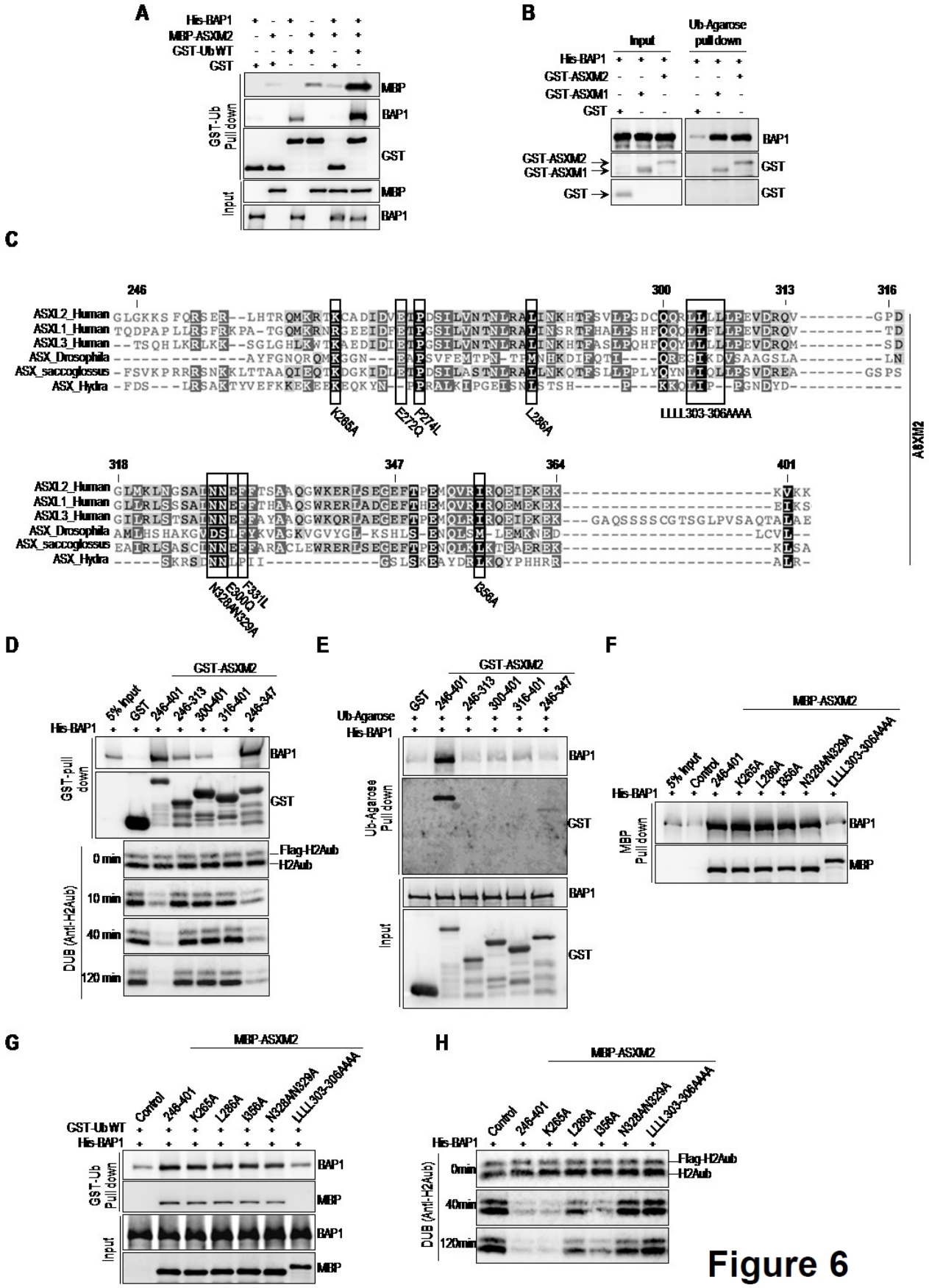
A
His-BAP1
MBP-ASXM2
GST-Ub WT
GST
GST-Ub Pull down
Input
MBP
BAP1
GST
B
Input
Ub-Agarose pull down
His-BAP1
GST-ASXM2
GST-ASXM1
GST
C
246
300
313
316
318
347
364
401
ASXL2_Human
ASXL1_Human
ASXL3_Human
ASX_Drosophila
ASX_saccoglossus
ASX_Hydra
K265A
E272Q
P274L
L286A
LLLL303-306AAAA
N328AN329A
E300Q
F331L
I356A
ASXM2
D
GST-ASXM2
6% Input
GST
246-401
246-313
300-401
316-401
246-347
His-BAP1
GST-pull down
BAP1
GST
Flag-H2Aub
H2Aub
DUB (Anti-H2Aub)
0 min
10 min
40 min
120 min
E
GST-ASXM2
Ub-Agarose
His-BAP1
Ub-Agarose Pull down
Input
F
MBP-ASXM2
5% Input
Control
246-401
K265A
L286A
I356A
N328AN329A
LLLL303-306AAAA
MBP Pull down
MBP
G
MBP-ASXM2
Control
246-401
K265A
L286A
I356A
N328AN329A
LLLL303-306AAAA
GST-Ub WT
His-BAP1
GST-Ub Pull down
Input
H
MBP-ASXM2
Control
246-401
K265A
L286A
I356A
N328AN329A
LLLL303-306AAAA
His-BAP1
Flag-H2Aub
H2Aub
DUB (Anti-H2Aub)
0min
40min
120min

Figure 6

Figure 6. ASXM enhances BAP1 binding to ubiquitin.
A) Recombinant His-BAP1 (1.6 μg, 20 nM) and MBP-ASXM2 (2 μg, 30 nM) were incubated with either GST or GST-Ubiquitin-Agarose beads (3 μg, 80 nM) and the pulled down fractions were analysed by immunoblotting. B) Recombinant His-BAP1 (1.6 μg, 20 nM) and GST-ASXM1 or GST-ASXM2 (2 μg, 40 nM) were incubated with ubiquitin-agarose beads and the pulled down fractions were analyzed by immunoblotting. C) Multiple sequence alignment between the ASXM domains of human ASXL1/2, Drosophila ASX and other paralogs and orthologs of ASX. The mutants of ASXM2 including the cancer-associated mutants used in panels F, G, H and Fig.9 are shown. D) GST pull down interaction assay and in vitro DUB reactions of H2A using His-BAP1 and GST-ASXM2 (full length and deletion mutant forms). For the pull down assay, His-BAP1 (1.6 μg, 20 nM) was incubated with GST-ASXM2 (2 μg, 40 nM) or the different fragment of GST-ASXM2 (2 μg, 50 nM). His-BAP1 (8 ng, 2 pM) and the different recombinant ASXM2 fragments (10 ng, 4 pM) were used for the DUB reactions. E) His-BAP1 (1.6 μg, 20 nM) and the different GST-fused fragments of ASXM2 (2 μg, 40 nM) were subjected to ubiquitin-Agarose pull down assay followed by immunoblotting. F) MBP-pull down interaction assay using recombinant MBP-ASXM2 (full length and mutant forms) (2 μg, 30 nM) and His-BAP1 (1.6 μg, 20 nM). G) GST-Ubiquitin pull down assay using MBP-ASXM2 full length and the different mutant forms with His-BAP1. The pull down was done as in (A). H) In vitro DUB reactions of H2A using His-BAP1 (8 ng, 2 pM) and the different recombinant MBP-ASXM2 (10 ng, 2,8 pM).

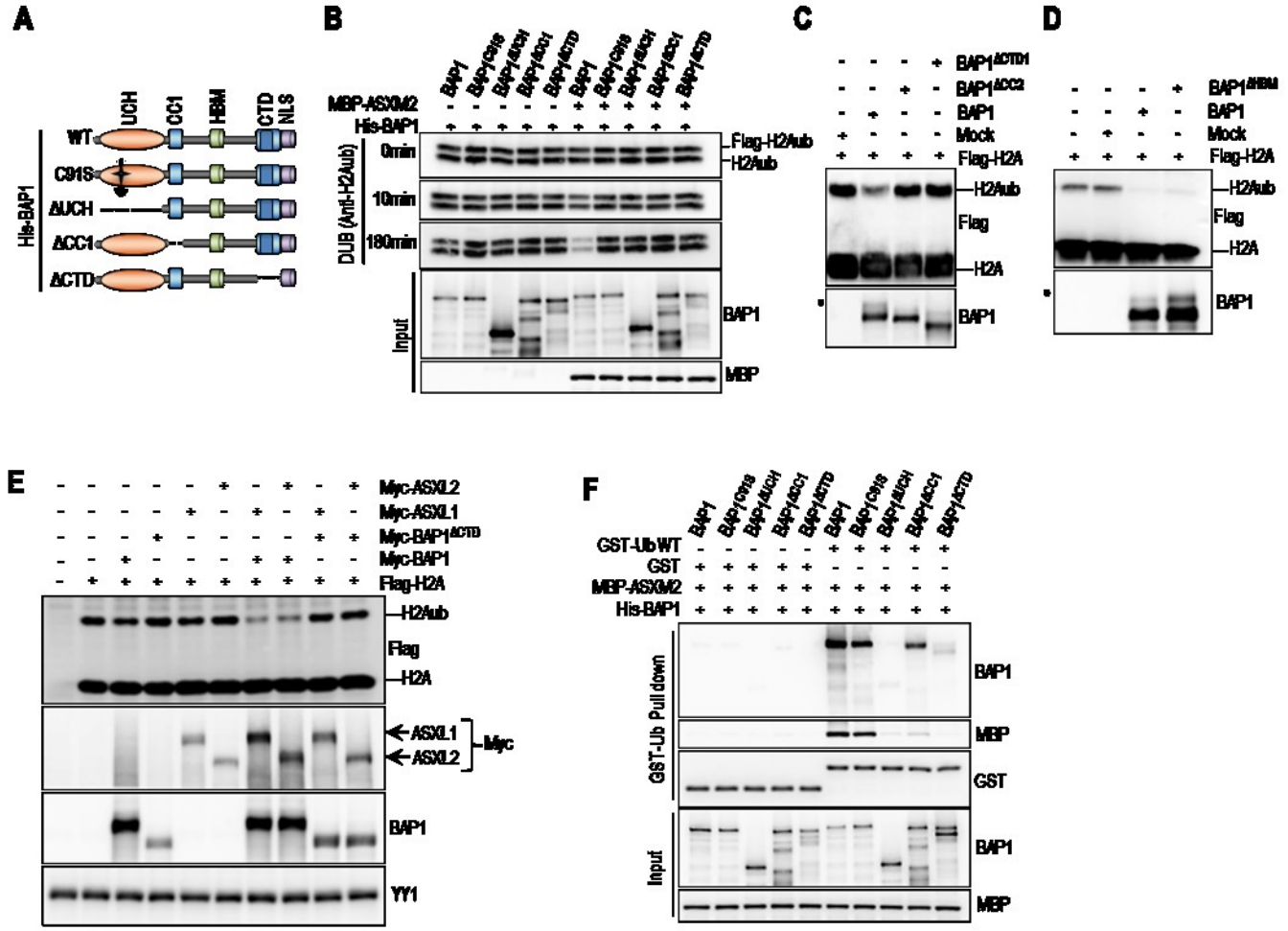

Figure 7. Intramolecular interaction in BAP1 is required to create an ASXM-inducible composite ubiquitin binding interface (CUBI).

A) Schematic representation of the different BAP1 mutants generated for in vitro experiments done in panel B. B) In vitro DUB reaction of nucleosomal H2A using His-BAP1 or its mutant forms (8 ng, 2 pM) in presence or absence of MBP-ASXM2 (10 ng, 2,8 pM). C-D) In vitro deubiquitination assay of nucleosomal histone H2A using purified Flag-HA BAP1, BAP1ΔCTD1 or BAP1ΔCC2 complexes. BAP1ΔHBM was used as a control since HCF-1 is not required for BAP1 DUB activity. E) In vivo DUB activity of BAP1ΔCTD is abolished due to the lack of interaction with ASXL1/2. Flag-H2A (0.2 µg) expression construct was co-expressed in 293T cells with either Myc-BAP1 (1 µg) or Myc-BAP1 ΔCTD (1 µg) with or without Myc-ASXL1 (4 µg) or Myc-ASXL2 (6 µg) expression constructs. Three days post-transfection, cells were harvested for immunoblotting. YY1 is used as a loading control. F) His-BAP1 mutants (1.6 µg, 20 nM) and MBP-ASXM2 (2 µg, 30 nM) were subjected to GST-Ubiquitin pull down assay followed by immunoblotting.

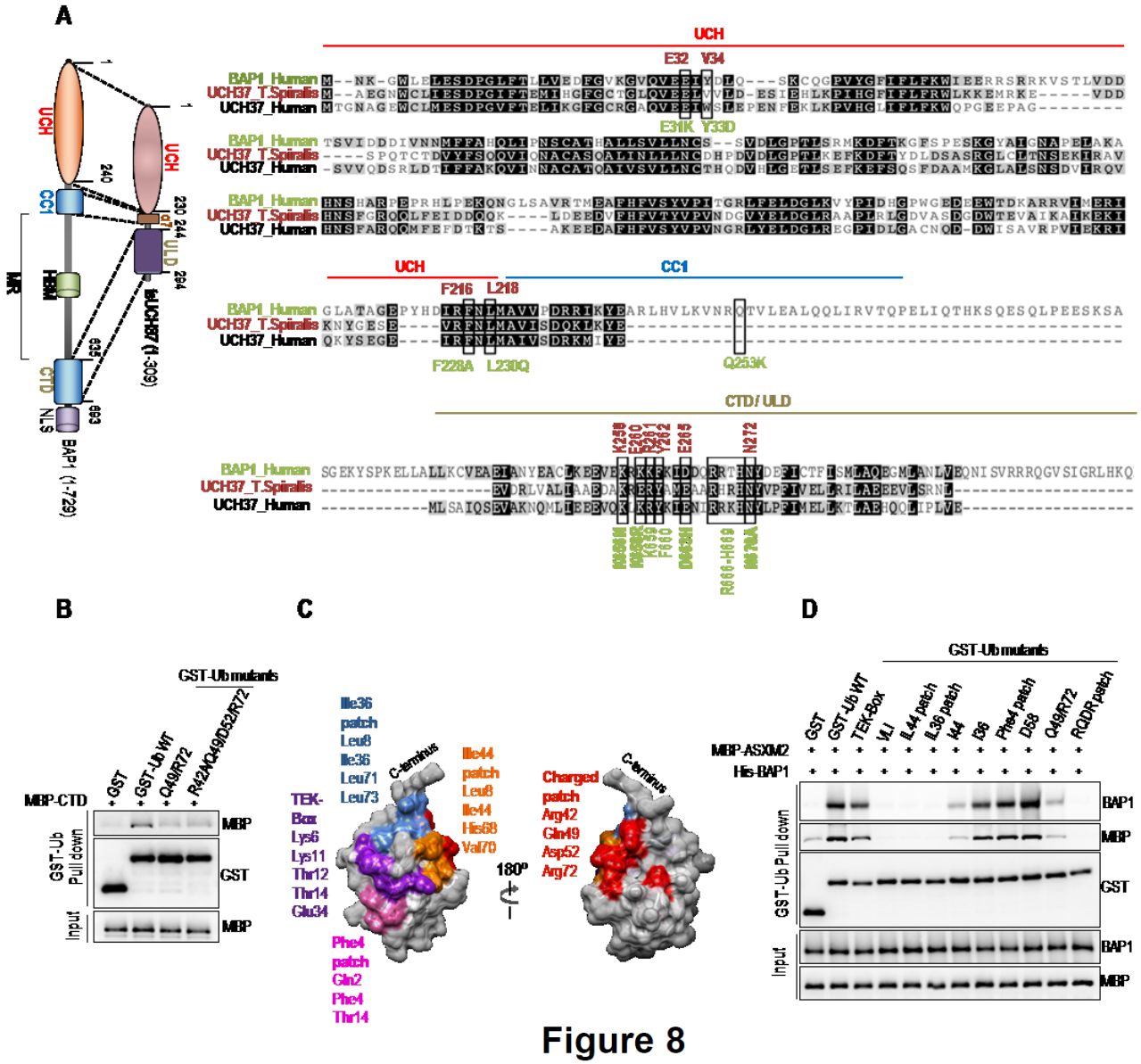

Figure 8

Figure 8. BAP1 CTD is an ubiquitin-interacting domain.

A) Comparison between BAP1 and UCH37. tsUCH37 of the worm Trichinella spiralis whose crystal structure was recently reported (38), was aligned with human UCH37 and BAP1. The functional conserved domains between BAP1 and tsUCH37 are shown in the left panel. The alignment (right panel) show conserved motifs and residues in the UCH, CC1 and CTD domains. The mutants of BAP1 including the cancer-associated mutants used in Fig. 9 are shown. Note the presence in the CTD of the cancer mutant BAP1R666-H669 with a deletion of the R666 to H669 amino acids. B) MBP-CTD (3 µg, 40 nM) of BAP1 was subjected to GST-Ubiquitin pull down assay using GST-Ubiquitin wild type or its mutant forms (3 µg, 80 nM) (all residues were converted to alanines) and then analysed by immunoblotting. C) Ubiquitin structure showing the various interaction interfaces. D) GST-Ubiquitin pull down interaction assays using GST-Ubiquitin wild type or its different mutant forms (all residues of each path were converted to alanines) and His-BAP1 with MBP-ASXM2 followed by immunoblotting. The pull down was done as in Fig. 7F.

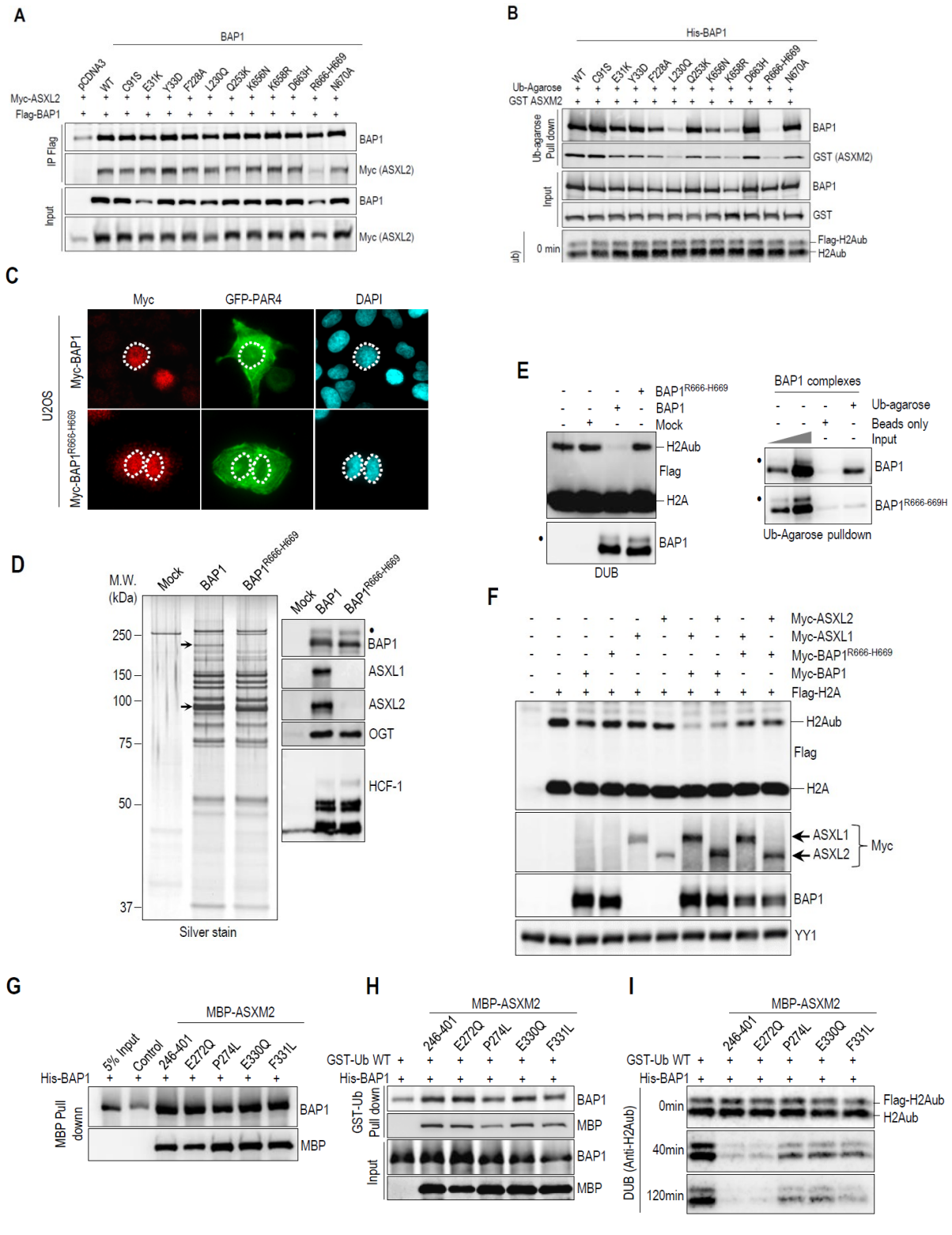
A
BAP1
pCDNA3
WT
C91S
E31K
Y33D
F228A
L230Q
Q253K
K656N
K658R
D663H
R666-H669
N670A
Myc-ASXL2
Flag-BAP1
IP Flag
BAP1
Myc (ASXL2)
Input
BAP1
Myc (ASXL2)
B
His-BAP1
Ub-Agarose
GST ASXM2
Ub-agarose Pull down
BAP1
GST (ASXM2)
Input
BAP1
GST
0 min
Flag-H2Aub
H2Aub
C
Myc
GFP-PAR4
DAPI
U2OS
Myc-BAP1
Myc-BAP1R666-H669
D
M.W. (kDa)
Mock
BAP1
BAP1R666-H669
250
150
100
75
50
37
BAP1
ASXL1
ASXL2
OGT
HCF-1
Silver stain
E
BAP1R666-H669
BAP1
Mock
H2Aub
Flag
H2A
BAP1
DUB
BAP1 complexes
Ub-agarose
Beads only
Input
BAP1
BAP1R666-669H
Ub-Agarose pulldown
F
Myc-ASXL2
Myc-ASXL1
Myc-BAP1R666-H669
Myc-BAP1
Flag-H2A
H2Aub
Flag
H2A
ASXL1
ASXL2
Myc
BAP1
YY1
G
MBP-ASXM2
His-BAP1
5% Input
Control
246-401
E272Q
P274L
E330Q
F331L
MBP Pull downn
BAP1
MBP
H
MBP-ASXM2
GST-Ub WT
His-BAP1
246-401
E272Q
P274L
E330Q
F331L
GST-Ub Pull down
BAP1
MBP
Input
BAP1
MBP
I
MBP-ASXM2
GST-Ub WT
His-BAP1
246-401
E272Q
P274L
E330Q
F331L
DUB (Anti-H2Aub)
0min
40min
120min
Flag-H2Aub
H2Aub

Figure 9

Figure 9. Disruption of BAP1 ubiquitin binding and DUB activity by cancer-associated mutations of BAP1 and ASXL2.

A) R666-H669 BAP1 cancer mutation abolishes its interaction with ASXL2. Myc-ASXL2 (6 μg) construct was co-transfected in 293T with either Flag-BAP1, Flag-BAP1 C91S or Flag-BAP1 mutants constructs (1 μg) and cells were harvested for Flag IP of BAP1 followed by immunoblotting. B) Ubiquitin pull down and in vitro DUB assays of nucleosomal H2A using GST-ASXM2 and His-BAP1, His-BAP1C91S or the different recombinant mutant forms of BAP1. The same amounts of recombinant proteins as presented in Fig. 5, 6 and 7 were used for the in vitro reactions. C) U2OS cells were transfected with either Myc-BAP1 (4 μg) or Myc- BAP1 R666-H669 (4 μg) along with GFP-PAR4 (0.5 μg). Three days later, cells were harvested for immunostaining using the indicated antibody. Cells expressing BAP1 or BAP1R666-H669 were encircled. D) BAP1 complexes were purified from HeLa cells stably expressing Flag-HA-BAP1 or Flag-HA-BAP1R666-H669. Left panel, silver stain shows the profiles of the complexes. Right panel, western blot detection of the major components of the BAP1 complexes. The high and low arrows indicate the position of ASXL2 and BAP1 respectively. E) In vitro DUB assay of nucleosomal H2A (top panel) and Ubiquitin pull down assay (bottom panel) using BAP1 and BAP1R666-H669 complexes. F) R666-H669 BAP1 cancer mutation results in the abrogation of its DUB activity in vivo. Flag-H2A (0.2 μg) construct was co-expressed in 293T cells with either Myc-BAP1 (1 μg) or Myc-BAP1 R666-H669 (1 μg) with or without Myc-ASXL1 (4 μg) or Myc-ASXL2 (6 μg) expression constructs. Three days post-transfection, cells were harvested for immunoblotting. G) His-BAP1 (1.6 μg, 20 nM) and MBP-cancer associated mutants forms of ASXM2 (2 μg, 30 nM) were subjected to MBP pull down interaction assays. H-I) His-BAP1 and MBP-ASXM2 mutants were subjected as done in Fig. 6, 7 and 8 to GST-Ubiquitin pull down assay (H) and in vitro DUB assay using nucleosomal H2A (I). The reactions were analyzed by immunoblotting. YY1 is used as a loading control. The dot indicates a monoubiquitinated form of BAP1 (31) (panels D, E).

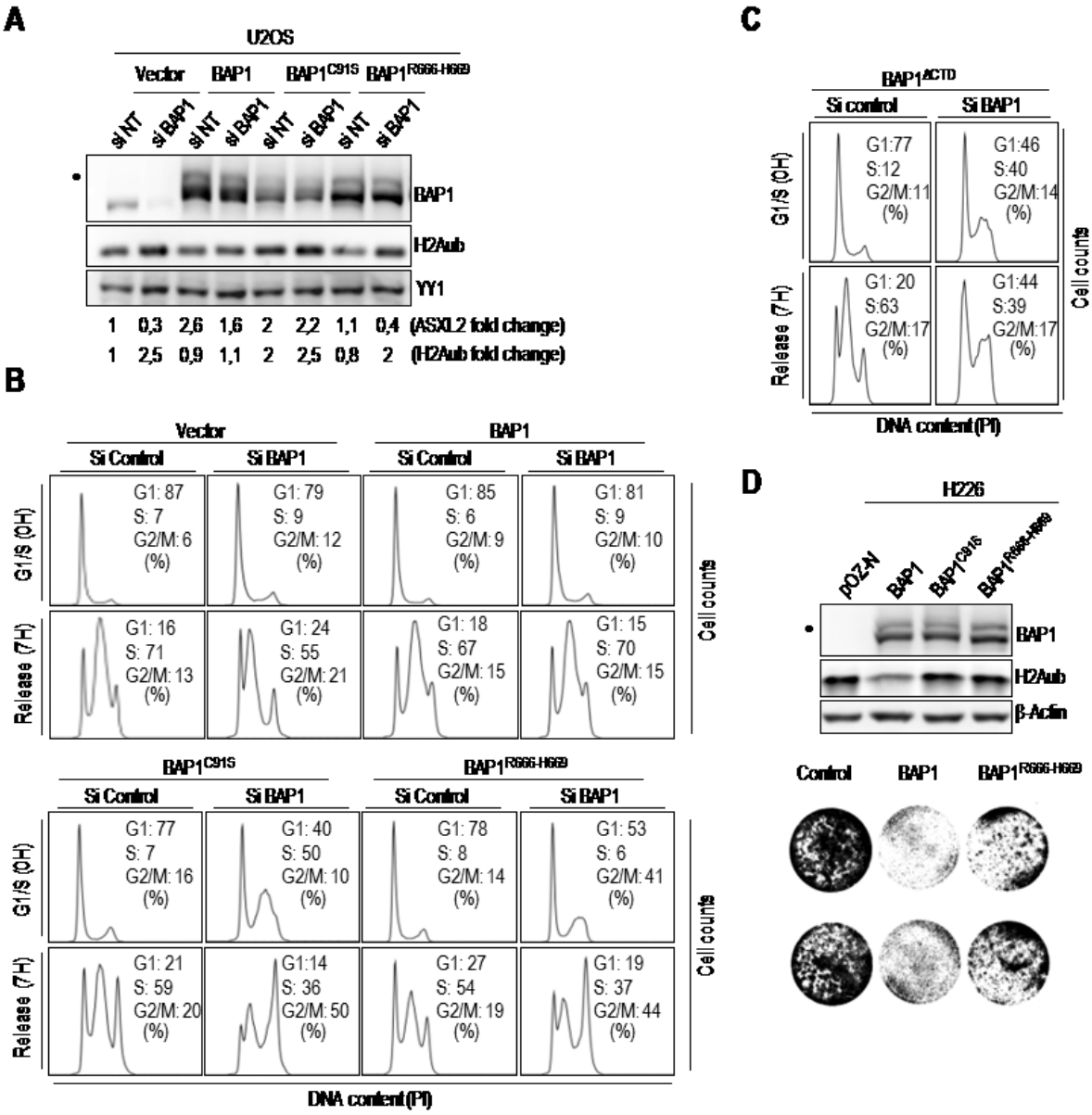

Figure 10

Figure 10. BAP1 regulates cell cycle progression in CTD-dependent manner.
A) Protein levels following depletion of endogenous BAP1 using siRNA in U2OS cells stably expressing siRNA-resistant BAP1, BAP1C91S or BAP1R666-H669. B-C) Mutations of CTD disrupts BAP1 function in regulating cell proliferation. Following siRNA for endogenous BAP1, U2OS cells stably expressing siRNA-resistant BAP1, BAP1C91S, BAP1R666-H669 or BAP1ΔCTD were synchronized by double thymidine block at the G1/S boundary and released 7 hours to progress through S phase and were then subjected to FACS analysis. D) H226 BAP1-null cells stably expressing BAP1, BAP1C91S or BAP1R666-H669 was analysed by immunoblotting (top panel). Similar numbers of cells were plated and cultured for 5 days prior staining with crystal violet dye (bottom panel). YY1 and β-Actin were used as a protein loading controls. The dot indicates a monoubiquitinated form of BAP1 (31) (panels A, D).

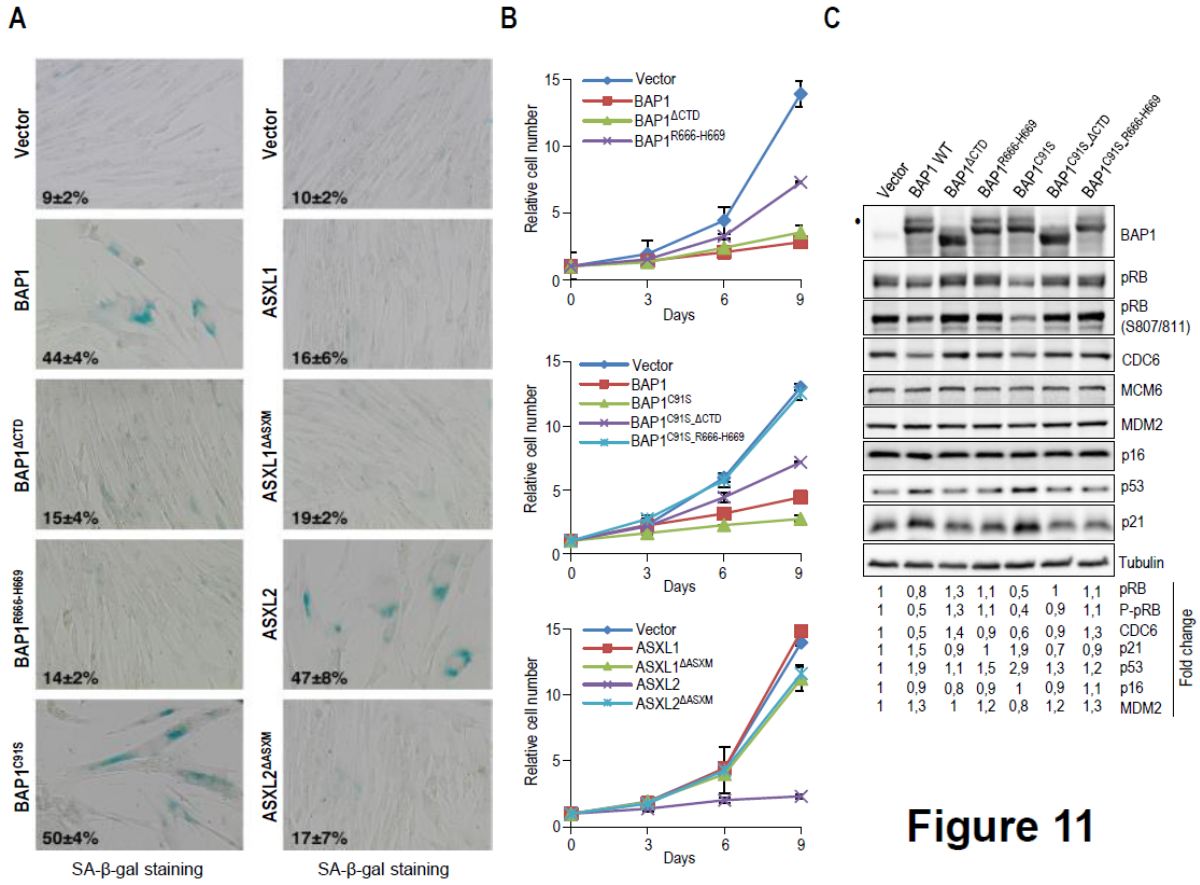

Figure 11. ASXL2 and BAP1 overexpression induce senescence in an ASXM- and CTD-dependent manner respectively.

A) IMR90 cells were infected using retroviral expression vectors for BAP1, ASXL1, ASXL2 and their respective mutant forms. Eight days post-selection the cells were fixed for staining of senescence-associated β-galactosidase assay (SA-β-gal). B) Cells were also transduced with retroviral expression vectors for BAP1, ASXL1, ASXL2 and their respective mutant forms and counted every three days after selection to follow cell proliferation. 100 cells were counted in triplicate and data presented as percentage of positive cells, average ± SD. C) BAP1 overexpression triggers cellular senescence and induces the p53/p21 DNA damage response in ASXL1/2 dependent manner. Eight days post-selection the senescent cells were harvested for immunoblotting. Quantification of band intensity was conducted relative to the empty vector transduced cells. Tubulin was used as a protein loading controls. The dot indicates a monoubiquitinated form of BAP1 (31) (panels C).

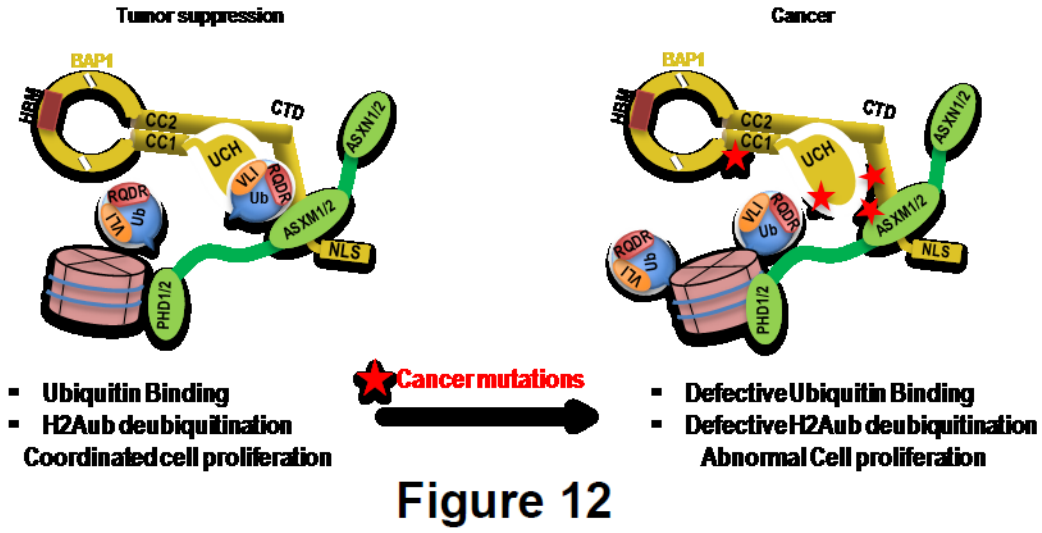

Figure 12

Figure 12. Model for the regulation of BAP1-mediated deubiquitination by ASXL1/2. An intramolecular interaction involving UCH/CC1 and CTD domains of BAP1 creates an ASXM-inducible composite ubiquitin binding interface (CUBI) that facilitates ubiquitin binding and catalysis. The red stars indicate cancer-associated mutations of BAP1 or ASXM that disrupt the CUBI.